2008

# Electrical Behavior of Non-Aqueous Formulations: Role of Electrostatic Interactions in Pressurized Metered Dose Inhalers (pMDIs)

Reshma Kotian
*Virginia Commonwealth University*

# ELECTRICAL BEHAVIOR OF NON-AQUEOUS FORMULATIONS: ROLE OF ELECTROSTATIC INTERACTIONS IN PRESSURIZED METERED DOSE INHALERS (pMDIs)

A Dissertation submitted in partial fulfillment of the requirements for the degree of Doctor of Philosophy at Virginia Commonwealth University.

by

RESHMA KOTIAN
M.Pharm., India, Mumbai University Institute of Chemical Technology, 2002
B.Pharm., India, Mumbai University Institute of Chemical Technology, 2000

Director: JOANNE PEART, Ph.D.
ASSOCIATE PROFESSOR, DEPARTMENT OF PHARMACEUTICS

Virginia Commonwealth University
Richmond, Virginia
May 2008

# Acknowledgement

I would like to take this opportunity to express my gratitude to all the people who have helped me along the path to a successful completion of my Ph.D. endeavor.

First and foremost, I would like to thank my advisor, Dr. Peart, for her constant guidance towards my research project. Her constant encouragement and her untiring efforts have helped me grow professionally and made me a more confident person today.

I am grateful to my committee members, Drs. Byron, Sakagami, Kellogg and Longest, for their valuable time and for providing me helpful suggestions and inputs towards my dissertation project.

I would like to thank Dr. Hindle for his help with the LC-MS method for analysis of albuterol. Thanks to Joan for helping me get acquainted with the aerosol research lab when I first joined the Department and for lending me a patient ear many a times.

I would like to acknowledge Dr. Karla Mossi from Department of Mechanical Engineering for providing me free access to the LCR meter in her laboratory as well as to her graduate student, Poorna Mane, who helped me with the instrument. I would like to thank Samir Vinchurkar, also from the Dept. of Mechanical Engineering, for his help with the AUTOCAD software, which I used for drawing the ELPI inlet.

Thanks are due to Mike and Pete at the Custom Design and Fabrication for accomodating my many requests and making the various pieces of equipment I used throughout my project. I would like to acknowledge the help I received from Ashutosh, Aurujit and Dr. Phil Mosier during my molecular modeling project. Thanks to the Pharmaceutics faculty for their help in the course of my graduate studies.

I extend special thanks to Pankaj and Anuprita, for being so kind and for helping me get settled when I first landed in the USA. Thanks to Vidya, Anuprita, Deepika, Soniya, Priya and Bhawana - my family away from home - for their friendship. Thanks to my good friends - Rena, Dave, Suparna, Nagesh, Poorna and Kumar for always being so helpful. Thanks to the Aerosol Research Group members and the graduate students in the Dept. of Pharmaceutics for making my time here at the VCU School of Pharmacy a memorable one. Laura, Mia, Keyetta, Chris and Romano deserve special thanks for being so efficient and dependable and making life in graduate school much easier.

I would like to thank Medical College of Virginia Foundation for funding the project as well as the School of Pharmacy for providing me financial support.

Finally, I would like to thank Girish for his love, understanding, encouragement and patience all these years. Last but not the least, thanks to my family - my parents and my brother for being there for me always. This dissertation is the result of my parents' love, blessings and their relentless efforts to keep me motivated at all times. Thanks to Mom and Dad for always believing in me.

# Table of Contents

Page

# List of Tables

Page

# List of Figures

Page

# List of Abbreviations

| | |
|---|---|
| ® | registered trademark |
| °C | degrees Celsius |
| ε | Dielectric constant |
| $\varepsilon_o$ | Electric permittivity of vacuum |
| $\varepsilon_{rs}$ | relative permittivity |
| η | Viscosity |
| μ | Electrophoretic mobility |
| ρ | Resistivity |
| ζ | Zeta potential |
| μg | Microgram |
| μL | Microliter |
| μm | Micrometer |
| a | hydrophobic atom constant |
| A | Cross-sectional area of electrodes |
| ACI | Andersen cascade impactor |
| AFM | Atomic Force Microscopy |
| ANOVA | analysis of variance |
| aPSD | Aerodynamic particle size distribution |
| C | Coulomb |
| $C_i$ | current distribution |
| CDF | Cumulative distribution function |
| CFC | Chlorofluorocarbon |
| CFC 11 | Trichlorofluoromethane |
| CFC 12 | Dichlorodifluoromethane |
| $cm^3$ | cubic centimeter |
| COD | Coefficient of Determination |
| d | Electrode gap |
| $D_{50}$ | Aerodynamic cut-off diameter |
| $D_p$ | particle diameter |
| DFN | Difference from nominal |
| DOS | di-octyl sebacate |
| DPI | dry powder inhaler |
| e | elementary charge |
| E | Electric Field |
| e.g. | for example |
| *et al.* | and others |
| ELPI | Electrical Low Pressure Impactor |

| | |
|---|---|
| EPDM | ethylene-propylene-diene-terpolymer |
| ESA | Electrokinetic Sonic Amplitude |
| fA | Femtoampere |
| FFD | Formoterol Fumarate Dihydrate |
| FPD | fine particle dose |
| g | gram |
| GSD | Geometric standard deviation |
| H-bond | Hydrogen bond |
| HFA 134a | 1,1,1,2-tetrafluoroethane |
| HFA 227 | 1,1,1,2,3,3,3-heptafluoropropane |
| HFA | hydrofluoroalkane |
| HINT | Hydropathic INTeractions |
| HPFP | 2H,3H-perfluoropentane |
| HPLC | high pressure liquid chromatography |
| Hz | Hertz |
| i.e. | that is |
| K | Resistivity cell constant |
| kcps | kilo counts per second |
| kV | kilovolt |
| kHz | kiloHertz |
| LC-MS | Liquid Chromatography-Mass Spectrometry |
| LDV | Laser Doppler Velocimetry |
| L/min | liter per minute |
| LogP | octanol-water partition coefficient |
| $m^3$ | cubic meter |
| mbar | millibar |
| MEK | Methyl ethyl ketone |
| mg | milligram |
| mL | milliliter |
| mL/min | milliliter per minute |
| mm | millimeter |
| mV | millivolts |
| MMAD | mass median aerodynamic diameter |
| MΩ.cm | MegaOhms-centimeter |
| MSC | Model Selection Criteria |
| n | average number of charges per particle |
| ng/mL | nanogram per milliliter |
| NGI | Next generation impactor |
| nm | nanometer |
| P | charger penetration |

| | |
|---|---|
| pA | picoampere |
| PBT | polybutylene terephthalate |
| PEG | Polyethylene glycol |
| pC | picocoulomb |
| pMDI | pressurized metered dose inhaler |
| PSD | Particle size distribution |
| PTFE | Polytetrafluoroethylene |
| PVP | Polyvinyl pyrollidone |
| Q | flow rate of calibration |
| R | Resistance |
| $r^2$ | coefficient of determination |
| RH | Relative humidity |
| RSD | relative standard deviation |
| SD | standard deviation |
| sec | second |
| SMPS | scanning mobility particle sizer |
| USP | United States Pharmacopeia |
| v | velocity |
| V | volt |
| VHC | Valved-holding chamber |
| V/cm | Volts/cm |
| v/v | volume per volume |
| w/v | Weight per volume |
| w/w | weight per weight |

# Abstract

ELECTRICAL BEHAVIOR OF NON-AQUEOUS FORMULATIONS: ROLE OF ELECTROSTATIC INTERACTIONS IN PRESSURIZED METERED DOSE INHALERS (pMDIs)

Reshma Kotian, M.S.

A dissertation submitted in partial fulfillment of the requirements for the degree of Doctor of Philosophy at Virginia Commonwealth University.

Virginia Commonwealth University, 2008

Director: JOANNE PEART, Ph.D.
ASSOCIATE PROFESSOR, DEPARTMENT OF PHARMACEUTICS

Aerosol electrostatics is an important property of pharmaceutical aerosols. The electrostatic properties of pMDI aerosols have been shown to be a function of both formulation and packaging components. The modified ELPI enables measurement of aerosol charge as a function of particle size, and the simultaneous determination of the mass distribution using chemical analysis. However, in order to fully assess the cause and

effects of aerosol electrostatics in terms of its biological and regulatory implications, it is necessary to understand the basic charging mechanisms inside the pMDI formulation.

Electrical resistivity and zeta potential measurements confirmed the presence of charged species within HFA based solutions and suspensions although the nature of these species remains unknown. These measurements were influenced by the cosolvent concentration and to a lesser extent by the presence of soluble drug and surfactant. The mean electrical resistivity of a 7% ethanol / 93% HFA 134a blend (0.83 ± 0.02 MΩ.cm) was significantly lower than that reported for HFA 134a (180 MΩ.cm). Albuterol sulfate demonstrated a positive zeta potential (75.9 ± 26.2 mV) in HFA 134a. Pilot molecular modeling studies, in conjunction with the analysis of particle interactions using HINT, provided an improved understanding of the possible interactions within albuterol sulfate HFA suspension pMDIs. The predominantly negative (-7597 ± 2063) HINT score signified unfavorable interactions between albuterol sulfate and HFA 134a molecules.

Systematic investigations of the electrical properties of HFA solution and suspension pMDIs using the modified ELPI demonstrated that the electrical properties were a function of the formulation type (solution/suspension), formulation components and particle size. Experimental BDP solution pMDIs produced predominantly electropositive aerosols (net charge: 160 ± 30 pC) while albuterol sulfate pMDIs produced bipolar charged aerosol clouds (net charge: -162 ± 277 pC). Finally, the modified ELPI was recalibrated using commercially available polydisperse pMDIs as calibration aerosols with a reference Andersen cascade impactor. The mean cut-off diameters for stages 4-12 obtained following recalibration of the modified ELPI were 0.44, 0.56, 0.70, 1.01, 1.40, 2.12, 3.03, 4.75, 6.37

μm, respectively in comparison to those reported by the manufacturer (0.16, 0.27, 0.39, 0.62, 0.96, 1.62, 2.42, 4.05, 6.67 μm, respectively).

# I. INTRODUCTION

## I.A. Significance and Background

Aerosol clouds produced by pressurized metered dose inhalers (pMDIs) are electrically charged and these charges may influence particle deposition behavior in the respiratory tract and valved holding chambers (VHCs) (Melandri *et al.* 1983, Peart *et al.* 1998, Bisgaard *et al.* 2002). In fact, VHCs made from electrically conductive or electrostatically dissipative material are now commercially available and have been suggested to improve drug delivery from pMDIs by minimizing electrostatic loss of drug in the chamber (Mitchell *et al.* 2004, Louca *et al.* 2006, Rau *et al.* 2006). Electrostatic properties of pMDI aerosol clouds have been shown to be a function of both formulation and packaging components (Peart *et al.* 1998). However, electrical properties of the formulation within the pMDI canister are not well characterized, primarily due to a lack of consensus on charge generation mechanisms and the experimental difficulties associated with the measurement of electrical properties in non-aqueous liquefied propellants (Sidhu *et al.* 1993, Sandstrom *et al.* 1994, Rogueda 2002, Traini *et al.* 2005). In order to fully assess the cause and effects of pMDI aerosol electrostatics in terms of its biological and regulatory implications, it is necessary to understand the basic charging mechanisms inside the pMDI formulation.

Electrical measurements in chlorofluorocarbon (CFC) and hydrofluoroalkane (HFA) containing formulations are challenging due to the need to maintain the propellants under pressure. Earlier studies have employed electrophoretic mobility measurements to demonstrate that drug particles suspended in model non-pressurized chlorinated solvents and CFC propellants can acquire surface charges (Wyatt and Vincent 1989, Sidhu *et al.* 1993). A limited number of studies have reported determination of zeta potential using electrophoretic mobility measurements for drug suspensions in a model non-pressurized HFA solvent, e.g., 2H,3H-perfluoropentane (HPFP), however, the role of surface charges in HFA based suspension pMDIs remains poorly understood (Rogueda 2002).

Although aerodynamic particle size is the major parameter influencing drug deposition from pMDIs, studies using animals, hollow-cast lung models, humans and theoretical lung models have demonstrated the importance of electrostatic charge on the deposition of aerosols in the respiratory tract (Fraser 1966, Chan *et al.* 1978, Melandri *et al.* 1983). The effect of electrostatic charge on particle size characterization methods is not known. It is therefore necessary to evaluate aerosol electrostatic properties in relation with the particle size distribution. With the introduction of the Electrical Low Pressure Impactor (ELPI), it is possible to measure the charge distribution of aerosols as a function of particle size and simultaneously determine the mass distribution using chemical analysis (Glover and Chan 2004a, Keil 2005, Kwok *et al.* 2005). Electrostatic charge characterization of commercial HFA based solution and suspension pMDIs using a modified ELPI has previously been reported (Kwok *et al.* 2005), however, a systematic study investigating the

differences in the electrostatic charging characteristics of solution and suspension HFA pMDIs is lacking.

This research project will focus on the particle interactions and, in particular, electrostatic interactions within hydrofluoroalkane based pMDI formulations in relation to their aerosol electrostatic properties.

**I.B. Particle Interactions within Pressurized Metered Dose Inhalers**

In order to better understand the formulation effects on electrical properties of pMDI aerosols, the particle interactions inside the pMDI formulation itself need to be considered. Most pMDIs are formulated as suspensions of micronized drug in liquefied propellant blends (Farr *et al.* 1994). Surfactants, e.g., lecithin, oleic acid and sorbitan trioleate have traditionally been used to stabilize these inherently unstable systems, which have a tendency to form agglomerates as a result of attractive particle-particle interactions such as van der Waals forces (Farr *et al.* 1994). According to DLVO theory, suspension stability is governed by the steric and / or electrostatic repulsive forces exceeding the attractive forces (Derjaguin and Landau 1941, Verwey and Overbeek 1948). Although traditional DLVO theory has been used to explain suspension stability within aqueous systems on the basis of van der Waals attractive forces and electrostatic repulsion, its application to non-aqueous systems, e.g., pMDI suspensions has not been validated (Vervaet and Byron 1999). The extent to which the above-mentioned forces influence particle interactions within the pMDI suspension is considered to vary depending on surface chemistry and morphology of drug, excipients and packaging components, e.g.,

canister coating material (Parsons *et al.* 1992, Clarke *et al.* 1993). Conventional wisdom states that suspension stability is predominantly achieved using surfactants via steric repulsion in non-aqueous media (Vervaet and Byron 1999). In such non-aqueous systems, due to the low dielectric constant and low ionic strengths within the suspensions, electrostatic repulsive forces are considered to be negligible (Pugh *et al.* 1983).

The formulation and device components of the pMDI have undergone major modifications due to the transition from the ozone-depleting CFCs to the ozone-friendly HFA propellants (Thiel 1996, Leach 2005). The difference in physicochemical properties of HFA and CFC propellants, particularly the solvent characteristics, has necessitated the use of different salt forms of drugs and the inclusion of polar cosolvents such as ethanol to dissolve surfactants traditionally used in CFC based pMDIs (Byron *et al.* 1994, Tzou *et al.* 1997, Jannick 2006). Solubility of water in HFAs is higher than that in CFCs, and HFA based pMDIs show an increased tendency for water ingress (Gelotte and Shaheed 1998, Williams 1999). HFA based suspension pMDIs also have a greater propensity for drug adhesion to the canister inner surface than CFC based suspensions and the use of fluorocarbon polymer coating such as PTFE (polytetrafluoroethylene) on the canister inner surfaces to minimize drug adhesion has been documented in the patent literature (Ashurst *et al.* 2000a, Ashurst *et al.* 2000b, Britto 2000, Britto 2001, Riebe *et al.* 2003). Novel suspension stabilizers to improve HFA based pMDI suspension stability have also been investigated (Stefely 2002, Looker *et al.* 2003). The addition of polymers, e.g., polyethylene glycol (PEG) and polyvinylpyrollidone (PVP) to formoterol fumarate dihydrate (FFD) suspensions in HPFP has been shown to decrease the attractive forces

between FFD particles, measured using atomic force microscopy (AFM), presumably via steric hindrance by polymer adsorption on to the particle surface (Rogueda 2002).

Traini *et al.* have suggested an alternative approach to DLVO theory in order to explain particle interactions within HFA propelled suspension pMDIs on the basis of surface energetics, proposed by van Oss (van Oss 1994, Traini *et al.* 2005). This alternative surface component approach considers short range Lewis acid-base (electron donor or electron acceptor) interactions including hydrogen bonding, in addition to dispersive van der Waals and the long range electrostatic repulsive forces, to explain particle interactions in pMDI suspensions (Traini *et al.* 2005). Particle interactions between drug, canister and polymeric coating materials in HPFP have been investigated; contact angle measurements were employed to determine the surface energy parameters while AFM measurements were used to determine the cohesive-adhesive interactions (Traini *et al.* 2006). Experimentally determined adhesion energies between albuterol sulfate particles and inner surfaces of pMDI canisters such as aluminum, anodized aluminum, and PTFE, using AFM have been correlated with theoretical calculations of adhesion energies using the surface component approach (Traini *et al.* 2006). These studies demonstrated that adhesion of drug particles to canister material was dependent on both the dispersive and polar components of particle interactions in an HPFP environment thus suggesting that partially fluorinated liquids are not apolar and that their weakly polar nature may also play an important role in particle interactions within pMDIs (Traini *et al.* 2006).

In their approach, Traini *et al.* assumed that the electrostatic component of particle interactions within HFA based suspension pMDIs was negligible, based upon the absence

of appreciable ionic concentration (Traini *et al.* 2005). However, this may not be entirely applicable to all HFA based formulations, which are more likely to form ionic species since they are relatively polar. The dielectric constant of a dispersion medium determines the dissociation of the electrolytes present in the solvent. Non-aqueous solvents may be categorized in terms of their dielectric constant (ε) into non-polar ($\varepsilon \leq 5$), weakly polar ($5 < \varepsilon \leq 12$), moderately polar ($12 < \varepsilon \leq 40$) and polar ($\varepsilon > 40$) (Delgado *et al.* 2005). Thus, propellants used in pMDI formulations may be classified on the basis of their dielectric constant as non-polar, e.g., CFC 11, CFC 12 or weakly polar, e.g., HFA 134a, HFA 227 solvents. Inclusion of ethanol as a cosolvent would increase the dielectric constant and the polarity of the dispersion medium, which in turn could influence ionic dissociation. The solubility of water in HFA 134a alone has been reported to be 2200 ppm (Pischtiak 2000a) while that in a 10% ethanol / 90% HFA 134a blend is much higher (13500 ppm; Gelotte and Shaheed 1998). The presence of water in these systems may also possibly influence the formation of ionic species and a subsequent increase in the conductivity of the ethanol / HFA blend. Although conventional wisdom suggests that steric repulsion is the only effective means for stabilization of non-aqueous suspension pMDIs (Vervaet and Byron 1999), the role of electrostatic charge in the relatively polar HFA based suspension pMDIs remains to be investigated.

**I.C. Electrostatic Interactions within Non-Aqueous Systems**

Comprehensive reviews addressing the mechanisms involving charge generation and electrostatic stabilization in non-aqueous systems have been published (Lyklema 1968,

Fowkes *et al.* 1982, Morrison 1993). Charging mechanisms in non-aqueous dispersions may involve: 1) acid-base mechanisms where proton or hydroxyl ions are potential determining ions (in protic liquids), or electron transfer mechanisms in aprotic liquids, 2) surface group dissociation, or 3) adsorption of uncharged electrolyte onto the particle followed by ion exchange with surface groups and dissociation of charged electrolytes, the most common ion exchanged being a proton (Morrison 1993).

While complete dissociation of electrolytes can be expected for polar solvents, incomplete dissociation of electrolytes is observed in moderately polar liquids, i.e., the concentration of charged ionic species may be lower than the concentration of the electrolytes present (Delgado *et al.* 2005). In weakly polar liquids, limited dissociation of electrolytes capable of forming large charged species, e.g., micelles or polymers, can occur (Morrison 1993). However the ionic concentration in such systems, which may be obtained from conductivity measurements, would be expected to be very low (Delgado *et al.* 2005).

Most of the studies investigating electrical charges in non-aqueous dispersions have investigated carbon black suspensions in hydrocarbons such as mineral oil, xylene, benzene with dispersants, e.g., sodium diethylhexylsulfosuccinate, calcium diisopropyl-salicylate, and various salicylates and succinimides. It has been suggested that charge forming species in these suspensions are inverse micelles formed by the dispersants. Trace amounts of water could enhance the formation of inverse micelles by forming links between the hydrophilic portions within the micelle in non-aqueous systems. These large association structures may spontaneously dissociate on the application of an electric field and give rise to electrical conductivity in non-aqueous media (Morrison 1993). Although

inverse micelle formation has been reported in CFCs (Matthews and Hirschhorn 1953), similar formation of inverse micelles has not been documented for HFA based suspensions containing a series of surfactants (Blondino 1995).

The influence of trace quantities of water on the surface charge of both hydrophilic solids like titanium dioxide and hydrophobic particles such as carbon black dispersed in non-aqueous solvents, e.g., p-xylene, cyclohexane, n-heptane has been reported (McGown and Parfitt 1966). Charge reversal of suspended titanium dioxide particles in p-xylene containing Aerosol OT (sodium diethylhexyl sulfosuccinate) from negative to positive was observed on moisture adsorption (McGown and Parfitt 1966). Romo has also shown that while charge reversal was observed for α-alumina dispersed in alcohol in the presence of water with a subsequent decrease in suspension stability, there was minimal effect of moisture on the surface charge of aluminum hydroxide (Romo 1966). The presence of water has also been implicated in the charging of surfaces in non-aqueous media by making the dispersion medium either acidic or basic via proton transfer (Lyklema 1968).

Electrical resistivity of CFC and HFA refrigerants have been reported; CFCs were found to be stronger insulators (poor conductors) than HFAs. The resistivity of CFC 12 was determined to be $0.51 \times 10^6$ MΩ.cm, while that of HFA 134a was 108.9 MΩ.cm (Meurer *et al.* 2001). Electrical resistivity of these refrigerants has been found to be dependent on water content and other impurities as well as the applied field strength (Meurer *et al.* 2001). Resistivity of pharmaceutical grade HFA 134a has been reported to be 180 MΩ.cm (Solvay Fluor Product Bulletin 2001), which is comparable to that of refrigerant 134a (108.9 MΩ.cm). HFA based pMDIs are relatively polar in nature due to

the presence of polar cosolvents and susceptible to water ingress as well; these factors would be expected to decrease the resistivity of HFA 134a containing formulations. Electrical resistivity measurements therefore could provide an indication of charged species in the solution and aid in understanding charging mechanisms in propellant containing formulations; such measurements have not yet been undertaken.

### I.C.1. Measurement of Surface Charge in Non-Aqueous Systems

Surface charge in non-aqueous systems can be determined using techniques including electroacoustic measurements, electrodeposition and electrophoretic mobility measurements (Wyatt and Vincent 1989, Morrison *et al.* 1991, Larson *et al.* 1992, Hunter 1998).

Electroacoustic characterization of colloidal dispersions can be used to determine dynamic mobility of charged particles. The technique is based on the generation of an ultrasonic wave by application of an alternating electric field to a colloidal suspension (Hunter 1998), and is also called the electrokinetic sonic amplitude (ESA) effect. Application of an electrical field causes oscillation of charged particles; these oscillations generate tiny acoustic dipoles, which cancel each other in the bulk of the suspension, but near the electrodes no such cancellation occurs. Instead, these tiny acoustic dipoles form an ultrasonic wave near the electrodes, which propagates at a particular amplitude and phase angle that can be related to the magnitude and polarity of the dynamic mobility of charged particles. This technique may be used for determination of zeta potential of colloidal

suspensions and is especially advantageous for measurements in concentrated suspensions (particle concentrations in excess of 1% by volume) (Hunter 1998).

Electrodeposition is a quantitative method to determine the average charge to mass ratio of suspended particles by applying a constant potential (e.g., a high electric field potential of 1 kV) between two parallel plate electrodes (electrode gap: 1 mm) for a known amount of time (3 - 6 sec) (Larson *et al.* 1992). The total number of electric charges passing through the cell is calculated and the mass of the particles plated on the electrode can be calculated from the electrode area and the concentration of particles in suspension (Larson *et al.* 1992).

Morrison *et al.* reported a technique to measure the charge on particles dispersed in insulating fluids. A sample of the dispersion to be tested is placed on a porous support or filter with a pore size sufficient to hold the particles but allows a rapid flow of the liquid (Morrison *et al.* 1991). As the insulating fluid is forced through the dispersion, the charged particles are collected on the filter while the countercharges are carried away and collected in a Faraday cup. The potential produced on the Faraday cup as the oil drains through the orifice is measured. Since the number of countercharges is the same as the number of charges on all the particles, and the mass of all the particles in the dispersion is known, the average charge to mass ratio can be calculated (Morrison *et al.* 1991). However, these techniques are challenging to adapt for measurements in pressurized formulations.

Surface charge of non-aqueous suspensions, including pMDI formulations, has also been determined by measuring the electrophoretic mobility of the suspended particles using either Laser Doppler Velocimetry (LDV) or phase analysis light scattering (PALS),

which is a variation of LDV (Wyatt and Vincent 1989, Morrison 1993, Sidhu *et al.* 1993). Electrophoresis is the movement of charged particles or polyelectrolytes, immersed in a liquid, under the influence of an external electric field (Delgado *et al.* 2005). Charged particles in suspension attract oppositely charged ions (countercharges) from the bulk of the dispersion medium. The countercharges in the vicinity of the particle form a tightly bound layer at the particle surface called the Stern layer. The liquid associated with the tightly bound layer of ions remains stationary with respect to the particle. The potential at the boundary of this stationary liquid layer and the bulk of the medium is called the electrokinetic or zeta potential. Delgado *et al.* have reviewed the status and recent progress in the understanding of electrokinetic theory and have given practical recommendations regarding electrokinetic measurement and interpretation of the results obtained (Delgado *et al.* 2005). For uniform and weak electric fields, a linear relationship exists between steady-state electrophoretic velocity, v and the applied field, E:

$$v = \mu.E \qquad \text{Equation I.C.1.1}$$

where μ is the electrophoretic mobility. In order to obtain zeta potential from measurements of electrophoretic mobility, it is essential to know the thickness of the electrical double layer, i.e., the layer of counterions around the charged particle, $\kappa^{-1}$, and the particle radius, a (Delgado *et al.* 2005). The value of κ is given by:

$$\kappa = \left\{ \frac{\sum_{i=1}^{N} e^2 z_i^2 n_i}{\varepsilon_{rs} \varepsilon_0 kT} \right\}^{1/2} \qquad \text{Equation I.C.1.2}$$

with $e$, the elementary charge; $z_i$ and $n_i$, the charge number and number concentration of ion $i$ (the solution contains $N$ ionic species), respectively; $\varepsilon_{rs}$, the relative permittivity of the electrolyte solution; $\varepsilon_{0,}$ the electric permittivity of vacuum; $k$, the Boltzmann constant; $T$, the thermodynamic temperature (Delgado *et al.* 2005).

Zeta potential can be calculated from the measured electrophoretic mobility using Henry's equation (Equation I.C.1.3):

$$\mu = \frac{2\varepsilon_{rs}\varepsilon_0\zeta f(\kappa a)}{3\eta} \qquad \text{Equation I.C.1.3}$$

where $\zeta$ is zeta potential and $\eta$ is the viscosity of the solution. In order to calculate $\kappa$, the conductivity of the solution as well as knowledge of the mobilities and valences of the ionic species present in the solution is required. The electrokinetic equations derived by Smoluchowski, for non-conducting particles, are valid for particles of any shape or pores inside a solid, provided the radius, a, largely exceeds the Debye length, $\kappa^{-1}$ (electrical double layer around charged particle is 'thin' due to high ionic concentration in the dispersion medium). The Helmholtz-Smoluchowski (HS) equation for electrophoresis is:

$$\mu = \frac{\varepsilon_{rs}\varepsilon_0\zeta}{\eta} \qquad \text{Equation I.C.1.4}$$

Smoluchowski, however, did not consider the case of strongly curved surfaces, i.e., the presence of a large double layer (Delgado *et al.* 2005). When $\kappa a << 1$ (electrical double layer around the charged particle is 'thick' due to low ionic concentration in the dispersion medium), the Hückel approximation as shown in Equation I.C.1.5 is applied.

$$\mu = \frac{2\varepsilon_{rs}\varepsilon_0\zeta}{3\eta} \qquad \text{Equation I.C.1.5}$$

The theories relating to electrokinetic potential assume that the equations relating electrophoretic mobility to zeta potential are applicable to any liquid characterized by two important properties: the electrical permittivity ($\varepsilon_{rs}\varepsilon_0$) and the viscosity ($\eta$). Although surface charges acquired in weakly polar or non polar solvents are much lower compared to those found in aqueous systems, because of the very low electrical double layer capacitance, the value of surface potential is of the same order of magnitude as in aqueous systems. Further, due to the low ionic concentration in these systems, surface potential decays slowly with distance. As a consequence of this, the surface potential is considered to be approximately equal to the zeta potential (Delgado *et al.* 2005).

### I.C.2. Surface Charge of Particles Dispersed in Non-Aqueous, Non-Pressurized and Pressurized Solvents

A limited number of studies have been undertaken to investigate the surface charge of drug particles suspended in model non-aqueous, non-pressurized as well as pressurized chlorinated solvents using an electrophoretic mobility technique (Clarke *et al.* 1993). However, there remains a lack of consensus on the range of zeta potential values that would be preferred for stable suspensions in non-aqueous media. Zeta potential values greater than 50 mV have been suggested in order to obtain stable suspensions in non-aqueous media (Fowkes *et al.* 1982), while Pugh *et al.* have reported zeta potential values in excess of 100 mV for stable dispersions of carbon black in non-aqueous solvents (Pugh *et al.* 1983).

Wyatt and Vincent determined the electrophoretic mobility of drug substances in a model CFC propellant, trichlorotrifluoroethane (P113), a liquid at room temperature, by PALS (Wyatt and Vincent 1989). The PALS technique uses the phase shift of the light scattered by the moving particles with respect to the reference beam instead of the Doppler frequency shift caused by the moving particles with respect to their velocity (Malvern Zetasizer Nano ZS Manual 2003). This technique is therefore much more sensitive in detecting small changes in mobility of charged suspended particles in the presence of other electrokinetic effects. The authors found that certain drugs possessed inherent charge, which could be modified by suitable excipients while other drug substances did not show measurable electrophoretic mobility but charge could be induced on these particles in the suspension in the presence of surfactants like lecithin. Unfortunately, the nature of the drugs tested was not disclosed.

Clarke *et al.* studied particle interactions in model pMDI suspensions in the presence of surfactants, e.g., albuterol base suspensions in P113 in the presence of oleic acid or sorbitan trioleate (Clarke *et al.* 1993). The adsorption of oleic acid on the albuterol base surface suspended in P113 was investigated using radiolabeled oleic acid as well as attenuated transmittance spectroscopy (ATS) coupled with Fourier Transform Infra-Red (FTIR) spectrometry. The oleic acid fraction adsorbed to albuterol increased with an increase in the initial oleic acid concentration (concentration range studied: 0.005 - 0.100 %w/v). The corresponding increase in the intensity of the asymmetric stretch of the oleate ion observed in the ATS-FTIR studies suggested that the interaction between oleic acid and albuterol base involved an acid-base mechanism, i.e., donation of a proton from oleic

acid to albuterol with the formation of an ion-pair. The electrophoretic mobility of albuterol base in P113, measured using LDV (ZetaSizer), was determined to be negative and the magnitude increased (electrophoretic mobility: $2.0x10^{-10}$ - $0.2x10^{-10}$ $m^2/V.s$) with increasing oleic acid concentration, which was hypothesized to be due to the presence of oleate ion at the electrical double layer (Clarke *et al.* 1993).

Adsorption of sorbitan trioleate, a non-ionic surfactant, to albuterol base suspended in P113 appeared to increase with initial surfactant or adsorbate concentration (0.025 - 0.160 %w/v) with respect to the adsorbent; however, no evidence of chemical interaction was found from the FTIR studies (Clarke *et al.* 1993). The authors also observed that there was no appreciable change in the electrophoretic mobility of albuterol base in P113 ($1.2x10^{-10}$ - $2.5x10^{-10}$ $m^2/V.s$) as the concentration of sorbitan trioleate was increased. The authors suggested that sorbitan trioleate adsorbed on to the albuterol base surface by a physical mechanism such as hydrogen bonding (Clarke *et al.* 1993). Zeta potentials measured for the albuterol base suspensions in P113 containing either oleic acid or sorbitan trioleate were much lower (albuterol / oleic acid system: 0.9 - 9.0 mV; albuterol / sorbitan trioleate system: 5.0 - 10.5 mV) than those reported for stable non-aqueous suspensions. The authors suggested that the electrostatic repulsion forces alone may not be effective and steric stabilization possibly plays a major role in stabilization of the suspensions studied (Clarke *et al.* 1993).

Electrophoretic properties of lactose and salbutamol sulfate suspensions in dried chloroform, chloroform and P113 have also been investigated using a non-aqueous electrophoresis cell coupled with LDV (Sidhu *et al.* 1993). Zeta potentials were calculated

from electrophoretic mobilities using the Hückel equation. Lactose was found to have a negative zeta potential (-23 ± 3 mV) in chloroform, which decreased in magnitude (-5 ± 2 mV) when dispersed in dry chloroform. In contrast, salbutamol sulfate was found to exhibit a positive zeta potential in chloroform (34 ± 5 mV), the magnitude of zeta potential (55 ± 2 mV) increased when dry chloroform was used (Sidhu *et al.* 1993).

Sidhu *et al.* also studied the effect of the addition of two surfactants, lecithin and Span 85 (sorbitan trioleate), at varying concentrations on particle charge in chloroform based dispersions (Sidhu *et al.* 1993). The addition of lecithin to the lactose / chloroform dispersion caused the lactose surface charge to reverse from negative to positive, with a maximum zeta potential reported at 0.01 %w/v lecithin; further increase in lecithin concentration (to 1 %w/v) had no additional effects. Addition of Span 85 showed similar trends, with a charge reversal from negative to positive observed at concentrations exceeding 0.001 %w/v. In contrast, the addition of lecithin to salbutamol sulfate suspensions in chloroform caused the zeta potential to become less positive; the zeta potential was reduced from +34 mV to +12 mV in the presence of 1% lecithin. Again similar trends were observed upon the addition of Span 85 (Sidhu *et al.* 1993). The authors concluded that the potential surrounding the charged particles was dependent upon the relative polarity of the solid and the dispersion media and on the type and concentration of the surfactant used. Furthermore, they considered lecithin and Span 85 to be positively charged and adsorbed to the negative lactose surface causing charge reversal, while the reduced zeta potential observed with salbutamol sulfate was believed to be due to double layer shielding effects. However, the measurements were conducted in non-pressurized

systems, and the authors failed to address the distribution of the surfactants between the drug particles and the solvents.

Sandstrom *et al.* characterized the surface charge of salbutamol base suspensions in propellant blends of CFC 11 and CFC 12 by the measurement of electrophoretic mobility using a modified electrophoresis cell, which allowed pressurized samples to be analysed (Sandstrom *et al.* 1994). The mobilities of particles in salbutamol base suspensions without oleic acid were $0.02x10^{-8}$ $m^2/V.s$ in CFC 11 and increased to $0.12x10^{-8}$ $m^2/V.s$ in propellant blend CFC 11 and CFC 12 (50:50) and $0.14x10^{-8}$ $m^2/V.s$ in a 30:70 propellant blend CFC 11 and CFC 12 (Sandstrom *et al.* 1994). Electrophoretic mobilities of salbutamol suspensions in propellant blends (different CFC 11: CFC 12 ratios) with increasing oleic acid concentrations were also investigated. The electrophoretic mobility of the particles initially increased with increase in oleic acid concentration, however, after reaching a maximum value, further increase in the concentration of oleic acid decreased the mobility and caused a corresponding increase in particle size of the dispersion. The authors hypothesized, and in a later paper illustrated, that oleic acid affected the mobility of salbutamol base suspensions in propellants by monolayer adsorption at low concentration and multilayer adsorption at high concentrations (Eriksson *et al.* 1995). A solvent series based upon the polarizability and on the dipole moment of the solvent molecules was constructed to estimate the acid-base character of the propellants. It was concluded that the type and amount of surfactant and the propellant blend played an important role in the formation of surface charge (Sandstrom *et al.* 1994).

Although attempts have been made to measure surface charge in HFA based suspensions, the role of electrostatics in these relatively polar systems remains poorly understood. The zeta potential of albuterol sulfate suspensions in a model HFA propellant, HPFP was found to be 33 ± 6 mV, while that of formoterol fumarate dihydrate (FFD) in HPFP was 75 ± 6 mV. The surface charge of these drugs in a pressurized propellant HFA 227 was also investigated; since it was difficult to establish stable signals for zeta potential measurements of FFD in HFA 227, the author reported two maxima, 19.9 and 40.6 mV, for the zeta potential of FFD in HFA 227. The zeta potential of FFD-HFA 227 suspensions increased up to 145 mV in the presence of small amounts of added water (Rogueda 2002). However, AFM measurements performed by the author to determine particle interactions within suspensions of albuterol sulfate and formoterol fumarate dihydrate (FFD) in model HFA propellant, HPFP could not confirm the presence of any long range electrostatic repulsive forces (Rogueda 2002).

In summary, it has been demonstrated that drug particles in suspension pMDIs can acquire surface charges that can be measured using electrophoretic mobility studies. In addition, it has also been shown that any surface charge is dependent upon the drug, the type and concentration of the surfactant, and the propellant composition. In order to understand the origin of charge in HFA based pMDI formulations, it is important to investigate any soluble ionic species due to which charges can arise by surface dissociation or adsorption (Rogueda 2005a). The presence of polar impurities, e.g., moisture as well as the inclusion of polar cosolvents could increase the polarity of HFA formulations and may influence charge formation. Taken together, the various formulation factors, which affect

the polarity of HFA based pMDIs, may play a role in charge formation inside these formulations.

**I.D. Characterization of Electrostatic Properties of Pharmaceutical Aerosols**

Electrical charges in pharmaceutical aerosols are generated by frictional contact or triboelectrification owing to the relative movement of particles against the device components (Byron *et al.* 1997). Triboelectrification is a complex surface phenomenon and the electrostatic charges acquired by pharmaceutical aerosols are influenced by both the formulation components as well as the device components (Byron *et al.* 1997, Peart *et al.* 1998). Electrostatic properties of dry powder inhalers (DPIs) and pressurized metered dose inhalers (pMDIs) have been characterized using the aerosol electrometer (a filter housed within a Faraday Cage), which measures the fine particle dose (particle size < 5 μm when operated at 30 L/min) charge. Byron *et al.* characterized the electrostatic charge acquired by aerosols produced by Bricanyl® and Pulmicort® Turbohalers, as well as experimental DPI formulations aerosolized using the Dryhaler DPI, using the aerosol electrometer and found that the inhaler components and the powder deaggregation mechanisms influenced the fine particle dose charge of the aerosols (Byron *et al.* 1997). Peart *et al.* have demonstrated that there is a significant difference between the electrostatic charge of aerosols produced by CFC and HFA suspension pMDIs (Peart *et al.* 1998). Electrostatic properties of pMDI aerosol clouds have been shown to be a function of both formulation and packaging components (Peart *et al.* 1998). The aerosol electrometer, however, does not differentiate bipolar aerosol clouds and chemical analysis of the fine particle dose is not

possible due to the method of dose capture (Peart *et al.* 1998). Hence, the relationship between aerosol charge and the drug mass cannot be elucidated using this technique.

Simultaneous particle charge and size determination has been achieved using dynamic as well as static charge measurement techniques. Dynamic particle charge measurement techniques are based on the principle of electrical mobility of charged particles; charged particles in motion have certain electrical mobility, which depends on the number of elementary charges on the particles as well as the particle size. The bipolar charge measurement system and electrical single particle aerodynamic relaxation time (ESPART) analyzer operate on this principle (Balachandran *et al.* 2003, Ali *et al.* 2007). In the bipolar charge measurement system, a DC electric field is applied perpendicular to the direction of flow of the aerosol particles; the charge on the particles is measured based on their electrical mobility while particle size is determined using phase Doppler anemometry (Balachandran *et al.* 2003).

In the ESPART analyzer, aerosol particles are drawn vertically downwards into the sensing volume of the instrument at a rate of 1 L/min; the aerosol particles cross the path of two converging laser beams as they move vertically down while simultaneously being subjected to an alternating electric field, which causes charged particles to oscillate in the horizontal direction (Ali *et al.* 2007). The phase lag of the particle motion, with respect to the AC field, is used to determine the aerodynamic diameter while the polarity and magnitude of particle charge is obtained from the direction and amplitude of its electrical migration velocity with respect to the electric field (Ali *et al.* 2007). However, the disadvantage of both the above-mentioned techniques is that the particle size determination

is not drug specific. In addition, the flow rate, at which the ESPART operates, favors charge measurement of stable continuous aerosols and is considered to be of limited use in the electrostatic characterization of short lived bursts typical of pMDI aerosol particles (Mitchell *et al.* 2007).

**I.E. Electrical Low Pressure Impactor**

The Electrical Low Pressure Impactor (ELPI) overcomes some of the above-mentioned limitations as it enables the measurement of the net inherent charge of aerosols as a function of particle size. Briefly the ELPI consists of a 13-stage low-pressure impactor with the lower 12 stages connected to a multichannel electrometer and a corona charger situated atop the impactor. The ELPI was originally designed to determine the size distribution of aerosols by subjecting them to a high voltage of approximately +5 kV via the corona charger; particle concentrations of the aerosols are determined from the electrical current induced by the charged particles depositing on the electrically isolated impactor stages (Keskinen *et al.* 1992). Previous studies have modified the ELPI to enable determination of inherent aerosol charge while simultaneously measuring particle size by chemical analysis (Glover and Chan 2004a, Orban and Peart 2004, Telko *et al.* 2007). In the modified set-up of the ELPI, the corona charger is removed, which enables measurement of the net inherent charge of the aerosol particles impacting on each stage for stages 1 - 12 of the ELPI. Furthemore, the particle size distribution can be simultaneously determined by chemical analysis of drug deposited on all impaction stages (Glover and Chan 2004a). Most of the studies to date have used the modified ELPI to investigate the

inherent electrostatic charge of commercially available pharmaceutical aerosols (Glover and Chan 2004a, Orban and Peart 2004, Keil 2005, Telko *et al.* 2007); a limited number of studies have investigated the particle sizing ability of the ELPI in comparison to standard compendial sizing techniques (Orban and Peart 2004, Keil 2005, Telko *et al.* 2007).

### I.E.1. Electrostatic Charge Characterization of Pharmaceutical Aerosols using the Electrical Low Pressure Impactor (ELPI)

The modified ELPI has been employed to characterize electrostatic charge of pressurized metered dose inhalers (Glover and Chan 2004a, Orban and Peart 2004, Kwok *et al.* 2005, Kwok *et al.* 2006), dry powder inhalers (Glover and Chan 2004b, Mikkanen *et al.* 2004, Telko *et al.* 2007, Young *et al.* 2007, Kwok and Chan 2008) and nebulizers (Kwok and Chan 2004) as a function of particle size. The electrostatic charge of pharmaceutical aerosols measured using the modified ELPI has been shown to be comparable to that measured using the aerosol electrometer. For example, the net fine particle dose charge (-184.21 ± 40.02 pC) for Ventolin CFC® determined by the modified ELPI has been found to be in good agreement with that determined using the aerosol electrometer (-171.00 ± 8.63 pC) (Orban and Peart 2004). In addition, the ELPI was able to discern that Ventolin CFC produced bipolar aerosol clouds; particles smaller than 0.96 μm were net electronegative while particles larger than 0.96 μm were net electropositively charged (Orban and Peart 2004).

The modified ELPI has been used to screen the electrostatic properties of Flixotide® and Ventolin HFA®, as a function of particle size (Glover and Chan 2004a).

Kwok et al extended the study and investigated a series of commercially available pMDI suspensions as well as QVAR®, which is a solution pMDI (Kwok *et al.* 2005). It was found that suspension pMDIs, e.g., Ventolin HFA and Flixotide, produced bipolar charged aerosol clouds (mean net charge: -1100 ± 220 pC for Ventolin HFA and +450 ± 30 pC for Flixotide). The testing protocol was shown to influence the electrostatic charge profiles. For example, Ventolin HFA produced a bipolar charge distribution profile when a single shot was actuated into the ELPI, whereas an aerosol produced after a series of continuous actuations of Ventolin HFA pMDI was electronegatively charged (Kwok *et al.* 2005).

In contrast, QVAR, a solution pMDI, was found to produce unipolar positively charged aerosol clouds (mean net charge: +290 ± 230 pC) (Kwok *et al.* 2005). The charge distribution from QVAR appeared to follow the drug mass distribution and the authors hypothesized that for a solution pMDI, a constant mass ratio of drug to excipients would be present in each of the aerosol droplets and therefore charge and drug mass would likely exhibit similar distribution profiles (Kwok *et al.* 2005). However, a systematic study investigating the apparent difference in the charge distribution profiles between suspension and solution pMDIs has not been investigated.

A comparison of the charge distribution profiles of Ventolin HFA and Flixotide revealed that net electronegative charge was measured on stages 1 - 7 for Ventolin HFA while particles depositing on stages 1 - 7 of the ELPI (corresponding to the manufacturer-reported aerodynamic cut-off diameter range: 0.03 - 0.62 μm) were net electropositively charged in the case of Flixotide (Kwok *et al.* 2005). Interestingly, chemical analysis showed that negligible amounts of drug were detected on these stages for both Ventolin

HFA and Flixotide aerosols (Kwok *et al.* 2005). The authors suggested that since negligible amount of drug was present on stages 1 - 7, the electrical charges detected on these stages might be due to propellant droplets or trace impurities, e.g., moisture; however, this hypothesis was not tested further.

A well-controlled investigation of the electrostatic properties of albuterol sulfate suspension HFA pMDIs containing a blend of propellant, cosolvent and surfactant using a modified ELPI showed that aerosol clouds from non-drug containing pMDIs were negligibly charged while albuterol sulfate suspension pMDIs produced net bipolar aerosol clouds (Keil 2005). Interestingly, particles on stages 1 - 5 (particles smaller than approx. 0.27 μm) were electronegatively charged and chemical analysis showed that no drug was present on these stages. The presence of albuterol sulfate particles in the propellant mixture appeared to modify the charging properties of non-drug aerosol droplets (Keil 2005). However, these aerosol droplets existed in multiple forms due to the presence of surfactant and cosolvent thereby confounding the effect of drug particles on aerosol charge. To understand the effect of drug on aerosol charge, it is necessary to investigate the electrostatic properties of a simple suspension comprising of albuterol sulfate and propellant HFA 134a in the absence of a surfactant and / or cosolvent.

The ELPI has also been used to study the use of spacers such as the Aerochamber Plus VHC in conjunction with commercially available pMDIs on the electrostatic charge and particle size distribution of Ventolin HFA pMDI aerosols (Kwok *et al.* 2006). The polarity of the aerosol charge distribution remained unchanged in the presence of a VHC, however, the magnitude of total charge on each of the ELPI stages decreased due to a

decrease in drug deposition in the impactor (Kwok *et al.* 2006). For example, the mean fine particle dose (FPD; particles smaller than 6.67 μm, i.e., the manufacturer reported cut-off diameter of ELPI Stage 12) of Ventolin HFA aerosols decreased from 60.08 ± 1.74 μg without the VHC to 11.61 ± 1.74 μg in the presence of a new untreated VHC. The mean total net FPD charge for Ventolin HFA aerosols decreased from -815.81 ± 135.73 pC when tested without a spacer to -81.50 ± 33.32 pC with an untreated spacer (Kwok *et al.* 2006).

The modified ELPI has only recently been used to characterize the electrostatic properties of dry powder inhalers (Telko *et al.* 2007, Young *et al.* 2007, Kwok and Chan 2008). The ELPI has been designed to operate at a flow rate of either 10 or 30 L/min and hence cannot be readily adapted to testing dry powder inhalers since higher flow rates are required to sample DPI aerosols (Kwok and Chan 2008). The effect of storage relative humidity ranging from 0 - 85% RH on aerosol performance as well as electrostatic charge of carrier-based dry powder inhalers (DPIs), e.g., albuterol and lactose powder blend filled capsules delivered from a Cyclohaler device, has been investigated using an ELPI (Young *et al.* 2007). However, their testing protocol was not in accordance with current compendial specifications for in-vitro testing of DPIs since the DPIs were aerosolized and sampled at 30 L/min from the ELPI. It has been recommended that DPIs be tested at a flow rate equivalent to a 4 kPa pressure drop across the device (USP 29 / NF 24 First Supplement 2006). For a Cyclohaler (ISF inhaler), this flow rate has been determined to be in the range of 100 - 120 L/min (Clark and Hollingworth 1993).

Further studies have attempted to modify the experimental set-up and aerosolize DPI aerosols at 60 L/min and sample the aerosols into the ELPI at 30 L/min (Telko *et al.*

2007, Kwok and Chan 2008). Telko *et al.* investigated the effect of various formulation and packaging factors on the electrostatic charge of experimental albuterol sulfate / lactose DPI aerosols (Telko *et al.* 2007). Briefly, the DPI was aerosolized at 60 L/min and sampled into a preseparator to remove the larger lactose particles, the aerosol flow was then split and simultaneously sampled into a modified ELPI and an Andersen Cascade Impactor (ACI) at 30 L/min. Both the magnitude and polarity of the electrostatic charge on the DPI aerosols were found to be influenced by the grade of lactose used (presence of lactose fines), capsule material as well as the type of inhaler used (Telko *et al.* 2007).

Kwok and Chan characterized the electrostatic charging properties of commercially available drug only dry powder inhalers, Pulmicort® and Bricanyl® Turbohalers (Kwok and Chan 2008). This enabled the authors to investigate the effect of drug, e.g., budesonide, terbutaline sulfate, on the tribocharging properties of the DPI aerosols. The DPIs were sampled into a USP induction port at 60 L/min and the experimental set-up utilized a Y-piece to divide the aerosol flow from the USP induction port such that the ELPI sampled the aerosol at 30 L/min while the remainder of the aerosol was drawn into a unit dose sampler at 30 L/min (Kwok and Chan 2008). Both the inhalers produced bipolar charged aerosols; particles depositing on stages 1 - 8 and stages 1 - 7 were electronegatively charged while particles depositing on stages 9 - 12 and stages 8 - 12 were electropositively charged for Pulmicort® and Bricanyl® aerosols, respectively. (Kwok and Chan 2008). Although the mass deposition within the ELPI was not affected, the authors found that relative humidity influenced the electrostatic charging characteristics of the two commercial DPIs. The authors found that the electrostatic properties of Pulmicort DPI

aerosols determined using the ELPI were found to correlate with that measured using the aerosol electrometer (Byron *et al.* 1997). Bricanyl Turbohalers were found to produce FPD charge in the same magnitude as that measured by Byron *et al.* using the aerosol electrometer; the specific charge and the number of elementary charges / particle reported by both the studies were also in the same order of magnitude (Byron *et al.* 1997, Kwok and Chan 2008).

### I.E.2. Particle Size Characterization of Pharmaceutical Aerosols using the Electrical Low Pressure Impactor (ELPI)

Few studies have evaluated the sizing ability of the ELPI for pharmaceutical aerosols (Crampton *et al.* 2004, Keil 2005, Telko *et al.* 2007). Crampton *et al.* have employed the ELPI in its standard mode of operation to measure the particle size based on the number distribution of commercially available pMDI aerosols using electrical detection. The authors reported that HFA propelled pMDIs, e.g., QVAR, Ventolin HFA, Flixotide produced a higher sub-micron aerosol fraction compared to their CFC counterparts, e.g., Becotide® and Atrovent Forte® based on their measurements using electrical detection of charged aerosol particles in the ELPI and the Scanning Mobility Particle Sizer (SMPS). The authors suggested that although sub-micron (particles smaller than 1 μm) and ultrafine (particles smaller than 0.1 μm) particles do not have appreciable mass, it might be relevant to measure the particle number or surface area to understand their physiological impact (Crampton *et al.* 2004).

Telko *et al.* have employed the ELPI in its standard mode of operation (with the corona charger switched on) to determine the particle size distribution (PSD) of experimental albuterol sulfate - lactose blend DPIs via electrical detection (Telko *et al.* 2007). The PSD of the experimental DPIs determined by electrical detection was found to compare well with that obtained subsequently by gravimetric analysis; discrepancy in particle size was observed on the lower stages where the use of the gravimetric sizing technique was found to be limited by the sensitivity of the analytical balance used (Telko *et al.* 2007). Both electrical and gravimetric detection measured particle size distribution of aerosols that were subjected to a high corona voltage of approximately +5 kV before being sampled into the ELPI. The particle size distribution obtained by both these techniques was not specific to drug mass and the results obtained therefore may be of limited use for the characterization of pharmaceutical aerosols.

Telko *et al.* also found that when aerosols produced by experimental DPIs containing micronized albuterol sulfate alone and those containing 1% albuterol sulfate in lactose were simultaneously sampled into a modified ELPI (without switching on the charger) and an ACI, the particle size distributions (PSDs) obtained were comparable (Telko *et al.* 2007). However the experimental set up used in the study was not comparable to that used with the standard compendial apparatus. Moreover, the authors have not compared the PSDs of these experimental albuterol sulfate - lactose blend DPIs determined using the non-standard experimental set-up to those determined using the ACI under standard compendial conditions to establish confidence in the PSD data thus obtained.

Keil has compared the PSD of Ventolin CFC® pMDI aerosols determined using the ELPI in its standard mode of operation (in the presence of the corona charger) via electrical detection to that obtained using the modified ELPI (charger-free) by chemical detection of drug deposited on the ELPI stages (Keil 2005). The mass median aerodynamic diameter (MMAD) of Ventolin CFC (3.36 ± 2.03 μm) obtained using the electrical detection technique was not comparable to that determined using chemical detection of albuterol (1.40 ± 0.06 μm); the overestimated particle size determined by the ELPI via electrical detection was attributed to the presence of larger excipient-containing particles such as oleic acid coated albuterol particles in the aerosol cloud (Keil 2005).

The modified ELPI appeared to undersize Ventolin CFC aerosols when particle size was determined by chemical analysis in comparison to that measured using the ACI, a compendial sizing apparatus (MMAD of Ventolin CFC: 2.10 ± 0.08 μm) (Keil 2005). It was speculated that the undersizing of Ventolin CFC aerosols by the modified ELPI might be due to the higher sub-micron fraction (particles smaller than 1.0 μm) detected by the ELPI (ELPI: 2.05 ± 0.41 μg, ACI: 0.02 ± 0.03 μg) (Keil 2005).

Although the ELPI was originally designed to measure near real time particle size of aerosols by electrical detection, the modified ELPI has offered the advantage of simultaneously determining inherent electrostatic charge and the particle size distribution of pharmaceutical aerosols. However, there does not appear to be a consensus on the efficiency of the modified ELPI in terms of its particle sizing ability for pharmaceutical aerosols in comparison to compendial sizing techniques. In order to have confidence in the

sizing ability of the modified ELPI, it is essential to compare the size distribution from the ELPI with that obtained using accepted industry standards.

**I.F. Overview**

This dissertation is organized to address the charging mechanisms and the particle interactions within HFA based solution and suspension formulations as well as the electrostatic properties of aerosols produced by these HFA based pMDI formulations. Chapter II states the individual hypotheses and the specific aims that will be addressed in the succeeding chapters. Chapter III describes the general experimental materials and methods together with an explanation of the operational principles of some of the instruments used in this research. Each of the chapters consists of a brief introduction, a materials and methods section, followed by a results and discussion section. Chapter IV describes the determination of the resistivity and the zeta potential of HFA based solution and suspension formulations. Chapter V discusses the construction of molecular models for albuterol sulfate HFA suspension pMDIs and subsequent analysis of interactions between the formulation components on a molecular level. Chapter VI investigates the influence of formulation as well as packaging components on the electrostatic charge and mass distribution of HFA propelled BDP solution and albuterol sulfate suspension pMDI aerosols using the modified ELPI. Chapter VII describes the recalibration of the modified ELPI using commercially available polydisperse pMDIs as calibration aerosols with the

ACI as the reference cascade impactor. Finally, Chapter VIII summarizes the results from each chapter as it relates to the original hypotheses.

# II. HYPOTHESES AND RESEARCH PLAN

## II.A. Hypothesis 1

The electrical properties of hydrofluoroalkane (HFA) based solution and suspension formulations are hypothesized to be a function of their electrical resistivity, which, in turn, will be influenced by the formulation components. It is also hypothesized that particles suspended in non-aqueous pressurized solvents including HFA propellants will acquire a surface charge, which will be a function of the formulation components.

The electrical resistivity of experimental HFA 134a based solutions and suspensions will be determined using a custom-built high-pressure resistivity cell in order to characterize any soluble ionic species present in these systems. In addition, zeta potential of albuterol suspensions in non-aqueous, non-pressurized and pressurized solvents including chloroform, CFC propellants and HFA 134a will be determined using an electrophoretic mobility technique. The influence of surfactant, cosolvent (ethanol) and moisture content of the formulations on the electrical resistivity and the zeta potential will be investigated.

**II.B. Hypothesis 2**

Molecular modeling can be used to characterize particle interactions at the molecular level within pressurized metered dose inhaler formulations.

In order to test this hypothesis, molecular models of simple pMDI formulations including albuterol sulfate in HFA 134a will be constructed and optimized and interactions between the drug and propellant molecules will be investigated using Hydropathic INTerations (HINT®) software. Interactions within albuterol sulfate suspensions in the presence of oleic acid (an anionic surfactant) and ethanol (a polar cosolvent) will also be studied.

**II.C. Hypothesis 3**

It is hypothesized that the electrical properties of experimental HFA-propelled solution and suspension pMDIs will be a function of the formulation type (solution or suspension) and the formulation components, as well as the particle size. The magnitude and polarity of aerosol clouds produced by experimental HFA-propelled pMDIs will be influenced by propellant, cosolvent, surfactant, and active drug. Differently sized particles within the aerosol cloud will be electrically charged to a different magnitude and polarity.

The influence of formulation components on the electrostatic charging characteristics of solution and suspension HFA pMDIs will be investigated using model HFA propelled beclomethasone dipropionate (BDP) solution pMDIs and albuterol sulfate suspension pMDIs. The mass distributions of the aerosols produced by drug containing

pMDIs will be simultaneously characterized by chemical analysis using the modified ELPI.

**II.D. Hypothesis 4**

It is hypothesized that the calibration of the ELPI, determined following electrical detection of corona-charged particles, cannot be extended to the modified ELPI (charger-free), where the particle size distribution is determined following chemical analysis of the drug deposited on each ELPI stage, since the electrical charge acquired by aerosol particles via the ELPI corona-charger will influence particle deposition within the ELPI.

The aerodynamic particle size distributions (aPSDs) of four independent, polydisperse, commercially available pMDIs with different median diameters characterized using an Andersen Cascade Impactor (ACI) and a modified ELPI will be compared. The modified ELPI will then be recalibrated based on the aPSDs of the four 'calibration' pMDIs obtained using the reference ACI and the new ELPI cut-off diameters will be validated using a previously untested commercially available pMDI.

# III. EXPERIMENTAL MATERIALS AND METHODS

## III.A. Preparation of Pressurized Solution and Suspension Formulations

### III.A.1. Materials

Beclomethasone dipropionate (BDP) and albuterol sulfate were provided by Dura Pharmaceuticals (San Diego, CA); albuterol base was donated by Armstrong Laboratories (West Roxbury, MA). Oleic acid was obtained from Fisher Scientific Company (Swannee, GA). Absolute ethanol was obtained from AAPER (Alcohol and Chemical Company, Shelbyville, KY). CFC 11 (monofluorotrichloromethane), CFC 12 (dichlorodifluoro-methane) and HFA 134a (1,1,1,2-tetrafluoroethane) were donated by Dupont (Wilmington, DE).

19-mL aluminum cut-edge canisters and 120 mL plastic coated glass bottles were obtained from Presspart (Blackburn, UK) and Wheaton Glass Company (Mays Landing, NJ), respectively. DF10/50 RCU/PBT 50 μL inverted metering valves and DF10/50 RCU/PBT modified continuous (non-metered) valves composed of a polybutylene terepthalate (PBT) metering chamber and valve stem and fitted with EPDM (ethylene-propylene-diene-terpolymer) elastomers were donated by Valois (Le Vaudreuil, France).

### III.A.2. Methods

#### III.A.2.1. Experimental HFA Based Solution Formulations

Experimental HFA 134a based solutions including propellant alone, an ethanol and propellant blend and BDP solutions were prepared by weight and packaged in clean, dry 19 mL aluminum cut-edge canisters. A Valois DF10/50 RCU/PBT 50μL metered valve or a continuous valve was crimped onto the canister (Model 2005/10, Pamasol Willi Mader AG, Pfaffikon, Switzerland).

Crimping parameters were in accordance with the valve suppliers' specifications for packaging in aluminum canisters (Valois DF10/50 crimp height = 5.7 ± 0.05 mm and crimp collet closing diameter = 17.70 mm). Propellant HFA 134a was added to the canister through the metering valve via a pressure burette (Aerosol Laboratory Equipment Model 35B, Walton, NY) overpressured with dry nitrogen. For preparation of an ethanol/propellant blend, an appropriate quantity of ethanol was weighed into an aluminum canister, a Valois DF10/50 valve (metered or continuous) was crimped on to the can and HFA 134a was pressure-filled through the valve to the target fill weight. BDP solution pMDIs were prepared by weighing an appropriate amount of a BDP solution in ethanol into an aluminum canister, followed by crimping the valve and pressure-filling HFA 134a to the target fill weight.

### III.A.2.2. Experimental HFA and CFC Based Suspension Formulations

Albuterol sulfate suspensions in 100% HFA 134a were prepared by weight and packaged in clean, dry 19 mL aluminum cut-edge canisters fitted with metered or continuous valves as described in Section III.A.2.1. Albuterol sulfate was micronized using a jet mill (Model 00 Jet-O-Mizer, Fluid Energy Processing Equipment Co., Hatfield, PA) and the volume median diameter of albuterol sulfate was determined to be 0.79 ± 0.01 μm (Mastersizer 2000, Malvern Instruments, Inc., Southborough, MA). Albuterol sulfate suspension pMDIs were prepared by weighing a fixed amount of albuterol sulfate into an aluminum canister, a metered or continuous Valois DF10/50 valve was crimped onto the canister, and propellant HFA 134a was pressure-filled through the valve. To prepare a suspension of albuterol sulfate in HFA 134a containing oleic acid and ethanol, appropriate amounts of albuterol sulfate and a stock solution of oleic acid in ethanol were weighed into the canister followed by pressure-filling HFA 134a to the target fill weight. After the addition of propellant, the inhalers were shaken on a wrist-action shaker (Burrell Corporation Model 75, Pittsburgh, PA) for 30 minutes.

Albuterol base suspensions in a CFC propellant blend (70% CFC 12: 30% CFC 11) were prepared and packaged in 120 mL plastic-coated glass bottles fitted with continuous valves. The volume median diameter of albuterol particles was determined to be 0.71 ± 0.19 μm (Mastersizer 2000, Malvern Instruments, Inc., Southborough, MA). Crimping parameters were in accordance with the valve suppliers' specifications for packaging in plastic-coated glass bottles (Valois DF 10 crimp height = 5.3 ± 0.05 mm and crimp collet closing diameter = 17.8 mm).

All the formulations were stored for 24 hours following preparation before measurements were performed.

## III.B. Determination of Electrostatic Charge and Mass Distribution of pMDIs using the Modified ELPI

The inherent electrostatic charge and subsequent mass distribution of aerosols produced by commercially available and experimental HFA 134a pMDIs were determined using a modified ELPI (Dekati Limited, Tampere, Finland). Table III.1 shows the manufacturer supplied aerodynamic cut-off diameters for the ELPI.

Table III.1. Manufacturer-Supplied Aerodynamic Cut-off Diameters of the ELPI Stages 1 - 13 at a Flow Rate of 29 L/min (Corrected to Two Decimal Places). Appendix A.I shows the ELPI Charger Efficiency Curve and the ELPI Datasheet with the Cut-Off Diameters for the ELPI used in these Experiments.

| Stage Number | Cut-off Diameter (µm) |
|---|---|
| 13 | 10.08 |
| 12 | 6.67 |
| 11 | 4.05 |
| 10 | 2.42 |
| 9 | 1.62 |
| 8 | 0.96 |
| 7 | 0.62 |
| 6 | 0.39 |
| 5 | 0.27 |
| 4 | 0.16 |
| 3 | 0.10 |
| 2 | 0.06 |
| 1 | 0.03 |

The commercially available ELPI consists of a 13-stage low-pressure impactor with the lower 12 stages connected to a multichannel electrometer and a corona charger situated atop the impactor. Figure III.1 illustrates the modified ELPI utilized in these studies.

Figure III.1. Photograph of the Charger-Free ELPI Cascade Impactor and the Standard ELPI Inlet (the Modified ELPI), with the USP Induction Port Attached. Schematic of the Modified ELPI (Adapted from Dekati Manual, Dekati, Finland) is also Shown.

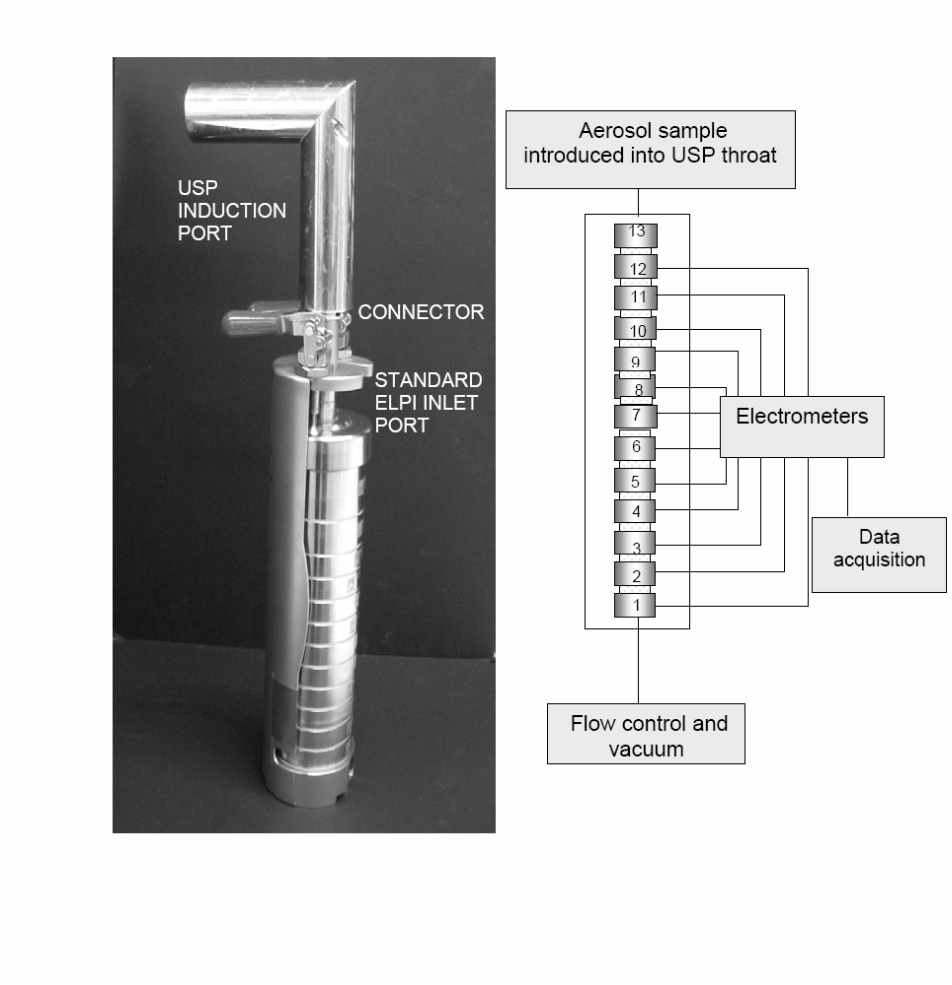

The original ELPI configuration was modified by removing the corona charger as well as the charger frame from the instrument in order to shorten the aerosol flow path into the ELPI and to make the aerosol entry conditions comparable to those in the ACI, a compendial sizing apparatus. The USP induction port was fixed atop the ELPI inlet port using a purpose-built, airtight stainless steel connector (Figure III.2).

Figure III.2. Cross Sectional View of the ELPI Inlet (as Supplied by Dekati with the Instrument), the Connector (Shown Cross-Hatched) and the Down Tube of the USP Induction Port in their Experimental Configuration. The Connector is shown in Greater Detail in the Figure Inset. All Dimensions are in Millimeters and the Diagram is Drawn to Scale. For Complete Dimensions for the USP Inlet see USP 29 / NF 24 First Supplement 2006.

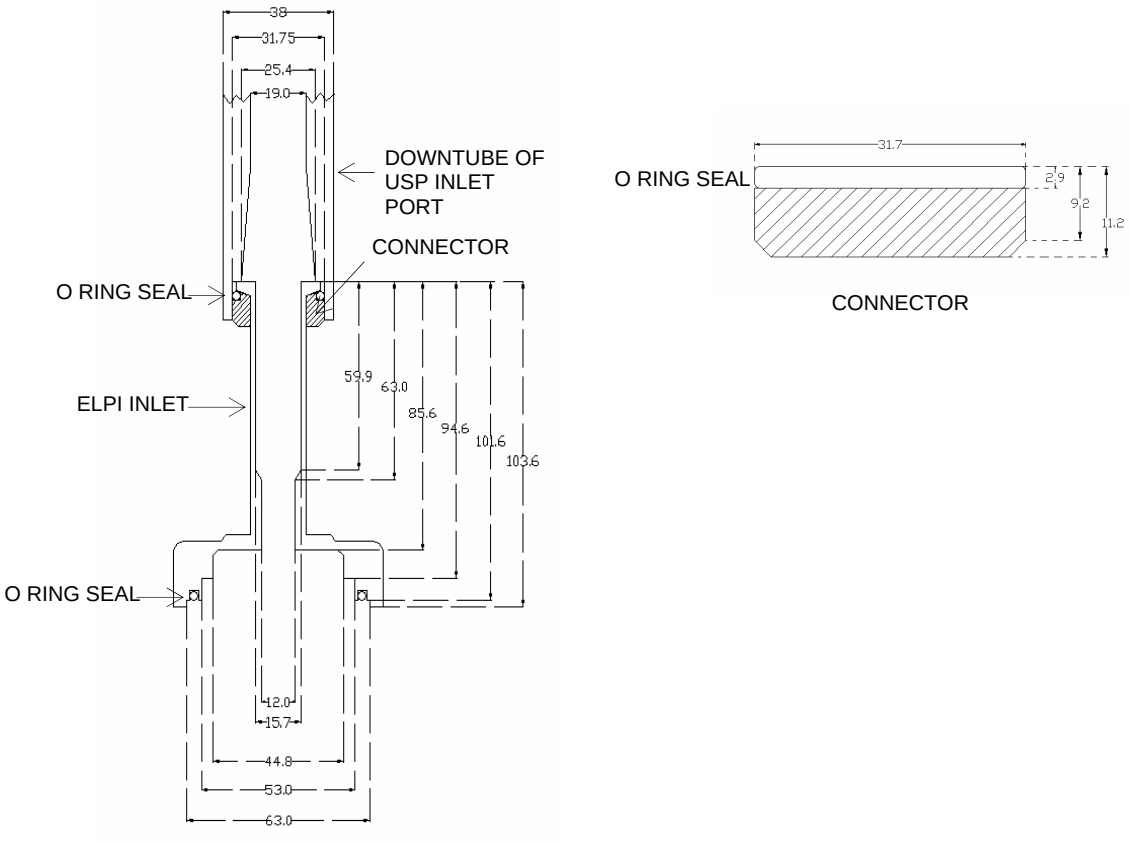

The ELPI was allowed to stabilize for an hour prior to operation while set-up requirements such as air leakage testing were performed in accord with the manufacturer's instructions and specifications. The current range setting was 40,000 fA. Silicone-coated (DS-515 grease spray; Dekati Ltd., Tampere, Finland) aluminum substrates were used on the impaction plates to collect drug particles for chemical analysis.

Inherent electrostatic properties of pMDIs were determined by actuating a single shot of the pMDI through a USP induction port into the modified ELPI (Figure III.1). The ELPI was operated at 100 mbar (below the lowest stage, i.e., Stage 1) to produce a flow rate of approximately 29 L/min, verified using an external flowmeter (Sierra Instruments, Inc., Monterey, CA). The electrical current induced by the charged aerosol particles, on each of the ELPI stages 1 - 12, was measured as a function of time (20 sec). Background current measurements were performed to ensure zeroing of the electrometer current readings before and after each experiment. An aerosol current (pA) vs. time (sec) profile was generated for each impactor stage. The area under each aerosol current vs. time profile represented the net inherent aerosol charge in picocoulombs (pC) for that stage (1 coulomb is equivalent to 1 ampere second). The net inherent charge of the aerosol cloud was calculated as the sum of the net charge on each of the impactor stages. Subsequently, the mass distribution of drug within the impactor was determined using chemical analysis.

**III.C. High Pressure Liquid Chromatography Analyses**

Validated high-pressure liquid chromatography (HPLC) methods were employed for detection of BDP, fluticasone propionate (FP) and albuterol in the samples obtained

from cascade impaction experiments. Mass of albuterol sulfate deposited on the lower stages (stages 1 - 4) of the ELPI was also determined using Liquid Chromatography-Mass Spectrometry (LC-MS).

### III.C.1. Materials

BDP and albuterol base were donated by Dura Pharmaceuticals (San Diego, CA) and Armstrong Laboratories (West Roxbury, MA), respectively. FP was purchased from Sigma Aldrich (St. Louis, MO). HPLC grade acetonitrile, methanol, ammonium acetate and ammonium formate were obtained from Fisher Scientific (Swannee, GA). Deionized water was freshly distilled in the laboratory.

### III.C.2. Methods

#### III.C.2.1. Analysis of BDP and FP using HPLC with UV Detection

For the HPLC assay of BDP and FP, a C-18 Spherisorb ODS-2 column (5 μm, 4.6 x 250 mm, Alltech Associates Inc., Deerfield, IL) was used. Both assays employed 60% acetonitrile / 40% water (flow rate: 1 mL/min) as mobile phase with UV detection at 238 and 236 nm for BDP and FP, respectively (2996 Photodiode Array Detector, 1515 Isocratic HPLC Pump, 717 plus Autosampler, Waters, Milford, MA). The sample injection volume used was 100 μL. Calibration curves of peak area vs. concentration were linear in the range of 0.05 - 2 μg/mL ($r^2 = 0.999$) for BDP and 0.05 - 2 μg/mL ($r^2 = 1$) for FP. The limit of detection (LOD), determined to be the smallest detectable peak on the HPLC chromatogram, was 0.04 μg/mL for both compounds. Typical values for precision (RSD)

and accuracy (%DFN) were less than 0.6% and 3.9% for BDP and less than 2.1% and 1.1% for FP, respectively.

### III.C.2.2. Analysis of Albuterol using HPLC with Fluorescence Detection

HPLC analysis of albuterol employed a C-18 Spherisorb ODS-2 column (5 μm; 4.6 x 150 mm, Alltech Associates, Deerfield, IL). The mobile phase (225 mL of 0.1% ammonium acetate solution and 800 mL methanol) was pumped at a flow rate of 0.8 mL/min. The sample injection volume used was 40 μL. Fluorescence detection was used with excitation and emission wavelengths of 276 and 609 nm, respectively (2475 Multi λ Fluorescence Detector, 1515 Isocratic HPLC Pump, 717 plus Autosampler, Waters, Milford, MA). Calibration curves of peak area versus concentration of drug were linear in the range of 0.05 - 1 μg/mL ($r^2 > 0.999$). The limit of detection (LOD), determined to be the smallest detectable peak on the HPLC chromatogram, was 0.04 μg/mL; typical values for precision (RSD) and accuracy (%DFN) were less than 0.6% and 0.8%, respectively.

### III.C.2.3. Analysis of Albuterol using LC-MS

A Waters Alliance 2695 separations module and a Micromass ZMD4000 single quadrupole mass spectrometer with ESI ionization probe (Waters Corp., Milford, MA) was used for analysis of albuterol. The mobile phase, 80% methanol / 20% water solution with 2 mM ammonium formate (used to adjust pH to 3.4) was pumped into an Allure PFP propyl column (5 μm, 3.2 x 150 mm, Restek Corporation, Bellefonte, PA) at a flow rate of 1 mL/min. A flow splitter (Upchurch Scientific Inc., Oak Harbor, WA) was used after the

HPLC column to introduce approximately 0.10 mL/min of the eluent into the mass spectrometer. Ionization conditions for MS were optimized with the source block and desolvation temperatures of 150 and 140 °C, respectively; the desolvation nitrogen flow was 700 L/hr. Samples were analyzed and the protonated molecular ion of albuterol was monitored at m/z = 240. The calibration curve of peak area of the single ion chromatogram vs. albuterol concentration was linear, $r^2 = 0.997$ over the concentration range of 1 - 50 ng/mL. The limit of detection (LOD), determined to be the smallest detectable peak on the chromatogram, was 0.5 ng/mL; typical values for precision (RSD) and accuracy (%DFN) were less than 5.2% and 4.5%, respectively.

# IV. INVESTIGATION OF CHARGE MECHANISMS OF NON-AQUEOUS LIQUEFIED PROPELLANT CONTAINING SOLUTIONS AND SUSPENSIONS

## IV.A. Introduction

In order to fully explain the effect of pMDI formulation components on the triboelectric charging properties of the aerosol clouds, it is important to determine the electrical charges within the pMDI formulation itself. However, electrical properties inside pMDIs have not been well characterized due to a lack of consensus on charge generation mechanisms and the experimental difficulties associated with the measurement of electrical properties in non-aqueous liquefied propellants (Sidhu *et al.* 1993, Rogueda 2002, Rogueda 2005a). Electrical measurements in CFC and HFA containing formulations are challenging due to the need to maintain the liquids under pressure.

The resistivity of a liquid is a measure of its electrical insulating properties; high resistivity would indicate low content of free ions and ion-forming particles and possibly a low concentration of conducting impurities (ASTM Standard D1169-02 2002). Electrical properties of CFC and HFA refrigerants have been measured in terms of their electrical resistivity (Meurer *et al.* 2001). For example, the resistivity of CFC 12 was determined to be $0.51 \times 10^6$ MΩ.cm while that of HFA 134a was 108.9 MΩ.cm (Meurer *et al.* 2001). Zeta potential measurements using an electrophoretic mobility technique can provide a measure

of the surface charge within suspensions; electrophoretic mobility measurements have demonstrated formation of charged species in non-polar, non-aqueous dispersions (Kitahara and Watanabe 1984). A limited number of studies have also reported zeta potential measurements for drug suspensions in a model non-pressurized HFA solvent e.g. HPFP; however, the role of electrostatics in HFA based suspension pMDIs remains poorly understood (Rogueda 2002).

In the present study, the electrical resistivity of experimental HFA 134a based BDP solutions and albuterol sulfate suspensions was determined in order to obtain an indication of the soluble ionic species present in these systems. In addition, zeta potential of albuterol suspensions in non-aqueous, non-pressurized and pressurized solvents including chloroform, CFC propellants and HFA 134a was determined using an electrophoretic mobility technique. The influence of surfactant, cosolvent, e.g., ethanol and moisture content of the formulations on electrical resistivity and zeta potential was investigated.

## IV.B. Electrical Resistivity of HFA Based Solution and Suspensions

### IV.B.1. Methods

#### IV.B.1.1. Preparation of HFA Based Solution and Suspensions

Resistivity measurements were performed using experimental HFA solutions and albuterol sulfate HFA suspensions. Table IV.1 summarizes the experimental HFA based solutions prepared and packaged using continuous valves as described in Chapter III.A.2.1.

Table IV.2 summarizes the experimental albuterol sulfate suspensions in HFA 134a containing increasing concentrations of oleic acid and ethanol, which were formulated and packaged using continuous valves as described in Chapter III.A.2.2.

Table IV.1. Experimental HFA 134a Based Solutions

| Beclomethasone Dipropionate (%w/w) | Ethanol (%w/w) | HFA 134a (%w/w) |
|---|---|---|
| 0 | 0 | 100 |
| 0 | 7 | 93 |
| 0.08 | 7 | 93 |

Table IV.2. Experimental HFA 134a Based Albuterol Sulfate Suspensions

| Albuterol Sulfate (%w/w) | Oleic Acid (%w/w) | Ethanol (%w/w) | HFA 134a (%w/w) |
|---|---|---|---|
| 0.2 | - | - | 100 |
| 0.2 | 0.02 | 5 | 95 |
| 0.2 | 0.03 | 5 | 95 |
| 0.2 | 0.04 | 5 | 95 |
| 0.2 | 0.02 | 10 | 90 |
| 0.2 | 0.02 | 15 | 85 |

### IV.B.1.2. Determination of Electrical Resistivity of Experimental HFA Based Solution and Suspensions

#### IV.B.1.2.a. Design and Validation of the Resistivity Cell

The electrical resistivity of HFA based solution and suspension formulations was determined by measuring the resistance of the formulation to an applied voltage. A unit volume resistivity cell was constructed from PTFE with two parallel stainless steel circular electrodes of cross-sectional area of 1 $cm^2$ and placed at a gap of 1 cm from each other (Figure IV.1).

Figure IV.1. Schematic Diagram of the Non-Pressurized Unit Volume Resistivity Cell

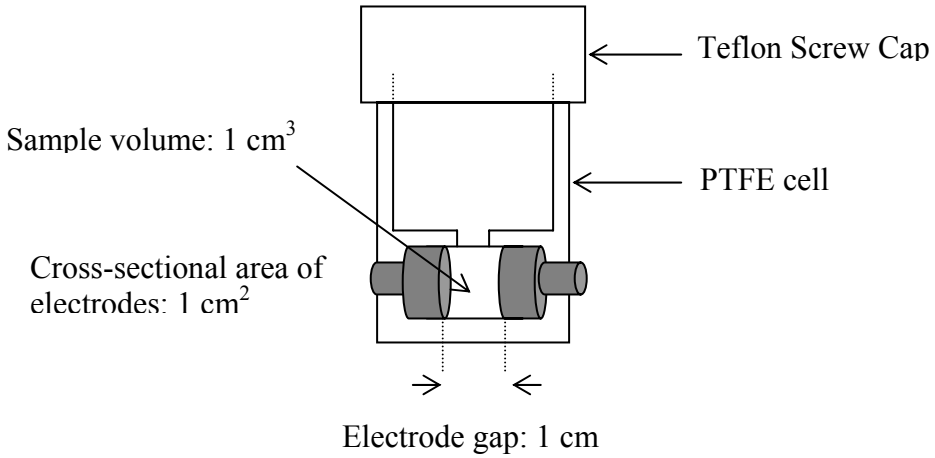


This unit volume cell was used to measure the resistivity of a model non-pressurized organic liquid, methyl ethyl ketone (MEK; Fisher Scientific, Swannee, GA). MEK was dried over 0.3 nm molecular sieve (Metrohm AG, Switzerland) for 24 hours before measuring the resistivity. Resistivity was calculated using the Equation IV.1:

$$\rho = R/K \qquad \text{Equation IV.1}$$

where ρ is the resistivity in Ω.cm, R is the measured resistance (Ω) = V/I where V is the applied voltage (volts), I is the measured current (amperes) and K is the cell constant ($cm^{-1}$). The cell constant is a function of the area of the electrodes (A), the electrode gap (d) and the electric field pattern between the electrodes in the cell. Theoretically, the cell constant may be calculated as the ratio of the electrode gap to the area of the electrodes (d/A). Since the cell constant was 1 $cm^{-1}$ for the unit volume resistivity cell, the value of the measured resistance would be identical to the resistivity.

In order to measure the electrical resistivity of HFA based solutions and suspensions, the resistivity cell was modified to hold pressurized samples. A custom-made PTFE high-pressure resistivity cell with 2 stainless steel electrodes, fitted with a continuous valve to enable direct transfer of pressurized formulations, was constructed for the resistance measurements (Figure IV.2).

Figure IV.2. Schematic Diagram of the High-Pressure Resistivity Cell

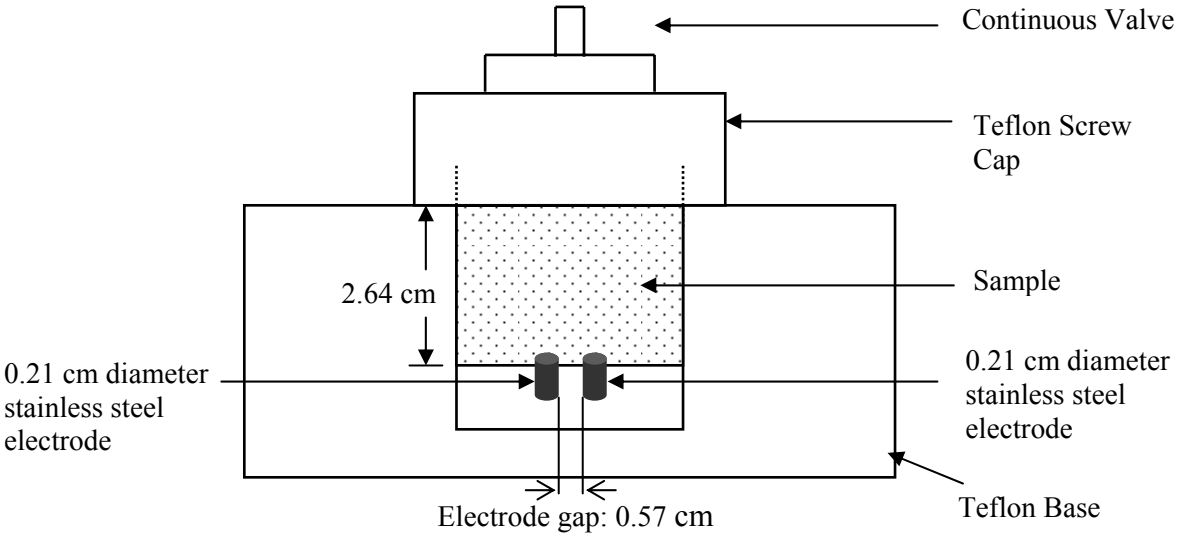


The cross-sectional area of the electrodes was 0.069 $cm^2$ and the electrode gap was 0.57 cm. Due to the design of the resistivity cell, it was difficult to determine the cell constant; the high-pressure cell was therefore calibrated using the non-pressurized unit volume cell (Figure IV.1). The cell constant (K) of the high-pressure resistivity cell was calculated using Equation IV.1 from the resistivity (ρ) of MEK measured with the non-pressurized unit volume resistivity cell and the resistance (R) measured with the high-pressure resistivity cell.

A 1920 Precision LCR meter (QuadTech Inc, Maynard, MA) was used to apply an AC voltage in order to prevent electrode polarization that may occur in the presence of polar cosolvents e.g. ethanol. The LCR meter uses a reference resistor whose resistance is accurately known; the voltages measured across the sample and across the reference resistor simultaneously, at a given AC frequency, are compared to obtain the final value of unknown (sample) resistance. The range of resistance measured by this instrument is 10 mΩ - 100 MΩ. The resistivity of MEK was measured using the one cubic centimeter resistivity cell and the high pressure cell using the Precision LCR meter by applying an electric voltage in the range of 20 - 100 mV with frequency ranging from 20 - 100 Hz; 20 readings were averaged per sample and 3 replicate samples were tested.

#### IV.B.1.2.b. Measurement of Electrical Resistivity of HFA Based Solutions and Suspensions

For determining the electrical resistivity of HFA based solutions and suspensions, the formulations were filled into the high-pressure resistivity cell (Figure IV.2) through a continuous valve via a PTFE coupler. The cell was weighed before and after sample transfer to fill approximately 2 g of the formulation into the cell each time. In order to ensure that the high-pressure cell was being filled with liquid formulation, both the resistivity cell and the canister containing the HFA based formulation were cooled in dry ice for about 5 minutes and the formulation then transferred into the cell through a continuous valve. The cell was allowed to stand for approximately 15 - 20 minutes and equilibrate to room temperature (21 °C) measured using thermocouples attached to the

electrodes. The cell was reweighed to check for leakage of the pressurized formulations. The cell was carefully cleaned five times between samples with acetone, and air dried.

Preliminary experiments with MEK showed that the resistance values remained unchanged at an applied voltage ranging from 20 mV to 1 V with a frequency range of 20 Hz to 1 kHz. Hence, lower voltages were used for further experiments to prevent any undesirable heating of the pressurized samples. The applied voltage was varied in the range 20 - 100 mV while the frequency was varied from 20 - 100 Hz. Twenty measurements were averaged per can, and 3 cans of each formulation were tested. All the measurements were performed at 21 - 22.5 °C and 18 - 40 % RH. Water content of the formulations was determined using Karl Fischer titration (Kulphaisal 2003).

### IV.B.2. Results and Discussion

#### IV.B.2.1. Determination of the Cell Constant of the High Pressure Resistivity Cell

In the present study, MEK, a non-aqueous, non-pressurized solvent was used for calibrating the high-pressure resistivity cell using the unit volume reference cell. The measured water content of MEK determined by Karl Fischer titration was 162 ± 11 ppm. The equation for resistance, $R = V/I$ does not take into account the frequency at which the voltage is applied and for all practical purposes, the resistance would not be expected to change with the frequency of the applied AC voltage. Table IV.3 shows that the mean resistivity values for MEK remained statistically similar ($p > 0.05$, one way ANOVA) over the range of the applied voltage (20 - 100 mV) and the frequency (20 - 100 Hz) tested

suggesting that there was a finite increase in the flow of current through the sample with an increase in the applied voltage.

Table IV.3. Electrical Resistivity (MΩ.cm) of Methyl Ethyl Ketone as a Function of Applied Voltage and Frequency (n = 3 Samples, 20 Readings Averaged per Sample)

| Applied Voltage (mV) | Applied Frequency | | |
|---|---|---|---|
| | 20 Hz | 50 Hz | 100 Hz |
| 20 | 0.48 ± 0.08 | 0.48 ± 0.08 | 0.48 ± 0.08 |
| 50 | 0.48 ± 0.08 | 0.48 ± 0.08 | 0.48 ± 0.08 |
| 100 | 0.48 ± 0.08 | 0.48 ± 0.08 | 0.49 ± 0.08 |

In order to compare the electrical properties of MEK measured in the present study using the unit volume resistivity cell with that reported in literature, the electrical conductivity (reciprocal of electrical resistivity) was calculated. The mean resistivity of MEK was 0.48 ± 0.08 MΩ.cm and the corresponding calculated electrical conductivity of MEK was 2.12 ± 0.34 μS/cm. This value was a magnitude higher than the reported electrical conductivity of MEK (0.2 μS/cm) measured using a DC test method (ASTM Standard D4308-95 2005) at 20 ºC, although the test voltage has not been reported (Shell Chemicals 2005). In the present study, AC resistivity measurements were employed since the presence of ethanol in HFA based formulations was considered likely to cause polarization of the electrodes. Electrical resistivity measurements are known to be influenced by water content, other impurities in the test sample and the applied voltage. MEK used in the present study was dried to minimize the moisture content but further purification of MEK by distillation to remove low-volatility impurities was not performed.

The presence of trace impurities may be a possible factor responsible for the decrease in the resistivity of MEK. The resistivity cell was cleaned thoroughly with acetone to remove water soluble impurities, if any, between measurements.

In order to calculate the cell constant for the high pressure cell, the electrical resistance was measured for MEK using the high pressure cell. The applied electric voltage and the frequency varied in the range 20 - 100 mV and 20 - 100 Hz, respectively. The cell constant of the high pressure cell was calculated as the ratio of the electrical resistance measured using the high pressure cell to the resistivity measured using the unit volume resistivity cell. Table IV.4 shows the resistivity (ρ) values obtained for MEK using the unit volume resistivity cell and the resistance (R) values measured using the high-pressure cell.

Table IV.4. Resistivity and Resistance Measurements for MEK as a Function of Applied Voltage and Frequency (n = 3 Samples, 20 Readings Averaged per Sample). The Cell Constants Determined for the High-Pressure Cell are also Included.

| Applied Voltage (mV) | Frequency (Hz) | Resitivity (ρ) in MΩ.cm (using unit volume cell) | Resistance (R) in MΩ (using high pressure cell) | Cell Constant in $cm^{-1}$ (R/ρ) |
|---|---|---|---|---|
| 20 | 20 | 0.48 ± 0.08 | 2.06 ± 0.52 | 4.28 |
| | 50 | 0.48 ± 0.08 | 2.12 ± 0.63 | 4.40 |
| | 100 | 0.48 ± 0.08 | 2.13 ± 0.67 | 4.43 |
| 50 | 20 | 0.48 ± 0.08 | 2.18 ± 0.70 | 4.51 |
| | 50 | 0.48 ± 0.08 | 2.19 ± 0.73 | 4.53 |
| | 100 | 0.48 ± 0.08 | 2.19 ± 0.74 | 4.54 |
| 100 | 20 | 0.48 ± 0.08 | 2.24 ± 0.76 | 4.61 |
| | 50 | 0.48 ± 0.08 | 2.23 ± 0.77 | 4.60 |
| | 100 | 0.49 ± 0.08 | 2.23 ± 0.78 | 4.54 |

Table IV.4 also includes the cell constant for the high resistivity cell derived from the Equation IV.1. The mean cell constant for the high pressure cell was calculated to be 4.5 $cm^{-1}$. In contrast, the theoretical cell constant obtained from the ratio of the electrode

gap to the cross-sectional area of the electrodes of the high pressure cell was 8.2 $cm^{-1}$. The experimental method of determining the cell constant involved standardization of the high-pressure cell based on the comparison of the electrical resistance of a stable non-aqueous solvent, MEK, in the unit volume reference resistivity cell with that measured in the high-pressure cell using the same device, 1920 Precision LCR meter and similar electrical connections. The mean cell constant for the high pressure cell was calculated to be 4.5 $cm^{-1}$. In contrast, the theoretical cell constant obtained from the ratio of the electrode gap to the cross-sectional area of the electrodes of the high pressure cell was 8.2 $cm^{-1}$. The experimental method of determining the cell constant involved standardization of the high-pressure cell based on the comparison of the electrical resistance of a stable non-aqueous solvent, MEK, in the unit volume reference resistivity cell with that measured in the high-pressure cell using the same device, 1920 Precision LCR meter and similar electrical connections. The experimentally calculated cell constant would therefore be expected to be valid for the measurements performed in similar conditions for the HFA based formulations and was used for further determination of resistivity for all the HFA based formulations.

**IV.B.2.2. Electrical Resistivity of HFA Based Solutions**

The electrical resistance of 100% HFA 134a was measured using the high pressure cell at an applied electrical voltage ranging from 20 - 100 mV and frequency ranging from 20 - 100 Hz. The measured resistance values varied from 59 - 402 MΩ while the

corresponding resistivity values ranged between 13 - 90 MΩ.cm. However, as the resistance meter used in the present study could only measure resistances in the range of 10 mΩ - 100 MΩ, the results should be viewed with caution. The electrical resistivity of pharmaceutical grade HFA 134a has been reported to be 180 MΩ.cm (Solvay Fluor Product Bulletin 2001). Although the measurements obtained for HFA 134a were highly variable, the resistivity of HFA 134a was found to be in the same order of magnitude as that reported in the literature. However, a resistance meter capable of measuring resistances greater than 100 MΩ would be required to obtain reliable resistivity measurements for HFA 134a.

The electrical resistivity of HFA based solution formulations including 7% ethanol / 93% HFA 134a and BDP solutions in 7% ethanol / 93% HFA 134a blend was determined. Table IV.5 summarizes the results for an applied electric voltage ranging from 20 - 100 mV with a frequency ranging from 20 - 100 Hz.

Table IV.5. Electrical Resistivity Measurements for HFA Based Solutions as a Function of Applied Voltage and Frequency

| Applied Voltage (mV) | Frequency (Hz) | Resistivity (MΩ.cm)[a] | |
|---|---|---|---|
| | | 7% Ethanol / 93% HFA 134a | 0.08% BDP / 7% Ethanol / 93% HFA 134a |
| 20 | 20 | 0.84, 0.81 | 2.38 ± 1.31 |
| | 50 | 0.84, 0.81 | 2.41 ± 1.36 |
| | 100 | 0.84, 0.81 | 2.39 ± 1.34 |
| 50 | 20 | 0.85, 0.78 | 2.42 ± 1.37 |
| | 50 | 0.85, 0.82 | 2.43 ± 1.38 |
| | 100 | 0.85, 0.80 | 2.42 ± 1.37 |
| 100 | 20 | 0.86, 0.82 | 2.46 ± 1.41 |
| | 50 | 0.86, 0.82 | 2.46 ± 1.41 |
| | 100 | 0.86, 0.83 | 2.47 ± 1.43 |

[a]20 measurements averaged / can, n = 2 cans for 7% ethanol / 93% HFA 134a, n = 3 cans for 0.08% BDP / 7% ethanol / 93% HFA 134a.

The electrical resistivities determined for 7% ethanol / 93% HFA 134a blend as well as 0.08% BDP / 7% ethanol / 93% HFA 134a solutions were found to remain consistent with the applied voltage (20 - 100 mV) and frequency (20 - 100 Hz) tested. The mean electrical resistivity of the ethanol-HFA 134a blend (0.83 ± 0.02 MΩ.cm) was significantly lower ($p < 0.05$) in magnitude than that reported for HFA 134a in the literature (180 MΩ.cm). The mean resistivity of BDP solutions in 7% ethanol / 93% HFA 134a blend (2.4 ± 1.14 MΩ.cm) was found to be slightly higher in comparison to that determined for the ethanol-HFA blend alone. It was observed that the resistivity values for the BDP HFA solutions showed variability between cans.

The addition of ethanol to HFA 134a would be predicted to lower the resistivity of the formulation since the polarity of the blend would be higher than that of HFA 134a alone. Delgado *et al.* classified non-aqueous liquids on the basis of their dielectric constant (ε) as weakly polar liquids ($5 < \varepsilon \leq 12$) and moderately polar liquids ($12 < \varepsilon \leq 40$) (Delgado *et al.* 2005). The dielectric constant of 100% HFA 134a is 9.5 (Purewal 1998) while that of ethanol is 25.3 (Wohlfarth 2007). Assuming that the blend of ethanol and HFA 134a forms an ideal mixture, the dielectric constant of the 7% ethanol / 93% HFA 134a blend can be approximated to be 10.61 (Appendix A.II), which is higher than that of 100% HFA 134a. The water content of 7% ethanol / 93% HFA 134a and the BDP HFA solutions was determined to be 654 ± 166 ppm and 567 ± 184 ppm, respectively. The high water content is not unexpected since these HFA based solutions containing ethanol have an increased tendency for water ingress through the valve during storage. The presence of

water may possibly confound the results of the electrical resistivity measurements for the ethanol / HFA blend.

### IV.B.2.3. Electrical Resistivity of HFA Based Suspensions

Commercially available albuterol sulfate suspensions in HFA 134a have been developed using two different formulation strategies; Ventolin HFA is a simple suspension of albuterol sulfate in 100% HFA 134a, while Proventil HFA is a more complex suspension of albuterol sulfate in HFA 134a since it contains oleic acid as a surfactant and a polar cosolvent, ethanol. In the present study, the electrical resistivity of simple suspensions of albuterol sulfate in 100% HFA 134a was not measured, since the resistance offered by 100% HFA 134a was found to be greater than the measurable range of resistance (10 mΩ - 100 MΩ) for the resistance meter used in the present study, making the results unreliable.

However, the electrical resistivities of albuterol sulfate suspensions in HFA 134a in the presence of oleic acid and ethanol, as shown in Table IV.2, were measured after diluting these suspensions. The resistivity values for albuterol sulfate suspensions in HFA 134a containing 0.02% oleic acid and different ethanol concentrations determined at an applied voltage of 20 - 100 mV and a frequency of 20 - 100 Hz are shown in Table IV.6. There was a marked decrease in the resistivity of HFA 134a with the addition of ethanol as observed earlier in Section IV.B.2.2. The resistivity values did not vary at the applied voltage and frequency range tested, however, variability existed in resistivity between

canisters. The difference in the mean resistivity of albuterol sulfate suspensions in HFA 134a containing 0.02% oleic acid with increasing ethanol concentrations was statistically significant ($p < 0.05$, one way ANOVA).

Table IV.6. Electrical Resistivity of 0.003% Albuterol Sulfate HFA 134a Suspensions Containing 0.02% Oleic acid as a Function of Ethanol Concentration, Applied Voltage and Frequency (20 Readings / Can, 3 Cans)

| Applied Voltage (mV) | Frequency (Hz) | Resistivity (MΩ.cm) | | |
|---|---|---|---|---|
| | | 5% Ethanol[a] | 10% Ethanol[b] | 15% Ethanol[c] |
| 20 | 20 | 1.71 ± 0.92 | 0.38 ± 0.05 | 0.30 ± 0.11 |
| | 50 | 1.72 ± 0.93 | 0.37 ± 0.05 | 0.29 ± 0.11 |
| | 100 | 1.71 ± 0.93 | 0.37 ± 0.05 | 0.29 ± 0.11 |
| 50 | 20 | 1.73 ± 0.95 | 0.38 ± 0.05 | 0.30 ± 0.11 |
| | 50 | 1.74 ± 0.96 | 0.37 ± 0.05 | 0.29 ± 0.11 |
| | 100 | 1.74 ± 0.96 | 0.37 ± 0.05 | 0.29 ± 0.11 |
| 100 | 20 | 1.76 ± 0.98 | 0.38 ± 0.05 | 0.30 ± 0.11 |
| | 50 | 1.76 ± 0.98 | 0.37 ± 0.05 | 0.29 ± 0.11 |
| | 100 | 1.77 ± 0.99 | 0.37 ± 0.05 | 0.29 ± 0.11 |

Water content of albuterol sulfate suspensions containing varying ethanol concentrations: [a]275 ± 42 ppm, [b]375 ± 28 ppm, [c]567 ± 85 ppm.
Dielectric Constant of formulations containing varying ethanol concentrations in HFA 134a: [a]10.29, [b]11.08, [c]11.87 (Appendix A.II).

The mean resistivity decreased by almost one-fifth when the ethanol concentration in albuterol sulfate suspensions containing 0.02% oleic acid in HFA 134a was increased from 5% to 10% w/w. However, further increase in ethanol concentration to 15% did not cause a corresponding decrease in resistivity of the suspensions.

The resistivity would be expected to decrease with the addition of ethanol to the HFA formulations, as shown by the increase in the calculated dielectric constants. For example, the dielectric constant of formulations containing a 5% ethanol / 95% HFA 134a blend was calculated to be 10.29, while those determined for 10% ethanol / 90% HFA

134a and 15% ethanol / 85% HFA 134a blends were 11.08 and 11.87, respectively (Appendix A.II). The water content of these formulations also increased significantly ($p < 0.05$, one-way ANOVA) with increase in ethanol concentration (Table IV.6), the presence of water may infleunce polarity of these formulations. The water content for albuterol sulfate suspensions in a 10% ethanol / 90% HFA 134a blend (375 ± 28 ppm) was lower than the HFA based solutions in a 7% ethanol / 93% HFA 134a blend (567 ± 184 ppm). The increased water content for the solution based formulations was considered to be related to the storage time of the formulations. Solution formulations were prepared approximately 2 weeks before the suspension formulations, and as a consequence, water ingress in the HFA based solutions on storage would be expected to be higher.

Table IV.7 shows the influence of oleic acid concentration on the electrical resistivity of albuterol sulfate suspensions at an applied voltage ranging from 20 - 100 mV with a frequency ranging from 20 - 100 Hz.

Table IV.7. Electrical Resistivity of 0.003 %w/w Albuterol Sulfate Suspensions in 5% Ethanol / 95% HFA 134a as a Function of Oleic Acid Concentration, Applied Voltage and Frequency (20 Readings Averaged / Can, 3 Cans)

| Applied Voltage (mV) | Frequency (Hz) | Resistivity (MΩ.cm) | | |
|---|---|---|---|---|
| | | 0.02% oleic acid[a] | 0.03% oleic acid[b] | 0.04% leic acid[c] |
| 20 | 20 | 1.71 ± 0.92 | 1.21 ± 0.36 | 0.88 ± 0.15 |
| | 50 | 1.72 ± 0.93 | 1.21 ± 0.36 | 0.88 ± 0.15 |
| | 100 | 1.71 ± 0.93 | 1.21 ± 0.36 | 0.88 ± 0.15 |
| 50 | 20 | 1.73 ± 0.95 | 1.23 ± 0.36 | 0.89 ± 0.15 |
| | 50 | 1.74 ± 0.96 | 1.23 ± 0.36 | 0.89 ± 0.15 |
| | 100 | 1.74 ± 0.96 | 1.24 ± 0.35 | 0.88 ± 0.15 |
| 100 | 20 | 1.76 ± 0.98 | 1.24 ± 0.36 | 0.90 ± 0.15 |
| | 50 | 1.76 ± 0.98 | 1.24 ± 0.36 | 0.90 ± 0.15 |
| | 100 | 1.77 ± 0.99 | 1.24 ± 0.35 | 0.90 ± 0.15 |

Water content of albuterol sulfate suspensions containing varying oleic acid concentrations: [a]275 ± 42 ppm, [b]198 ± 17 ppm, [c]256 ± 28 ppm.

The mean resistivity of albuterol sulfate suspensions in HFA 134a containing oleic acid and ethanol decreased with increase in oleic acid concentration, however the decrease was not statistically significant ($p > 0.05$, one-way ANOVA) due to considerable variation in the resistivity values between canisters. Table IV.7 shows that the resistivity values were consistent at the applied voltage and frequency range tested.

Although increasing the oleic acid concentration caused a decrease in the resistivity of the ethanol containing albuterol sulfate HFA suspensions, this decrease was not statistically significant. The water content of albuterol sulfate suspensions in a 5% ethanol / 95% HFA 134a blend containing varying concentrations of oleic acid (275 ± 42 ppm, 198 ± 17 ppm and 256 ± 28 ppm for suspensions containing 0.02, 0.03 and 0.04 %w/w oleic acid, respectively) differed significantly ($p < 0.05$, one-way ANOVA). The presence of moisture in these formulations may possibly confound the electrical resistivity measurements.

In summary, the resistivity measurements have provided an indication that ionic species are present in HFA based solutions. Although HFA 134a has high resistivity, which could not be measured reliably in the present study, the presence of ethanol in the control HFA solutions tested increased the polar nature of the formulation and subsequently decreased the resistivity. The presence of trace quantities of water may possibly influence the formation of charged ionic species in ethanol-HFA based formulations and confound the results obtained for the resistivity measurements. The use of ethanol dried over molecular sieves may be able to distinguish the influence of water on the resistivity measurements. The variability in the resistivity measurements of these

pressurized formulations made it difficult to discern subtle changes in the resistivity due to the addition of excipients. For albuterol sulfate suspensions in HFA 134a containing ethanol and oleic acid, the resistivity measurements decreased with increase in the ethanol concentration, however, no significant effect of oleic acid concentration on resistivity was observed for the concentrations studied. The resistivity measurements suggested that ethanol containing HFA formulations are relatively polar and may likely produce charged species in these systems.

## IV.C. Zeta Potential of Albuterol Suspensions in Non-Aqueous Solvents

### IV.C.1. Methods

#### IV.C.1.1. Preparation of Albuterol Suspensions in Non-Aqueous Solvents

The electrophoretic mobility technique used in the present study was validated for measurements in non-aqueous suspensions using model albuterol suspensions in non-pressurized and pressurized chlorinated solvents. 0.001 - 0.004 %w/v albuterol sulfate suspensions in chloroform (Fisher Scientific, Swannee, GA) were prepared as model suspensions in a non-aqueous, non-pressurized chlorinated solvent and tested in order to compare the zeta potential values obtained to that reported in the literature. In addition, albuterol base suspensions in a CFC 11: CFC 12 blend containing oleic acid were prepared as outlined in Chapter III.A.2.2 as model suspensions in non-aqueous pressurized chlorinated solvents. A 0.09 % w/w albuterol base suspension in a mixture of CFC 11:

CFC 12 with 0.015% w/w oleic acid (drug-surfactant ratio of 6:1) was prepared and tested in order to compare the zeta potential with that reported in the literature for a similar concentration. Further, in order to study the effect of albuterol base and oleic acid concentration on the zeta potential, a series of albuterol base suspensions in a mixture of CFC 11: CFC 12, with oleic acid as the surfactant were prepared (Table IV.8 and IV.9).

Table IV.8. Albuterol Base Suspensions in Chlorofluorocarbon (CFC) 11 and 12 Blend with a Fixed Drug-Surfactant Ratio of 6:1

| Albuterol base (%w/w) | Oleic acid (%w/w) | CFC 11 (%w/w) | CFC 12 (%w/w) |
|---|---|---|---|
| 0.001 | 0.00016 | 30 | 70 |
| 0.005 | 0.0008 | 30 | 70 |
| 0.03 | 0.005 | 30 | 70 |
| 0.06 | 0.01 | 30 | 70 |
| 0.09 | 0.015 | 30 | 70 |

Table IV.9. Albuterol Base Suspensions in Chlorofluorocarbon (CFC) 11 and 12 Blend with varying Oleic Acid Concentration

| Albuterol base (%w/w) | Oleic acid (%w/w) | CFC 11 (%w/w) | CFC 12 (%w/w) |
|---|---|---|---|
| 0.03 | 0.002 | 30 | 70 |
| 0.03 | 0.003 | 30 | 70 |
| 0.03 | 0.005 | 30 | 70 |
| 0.03 | 0.0075 | 30 | 70 |
| 0.03 | 0.01 | 30 | 70 |

After validation of the electrophoretic mobility technique, the zeta potential of HFA based albuterol sulfate suspensions was determined. In order to prepare samples for electrophoretic measurements for concentrated suspensions, careful dilution preserving the existing state of the particle surface is recommended (Delgado *et al.* 2005). Table IV.2 summarizes the dilute albuterol sulfate HFA suspensions (approximately 0.003 %w/w albuterol sulfate) used for the zeta potential measurements.

### IV.C.1.2. Determination of Zeta Potential of Albuterol Suspensions in Non-Aqueous Solvents

Zeta potential was determined by measuring the electrophoretic mobility of charged particles in suspension. Electrophoretic measurements were performed using Laser Doppler Electrophoresis with a Malvern Zetasizer 2000 (Malvern Instruments, Inc., Southborough, MA) and a custom-built pressurized non-aqueous electrophoresis cell (Figure IV.3).

Figure IV.3. Schematic Diagram of the High-Pressure Electrophoresis Cell

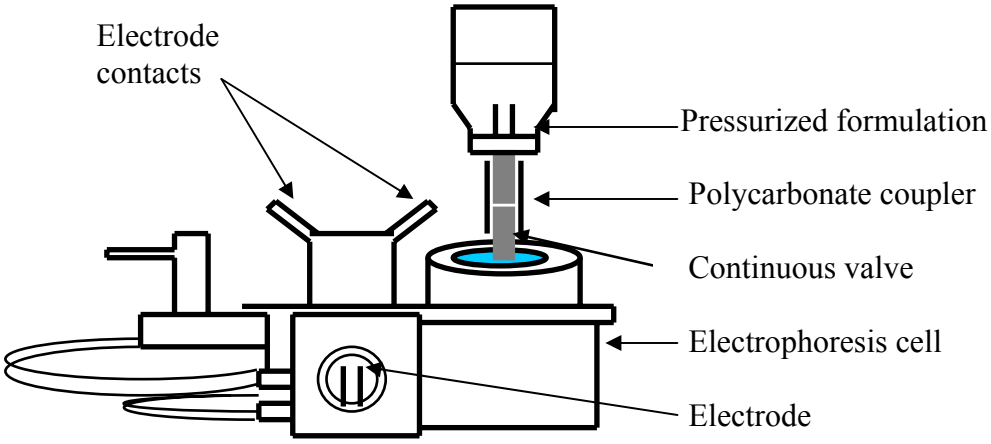


The electrophoresis cell was designed to hold pressurized samples and incorporated with a continuous valve to enable direct transfer; low voltages could be applied to minimize sample heating since the electrode gap in the cell was only 2 mm. The Zetasizer 2000 uses heterodyne detection; one of the laser beams was modulated at 250 Hz to detect the direction of movement and hence the sign of the charge on the particles. The applied electric field was reversed at a frequency of 2 Hz to prevent electrode polarization. The

Zetasizer 2000 measures the electrophoretic mobility of particles suspended in the dispersion medium. In order to determine zeta potential values from the measured electrophoretic mobility, the Zetasizer 2000 software uses the Henry's formula as given by Equation IV.2.

$$\zeta = \frac{3\eta\mu}{2 f(\kappa a)\varepsilon_{rs}\varepsilon_0} \qquad \text{Equation IV.2}$$

where $\zeta$ is the zeta potential, $\eta$ is the viscosity, $\mu$ is the electrophoretic mobility, $\kappa a$ is the ratio of the electrical double layer ($\kappa^{-1}$) and the particle radius (a) and $\varepsilon_{rs}$ is the electrical permittivity of the medium and $\varepsilon_0$ is the electrical permittivity of the vacuum. The values of dielectric constant ($\varepsilon_{rs}/\varepsilon_0$) and viscosity of the formulations tested (Table IV.10) were entered into the Zetasizer software.

Table IV.10. Summary of the Dielectric Constants and Viscosity of the Dispersion Media of the Albuterol Suspensions

| Dispersion Medium | Dielectric Constant | Viscosity (cP) |
|---|---|---|
| 100% Chloroform | 4.8[a] | 0.54[a] |
| 30% CFC 11 / 70% CFC 12 | 2.17[a] | 0.30[a] |
| 100% HFA 134a | 9.5[b] | 0.21[d] |
| 5% ethanol / 95% HFA 134a | 10.29[c] | 0.23[e] |
| 10% ethanol / 90% HFA 134a | 11.08[c] | 0.30[e] |
| 15% ethanol / 85% HFA 134a | 11.87[c] | 0.33[e] |

[a]Sandstrom *et al.* 1994, [b]Purewal, 1998, [c]Appendix A.II, [d]Solvay Fluor HFA 227 and HFA 134a Datasheet 2003, [e]DeStefano and McNamara 1996.

In order to estimate the surface charge of albuterol sulfate particles in these HFA based suspensions, f($\kappa a$) was assigned a value of 1.0 in the Zetasizer software. This corresponds to the Hückel approximation. In the case of HFA based suspensions, the presence of a polar cosolvent, ethanol, makes these formulations more polar, as suggested

by the resistivity measurements. For these HFA formulations, it may be possible that the value of f(κa) lies between 1.0 and 1.5, which are generally used for non-aqueous formulations and aqueous formulations, respectively. The resistivity measurements for the HFA based formulations performed in Section IV.B confirmed the presence of charge ionic species, however, the nature of these species is not known. Hence, κ (reciprocal of the electrical double layer) could not be calculated for the HFA based suspension formulations.

Preliminary experiments were performed by applying an electrical field in the range of 50 - 120 V/cm with the model albuterol suspensions in chloroform and CFC 11: CFC 12 blend. The zeta potential values remained consistent in the range of the applied electric field tested. Further experiments with HFA based suspensions were performed using an electrical field of 100 V/cm. Five measurements were averaged per can, 3 cans were tested per formulation. The cell was carefully cleaned with methanol five times between samples.

### IV.C.2. Results and Discussion

#### IV.C.2.1. Zeta Potential of Albuterol Suspensions in Non-Pressurized and Pressurized Chlorinated Solvents

Figure IV.4 summarizes the results of zeta potential measurements of albuterol sulfate suspensions in chloroform as a function of applied electric field (50 - 120 V/cm) and albuterol sulfate concentration (0.001 - 0.004 %w/v). Zeta potential was not

significantly different ($p > 0.05$, one-way ANOVA) as a function of the applied electric field for all the concentrations tested. Zeta potential of albuterol sulfate in chloroform did not differ significantly ($p > 0.05$, one-way ANOVA) as a function of the albuterol sulfate concentrations measured at an applied electric field in the range of 50 - 120 V/cm.

Figure IV.4. Zeta Potential of Albuterol Sulfate Suspensions in Chloroform as a Function of Electric Field Strength and Concentration of Albuterol Sulfate. Error Bars Represent S.D., n=9 (3 Samples, 3 Replicates / Sample)

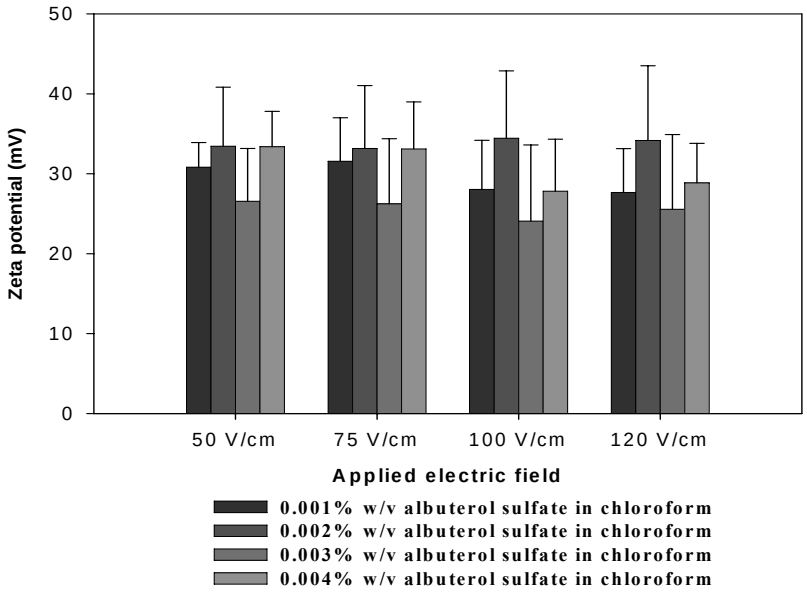


Albuterol sulfate suspensions in chloroform were tested in order to compare the zeta potential values obtained to that reported in literature. However, the concentration of albuterol sulfate used in these studies was not reported (Sidhu *et al.* 1993). Low concentrations of albuterol sulfate suspensions in chloroform (0.001 - 0.004% w/v) have been suggested for the determination of zeta potential using laser Doppler electrophoresis (Rogueda 2005b). The mean zeta potential for albuterol sulfate suspensions in chloroform,

in the concentration range of 0.001 - 0.004 %w/v, determined at an applied electric field of 100 V/cm was +28.6 ± 4.3 mV, which was comparable to +34 ± 5 mV as reported in the literature (Sidhu *et al.* 1993). The results suggested that albuterol sulfate particles possibly acquired a positive surface charge in chloroform.

Table IV.11 summarizes the electrophoretic mobility and zeta potential data for albuterol base suspensions containing 0.09 %w/w albuterol base and 0.015 %w/w oleic acid at an applied electric field in the range of 50 - 120 V/cm, which was found to have an insignificant effect on the zeta potential ($p$ = 0.90).

Table IV.11. Zeta Potential and Electrophoretic Mobility for 0.09 %w/w Albuterol Base / 0.015 %w/w Oleic Acid / CFC 11:12 (30:70) Suspensions as a Function of Applied Electrical Field (n = 6; 2 Samples, 3 Replicates/ Sample)

| Applied Electrical Field (V/cm) | Electrophoretic Mobility ($10^{-8}$ $m^2V^{-1}s^{-1}$) | Zeta Potential (mV) |
|---|---|---|
| 50 | 0.30 ± 0.09 | 72.9 ± 21.3 |
| 75 | 0.30 ± 0.11 | 74.9 ± 27.2 |
| 100 | 0.35 ± 0.08 | 82.3 ± 23.3 |
| 120 | 0.36 ± 0.09 | 88.7 ± 22.8 |

Electrophoretic mobility for albuterol base CFC suspensions containing 0.09 %w/w albuterol base and 0.015 %w/w oleic acid was 0.35 ± 0.08 ($10^{-8}$) $m^2V^{-1}s^{-1}$, which was comparable to that reported in the literature (0.43 x $10^{-8}$ $m^2V^{-1}s^{-1}$; Sandstrom *et al.* 1994) for albuterol base suspensions of equivalent composition. The corresponding zeta potential for the same formulation (82.3 ± 24.1 mV) obtained in this study was also similar to that reported by Sandstrom *et al.* (80mV; Sandstrom *et al.* 1994). However, in the present study, the suspensions tested were found to be too concentrated for electrophoretic mobility measurements using light scattering. The signals obtained during the

electrophoretic mobility measurements were influenced by the sample particle concentration.

An indication of sample concentration is obtained from the number of photons counted per second expressed as kilo counts per second (kcps). The reference beam contributes between 2000 - 2500 kcps to the photon count rate used in the measurement sequence. Ideally, the scattering beam or the light beam from the sample should contribute between 100 and 1000 kcps. A kcps value of 2400 - 3000 during the measurement sequence indicates an acceptable suspension concentration. A count rate above 4000 kcps suggests a concentrated suspension. The sample data extracted from the corellogram after processing the signal is displayed as a fringe model. An acceptable fringe model will have a symmetric decay about zero and a large depth of modulation of the signal, which is indicative of an appropriately prepared sample. A sample with too high or too low particle concentration will yield a signal, which does not display a good depth of modulation as seen from Figure IV.5. It is difficult to dilute pressurized suspensions; hence in order to keep the dispersed phase in an acceptable concentration range for the technique used, suspensions containing lower concentrations of albuterol were prepared. Suspensions containing a fixed drug-surfactant ratio of 6:1 and albuterol base concentration in the range of 0.001 - 0.09% w/w were prepared to investigate the effect of particle concentration on the measured electrophoretic mobility and the zeta potential tested at an applied electric field of 100 V/cm (Table IV.12).

Figure IV.5. Example of an Acceptable and Poor Fringe Model from Electrophoretic Mobility Measurements of 0.001 %w/w and 0.09 %w/w Albuterol Base Suspensions in CFC 11: CFC 12 blend, respectively.

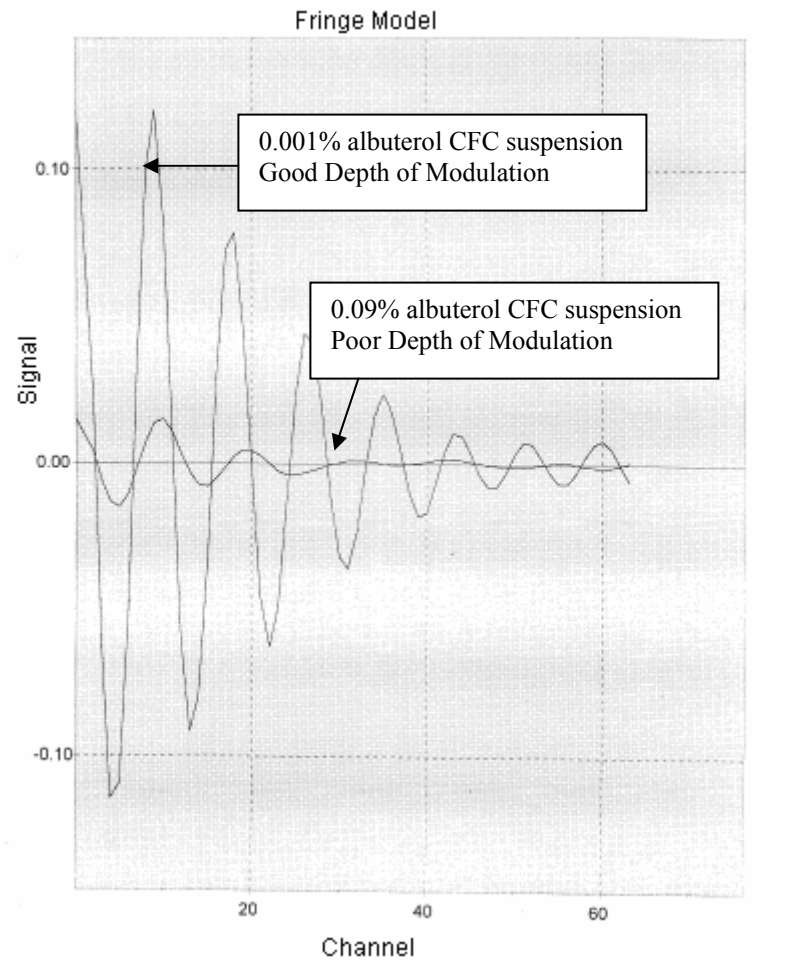


Table IV.12. Electrophoretic Mobility and Zeta Potential of CFC Based Suspensions at an Electrical Field of 100 V/cm (n = 9; 3 Samples, 3 Replicates / Sample)

| Albuterol base %w/w | Oleic Acid %w/w | Electrophoretic Mobility ($10^{-8}$ $m^2V^{-1}s^{-1}$) | Zeta Potential (mV) | Photon Count Rate (kcps) |
|---|---|---|---|---|
| 0.001 | 0.00016 | 0.67±0.03 | 164±9 | 5724 ± 230 |
| 0.005 | 0.0008 | 0.52±0.07 | 128±17 | 8630 ± 620 |
| 0.03 | 0.005 | 0.41±0.01 | 111±23 | 5929 ± 1032 |
| 0.06 | 0.01 | 0.47±0.04 | 116±11 | 7404 ± 908 |
| 0.09[a] | 0.015 | 0.35±0.08 | 82±23 | 8828 ± 697 |

[a]n = 6; 2 samples, 3 replicates/ sample

There was a statistically significant difference in the measured zeta potential across the particle concentration range studied ($p < 0.0001$, one way ANOVA). Post-hoc analysis using Tukey's HSD showed that the difference in the mean zeta potential was significant between the highest concentration of 0.09 %w/w albuterol and the lower concentrations of 0.005 and 0.001 %w/w albuterol base suspensions. The mean zeta potential for suspensions with albuterol concentration 0.005%, 0.03%, 0.06 %w/w was not significantly different. The photon count rate decreased with decrease in albuterol base concentration in the suspensions but still remained above 4000 kcps even for the lowest albuterol base concentration studied. However, the fringe pattern of the data improved as observed in Figure IV.5. Unfortunately, the low albuterol base concentrations used for zeta potential measurements are not reflective of the concentration of albuterol base in the marketed CFC formulation, for example, Ventolin CFC, which contains 0.12 %w/w albuterol base suspended in a CFC 11: CFC 12 propellant blend with oleic acid as a surfactant. Hence, application of the zeta potential data to commercially available suspensions with higher drug concentrations is considered to be limited.

Further, keeping the particle concentration unchanged, the effect of surfactant concentration on the particle mobility and the zeta potential was investigated using 0.03% w/w albuterol base suspensions in CFC 11: CFC 12 blends containing varying concentrations of oleic acid. The mean zeta potential measured for albuterol suspensions in CFC 11: CFC 12 in the absence of oleic acid was +58.1 ± 18.1 mV and became more positive on the addition of oleic acid (Table IV.13). Variability in the measurements was

found to be high, probably due to the high particle concentration (photon count rates in the range of 6000 kcps).

Table IV.13. Effect of Oleic Acid Concentration on Electrophoretic Mobility and Zeta Potential of Albuterol Suspensions in CFC 11:12 Blend (n = 9, 3 Samples, 3 Replicates / Sample)

| Albuterol Base % w/w | Oleic Acid % w/w | Electrophoretic Mobility ($10^{-8}$ $m^2V^{-1}s^{-1}$) | Zeta Potential (mV) |
|---|---|---|---|
| 0.03 | - | 0.26±0.10 | 58±18 |
| 0.03 | 0.0015 | 0.43±0.04 | 106±10 |
| 0.03 | 0.003 | 0.37±0.16 | 90±39 |
| 0.03 | 0.005 | 0.41±0.01 | 111±23 |
| 0.03 | 0.0075 | 0.55±0.03 | 136±10 |
| 0.03 | 0.01 | 0.55±0.07 | 135±18 |

The zeta potential of albuterol base suspensions was observed to increase with increasing oleic acid concentration from 0.003 - 0.0075 %w/w. The mean zeta potential did not increase further at an oleic acid concentration of 0.01 %w/w. The effect of oleic acid concentrations above 0.01% w/w on the zeta potential of albuterol base CFC suspensions was not tested. These studies have indicated that the addition of oleic acid increased the positive charge on the albuterol particle surface. In comparison, Sandstrom et al reported that the zeta potential of 0.09 %w/w albuterol base in a CFC 11: CFC 12 (30:70) blend increased until a maximum value of +80 mV at an oleic acid concentration range of 0.01 - 0.02 %w/w and further increase in oleic acid concentration caused a decrease in the zeta potential values (Sandstrom *et al.* 1994).

The present study showed that the electrophoretic mobility of albuterol suspensions in non-aqueous pressurized solvents can be measured and was in good agreement with the data reported in the literature. Although, the experiments have indicated that albuterol

suspensions in chloroform and CFC propellant blend exhibit positive zeta potentials, low particle concentrations were required to obtain acceptable measurements for the electrophoretic mobility technique employed in this study. Unfortunately, these concentrations do not reflect the concentration of drug present in commercially available suspension pMDIs and hence the results obtained are difficult to extrapolate to commercial products.

### IV.C.2.2. Zeta Potential of Albuterol Sulfate Suspensions in HFA 134a

The electrophoretic mobility of albuterol sulfate suspensions in HFA 134a determined at an alternating electric field of 100 V/cm was 2.20 ± 0.70 ($10^{-8}$) $m^2V^{-1}s^{-1}$, while the corresponding zeta potential was 76 ± 26 mV. There was variability in the measurements both within can and between cans, which was also observed with measurements within pressurized albuterol base CFC suspensions. A simple suspension of albuterol sulfate in 100% HFA 134a was tested to investigate the presence of surface charge on albuterol sulfate particles in the absence of excipients, e.g., surfactants and cosolvents.

The electrophoretic mobility determined for albuterol sulfate suspensions in HFA 134a was higher than that achieved by albuterol base suspensions in CFC 11: CFC 12 propellants. For example, the electrophoretic mobility for 0.09 %w/w albuterol base / 0.015 %w/w oleic acid / CFC 11: CFC 12 suspensions measured at 100 V/cm was 0.35 ± 0.08 ($10^{-8}$) $m^2V^{-1}s^{-1}$. HFA 134a has a higher dielectric constant ($\varepsilon = 9.5$) than a 30:70 blend

of CFC 11: CFC 12 (ε = 2.2). Zeta potential is directly proportional to electrophoretic mobility and viscosity, while it is inversely proportional to the dielectric constant. By virtue of the higher dielectric constant of HFA 134a, albuterol sulfate particles in HFA 134a would be predicted to have a higher electrophoretic mobility compared with albuterol base particles suspended in CFC 11: CFC 12 propellant blends for similar zeta potential values.

For albuterol sulfate suspensions in HFA 134a in the absence of surfactant, it is difficult to explain the formation of surface charge due to the absence of any ionic species. The electrical resistivity of 100% HFA 134a could not be reliably measured since the resistance meter used was not capable of measuring resistances above 100 MΩ.cm. This suggested that the conductivity of the propellant HFA 134a by itself is very low. Sidhu et al showed that presence of trace water can influence surface charge. Lactose suspensions in dry chloroform produced a zeta potential of –5 ± 2 mV as compared to –23 ± 5 mV when dispersed in non-dry chloroform (water content approximately 100 ppm; (Sidhu *et al.* 1993). Surface potentials in HFA 134a may possibly be influenced by the presence of soluble impurities from both the formulation components e.g. albuterol sulfate, HFA 134a as well as the packaging components e.g. extractables and leachables from valve elastomers or the presence of moisture. Valois DF10/50 continuous valves with EPDM elastomers were used in this study. EPDM elastomers do not contain carbon fillers, have low tendency for water ingress as well as limited swelling on contact with HFA 134a (Williams and Tcherevatchenkoff 1998, Cummings 1999, Pischtiak 2000b). HFA 134a may contain trace quantities of processing impurities including hydrogen fluoride (HF) as

well as water (Solvay Fluor HFA 227 and HFA 134a Datasheet 2003). In the present study, the water content of albuterol sulfate suspensions in HFA 134a was 59 ± 7 ppm. It is difficult to remove traces of water from non-aqueous systems, especially in pressurized dispersion media e.g. HFA 134a.

The effect of ethanol concentration on the zeta potential of albuterol sulfate suspensions in HFA 134a containing 0.02 % oleic acid was investigated. Table IV.14 summarizes the electrophoretic mobility, zeta potential, resistivity and water content of albuterol sulfate suspensions in HFA 134a containing 0.02% oleic acid and increasing concentration of ethanol.

Table IV.14. Electrophoretic Mobility and Zeta Potential of Albuterol Sulfate in HFA 134a Containing 0.02% Oleic Acid as a Function of Ethanol Concentration (n = 30; 5 Readings / Sample, 2 Samples / Can, 3 Cans)

| Albuterol sulfate %w/w | Ethanol %w/w | Electrophoretic Mobility ($10^{-8}$ $m^2V^{-1}s^{-1}$) | Zeta Potential (mV) | Resistivity (MΩ.cm) | Water Content (ppm) |
|---|---|---|---|---|---|
| 0.003 | 5 | 1.07±0.22 | 40±8 | 1.74±0.02 | 275 ± 42 |
| 0.003 | 10 | 0.48±0.31 | 24±13 | 0.37±0.00 | 375 ± 28 |
| 0.003 | 15 | 0.38±0.23 | 15±10 | 0.29±0.00 | 567 ± 85 |

The mean electrophoretic mobility and the corresponding zeta potential of albuterol sulfate particles decreased significantly ($p < 0.0001$, one way ANOVA) with an increase in the ethanol concentration from 5 - 15 % w/w. Table IV.14 also summarizes the resistivity of these formulations, which also decreased with an increase in the ethanol concentration. The water content of albuterol sulfate HFA suspensions increased significantly ($p < 0.05$, one way ANOVA) with increasing ethanol concentration as shown in Table IV.14. The presence of ethanol in these albuterol sulfate HFA suspensions may possibly contribute to

formation of ionic species as implied by the decrease in electrical resistivity, which may have a role in decreasing the overall surface charge in suspensions containing increasing concentrations of ethanol.

Table IV.15 shows the effect of oleic acid concentration on the electrophoretic mobility and the zeta potential of albuterol sulfate suspensions in a 5% ethanol / 95% HFA 134a blend. The mean zeta potential of albuterol sulfate suspensions in a 5% ethanol / 95% HFA 134a blend containing 0.02 % oleic acid was 40 ± 8 mV, while that for suspensions containing 0.03 % w/w oleic acid was 47 ± 16 mV. Variability in the measurements was high.

Table IV.15 Electrophoretic Mobility and Zeta Potential of Albuterol Sulfate in 5% Ethanol / 95% HFA 134a Blend as a Function of Oleic Acid Concentration (n = 30; 5 Readings / Sample, 2 Samples / Can, 3 Cans)

| Albuterol sulfate (%w/w) | Oleic acid (%w/w) | Electrophoretic Mobility ($10^{-8}$ $m^2V^{-1}s^{-1}$) | Zeta Potential (mV) | Resistivity (MΩ.cm) | Water Content (ppm) |
|---|---|---|---|---|---|
| 0.003 | 0.02% | 1.07±0.22 | 40±8 | 1.74±0.02 | 275 ± 42 |
| 0.003 | 0.03% | 1.27±0.43 | 47±16 | 1.23±0.01 | 198 ± 17 |
| 0.003 | 0.04% | 0.70±0.45 | 30±14 | 0.89±0.01 | 256 ± 28 |

Table IV.15 also shows the resistivity of the formulations, which slightly decreased with increase in the oleic acid concentration. On further increase in the oleic acid concentration to 0.04 % w/w, the mean zeta potential decreased to 30 ± 14 mV. There was a statistically significant difference ($p < 0.0001$, one-way ANOVA) in the zeta potential values between the formulations with three different oleic acid concentrations. Due to high variability in the measurements, the effect of increasing the oleic acid concentration on the

zeta potential was not clear. In addition, the presence of water may have had an adverse effect on the surface charge of albuterol sulfate in these suspensions as well.

The typical concentration range of surfactants used in suspension pMDIs is usually 0.01 - 1 %w/w depending upon the concentration of drug; higher surfactant concentrations are used for high drug concentration suspensions (Dalby 1990). In this study, oleic acid concentrations were varied between 0.02 - 0.04 %w/w of the formulation, which was 10 - 20 % of the initial concentration of albuterol sulfate in the suspensions. In general, the electrophoretic mobility and the corresponding zeta potential values for albuterol sulfate suspensions in HFA containing oleic acid and ethanol were lower than those obtained for albuterol sulfate HFA suspensions without surfactant. In contrast, the electrophoretic mobilities of albuterol sulfate particles suspended in HFA 134a containing oleic acid and ethanol were higher than those determined for albuterol particles suspended in a CFC 11: CFC 12 blend containing oleic acid.

In summary, electrophoretic mobility studies in a simple albuterol sulfate suspension in 100% HFA 134a showed that albuterol sulfate acquired a positive zeta potential although there was variability in the measurements. Albuterol sulfate concentrations in these suspensions (approximately 0.003 %w/w) were significantly lower than that present in commercially available albuterol sulfate HFA suspension pMDIs e.g. Ventolin HFA, which contains 0.14 %w/w albuterol sulfate in 100 % HFA 134a. It may be speculated that surface charge formation in such formulations may be due to the presence of trace water or impurities, however, these studies are difficult to undertake. The electrophoretic mobility of albuterol sulfate decreased in the presence of oleic acid and

ethanol; increasing the concentration of ethanol decreased the mobility and the corresponding zeta potential of albuterol sulfate HFA suspensions. However, the limitation of these techniques used to measure electrical charge is that dilute particle concentrations are required. Other techniques such as electroacoustic techniques could possibly be used to measure charge in high particle concentration suspensions, however, electroacoustics has not been adapted for pressurized formulations.

Both the resistivity and electrophoretic mobility measurements have confirmed the presence of charged species within HFA based solutions and suspensions. However, whether these species have a role in the overall suspension stability of HFA suspensions would depend on the type of soluble species present and their interactions within these formulations. Chapter V describes a theoretical approach to study the particle interactions within model albuterol sulfate HFA suspension pMDIs.

# V. MODELING PARTICLE INTERACTIONS IN SUSPENSION BASED METERED DOSE INHALERS

## V.A. Introduction

Most pMDIs are formulated as suspensions of micronized drug in liquefied propellant blends (Farr *et al.* 1994). Surfactants such as lecithin, oleic acid and sorbitan trioleate have been traditionally used to stabilize these inherently unstable systems (Farr *et al.* 1994). Although traditional DLVO theory has been used to explain suspension stability within aqueous systems on the basis of van der Waals attractive forces and electrostatic repulsion, its application to non-aqueous systems including pMDI suspensions has not been validated (Vervaet and Byron 1999). The extent to which the above-mentioned forces influence particle interactions within the pMDI suspension is considered to vary depending on surface chemistry and surface morphology of drug, excipients and packaging components like the canister coating material (Parsons *et al.* 1992, Clarke *et al.* 1993).

The pMDI formulation and device components have undergone major modifications due to the transition from the ozone-depleting CFCs to the ozone-friendly HFA propellants (Thiel 1996, Leach 2005). The difference in physicochemical properties of HFA and CFC propellants, particularly the solvent characteristics, has necessitated the use of different salt forms of drugs and the inclusion of polar cosolvents like ethanol to

dissolve surfactants traditionally used in CFC based pMDIs (Byron *et al.* 1994, Tzou *et al.* 1997, Jannick 2006). For example, Proventil HFA® is a suspension of albuterol sulfate in HFA 134a containing oleic acid as a surfactant and a polar cosolvent, ethanol. In contrast, Ventolin HFA is a simple suspension of albuterol sulfate in 100% HFA 134a. HFA based suspension pMDIs also have a greater propensity for drug adhesion to the canister inner surface than CFC based suspensions (Ashurst *et al.* 2000a). Recent studies have employed atomic force microscopy and surface tension measurements to explain particle interactions between drug, excipients and canister material (Traini *et al.* 2005). However, a theoretical understanding of the interactions within pressurized suspension formulations on a molecular level is still lacking.

In this pilot study, molecular models of simple pMDI formulations including albuterol sulfate in HFA 134a were constructed and optimized to investigate interactions between the drug and propellant molecules. Interactions within albuterol sulfate suspensions in the presence of oleic acid (an anionic surfactant) and ethanol (a polar cosolvent) were also studied.

## V.B. Molecular Modeling

### V.B.1. Construction and Optimization of the Molecular Models

Molecular modeling was undertaken using Sybyl software (Version 7.3, Tripos, Inc., St. Louis, MO), which employs molecular mechanics or the force field method to calculate the molecular geometry, energies and various other properties of the compound

of interest (Tripos Bookshelf Force Field Manual 2006). A molecule is considered to be a mechanical system in which particles (atoms) are connected by springs (bonds) and the elasticities of the springs are the force constants. A force field is used to calculate the interaction forces for both bonding (covalent) and non-bonding (van der Waals and electrostatic) interactions for all the atoms in the molecule. The molecule can rotate, vibrate and translate in response to the inter- and intramolecular forces acting upon it, to attain its most favored conformation in space (Schlick 2002).

Electrostatic point charges on the atoms in a molecule drawn in Sybyl can be calculated using various empirical methods. The Gasteiger-Huckel method is one commonly used method, where the calculation of charges on the molecule is based on the relationship between the orbital electronegativity and the atomic charge given by Equation V.1 (Tripos Bookshelf Force Field Manual 2006):

$$X_A=a_A+b_A.Q+c_A.Q^2 \qquad \text{Equation V.1}$$

where $X_A$ = orbital electronegativity and is represented as a function of the total charge (Q) on an atom (A), and $a_A$, $b_A$ and $c_A$ are the coefficients of the quadratic equation based on the ionization potential and electron affinity of the atom.

The energy associated with a molecular model of a compound is a function of its atomic coordinates. After constructing a molecular model in Sybyl, the energy is minimized by changing the atomic coordinates of the molecular model iteratively until a minimum energy value relative to the energy associated with the inital set of atomic coordinates is obtained. The resulting atomic coordinates corresponding to the local energy

minimum correspond to the favored structural conformation of the molecule in space (Tripos Bookshelf Force Field Manual 2006).

Sybyl can be used to study properties of the molecule in a vacuum. However, since almost all chemical interactions occur in a solvent medium, the software offers three options to take into account the solvent effects in the study of molecular interactions. These include using a distance dependent dielectric screening term in the force field to simulate solvent screening effects on electrostatic charges, implicit solvation of molecules by adding a new term/terms to the force field to account for solvent effects or explicitly including solvent molecules in the calculation of intermolecular forces (Tripos Bookshelf Force Field Manual 2006).

### V.B.2. Estimation of Molecular Interactions Using the Hydropathic INTeractions (HINT®) Scores

The HINT program in Sybyl has been designed to classify and quantitatively score non-covalent interactions e.g. hydrogen bonding, acid-base, Coulombic attractions and hydrophobic interactions (Kellogg and Abraham 2000). Experimental data from solvent partition experiments between water and 1-octanol ($\log P_{o/w}$) have been used to develop the HINT program. The HINT model scores each atom-atom interaction, within or between molecules, with the following equation:

$$b_{ij} = a_i S_i \, a_j S_j \, T_{ij} R_{ij} + r_{ij} \qquad \text{Equation V.2}$$

where $b_{ij}$ is the interaction score between atoms i and j, a is the hydrophobic atom constant, S is the solvent accessible surface area ($H_2O$ probe), $T_{ij}$ is a logic function which returns a value of 1 or –1; depending on the character of the interacting polar atoms ($a < 0$ for polar atoms), there are three possibilities: acid-acid, base-base and acid-base of which only acid-base interactions are scored favorably. $T_{ij}$ also flags hydrogen bonds, which are considered a special case of acid-base interactions. $R_{ij}$ is the exponential $e^{-r}$ (r is the distance between the two atoms i and j) and $r_{ij}$ is an implementation of the Lennard-Jones potential function (Levitt 1983, Levitt and Perutz 1988). The $r_{ij}$ term serves as a penalty function to flag van der Waals violations. The total HINT interaction score for the system is given by the sum of all the individual interaction scores ($\Sigma\Sigma b_{ij}$). The HINT convention is that favorable interactions are scored positively ($b_{ij} > 0$) and unfavorable interactions are scored negatively ($b_{ij} < 0$) (Kellogg and Abraham 2000). HINT has typically been used to calculate an empirical hydropathic field in or around a protein or small molecule, and displaying contours to qualitatively visualize hydrophobic and polar regions of the molecules; to determine the effects of site-directed mutagenesis on substrate-binding or protein subunit-subunit interactions; to calculate a predicted binding interaction constant that is the sum of all atom-atom interactions between two species and to calculate LogP and hydropathic maps for use with conventional and 3D QSAR (quantitative structure-activity relationship) (Tripos Bookshelf HINT Manual 2006).

**V.C. Methods**

Molecular models of albuterol sulfate suspensions in HFA 134a were constructed and optimized in Sybyl. Figure V.1 shows the molecular structures of all the formulation components studied in the present study.

Figure V.1. Chemical Structures of the Formulation Components of Albuterol Sulfate HFA Suspension pMDIs studied

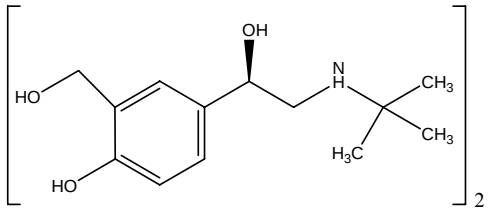


Albuterol Sulfate

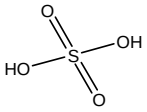


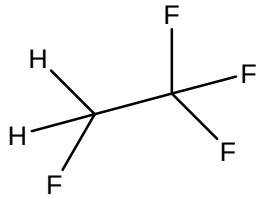


HFA 134a

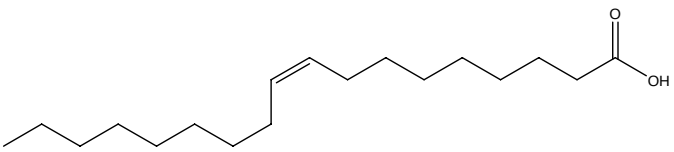


Oleic Acid

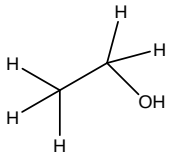


Ethanol

The molecular structure of albuterol sulfate was downloaded directly from the Cambridge small molecule crystallographic database. The crystal structure of a compound can be described in terms of a unit cell, which is the smallest arrangement of molecules, having the same symmetry and properties as that of the crystal; the unit cell repeats itself in a regular pattern to form a crystal lattice. The terms a, b, and c are the lengths of the edges of the unit cell while α, β and γ are the inclination angles of the edges of the unit

cell. The space group is a mathematical description of the symmetry inherent to a crystal structure. Albuterol sulfate consists of a monoclinic crystal structure and has the following parameters: a = 28.069, b = 6.183, c = 16.914 Å, α= γ=90˚, β = 81.9˚, Cc space group (Leger *et al.* 1978).

The chemical structures of HFA 134a, ethanol and oleic acid were drawn in Sybyl and energy minimization was performed. In the present study, energy minimization was performed until the difference in the energy values between two consecutive iterations was 0.005 kcal/mol Å or a maximum number of 1000 iterations (Tripos Bookshelf Force Field Manual 2006). The Gasteiger-Huckel method was employed to calculate the atomic charges for the molecule.

In order to study the interactions between albuterol sulfate (solvate) and the propellant (HFA 134a) molecules surrounding it, the explicit solvation technique available in Sybyl was used. The 'Precomputed Box' option in the 'Solvent' algorithm in Sybyl was used to create a three-dimensional periodic box lattice for the optimized molecular model of HFA 134a. The 3-D solvent lattice was generated and optimized; the density of HFA 134a at room temperature (1.21 g/cm$^3$ at 20 °C; Purewal 1998) was specified in the algorithm in order to simulate the pressurized liquid within the pMDI canister. The molecule of interest was solvated in the solvent box, i.e., it was placed in the solvent box and the energy of this solvate-solvent system was minimized. The process of energy minimization was used to optimize the conformation of solvent molecules in the vicinity of the solvate molecule in the periodic box. Energy minimization was performed with Gasteiger-Huckel charges and the dielectric constant of HFA 134a (ε = 9.5).

Using the above technique, an initial prototype molecular model of a single albuterol sulfate molecule in HFA 134a was built and energy minimized. Following preliminary investigation of the intermolecular interactions between albuterol sulfate and HFA 134a molecules, a unit cell of an albuterol sulfate crystal (consisting of eight molecules of albuterol and 4 sulfate groups; Leger *et al.* 1978) was used to create the remaining molecular models for albuterol sulfate suspensions in a propellant medium. Since non-covalently bonded interaction forces decrease exponentially with distance, interactions of albuterol sulfate with propellant molecules beyond a distance of 5 Å were not considered.

In order to study the interactions of oleic acid and ethanol with albuterol sulfate and HFA 134a, an approximate number of molecules of oleic acid and ethanol were calculated based on the number of HFA 134a molecules within a 5 Å radius around the albuterol sulfate unit cell. In the molecular models of the albuterol sulfate unit cell in a HFA 134a solvent box, an average of 84 molecules of HFA 134a were present within a 5 Å radius of the unit cell. The concentration of oleic acid and ethanol was assumed to be 0.02% and 15% w/w, corresponding to 0.03% and 19 %v/v, respectively. The approximate number of oleic acid and ethanol molecules that would occupy 0.03% and 19%, respectively, of the total volume occupied by an average of 84 molecules of HFA 134a was calculated. 20 molecules of ethanol were placed together with a unit cell of an albuterol sulfate crystal. Since the number of molecules of oleic acid (0.03% v/v) was less than 1, two oleic acid molecules were randomly placed near the albuterol sulfate unit cell such as to expose different regions of the unit cell to the surfactant molecule. The albuterol sulfate unit cell,

along with the ethanol and oleic acid molecules, was then solvated in a HFA 134a solvent lattice and energy minimization of this entire system was performed. The density of the HFA 134a solvent box was maintained constant at 1.21 g/cm$^3$ for all the molecular models constructed and hence the volume of the box and the number of HFA 134a molecules included increased in comparison to the model containing only the unit cell in the HFA solvent box.

For all the molecular models containing unit cell structures of albuterol sulfate, the positions of the solvated molecules were modified and energy minimization of the system was performed (n = 3). Following energy minimization, the molecular interactions within these systems were investigated using the HINT program within Sybyl. The total HINT score was the sum of individual contributions from the favorable interactions such as hydrophobic, acid-base and hydrogen bonds, as well as unfavorable interactions, e.g., hydrophobic-polar, base-base and acid-acid interactions. HINT also reported the individual contributions, in addition to the total HINT score, if the absolute value of the scores for the unfavorable or favorable interactions was greater than 10. Interaction scores lower than 10 would indicate weak interactions possibly due to the increasing distance between the interacting atoms. Nevertheless, the total HINT score for the interacting molecules included all those weak interactions. The interactions of the solvated molecule with solvent molecules beyond a radius of 5 Å around it were not considered since non-covalently bonded interaction forces decrease exponentially with distance.

## V. D. Results and Discussion

### V.D.1. Molecular Models of Albuterol Sulfate Suspensions in HFA 134a

Figure V.2.a shows the molecular model of a single albuterol sulfate molecule in a HFA 134a solvent box. A single molecule of albuterol sulfate was used to build a prototype of a simple suspension of albuterol sulfate in HFA 134a in order to study the interactions between the drug and the propellant molecules. Figure V.2.b shows the molecular model of albuterol sulfate in HFA 134a, which was used for determining the interactions between the drug and propellant molecules; only interactions within a 5 Å radius around the albuterol sulfate molecule were considered.

Figure V.2.a. Model of a Single Albuterol Sulfate Molecule Solvated in HFA 134a Solvent Lattice

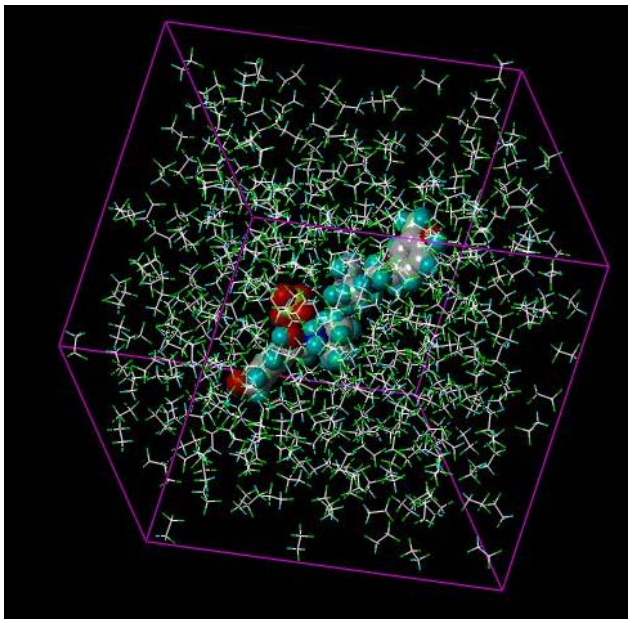

Figure V.2.b. Molecular Model of Albuterol Sulfate with HFA 134a Molecules Within a 5 Å Radius

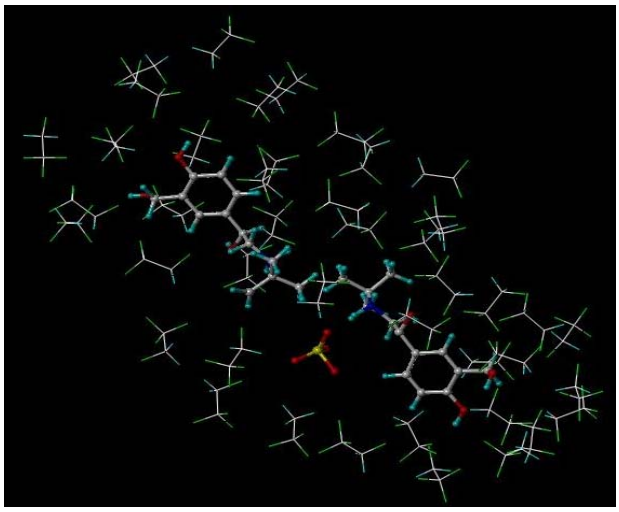

Molecular modeling software such as Sybyl is not adapted to study particle interactions (approximate particle size range 3 - 5 μm). Hence, in order to determine the feasibility of using Sybyl to build a model of a suspension pMDI, a preliminary prototype of an albuterol sulfate suspension in HFA 134a was first modeled by solvating a single albuterol sulfate molecule in a HFA 134a solvent lattice. Although HFA 134a could not be modeled as a pressurized liquid, the solvent lattice of HFA 134a was created so as to take the density of the propellant at room temperature (20 °C) into account. In addition, the dielectric constant used during the energy minimization was specified to be equal to that of the propellant. In order to obtain a practical model of albuterol sulfate particles suspended in HFA 134a, a unit cell of an albuterol sulfate crystal (consisting of eight albuterol molecules and four sulfate groups; Figure V.3) was solvated in HFA 134a using the same parameters as those set for the initial prototype model of albuterol sulfate molecule in HFA 134a.

Figure V.3. Model of an Albuterol Sulfate Unit Cell

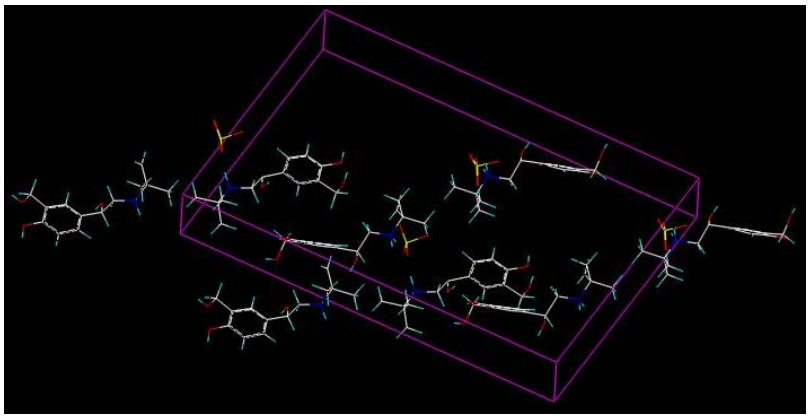

Two approaches have been employed to formulate commercial albuterol sulfate HFA suspension pMDIs. Ventolin HFA is a simple suspension of albuterol sulfate in 100% HFA 134a without any surfactant. Another marketed albuterol sulfate HFA suspension pMDI, Proventil HFA, is a more complex suspension of albuterol sulfate suspension in HFA 134a containing oleic acid as a surfactant and ethanol as a cosolvent. In order to study the interactions of oleic acid and ethanol with albuterol sulfate and HFA 134a, molecular models containing an albuterol sulfate unit cell, 2 molecules of oleic acid and 20 molecules of ethanol solvated in a HFA 134a solvent box were created. Figure V.4 shows the albuterol sulfate unit cell as a space-filling model with ethanol and oleic acid molecules placed in the vicinity of the unit cell. Figure V.5 shows the three solvated components surrounded by HFA 134a molecules within a 5 Å radius.

Figure V.4. Representative Model of the Albuterol Sulfate Unit Cell (Space-filling Model) Along with Ethanol and Oleic Acid Molecules in the Vicinity of the Unit Cell

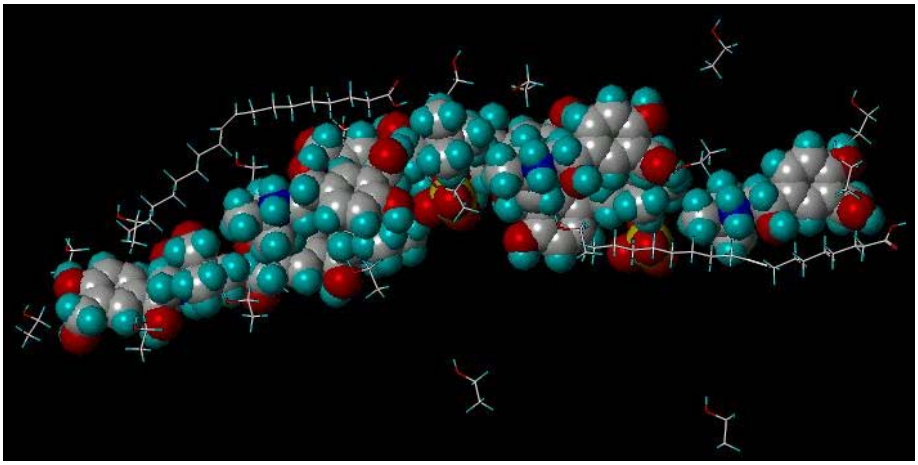

Figure V.5. Molecular Model of Albuterol Sulfate Unit Cell, Oleic Acid and Ethanol Molecules Surrounded by HFA 134a Molecules Within a 5 Å Radius

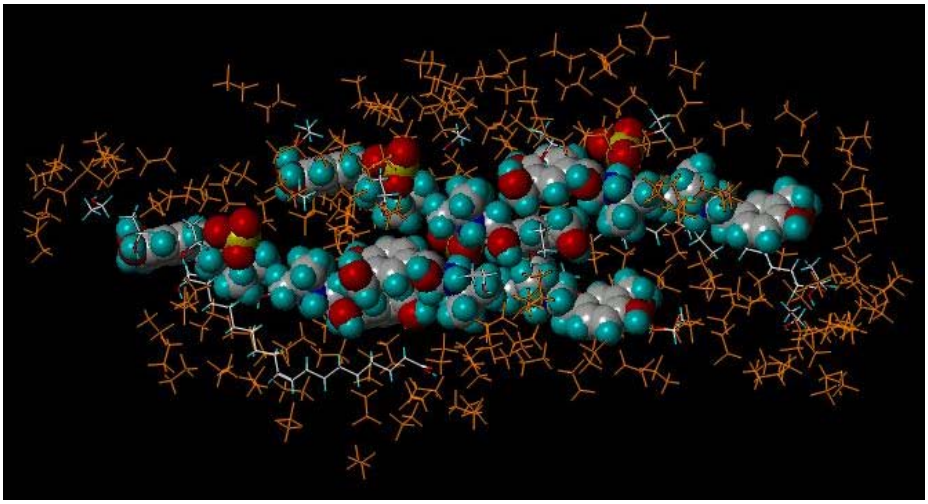

The molecular interactions within these optimized molecular models of albuterol sulfate HFA suspensions were analyzed using the HINT program.

## V.D.2. Interactions within Albuterol Sulfate HFA Suspensions

### V.D.2.1. Interactions Between Albuterol Sulfate and HFA 134a Molecules

The HINT program accounted for the interactions between a single molecule of albuterol sulfate and each individual HFA 134a molecule within the 5 Å radius around it. For the molecular model containing a single albuterol sulfate molecule, 31 molecules of HFA 134a were within this range. The composite logP value calculated by the HINT program for the 31 molecules of HFA 134a was 36.51. Therefore, the logP for a single molecule of HFA 134a could be approximated to be 1.17, which was in good agreement with that reported in literature ($logP_{o/w}$: 1.06; Solvay Chemicals Solkane 134a MSDS 2003). The logP value for the albuterol sulfate molecule determined by HINT was -15.82. The HINT program calculates the logP based on the hydrophobic atom constants (a) for each atom in the molecule and denotes the hydrophobic nature of the molecule. The logP value can be positive or negative depending on the hydrophobic or polar nature of the atoms present in the molecule since $a < 0$ for polar atoms e.g. oxygen and halogen atoms and positive for hydrophobic atoms e.g. carbon. The logP values suggested that HFA 134a molecule was hydrophobic in comparison to albuterol sulfate.

Figure V.6 shows the chemical structure of HFA 134a, which contains two small asymmetrically placed hydrogen atoms along with the electronegative fluorine atoms together forming the mantel (surface atoms) of the molecule. The presence of electronegative fluorine atoms creates distinct dipoles in the carbon-hydrogen bonds in HFA 134a.

Figure V.6. Chemical Structure of HFA 134a and the Hydrophobic Atom Constants for the Carbon and Fluorine Atoms in HFA 134a

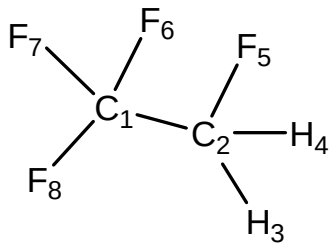


| Atom | Hydrophobic Atom Constant (a) |
|---|---|
| $C_1$ | 0.984 |
| $C_2$ | -0.472 |
| $F_5$ | -0.428 |
| $F_6$ | 0.255 |
| $F_7$ | 0.255 |
| $F_8$ | 0.255 |

The fluorine atom ($F_5$) attached to $C_2$ (which also has the two asymmetric hydrogen atoms ($H_3$ and $H_4$) attached to it) has a negative hydrophobic atom constant of –0.428. Due to the dipole created between the C-H bonds in HFA 134a, $C_2$ also has a negative hydrophobic atom constant of –0.472. The hydrophobic atom constant calculated by HINT for all three fluorine atoms ($F_6$, $F_7$, $F_8$) attached to $C_1$ was +0.255, while that for $C_1$ was 0.984 implying that these atoms are hydrophobic relative to $C_2$ and $F_5$. Thus the fluorine atoms in HFA 134a show both hydrophobic as well as polar (electronegative) characteristics.

The total HINT interaction score was calculated as the sum of the individual HINT scores for interactions between albuterol sulfate and each of the 31 molecules of HFA 134a. Table V.1 summarizes the individual contributions from the various non-covalent interactions including hydrophobic, hydrogen bonding, acid-base, hydrophobic-polar and base-base, to the total HINT score.

Table V.1. HINT Score Analysis for the Contributing Interactions Within a Molecular Model of a Single Albuterol Sulfate Molecule in HFA 134a

| Type of Interaction | | | | | |
|---|---|---|---|---|---|
| Hydrophobic | H-Bond | Acid-Base | Hydrophobic/ Polar | Base-Base | Total |
| 960 | 469 | 150 | -3402 | -720 | -2543 |

The total HINT score was predominantly negative (HINT score: -2543) signifying unfavorable interactions between the albuterol sulfate molecule and the surrounding HFA 134a molecules. Hydrophobic interactions, hydrogen bonds and acid-base interactions contributed to favorable or positive interaction scores between albuterol sulfate and HFA 134a molecules while hydrophobic-polar and base-base interactions accounted for the unfavorable or negative HINT scores. Table V.1 shows that negative or unfavorable interactions were predominantly contributed by hydrophobic-polar interactions in the albuterol sulfate / HFA 134a system. Hydrophobic-polar interactions arise when polar atoms or groups, either acidic or basic, are either trapped in a hydrophobic pocket or come in close proximity to the hydrophobic groups of the neighboring molecule). These interactions represent the energy required to desolvate the polar groups and place them in an unfavorable (hydrophobic) environment and hence are negatively scored by HINT (Kellogg and Abraham 2000).

Figure V.7.a summarizes the likely interactions between atoms, which could contribute to favorable interactions between albuterol sulfate and HFA 134a molecules as determined by HINT analysis. Hydrophobic interactions included those between carbon atoms on the side chain of albuterol sulfate and the two carbon atoms present in HFA 134a.

Interactions between the sulfur (sulfate group) of albuterol sulfate and carbon atoms of HFA 134a have also been classified as favorable hydrophobic type, however, this interaction is unlikely to occur and may therefore be an artefact. Interactions between fluorine atoms of HFA 134a connected to $C_1$ and carbon atoms on the albuterol sulfate side chain were also hydrophobic in nature which would be expected since fluorine atoms in the $-CF_3$ group of HFA 134a were classified as having hydrophobic character (a = +0.255).

Figure V.7.a. Examples of Favorable Non-covalent Interactions Between Albuterol Sulfate and HFA 134a Molecules

Hydrophobic interactions between $CH_3$ of albuterol sulfate and $CF_3$ of HFA 134a

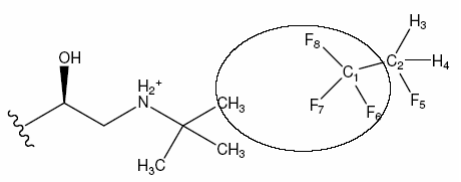


Hydrophobic interactions between $C_1$ and $S_1$

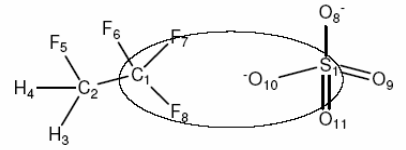


Acid-base or H-bond interactions between N and F, O and F

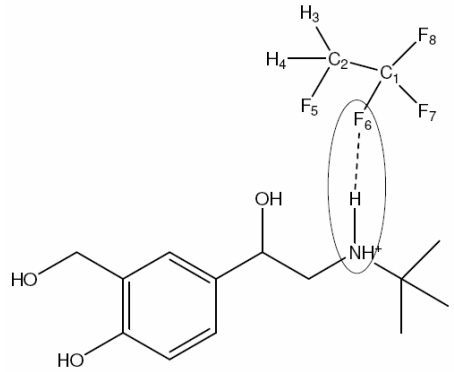


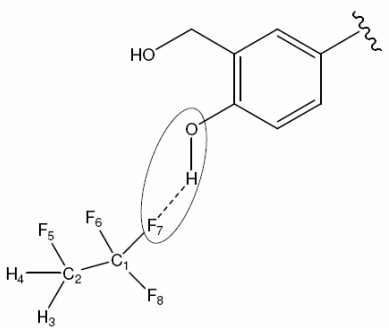


In addition to its hydrophobic character in HFA 134a, since fluorine atom needs only one electron to completely fill its valence shell, the atom is very electronegative and

may therefore also contribute to acid-base type interactions with polar groups in albuterol sulfate. Figure V.7.a displays possible acid-base interactions including those between fluorine atoms of HFA 134a and the -OH or -NH group of the albuterol sulfate molecule. When the distance between the interacting atoms is less than 3.65 Å, acid-base interactions were classified as hydrogen bonds. The hydrogen bond length between fluorine atoms of HFA 134a and the oxygen (hydroxyl group) or nitrogen (amine group) atoms of albuterol sulfate ranged from 2.67 - 3.65 Å. Figure V.7.a displays hydrogen bonds (shown as -----) between albuterol sulfate and HFA 134a molecules. Figure V.7.b illustrates the likely atoms involved in unfavorable interactions between albuterol sulfate and HFA 134a molecules.

Figure V.7.b. Examples of Unfavorable Non-covalent Interactions Between Albuterol Sulfate and HFA 134a Molecules

Hydrophobic-polar interactions between $C_1$ and O

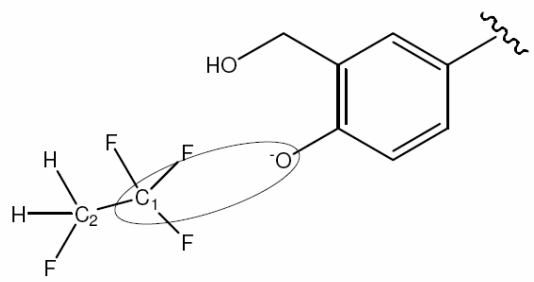


Base-Base Interactions between $C_1$ and N

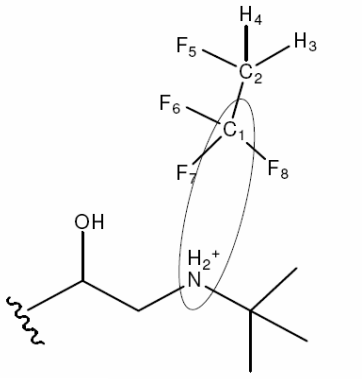


Base-Base Interactions between $F_7$ and $O_{10}$

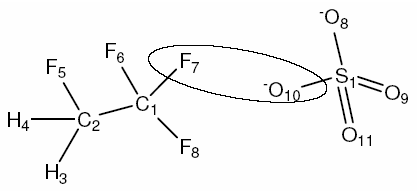

Negative HINT scores were contributed by unfavorable interactions between the hydrophobic carbon atoms of the HFA 134a molecule and the polar oxygen (hydroxyl) or nitrogen (amine) atoms of the albuterol base molecule. Unfavorable base-base type interactions included those between the fluorine atoms of HFA 134a and the oxygen atoms attached to the sulfate group of the albuterol sulfate molecule.

Placing the solvate (albuterol sulfate) molecule in the solvent (HFA 134a) box involves removal of solvent molecules to fit in the solvate molecule, and this may sometimes result in either empty spaces between the solvate and the surrounding solvent molecules or the solvate and some of the solvent molecules being placed too close together. Minimization of energies will prevent any unreasonable interactions between closely placed molecules by optimizing the conformation of the molecules. However, a visual check was performed to ensure that the negative interactions were not due to the solute and solvent molecules placed too close to each other.

Since albuterol sulfate consists of polar hydroxyl groups on its surface (Figure V.1), formation of hydrogen bonds with the mantel fluorine atoms would be expected, while interactions between the sulfate group and fluorine atoms would be repulsive. Solubility of albuterol sulfate in 100% HFA 134a has been reported to be negligible (lower than 0.0005 μg/mg using a UV-Visible detection technique; Tzou *et al.* 1997), which would be predictable since the interactions between the two molecules were observed to be predominantly unfavorable.

### V.D.2.2. Interactions between the Albuterol Sulfate Unit Cell and HFA 134a Molecules

For the molecular model containing an albuterol sulfate unit cell in HFA 134a, the interaction of the unit cell with an average of 84 molecules of HFA 134a within a 5 Å radius was considered. The HINT calculated logP values for the albuterol sulfate unit cell and the surrounding HFA 134a molecules were –63.65 and 143, respectively. Since four units of the albuterol sulfate molecule are present in the unit cell of the crystal, the calculated LogP for the unit cell was approximately four times that of a single albuterol sulfate molecule. Table V.2 summarizes the individual contributions to the total HINT score for the interactions of the albuterol sulfate unit cell with each of the surrounding HFA 134a molecules.

Table V.2. HINT Score Analysis with the Contributing Interactions for the Albuterol Sulfate Unit Cell Solvated in HFA 134a

| Albuterol sulfate unit cell in HFA 134a | Type of Interaction | | | | | |
|---|---|---|---|---|---|---|
| | Hydrophobic | H-Bond | Acid/Base | Hydrophobic/ Polar | Base/Base | Total |
| 1 | 4158 | 1412 | 1918 | -10108 | -6503 | -9122 |
| 2 | 4284 | 2582 | 2067 | -9958 | -7395 | -8420 |
| 3 | 3373 | 1531 | 1706 | -6920 | -4940 | -5249 |
| Mean | 3939 | 1842 | 1897 | -8995 | -6280 | -7597 |
| SD | 494 | 644 | 182 | 1799 | 1243 | 2063 |

The mean total HINT score was negative (-7597 ± 2063) and small changes in the position of the unit cell of albuterol sulfate within the HFA 134a solvent box did not cause a marked change in the total HINT interaction score. The interactions remained similar to

those observed for the albuterol sulfate molecule-HFA 134a model but the scores were higher since both the number of albuterol sulfate molecules and the HFA 134a molecules surrounding the unit cell were higher. In order to obtain a better understanding of all the possible interactions between the unit cell and HFA 134a molecules and to have confidence in the HINT scores for these interactions, a large number of replicates (approximately 20 replicates) would be required. Nevertheless, this pilot study provided a theoretical understanding of intermolecular interactions possible within an albuterol sulfate - HFA 134a suspension pMDI.

Further analysis of the individual HINT scores for interactions between the albuterol sulfate unit cell and each individual HFA 134a molecule revealed that the HINT interaction scores could be either positive or negative depending upon the relative position of the molecules (Appendices A.III.1 and A.III.2). The majority of the HFA 134a molecules (an average of 73% of HFA 134a molecules) surrounding the albuterol sulfate unit cell exhibited a net negative HINT score. Fewer hydrophobic-polar and base-base interactions were found for HFA 134a molecules with net positive interactions with the albuterol sulfate unit cell as compared to those with a net negative HINT interaction score. The range of net negative HINT scores obtained for interactions between the albuterol sulfate unit cell and a single molecule of HFA 134a was –1 to –1080, while the net positive HINT scores for albuterol sulfate unit cell interacting with individual HFA 134a molecules was +1 to +239 over the three models studied. The average HINT score calculated for net positive and negative interactions between albuterol sulfate and a single HFA 134a molecule were +35 ± 18 and –136 ± 32, respectively.

The present study showed that interactions between albuterol sulfate and HFA 134a molecules are a composite of hydrophobic and polar interactions. Since most of the interactions between the two molecules are accounted for by unfavorable hydrophobic-polar interactions, it would not be unexpected to observe drug adhesion to canister walls and/or the valve-metering chamber in pMDIs. Recent studies employing AFM and surface energy measurements have demonstrated that adhesion of drug particles such as albuterol sulfate to canister material such as aluminum or PTFE was dependent on both the dispersive and polar components of particle interactions in a model HFA propellant (HPFP) (Traini *et al.* 2006). In the present study, interactions between albuterol sulfate and HFA 134a were observed to be a function of both unfavorable hydrophobic-polar and base-base interactions as well as favorable hydrophobic and polar acid-base interactions. Future studies using molecular modeling of albuterol sulfate in HFA 134a in the presence of different canister coating materials may provide an improved understanding of these experimentally derived results.

### V.D.2.3. Interactions within Albuterol Sulfate Suspensions in HFA 134a containing Oleic Acid and Ethanol

Table V.3 displays the HINT calculated logP values for the formulation components of the molecular model of albuterol sulfate HFA suspension pMDI containing ethanol and oleic acid. The logP values for albuterol sulfate and HFA 134a were similar to those obtained for the albuterol sulfate unit cell-HFA 134a model. Oleic acid has a high

logP value (7.61) indicating its hydrophobic nature. A negative logP of –0.32 signifies the polar nature of ethanol.

Table V.3. LogP of Formulation Components of Albuterol Sulfate Suspension pMDI Calculated by HINT

| Formulation Components | Total number of molecules | Total logP | LogP/Molecule |
|---|---|---|---|
| Albuterol Sulfate Unit Cell | 4 | -63.65 | -15.91 |
| Oleic Acid | 2 | 15.22 | 7.61 |
| Ethanol | 20 | -6.48 | -0.32 |
| HFA 134a (Average) | 169 | 142 | 0.84 |

In order to determine the interactions within this complex albuterol sulfate HFA formulation, interactions between each of the following components: albuterol sulfate, oleic acid and ethanol with the surrounding HFA 134a molecules were individually analyzed using HINT. Interactions between albuterol sulfate, oleic acid and ethanol molecules were also analyzed. The HINT scores for the three molecular models built and optimized by changing the positions of the solvated molecules within the HFA 134a solvent box have been summarized in Table V.4. These scores are the sum of the interactions between individual molecules within the model. It was observed that the total HINT interaction score for all the molecules studied was net negative with the exception of interactions between oleic acid and HFA 134a molecules suggesting that the net interactions between oleic acid and HFA 134a were favorable.

Table V.4 Summary of the Mean HINT Scores for Interactions Between the Albuterol Sulfate Unit Cell, Oleic Acid, Ethanol and HFA 134a Molecules. Values in Parentheses are Standard Deviation (n=3 models)

| Interacting Molecules | | Type of Interaction | | | | | |
|---|---|---|---|---|---|---|---|
| Molecule 1 | Molecule 2 | Hydrophobic | H-bond | Acid/ Base | Hydrophobic/ Polar | Base/ Base | Total |
| HFA 134a | Albuterol sulfate unit cell | 2641 (491) | 1435 (87) | 1443 (167) | -6850 (208) | -5200 (582) | -6531 (1366) |
| | Oleic Acid | 2619 (1263) | 344 (102) | 537 (159) | -1878 (553) | -1148 (401) | 474 (1266) |
| | Ethanol | 6774 (564) | 2685 (24) | 1426 (42) | -8321 (341) | -4605 (214) | -2041 (486) |
| Albuterol Sulfate Unit Cell | HFA 134a | 2641 (491) | 1435 (87) | 1443 (167) | -6850 (208) | -5200 (582) | -6531 (1366) |
| | Oleic acid | 378 (269) | 305 (239) | 328 (127) | -1326 (889) | -426 (306) | -846 (581) |
| | Ethanol | 936 (190) | 3025 (307) | 1565 (189) | -4686 (819) | -2940 (396) | -3584 (810) |
| Oleic Acid | HFA 134a | 2619 (1263) | 344 (102) | 537 (159) | -1878 (553) | -1148 (401) | 474 (1266) |
| | Albuterol sulfate unit cell | 378 (269) | 305 (239) | 328 (127) | -1326 (889) | -426 (306) | -846 (581) |
| | Ethanol | 212 (90) | 161 (280) | 223 (223) | -547 (206) | -211 (271) | -229 (113) |
| Ethanol | HFA 134a | 6774 (564) | 2685 (24) | 1426 (42) | -8321 (341) | -4605 (214) | -2041 (486) |
| | Albuterol sulfate unit cell | 936 (190) | 3025 (307) | 1565 (189) | -4686 (819) | -2940 (396) | -3584 (810) |
| | Oleic Acid | 212 (90) | 161 (280) | 223 (223) | -547 (206) | -211 (271) | -229 (113) |

The interactions within the molecular model of albuterol sulfate molecule and the unit cell in HFA 134a alone were simpler to analyze since the models contained only two components. However, the analysis of the interactions within a complicated formulation of albuterol sulfate in HFA 134a containing ethanol and oleic acid becomes challenging. Due to the nature of the HINT program, the interactions between all four components could not be analyzed simultaneously. Instead, the interactions between two components were analyzed individually and the results are summarized in Table V.4. The individual interactions summarized in Table V.4 will be discussed separately in the following sections.

### V.D.2.3.a. Interactions Between the Albuterol Sulfate Unit Cell and HFA 134a in the Presence of Oleic Acid and Ethanol

Table V.5 summarizes the total HINT scores and the contribution of the favorable and unfavorable interactions of albuterol sulfate with HFA 134a molecules in the presence of oleic acid and ethanol. Table V.5 shows that the interactions between the albuterol sulfate unit cell and the surrounding HFA 134a molecules were predominantly unfavorable (-6531 ± 1336) as observed in Section V.D.2. The types of atoms involved in the interactions characterized by HINT were similar to those described in Section V.D.2. Table V.5 shows that the mean total HINT score was similar to that obtained for albuterol sulfate unit cell in HFA 134a alone (-7597 ± 2063).

Table V.5. HINT Score Analysis with the Contributing Interactions for Albuterol Sulfate Unit Cell Solvated in HFA 134a Containing Oleic Acid and Ethanol

| Albuterol sulfate unit cell/ HFA 134a | Type of Interaction | | | | | |
|---|---|---|---|---|---|---|
| | Hydrophobic | H-bond | Acid/Base | Hydrophobic/ Polar | Base/Base | Total |
| 1 | 3199 | 1387 | 1621 | -6636 | -4529 | -4959 |
| 2 | 2448 | 1536 | 1417 | -7051 | -5557 | -7206 |
| 3 | 2276 | 1383 | 1291 | -6865 | -5515 | -7429 |
| Mean | 2641 | 1435 | 1443 | -6850 | -5200 | -6531 |
| SD | 491 | 87 | 167 | 208 | 582 | 1366 |

An average of 107 molecules of HFA 134a showed significant interactions with the unit cell of albuterol sulfate with 68% of the HFA 134a molecules exhibiting net negative interactions. Appendices A.III.3 and A.III.4 show the summary of net positive and negative interactions for the albuterol sulfate unit cell with HFA 134a molecules in the presence of oleic acid and ethanol. The maximum net negative HINT score for interactions between the albuterol sulfate unit cell and individual HFA 134a molecules was –1119 while that for net positive interactions between albuterol sulfate unit cell and a single HFA 134a molecule was +249. The average net negative and positive HINT scores calculated for interactions between the unit cell and a single HFA 134a molecule were –97 ± 1 and +14 ± 11, respectively. Unfavorable interactions were predominant similar to that observed for the albuterol sulfate unit cell-HFA 134a model.

### V.D.2.3.b. Interactions between Oleic Acid and HFA 134a molecules in the Presence of Albuterol Sulfate and Ethanol

Table V.6 shows that the average total HINT score for interactions between oleic acid and HFA 134a molecules was +474 ± 1266. The variability in the total HINT scores was high as shown in Table V.6. For the first model, the HINT score was net negative (-632) while it was positive for the other two models (199 and 1855). Changing the position of oleic acid molecules with respect to the albuterol sulfate unit cell in the molecular model resulted in favorable interactions between oleic acid and the surrounding HFA 134a molecules. The hydrophobic interactions between oleic acid and HFA 134a molecules were predominantly responsible for the favorable interactions.

Table V.6. HINT Score Analysis with the Contributing Interactions for 2 Oleic Acid Molecules Solvated in HFA 134a in the Presence of Albuterol Sulfate Unit Cell and Ethanol

| Oleic acid/ HFA 134a | Type of Interaction | | | | | |
|---|---|---|---|---|---|---|
| | Hydrophobic | H-bond | Acid/Base | Hydrophobic/ Polar | Base/Base | Total |
| 1 | 2172 | 444 | 643 | -2448 | -1443 | -632 |
| 2 | 1640 | 240 | 354 | -1344 | -691 | 199 |
| 3 | 4044 | 348 | 613 | -1842 | -1309 | 1855 |
| Mean | 2619 | 344 | 537 | -1878 | -1148 | 474 |
| SD | 1263 | 102 | 159 | 553 | 401 | 1266 |

Since the two oleic acid molecules in the molecular model were arbitrarily placed in the vicinity of the albuterol sulfate unit cell, not all HFA 134a molecules present in the molecular model interacted with the two oleic acid molecules since the interactions between the molecules decrease exponentially as a function of distance. An average of 59

molecules of HFA 134a exhibited significant interactions with the oleic acid molecules. It was observed that an average of 40 HFA 134a molecules exhibited favorable interactions with the oleic acid molecules while an average of 18 HFA 134a molecules exhibited net unfavorable interactions (Appendices A.III.5 and A.III.6). The average net positive HINT score for interactions between oleic acid and a single HFA 134a molecule was estimated to be 39 ± 11, which was lower than the average net negative HINT score (-63 ± 11). The maximum net positive score for interactions between oleic acid molecules and a single molecule of HFA 134a was +170, while that for net negative HINT score was –296. Unfavorable hydrophobic-polar and base-base interactions were predominant for the molecules with a net negative HINT interaction score.

Figures V.8.a summarizes the atoms involved in the favorable interactions between oleic acid and HFA 134a molecules as determined by HINT. Interactions between any of the three fluorine atoms attached to $C_1$ of HFA 134a with the non-polar carbon atoms on oleic acid was classified as a favorable hydrophobic interaction (Figure V.8.a). Favorable acid-base interactions included those between –COOH group of oleic acid and the fluorine atoms in the HFA 134a molecule. Hydrophobic interactions also involved the non-polar carbon atoms, for example, as shown in Figure V.8.a, interactions between $C_6$ on the oleic acid and $C_1$ on the HFA 134a molecule.

Figure V.8.b shows some of the possible unfavorable interactions, which included hydrophobic-polar as well as base-base interactions. Hydrophobic-polar interactions included interactions between the polar –COOH group of oleic acid and the carbon atoms in HFA 134a as well as interactions with any of the fluorine atoms attached to $C_1$. Base-

base interactions included those between $–COO^-$ of oleic acid and the fluorine atoms of HFA 134a.

Figure V.8.a. Examples of Favorable Interactions Between Oleic Acid and HFA 134a Molecules

Hydrophobic interactions between $C_4$ and $F_8$

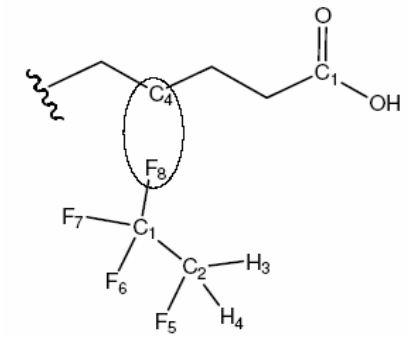


Acid-Base interactions between $F_5$ and –COOH

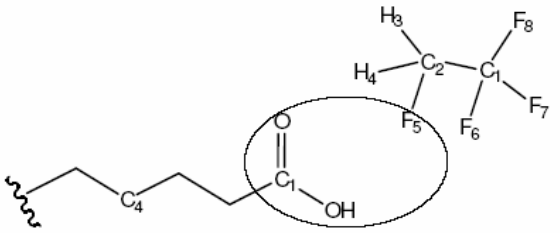


Hydrophobic interactions between C6 and $C_1$

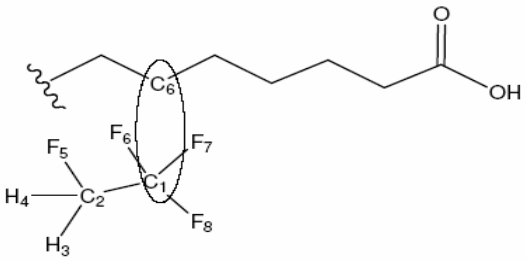


Figure V.8.b. Examples of Unfavorable Interactions Between Oleic Acid and HFA 134a Molecules

Hydrophobic-Polar Interactions between $C_1$ and O

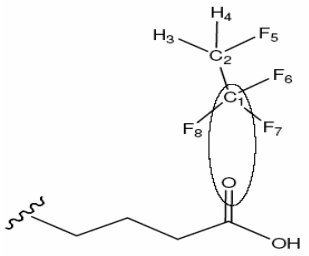


Base-Base Interactions Between $F_6$ and O

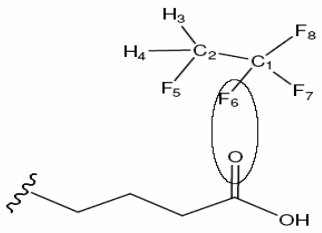

Oleic acid is insoluble in HFA 134a and hence cannot be used as a suspending agent in suspensions containing HFA 134a alone. Ethanol is used as a cosolvent for oleic acid in HFA suspension pMDIs. It has been suggested that the reason for the poor performance of oleic acid as a surfactant in suspensions containing HFA 134a alone may possibly be the unfavorable interactions between the polar HFA 134a molecules and the hydrophobic portion of oleic acid (Byron et al. 1994). However, the same study has shown that precoating micronized albuterol with oleic acid before formulating a suspension in HFA 134a alone increased the time required for the drug to flocculate indicating that restricting the surface interactions of oleic acid molecules may improve its surfactant behavior in HFA 134a in the absence of a cosolvent. Analysis of molecular interactions between oleic acid and HFA 134a in the models of albuterol sulfate suspension in HFA 134a containing oleic acid and ethanol indicated that in addition to the unfavorable interactions between oleic acid and HFA 134a due to hydrophobic-polar interactions, favorable interactions between oleic acid and HFA 134a molecules were also likely due to both hydrophobic and acid-base type interactions.

#### V.D.2.3.c. Interactions between Ethanol and HFA 134a molecules in the presence of Albuterol Sulfate and Oleic Acid

Table V.7 summarizes the HINT scores for interactions between ethanol molecules and the surrounding HFA 134a molecules along with the individual contributions to the total HINT score.

Table V.7. HINT Score Analysis with the Contributing Interactions for 20 Ethanol Molecules Solvated in HFA 134a in the Presence of Albuterol Sulfate Unit Cell and Oleic Acid

| Ethanol/ HFA 134a | Type of Interaction | | | | | |
|---|---|---|---|---|---|---|
| | Hydrophobic | H-bond | Acid/Base | Hydrophobic/ Polar | Base/Base | Total |
| 1 | 6123 | 2710 | 1396 | -8244 | -4384 | -2399 |
| 2 | 7112 | 2684 | 1473 | -8694 | -4811 | -2235 |
| 3 | 7087 | 2662 | 1408 | -8025 | -4620 | -1488 |
| Mean | 6774 | 2685 | 1426 | -8321 | -4605 | -2041 |
| SD | 564 | 24 | 42 | 341 | 214 | 486 |

The mean total HINT score was negative (-2041 ± 486) for interactions between 20 ethanol molecules and an average of 143 molecules of HFA 134a. The contribution of hydrophobic interactions to the favorable interactions was higher than that of hydrogen bonds and acid-base interactions. Most of the unfavorable interactions were contributed by the hydrophobic-polar interactions between the cosolvent and propellant molecules. Base-base interactions also contributed to the unfavorable interactions.

Appendices A.III.7 and A.III.8 provides a summary of the net positive and negative HINT scores for interactions between ethanol and HFA 134a molecules. The average number of HFA 134a molecules in the model exhibiting positive interactions (74 ± 7) with ethanol molecules was not significantly different ($p < 0.05$) than those exhibiting negative interactions (69 ± 11). The average net positive and negative HINT scores for interactions between ethanol molecules with an individual HFA 134a molecule were 26 ± 5 and –59 ± 11, respectively. The maximum net positive HINT score for interactions between ethanol and a single HFA 134a molecule for the three molecular models tested was +128 while that for the net negative score was –326. It was observed that hydrophobic interactions between

ethanol and HFA 134a molecules were predominantly responsible for the net positive interaction scores while hydrophobic-polar interactions were predominantly responsible for the net negative HINT score.

Figure V.9.a illustrates examples of favorable interactions between ethanol and HFA 134a molecules. Interactions between the carbon atoms of ethanol and HFA 134a molecules would be hydrophobic while acid-base or H-bonds would be contributed by interactions between the hydroxyl group of ethanol and fluorine atoms of HFA 134a.

Figure V.9.a. Examples of Favorable Interactions Between Ethanol and HFA 134a Molecules

Hydrophobic Interactions between $C_1$ of HFA and $C_2$ of ethanol

Acid-base Interactions between $F_8$ of HFA and -OH of ethanol

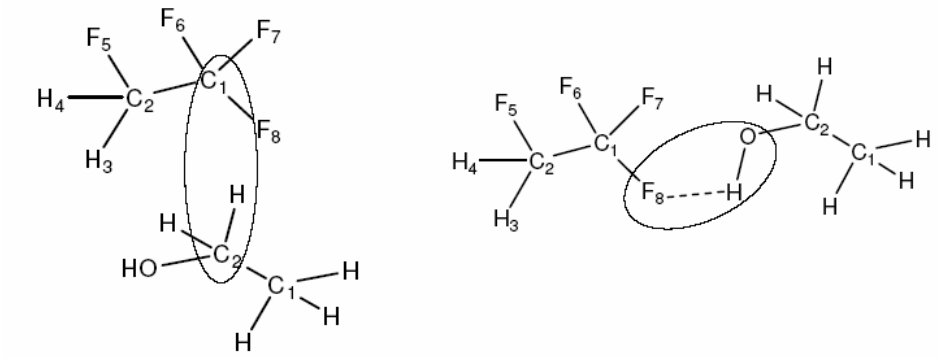


Figure V.9.b shows some of the possible unfavorable interactions between ethanol and HFA 134a molecules. Interactions between the carbon atoms (e.g. $C_1$) of the HFA 134a molecule and the hydroxyl group of ethanol as well as those between carbon atoms of ethanol (e.g. $C_1$) and the fluorine atom ($F_5$) attached to the $C_1$ atom of HFA 134a were

classified as hydrophobic-polar. Base-base interactions would possibly involve interactions between the hydroxyl group of ethanol and fluorine atoms of HFA 134a.

Figure V.9.b. Examples of Unfavorable Interactions Between Ethanol and HFA 134a Molecules

Hydrophobic-polar interactions between $C_1$ of HFA and –OH of ethanol

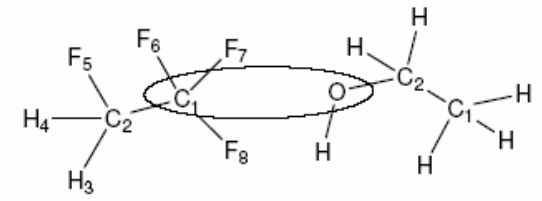


Base-base interactions between $F_7$ of HFA and –OH of ethanol

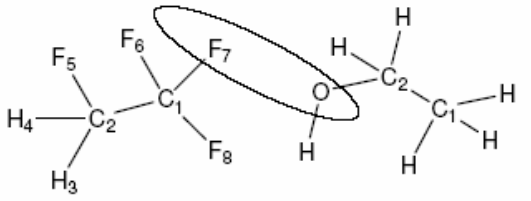


Hydrophobic-polar interactions between $F_5$ of HFA and $C_1$ of ethanol

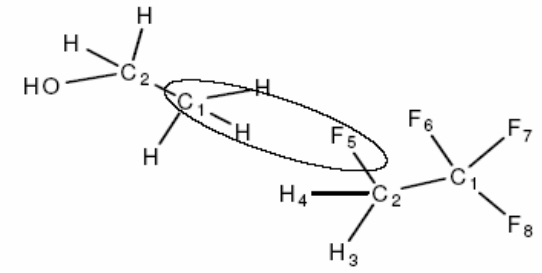


Conventional wisdom suggests that interactions between ethanol and HFA 134a would be favorable owing to the polar nature of ethanol as well as due to the possibility of strong dipole formation in HFA 134a molecule (Vervaet and Byron 1999). In the present study, ethanol molecules were placed arbitrarily around the albuterol sulfate unit cell, hence interactions between HFA 134a molecules and the ethanol molecules within such a molecular model will depend on both the distance and the orientation of the molecules.

Although, the interactions were predominantly unfavorable, there was evidence of favorable polar interactions, e.g., acid-base and hydrogen bonding between ethanol and HFA 134a molecules.

### V.D.2.3.d. Interactions Between Albuterol Sulfate, Oleic Acid and Ethanol Molecules in the presence of HFA 134a

Interactions between the solvate components of the molecular model containing albuterol sulfate, oleic acid and ethanol in HFA 134a were analyzed using HINT and the results are shown in Tables V.8 - V.10. Each set of interactions will be discussed separately.

**Molecular Interactions between the Albuterol Sulfate Unit cell and Oleic Acid**

Table V.8 summarize the total HINT scores for interactions between the albuterol sulfate unit cell and oleic acid molecules in the presence of ethanol and HFA 134a.

Table V.8. HINT Score Analysis with the Contributing Interactions for Albuterol Sulfate Unit Cell with Oleic Acid in the Presence of Ethanol and HFA 134a

| Albuterol Sulfate Unit Cell/ Oleic Acid | Type of Interaction | | | | | |
|---|---|---|---|---|---|---|
| | Hydrophobic | H-bond | Acid/Base | Hydrophobic/ Polar | Base/Base | Total |
| 1 | 473 | 40 | 184 | -1228 | -109 | -659 |
| 2 | 586 | 371 | 372 | -2260 | -451 | -1497 |
| 3 | 74 | 504 | 427 | -491 | -718 | -381 |
| Mean | 378 | 305 | 328 | -1326 | -426 | -846 |
| SD | 269 | 239 | 127 | 889 | 306 | 581 |

The HINT scores suggested that interactions between albuterol sulfate and oleic acid were unfavorable (-846 ± 581), which were predominantly due to hydrophobic-polar interactions. Changes in the position of oleic acid molecules resulted in a decrease in hydrophobic interactions while the number of H-bond and acid-base interactions increased as shown in Table V.8. It was observed that the unfavorable hydrophobic-polar interactions decreased from –1228 for molecular model 1 to –491 for model 3. However, the total unfavorable base-base interactions increased from –108 to -718.

Figure V.10.a shows some of the possible interactions between albuterol sulfate and oleic acid molecules contributing to favorable interactions.

Figure V.10.a. Examples of Favorable Interactions Between Albuterol Sulfate and Oleic Acid Molecules

Favorable Acid-Base Interaction between N and O

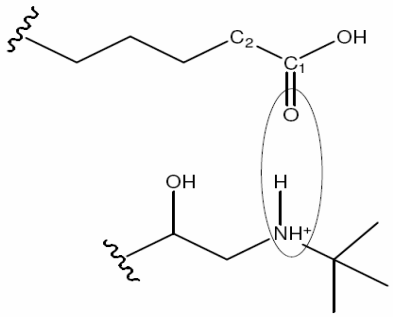


Favorable Hydrophobic Interactions between carbon atoms

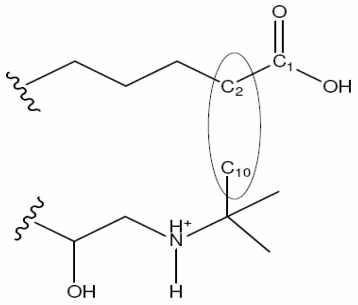


Favorable hydrophobic interaction between $C_2$ of oleic acid and S of albuterol sulfate

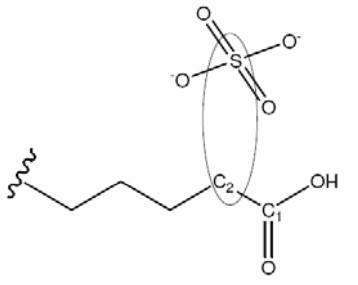

Favorable acid-base interactions included those between the oxygen atoms of the –COOH group of oleic acid and nitrogen from the amine group in albuterol sulfate. Figure V.10.a illustrates the favorable interactions contributed by hydrophobic interactions between carbon atoms of oleic acid and either carbon or sulfur atoms of albuterol sulfate.

Figure V.10.b shows examples of unfavorable interactions between albuterol sulfate and oleic acid. Interactions between the hydrophobic carbon atoms of oleic acid and polar amine or hydroxyl groups of the albuterol sulfate molecule were classified as unfavorable interactions.

Figure V.10.b. Examples of Unfavorable Interactions Between Albuterol Sulfate and Oleic Acid Molecules

Unfavorable hydrophobic-polar interaction between carbon atoms of oleic acid and amine group of albuterol sulfate

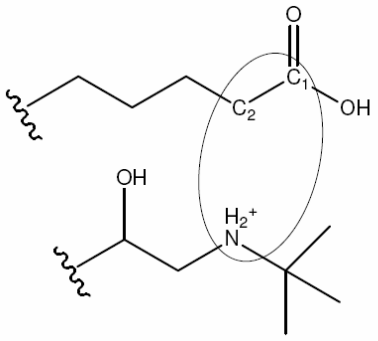


Unfavorable hydrophobic-polar interaction between $C_{18}$ and hydroxyl group

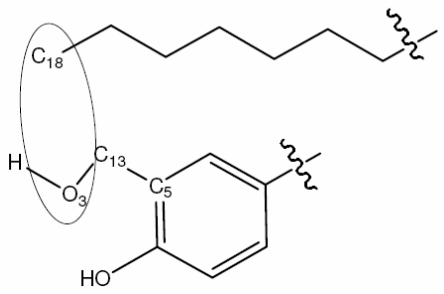

The interactions between oleic acid and the albuterol sulfate unit cell determined by HINT were dependent on the placement of the surfactant molecules around the unit cell in the model. The oleic acid molecules were arbitrarily placed near the albuterol sulfate unit cell and small changes in the orientation of the molecules with respect to the unit cell were made for the three molecular models. It may be possible to obtain a more representative value for the HINT scores for interactions between albuterol sulfate and oleic acid by repeating the above procedure multiple times, however, this would result in increased computational time for optimizing the models generated.

**Molecular Interactions between Albuterol Sulfate unit cell and Ethanol molecules**

Table V.9 shows that interactions between albuterol sulfate and ethanol were found to be predominantly negative (-3584 ± 810). The individual interaction scores contributing to the total HINT score were in the same order of magnitude between the three molecular models.

Table V.9. HINT Score Analysis with the Contributing Interactions for Albuterol Sulfate Unit Cell with Ethanol Molecules Solvated in HFA 134a

| Albuterol Sulfate Unit Cell/ Ethanol | Type of Interaction | | | | | |
|---|---|---|---|---|---|---|
| | Hydrophobic | H-bond | Acid/Base | Hydrophobic/ Polar | Base/Base | Total |
| 1 | 1155 | 2875 | 1711 | -5624 | -3201 | -4512 |
| 2 | 839 | 3378 | 1633 | -4322 | -3134 | -3216 |
| 3 | 814 | 2823 | 1352 | -4112 | -2484 | -3024 |
| Mean | 936 | 3025 | 1565 | -4686 | -2940 | -3584 |
| SD | 190 | 307 | 189 | 819 | 396 | 810 |

Figure V.11.a shows some of the possible interactions between albuterol sulfate and ethanol molecules contributing to favorable interactions. Favorable hydrophobic interactions included those between the carbon atoms of albuterol sulfate and ethanol molecules. Figure V.11.a also illustrates the favorable acid-base or hydrogen bond interactions between the hydroxyl groups of the two molecules. Figure V.11.b illustrates examples of possible unfavorable interactions between atoms of albuterol sulfate and ethanol. For example, as shown in Figure V.11.b, hydrophobic-polar interactions would include those between $C_1$ of ethanol and $O_3$ of albuterol sulfate. Hydrophobic-polar interactions can also be contributed by interactions between the sulfur group of albuterol sulfate and hydroxyl group of ethanol while base-base interactions can involve interactions between the hydroxyl group of ethanol and oxygen atom from the sulfate group of albuterol sulfate.

Figure V.11.a. Examples of Favorable Interactions Between Albuterol Sulfate and Ethanol Molecules

Favorable Hydrophobic Interactions between $C_{25}$ and $C_1$

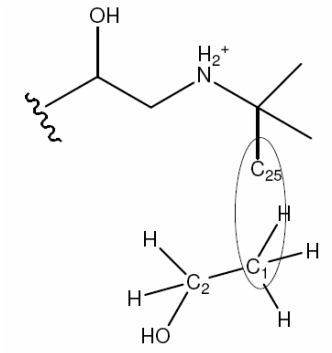


Favorable H-bond between the oxygen atoms attached to $C_2$ of ethanol and $C_{13}$ of albuterol sulfate

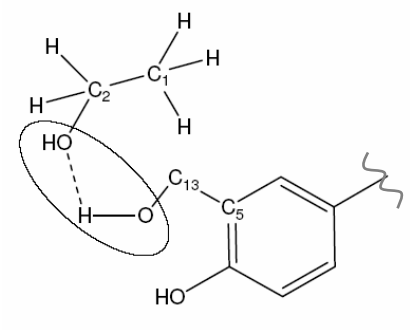

Figure V.11.b Examples of Unfavorable Interactions Between Albuterol Sulfate and Ethanol Molecules

Unfavorable hydrophobic-polar interactions between $C_1$ and $O_3$

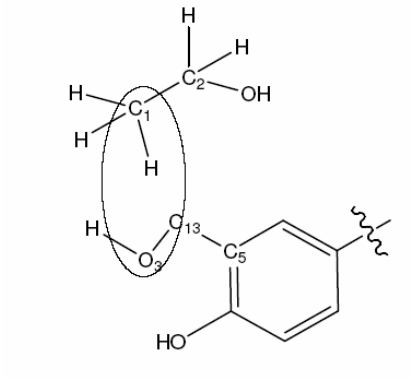


Unfavorable hydrophobic-polar interactions between $S_1$ and $O_3$ and base-base interactions between $O_3$ and $O_{10}$

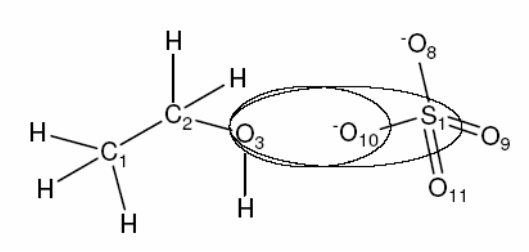


Ethanol is a polar molecule capable of forming hydrogen bonds with polar molecules such as albuterol sulfate within these formulations (Tzou *et al.* 1997), hence the interactions between the two molecules would be expected to be net positive or favorable. However, molecular modeling results showed that interactions between the two molecules were made up of both negative hydrophobic-polar and positive acid-base interactions. The orientation of the ethanol molecules as well as the distance between the respective atoms involved in the interactions would influence the interactions determined by HINT. In order to obtain a more reliable HINT score, all the likely interactions between ethanol and the albuterol sulfate unit cell arising from possible conformation of ethanol molecules with respect to albuterol sulfate would have to be considered. Although the three molecular models tested may not completely represent the possible particle interactions within an

albuterol sulfate suspension pMDI, an indication of the likely types of interactions could be obtained from the analysis of these models.

**Molecular Interactions between Oleic Acid and Ethanol Molecules**

Interactions between oleic acid and ethanol molecules are summarized in Table V.10. The average net HINT score for interactions between oleic acid and ethanol was negative (-229 ± 113). As observed in the Table V.10, the individual contributions e.g. hydrogen-bonding, acid-base and base-base interaction scores to the total HINT score increased from model 1 to model 3 due to the change in the positions of oleic acid and ethanol molecules. Since the oleic acid and ethanol molecules were randomly placed within the solvent box, it may be possible that some of the ethanol molecules do not interact with the oleic acid molecules or may exhibit weak interactions.

Table V.10. HINT Score Analysis with the Contributing Interactions Between Oleic Acid and Ethanol Molecules Solvated in HFA 134a

| Oleic Acid/ Ethanol | Type of Interaction | | | | | |
|---|---|---|---|---|---|---|
| | Hydrophobic | H-bond | Acid/Base | Hydrophobic/ Polar | Base/Base | Total |
| 1 | 316 | 0 | 58 | -662 | -38 | -340 |
| 2 | 167 | 0 | 135 | -308 | -72 | -114 |
| 3 | 153 | 484 | 476 | -669 | -523 | -232 |
| Mean | 212 | 161 | 223 | -547 | -211 | -229 |
| SD | 90 | 280 | 223 | 206 | 271 | 113 |

Figure V.12 shows examples of possible unfavorable and favorable interactions between oleic acid and ethanol molecules. Hydrophobic interactions between the carbon atoms of oleic acid and ethanol molecules contribute to the favorable interactions. Acid-

base interactions between the hydroxyl group of ethanol and –COOH group of the oleic acid molecules were also classified as favorable interactions. Unfavorable interactions were contributed by hydrophobic-polar interactions. For example, Figure V.12 illustrates an example of an unfavorable interaction between hydrophobic carbon atom ($C_1$) of oleic acid and the polar hydroxyl group of ethanol.

Figure V.12. Examples of Favorable and Unfavorable Interactions between oleic acid and ethanol molecules

Favorable hydrophobic interactions between carbon atoms of the two molecules

Favorable acid-base interactions between –OH of ethanol and oxygen atom of –COOH of oleic acid

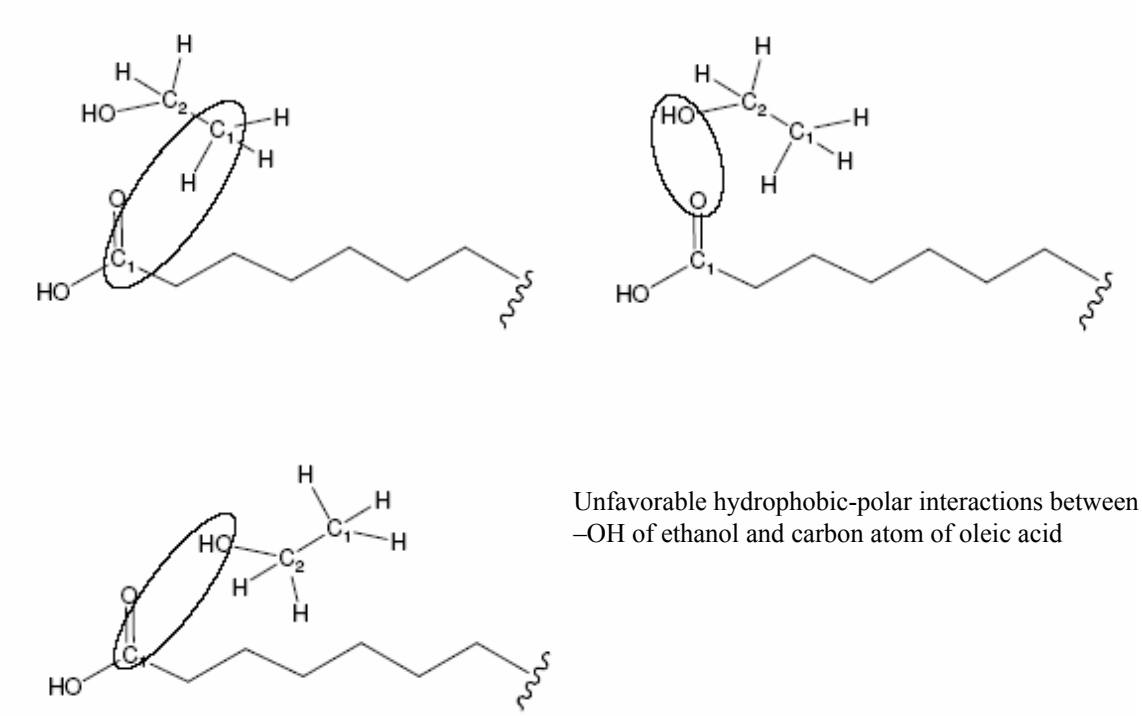

Unfavorable hydrophobic-polar interactions between –OH of ethanol and carbon atom of oleic acid

Not all interactions between the two oleic acid molecules and the ethanol molecules were significant since the oleic acid and ethanol molecules were placed such that selected

sections of the albuterol sulfate unit cell were exposed to the surfactant and solvent molecules. As a result, only those ethanol molecules in the vicinity of oleic acid such that the interacting atoms were at a distance of about 5 Å exhibited significant interactions with the oleic acid molecules.

In summary, this pilot study involving molecular modeling of albuterol sulfate HFA suspension pMDIs provided an improved understanding of the possible interactions between the various components within the formulation. Analysis of interactions in two-component models, for example, the interactions between a single albuterol sulfate molecule and those of the albuterol sulfate unit cell with the surrounding HFA 134a molecules is possible with HINT. However, the study of interactions within a complex formulation, e.g., interactions within a molecular model containing albuterol sulfate unit cell, oleic acid and ethanol molecules solvated in a HFA 134a solvent box are significantly more challenging compared to the two-component system.

The molecular models were created such that the oleic acid and ethanol molecules were arbitrarily placed around the albuterol sulfate unit cell and finally placed inside the solvent box. It was therefore not possible to take into consideration the interactions between the solvated components within the model for every possible conformation with respect to the interacting molecules. Also, further analysis of the net negative and positive HINT scores for interactions per molecule between the solvated molecules, albuterol sulfate unit cell, oleic acid and ethanol, was not performed. Although, it was possible to obtain an overall understanding of interactions within a complex albuterol sulfate HFA suspension pMDI in this pilot study, further studies (large number of replicates) appear

warranted to better optimize the molecular models and to have increased confidence in the prediction of the possible interactions within these models.

The use of molecular dynamics could possibly provide improved molecular models of the albuterol sulfate HFA suspension pMDIs. However, the analysis of the interactions would still be extensive due to the number of interactions possible between these components. Nevertheless, molecular modeling in conjunction with the analysis of interactions using HINT may serve as a useful tool to provide a better understanding of interactions between pMDI formulation components. Studies could also usefully be extended to the investigation of canister coating materials used in pMDI canisters.

# VI. ELECTROSTATIC CHARGE AND SIZE DISTRIBUTION OF HYDROFLUOROALKANE (HFA) SOLUTION AND SUSPENSION PRESSURIZED METERED DOSE INHALERS (pMDIs)

## VI.A. Introduction

Aerosol clouds produced by pressurized metered dose inhalers (pMDIs) are highly charged and these charges may influence particle deposition behavior in the respiratory tract and valved holding chambers (VHCs) (Melandri *et al.* 1983, Peart *et al.* 1998, Bisgaard *et al.* 2002). Although, aerodynamic particle size is the major parameter influencing deposition in pMDIs, studies have also demonstrated that charge can influence particle deposition from aerosols (Melandri *et al.* 1983, Balachandran *et al.* 1991, Balachandran *et al.* 1997). In order to understand the impact of pMDI aerosol electrostatics on drug deposition, in-vitro measurement of aerosol electrostatic properties in relation to the particle size distribution is important. The modified Electrical Low Pressure Impactor (ELPI) enables measurement of the charge distribution of aerosol clouds as a function of particle size, and the simultaneous determination of the mass distribution using chemical analysis. Electrostatic charge characterization of commercial HFA based solution and suspension pMDIs using a modified ELPI has been reported (Kwok *et al.* 2005). QVAR, a solution HFA pMDI, was found to produce unipolar positively charged aerosol clouds

(mean net charge: +290 ± 230 pC) while suspension pMDIs such as Ventolin HFA and Flixotide produced bipolar charged aerosol clouds (mean net charge: -1100 ± 220 pC for Ventolin HFA and +450 ± 30 pC for Flixotide; (Kwok *et al.* 2005). However, a systematic study investigating the differences in the electrostatic charging characteristics of solution and suspension HFA pMDIs is lacking.

The objective of this study was to investigate the influence of formulation components on the electrostatic charging characteristics of solution and suspension HFA pMDIs. HFA propelled beclomethasone dipropionate (BDP) solution pMDIs and albuterol sulfate suspension pMDIs were chosen as the model pMDIs. The mass distributions of the aerosols produced by drug containing pMDIs were simultaneously characterized by chemical analysis using the modified ELPI.

## VI.B. Materials and Methods

### VI.B.1. HFA Propelled Solution pMDIs

#### VI.B.1.1. Commercially Available HFA Propelled BDP Solution pMDIs

QVAR 40 and 80 μg (Ivax Laboratories Inc., Miami, FL, USA; Lot # ED037A and Lot # 060086, respectively), BDP solutions in HFA 134a and ethanol, were obtained commercially and tested prior to their expiry dates.

### VI.B.1.2. Experimental HFA Propelled Solution pMDIs

QVAR pMDI is packaged using 3M Spraymiser valves. However, the experimental HFA solution pMDIs used in the present study were packaged in canisters crimped with Valois metered valves. Hence, the contents of QVAR 40 were repackaged into aluminum canisters fitted with 50 μL Valois metering valves, to allow the comparison of results which would not be confounded by changes in the particle charge and size distribution due to different packaging components between commercial and experimental HFA solution pMDI formulations.

HFA experimental solution pMDIs (lot size: 3 pMDIs for each formulation) including 100% HFA 134a, an ethanol and propellant blend (7% ethanol / 93% HFA 134a), and a BDP solution (0.08% BDP in 7% ethanol / 93% HFA 134a) were prepared by weight based on a targeted 10 g fill and packaged in 19 mL aluminum cut-edge canisters and fitted with Valois DF10/50 RCU/PBT 50 μL metered valves using the technique described in Chapter III.A.2.1. The BDP solution formulation provided a theoretical ex-valve dose of BDP equal to 50 μg / 50 μL.

### VI.B.2. HFA Propelled Suspension pMDIs

#### VI.B.2.1. Commercially Available HFA Propelled Albuterol Sulfate Suspension pMDIs

Ventolin HFA 100 μg (GlaxoSmithKline, Raleigh, NC, USA; Lot 4ZP3714), an albuterol sulfate suspension in HFA 134a, was obtained commercially and tested prior to its expiry date.

**VI.B.2.2. Experimental HFA Propelled Suspension pMDIs**

HFA experimental suspension pMDIs (lot size: 3 pMDIs for each formulation) including 100% HFA 134a and an albuterol sulfate suspension (0.2% albuterol sulfate in 100% HFA 134a) were prepared by weight based on a targeted 15 g fill and packaged in 19 mL aluminum cut-edge canisters fitted with Valois DF10/50 RCU/PBT 50 μL metered valves as described in Chapter III.A.2.2. The metering valves used were similar to those used for packaging Ventolin HFA pMDIs. Each canister of the albuterol sulfate suspension pMDIs provided a theoretical ex-valve dose of albuterol sulfate equal to 120 μg / 50 μL (equivalent to 100 μg albuterol base).

In order to test the influence of any soluble impurities on the electrostatic charging properties of the experimental albuterol sulfate suspension pMDIs, removal of the suspended drug from the formulations was necessary. The contents of the experimental 0.2% albuterol sulfate / 100% HFA 134a suspension pMDIs were transferred to aluminum canisters fitted with Valois continuous valves by the cold-filling technique. Briefly, the pMDI containing the formulation as well as the aluminum canister into which the formulation was to be transferred were cooled using a mixture of methanol and dry ice, following which the valve on top of the pMDI was removed, the formulation was quickly transferred to the chilled empty canister and a continuous valve was crimped in place.

After transfer into canisters with continuous valves, albuterol sulfate suspensions in HFA 134a (n = 3) were filtered through a filtration assembly (Dalby *et al.* 1991) into canisters fitted with Valois continuous valves. The filtration assembly comprised of a stainless steel microsyringe filter housing containing a 25 mm diameter Type A/E glass

fiber filter (Pall Corp., Ann Arbor, MI) sandwiched between stainless steel support screens (Millipore, Bedford, MA). Figure VI.1 is a schematic representation of the filtration technique used.

Figure VI.1. Schematic Diagram of the Filtration Assembly used for Filtration of Albuterol Sulfate Suspensions in HFA 134a

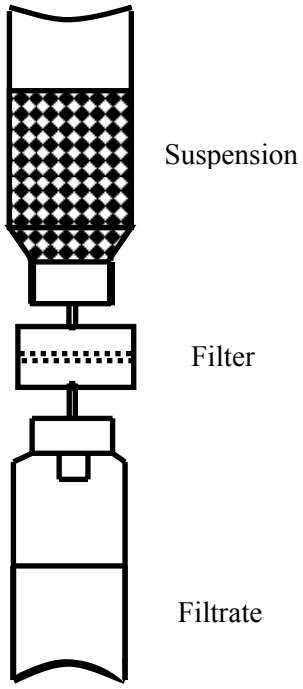


The filtrate obtained was then transferred into canisters fitted with Valois RCU/PBT DF 10/50 50 μL metered valves using the cold-filling technique described earlier. These pMDIs were stored overnight in a desiccator before testing to allow for any electrostatic charge acquired during the filtration process to be discharged through the conductive aluminum canister. Experimental 100% HFA 134a pMDIs subjected to the

same treatment, as described for the suspension pMDIs, served as the control pMDIs for the experiment.

All the experimental solution pMDIs were actuated using polypropylene actuators with an orifice diameter of 0.7 mm (Valois, Le Vaudreuil, France). The experimental pMDIs were stored in a desiccator immediately after manufacture and tested within 2 weeks.

### VI.B.3. Determination of Electrostatic Charge and Mass Distribution of Commercially Available and Experimental HFA 134a Solution and Suspension pMDIs using the Modified ELPI

The inherent electrostatic charge and subsequent mass distribution of aerosols produced by commercially available and experimental HFA 134a pMDIs were determined using a modified ELPI (Dekati Limited, Tampere, Finland) as described in Chapter III.B. Single shots of the pMDIs were actuated, n = 5 (5 shots / can, 1 can) for commercial pMDIs and n = 9 (3 shots / can, 3 cans) for experimental pMDIs, using a randomized block design, through a USP induction port into a modified ELPI (Figure III.1) operated at approximately 29 L/min. The canister was shaken for 5 sec and primed by firing either 2 or 4 shots to waste for HFA based solution and suspension pMDIs, respectively. The canister, fitted with a clean actuator, was then weighed, shaken for 5 sec, and actuated into the ELPI. The mass of each inhaler was recorded prior to, and following, each actuation into the ELPI as a procedural check to ensure accurate valve function, by checking to assess that the shot weight was within 5% of the target weight for that product.

The electrical current induced on each stage of the impactor by the tribocharged aerosol particles was measured as a function of time (20 sec); the net charge on each impactor stage was calculated as the area under the current vs. time curve. Background current measurements were performed. The correction algorithm employed by the ELPI software to account for diffusion losses of smaller particles was not used in these experiments (Dekati Ltd. Technical Note 2002). The net inherent charge of the aerosol cloud was calculated as the sum of the net charge on each of the impactor stages. Subsequently, the ELPI was disassembled and the actuator, USP induction port and thirteen impactor stages were washed with appropriate washing solvents, 60% acetonitrile / 40% water solution for BDP samples and 75% methanol / 25% water solution for albuterol sulfate samples. Drug deposition in the impactor for BDP and albuterol containing pMDI aerosols was quantified using validated HPLC analytical methods as described in Chapter III.C.2.1 and III.C.2.2, respectively. Trace quantities of albuterol deposited on stages 1-4 were determined using LC-MS (Chapter III.C.2.3). The mass of drug depositing on all stages below stage 11 of the ELPI (particles smaller than 4.05 μm, manufacturer-reported cut-off diameter of stage 11) was defined as the fine particle dose (FPD). The sum of the electrical charge of particles depositing below stage 11 was defined as the FPD charge.

All pMDIs were tested at temperatures between 23 - 24 $^{\circ}$C and relative humidity ranging from 20 - 43 %. The water content of the experimental pMDIs was also determined using Karl Fischer titration (Kulphaisal 2003). Precautions were taken to ensure that all inhalers and actuators were subjected to the same procedures throughout the study.

## VI.C. Results and Discussion

### VI.C.1. Electrostatic Charge and Mass Distribution of HFA Propelled Solution pMDIs

#### VI.C.1.1. Effect of BDP Concentration in HFA Based BDP Solution pMDIs on Electrostatic Charge

Figure VI.2 summarizes the mean net inherent charge of aerosols produced by QVAR 40 and QVAR 80 pMDIs on stages 1 - 12 of the ELPI.

Figure VI.2. Electrostatic Charge Distribution of Aerosols Produced by QVAR 40 and QVAR 80 pMDIs (n = 5 Shots / Can, 1 Can). Appendices A.IV.1.1 - A.IV.1.4 List the Electrostatic Charge Data for Background Measurements and Individual Shots.

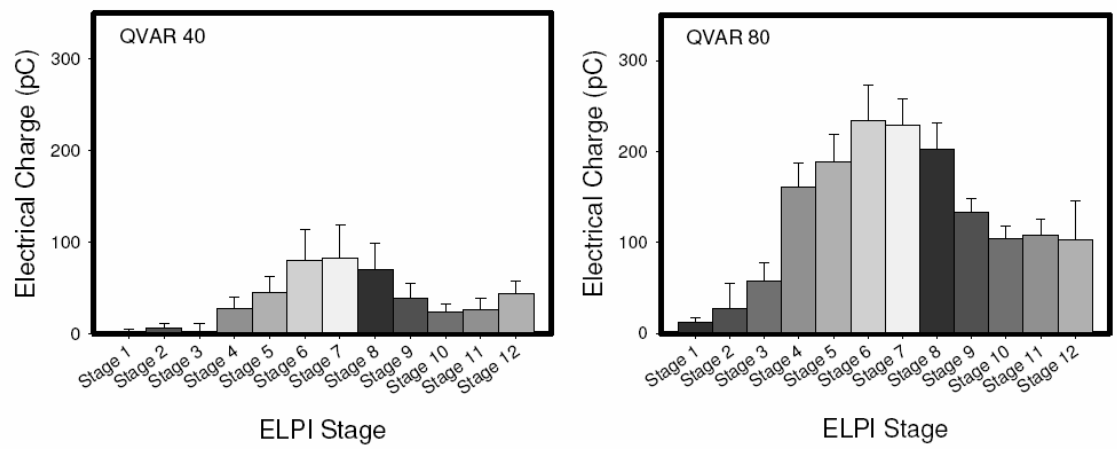


Both strengths of QVAR pMDIs produced unipolar predominantly electropositive aerosol clouds with a mean total net electrostatic charge of +449 ± 254 pC and +1314 ± 364 pC. Background measurements for QVAR 40 and QVAR 80 were negligible (+0.13 ±

0.17 pC and –0.05 ± 0.16 pC, respectively), corresponding to less than 0.04 % of the total net inherent charge (Appendices A.IV.1.1 and A.IV.1.2).

The electrostatic charging properties of QVAR 40 obtained in the present study were in good agreement with results previously obtained in our laboratory (mean total net charge for QVAR 40 determined using a modified ELPI: +563 ± 314 pC; Keil 2005). Kwok *et al.* have determined the electrostatic charge characteristics of QVAR 80 aerosols; the aerosols produced from QVAR 80 were found to be unipolar electropositively charged as well, although the mean total net charge (300 ± 240 pC; Kwok *et al.* 2005) was lower than that observed in the present study.

Table VI.1 summarizes the mass distribution data for aerosols from QVAR 40 and QVAR 80 pMDIs. The delivered mass (shot weight) of the formulation for QVAR 40 and QVAR 80 was 57 ± 2 and 60 ± 1 mg, respectively, which suggested that QVAR 80 contains a more concentrated solution of BDP compared to QVAR 40.

Table VI.1. Actuator Dose, Emitted Dose, Throat Deposition, Impactor Dose, and Fine Particle Dose of QVAR 40 and QVAR 80 pMDIs. Results Represent Mean (S.D.) (n = 5; 5 shots / can, 1 can)

| Formulation | Actuator Deposition* (μg) | Emitted Dose* (μg) | Throat Deposition* (μg) | Impactor Dose* (μg) | Fine Particle Dose* (μg) |
|---|---|---|---|---|---|
| QVAR 40 | 11.1 (1.5) | 34.8 (4.5) | 10.6 (3.6) | 24.2 (1.3) | 24.0 (1.2) |
| QVAR 80 | 26.6 (5.3) | 70.3 (5.6) | 31.2 (2.5) | 39.1 (7.0) | 39.0 (7.1) |

*Difference between QVAR 40 and QVAR 80 was significant.

Table VI.1 shows that the actuator deposition from QVAR 80 was significantly higher ($p < 0.05$) than that from QVAR 40 aerosols, which would be expected since QVAR 80 consists of a higher concentration of BDP in solution. The ballistic fraction of QVAR 80 aerosols collected in the USP induction port was also greater (47.0 ± 7.5 % of the emitted dose) than that of QVAR 40 aerosols (29.8 ± 7.6 % of the emitted dose). As would be expected, the mass of drug recovered in the impactor for QVAR 80 (39.1 ± 7.0 µg) was significantly higher ($p < 0.05$) than that recovered for QVAR 40 (24.2 ± 1.3 µg). Since a larger fraction of the emitted QVAR 80 aerosols deposited on the USP throat than that for QVAR 40 aerosols, the impactor dose for QVAR 80 was not proportionately higher than that for QVAR 40 aerosols. Figure VI.3 illustrates the BDP mass distribution for both strengths of QVAR pMDIs. BDP predominantly deposited on stages 1 - 10 of the ELPI for both QVAR 40 and QVAR 80.

Figure VI.3. Mass Distribution of BDP Determined Using the Modified ELPI for QVAR 40 and QVAR 80 pMDI Aerosols (n = 5; 5 shots / can, 1 can)

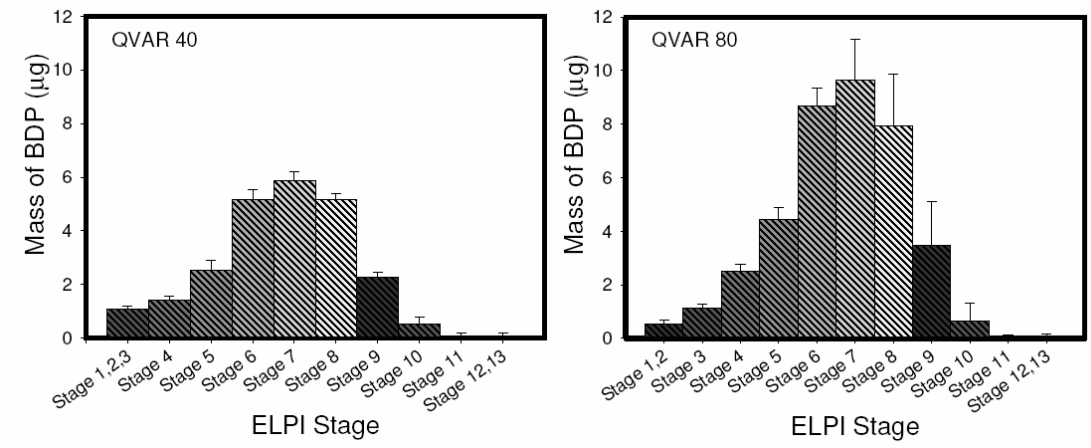

The fine particle doses (FPD) for QVAR 40 and QVAR 80 were 24.0 ± 1.2 and 39.0 ± 7.1 μg, respectively, which were not significantly different ($p > 0.05$) from the impactor doses since drug deposition on stages 11 - 13 was negligible. In order to normalize the electrostatic charge data for each stage with respect to the mass of BDP deposited on the corresponding stage, the net charge for each stage was divided by the mass of BDP deposited on that stage to obtain the charge to mass ratio for QVAR 40 and QVAR 80 and the results are shown in Table VI.2. The charge to mass ratio for stages 4 - 10 was higher for QVAR 80 than that for QVAR 40, i.e., more electrostatic charge was associated with QVAR 80 pMDI aerosols on each stage when compared with QVAR 40 pMDI aerosols. However, due to high variability, the charge to mass ratios for stages 4 - 10 were not statistically different ($p > 0.05$) between the two strengths of QVAR pMDIs. Charge to mass ratios were not obtained for stages 1 - 3 and 11 - 12 for both the aerosols; stages 1 - 3 were combined for washings in order to determine the mass of BDP deposited while there was no drug detected on stages 11 - 12.

Table VI.2. Mean Charge to Mass Ratio (pC/μg) of QVAR 40 and 80 pMDIs (Values in Parentheses are Standard Deviation, n = 5; 5 shots / can, 1 can).

| Stage | 4 | 5 | 6 | 7 | 8 | 9 | 10 |
|---|---|---|---|---|---|---|---|
| QVAR 40 | 19.85 (11.77) | 18.03 (7.71) | 15.81 (7.43) | 14.00 (6.42) | 13.55 (6.09) | 17.27 (8.00) | 51.32 (26.80) |
| QVAR 80 | 47.83 (26.61) | 36.02 (17.04) | 24.31 (6.96) | 22.02 (6.87) | 24.74 (9.11) | 42.22 (22.02) | 192.30 (172.68) |

Results for individual shots are listed in Appendices A.IV.1.5 and A.IV.1.6.

QVAR pMDI contains a solution of BDP in ethanol and HFA 134a, and it should be noted that the electrostatic charge on the ELPI stages would be due to all of the

formulation components while the mass is only due to BDP. However, for a solution based pMDI aerosol, it can be assumed that each droplet formed has a uniform distribution of the drug and the excipients (Stein and Myrdal 2004). Therefore, it is reasonable to assume that the electrostatic charge on the aerosol droplets of QVAR solution pMDI depositing on stages 1 - 12 will be proportional to the corresponding mass of the drug on those stages.

The effect of the mass of BDP on the aerosol charge was studied by comparing the charge to mass ratios for stages 4 - 10 of the ELPI for QVAR 40 and QVAR 80, which are the same BDP HFA solution formulations with different BDP concentrations. The mass of drug in each droplet of the aerosol for QVAR 80 would therefore be greater as compared to that in QVAR 40 aerosol droplets. The charge to mass ratios for QVAR 80 were not statistically different from those obtained for QVAR 40 suggesting that the electrostatic charge developed in aerosol droplets produced by QVAR solution pMDIs was proportional to the mass of BDP present in the aerosol.

### VI.C.1.2. Effect of Packaging Components of HFA Based BDP Solution pMDIs

Figure VI.4 compares the electrostatic charge distribution of QVAR 40 pMDIs, as obtained, and the repackaged formulations. Repackaged QVAR pMDIs produced net positively charged aerosols similar to those produced by QVAR pMDIs; however, the magnitude of charge was significantly lower ($p = 0.0079$) when compared to that produced by QVAR pMDIs (repackaged pMDIs: $+175 \pm 56$ pC, QVAR pMDIs: $+449 \pm 254$ pC). Background measurements were found to be less than 0.07% of the total net charge of

repackaged QVAR aerosols (0.12 ± 0.28 pC). Appendix A.IV.1.7 summarizes the net charge for background measurements.

Figure VI.4. Electrostatic Charge Distribution of QVAR 40 pMDIs (n=5; 5 shots / can, 1 Can) and Repackaged QVAR 40 pMDIs (n = 9; 3 Shots / Can, 3 Cans). Electrostatic Charge Data for Individual Shots of Repackaged pMDIs are listed in Appendix A.IV.1.8.

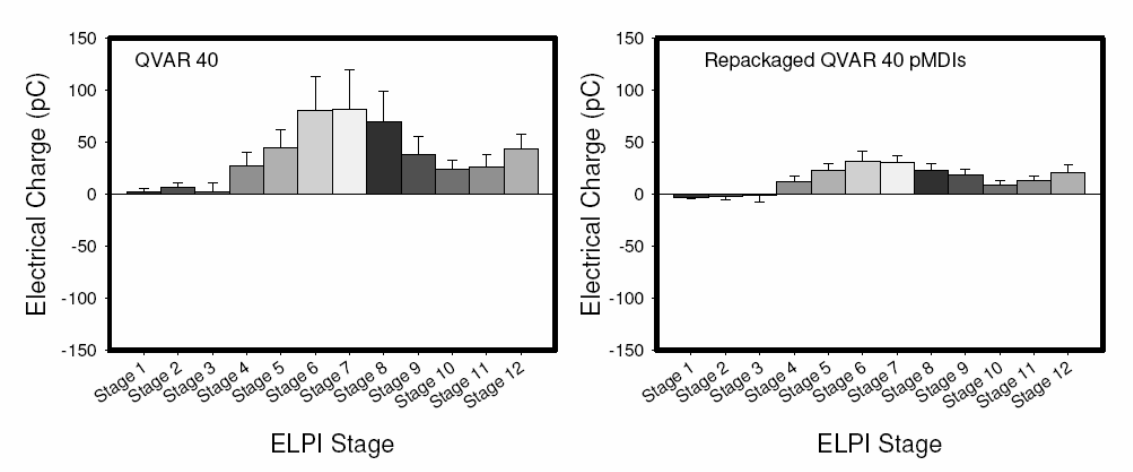


The net charge on stages 1 - 3 was negligible but electronegative which may possibly be an effect of changing the valve and the actuator combination in the repackaged QVAR pMDIs. 3M Spraymiser valves consist of a stainless steel valve stem and metering chamber while Valois valves used with the experimental pMDIs were comprised of a PBT valve stem and metering chamber. A Valois actuator was used with the experimental solution pMDIs in order to fit the Valois valves.

Table VI.3 summarizes the mass distribution data for aerosols from QVAR pMDIs as obtained and the repackaged QVAR pMDIs. Emitted doses for the pMDIs were not significantly different ($p = 0.2794$). However, deposition within the USP induction port from the repackaged pMDIs was significantly higher ($p < 0.0001$) in comparison with

marketed QVAR 40 pMDIs. Not unexpectedly, the mean impactor dose (10.6 ± 2.7 μg) from the repackaged QVAR 40 pMDIs was found to be approximately half of the impactor dose obtained from the commercially available QVAR 40 pMDIs (24.2 ± 1.3 μg). Previous studies have illustrated the effect of the actuator orifice diameter on the FPD (particles smaller than 4.7 μm) characterized using an ACI; the FPD was found to decrease with increase in the actuator orifice diameter (Lewis *et al.* 1998). The Valois actuator has a large orifice diameter (0.7 mm) intended for use with suspension pMDIs; in comparison, the QVAR actuator has a smaller orifice diameter (0.25 mm; Nithyanandan *et al.* 2007). It would therefore be predictable to observe a higher ballistic fraction and a lower impactor dose for the repackaged pMDI aerosols in comparison to those for QVAR 40 pMDIs.

Table VI.3. Actuator Dose, Emitted Dose, Throat Dose, Impactor Dose and FPD of QVAR 40 (n = 5; 5 shots / can, 1 can) and Repackaged QVAR pMDIs (n = 9; 3 Shots / Can, 3 Cans). Results Represent Mean (S.D.)

| Formulation | Actuator Deposition* (μg) | Emitted Dose (μg) | Throat Deposition* (μg) | Impactor Dose* (μg) | FPD* (μg) |
|---|---|---|---|---|---|
| QVAR 40 | 11.1 (1.5) | 34.8 (4.5) | 10.6 (3.6) | 24.2 (1.3) | 24.0 (1.2) |
| Repackaged QVAR 40 | 8.1 (0.5) | 37.4 (2.8) | 26.8 (2.4) | 10.6 (2.7) | 10.2 (2.6) |

*Difference between QVAR 40 and Repackaged QVAR pMDIs was significant.

Figure VI.5 illustrates the BDP mass distributions of QVAR 40, as obtained and repackaged QVAR pMDIs. It was observed that BDP predominantly deposited on stages 5 - 10 of the ELPI as determined by chemical analysis.

Figure VI.5. Mass Distribution of BDP for QVAR 40 pMDIs (n = 5; 5 Shots / Can, 1 Can) and Repackaged QVAR 40 pMDIs (n = 9; 3 Shots / Can, 3 Cans)

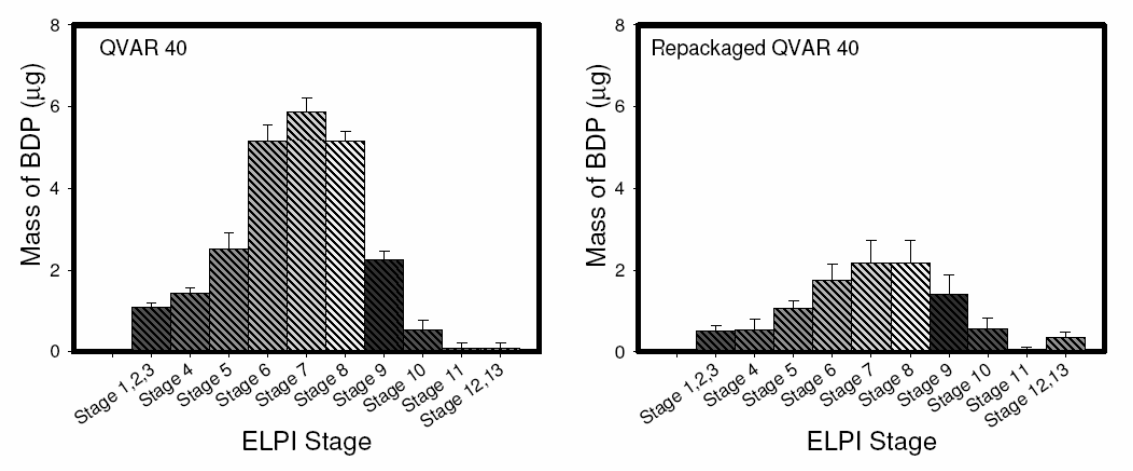


Table VI.4. Mean Charge to Mass Ratio (pC/µg) of QVAR 40 pMDIs (as obtained) and Repackaged QVAR 40 pMDIs (Values in Parentheses are Standard Deviation, n = 5; 5 Shots / Can, 1 Can for QVAR as is and n = 9; 3 Shots / Can, 3 Cans for Repackaged QVAR).

| Stage | 4 | 5 | 6 | 7 | 8 | 9 | 10* |
|---|---|---|---|---|---|---|---|
| QVAR 40 | 19.85 (11.77) | 18.03 (7.71) | 15.81 (7.43) | 14.00 (6.42) | 13.55 (6.09) | 17.27 (8.00) | 51.32 (26.80) |
| Repackaged QVAR 40 | 18.47 (10.77) | 22.24 (7.24) | 19.11 (6.56) | 14.79 (4.92) | 11.37 (4.12) | 14.60 (6.49) | 18.71 (9.43) |

Results for individual shots are listed in Appendices A.IV.1.5 and A.IV.I.9.
*Difference between QVAR 40 and Repackaged QVAR pMDIs was significant.

To normalize the charge data between the QVAR 40 formulations packaged in the two different valve and actuator combinations, the mean charge to mass ratio for each of the ELPI stages was calculated (Table VI.4). The charge to mass ratio was not calculated for stages 1 - 3 and 11 - 12 since stages 1 - 3 were combined for analysis while deposition

of BDP on stages 11 and 12 was negligible. There was no significant difference in the mean charge to mass ratio for stages 4 - 9 ($p > 0.05$ for each of the stages) between the QVAR pMDIs in two different packaging configurations. The mean charge to mass ratio on stage 10 was significantly different ($p < 0.05$) between QVAR, as is, and repackaged pMDIs. The similar mean charge to mass ratio data confirmed that the formulations packaged in different valve and actuator combinations were in effect the same and the difference in the magnitude of the charge was due to a decrease in the impactor dose.

### VI.C.1.3. Effect of Formulation Components of HFA Based BDP Solution pMDIs

Figure VI.6 shows the electrostatic charge distribution of aerosol produced by the experimental HFA solution pMDIs. The experimental 100% HFA 134a pMDIs produced primarily net electropositively charged aerosol clouds as shown in Figure VI.6.a ($68 \pm 100$ pC). There was both shot to shot and can to can variability in the net electrostatic charge distribution of aerosols produced by 100% HFA 134a pMDIs.

Background measurements were less than 0.2% of the total net charge of the propellant aerosol clouds ($0.13 \pm 0.43$ pC; Appendix A.IV.1.10 provides a summary of the background measurements). Figure VI.6.b represents the mean net inherent charge for ethanol/propellant blend aerosol clouds, which was also predominantly electropositive ($108 \pm 11$ pC).

Figure VI.6. Electrostatic Charge Distribution of Control HFA Solution pMDIs and Repackaged QVAR pMDIs (n = 9; 3 Shots / Can, 3 Cans). Electrostatic Charge Data for Individual Shots are listed in Appendices A.IV.1.11 - A.IV.1.13.

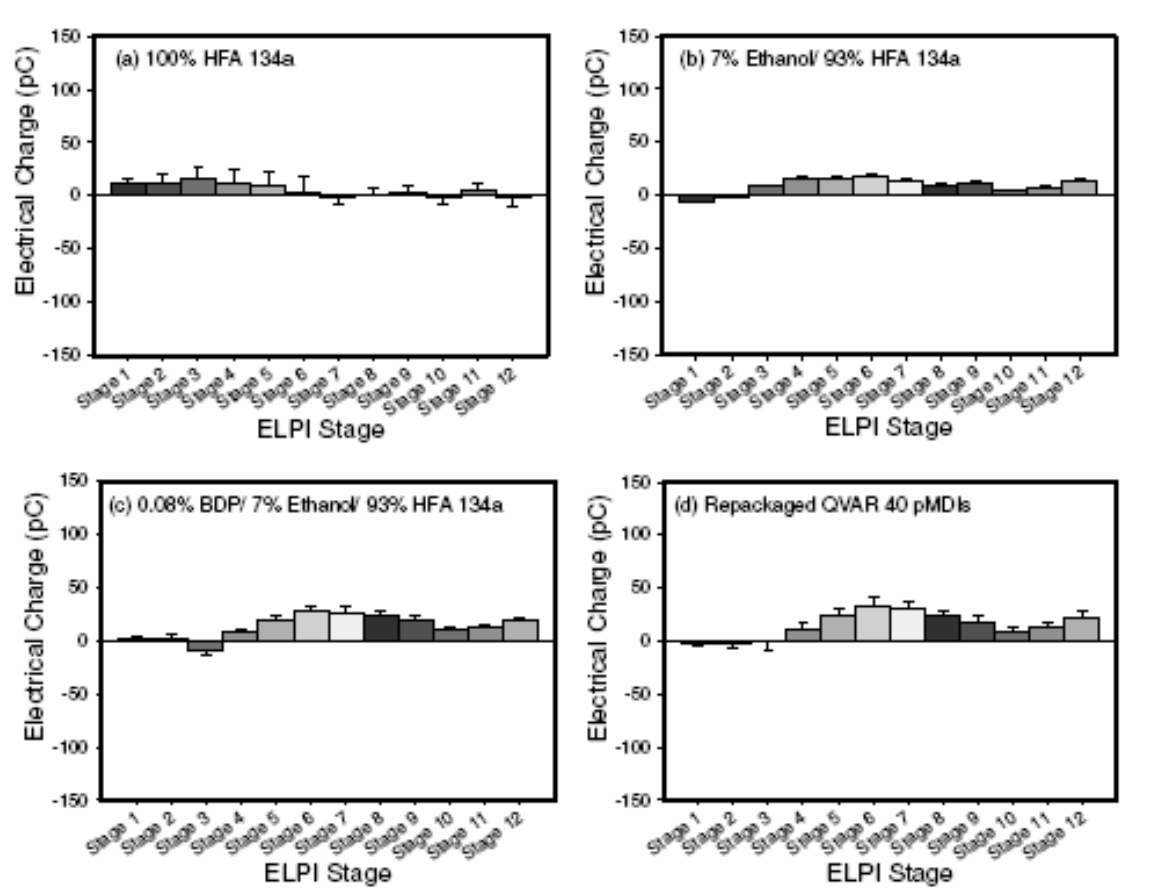


The experimental BDP solution pMDIs produced predominantly electropositive clouds (Figure VI.6.c) with a mean net electrostatic charge of 160 ± 30 pC, which was significantly higher ($p = 0.0069$) than that obtained for ethanol / propellant blend pMDIs but not significantly different ($p < 0.0001$) from that obtained for repackaged QVAR pMDIs (+175 ± 56 pC; Figure VI.6.d). Droplets depositing on stages 4 - 12 were found to be net positively charged, whereas stages 1 and 2 were negligibly charged. Stage 3 was net

electronegatively charged which may possibly be a function of the metering valve and actuator combination used.

Chemical analysis of the drug deposited in the impactor enabled determination of the mass distribution of the experimental BDP pMDI aerosols. Table VI.5 compares the actuator dose, emitted dose, throat deposition, impactor dose and FPD of experimental BDP solution pMDIs and repackaged QVAR 40 pMDIs determined by the ELPI. There was a small but statistically significant difference ($p < 0.0001$) in the actuator deposition as well as the emitted dose from the experimental BDP solution pMDIs and that obtained from the repackaged pMDIs. The ballistic fraction from the experimental BDP solution pMDIs was 69.2 ± 1.2 % of the emitted dose, which was comparable ($p > 0.05$) to that observed with the repackaged QVAR pMDIs (71.8 ± 5.5 % of the emitted dose). The mean impactor dose (9.8 ± 0.4 μg) was not significantly different ($p = 0.3890$) from that obtained for the repackaged QVAR pMDIs. The FPD (9.6 ± 0.4 μg) accounted for 98 % of the mass of drug depositing in the impactor since negligible amount of drug deposited on stages 11 - 13.

Table VI.5. Actuator Dose, Emitted Dose, Throat Deposition, Impactor Dose and FPD of Experimental BDP Solution pMDIs (n = 9; 3 Cans, 3 Shots / Can) and Repackaged QVAR pMDIs. Results Represent Mean (S.D.).

| Formulation | Actuator Deposition* (μg) | Emitted Dose* (μg) | Throat Deposition* (μg) | Impactor Dose (μg) | FPD (μg) |
|---|---|---|---|---|---|
| Experimental BDP Solution pMDIs | 6.7 (0.6) | 31.8 (1.5) | 22.0 (1.3) | 9.8 (0.4) | 9.6 (0.4) |
| Repackaged QVAR 40 | 8.1 (0.5) | 37.4 (2.8) | 26.8 (2.4) | 10.6 (2.7) | 10.2 (2.6) |

*Differences between experimental BDP pMDIs and Repackaged QVAR pMDIs are significant

Figure VI.7. Electrostatic Charge and Mass Distribution of BDP for Experimental BDP Solution pMDIs (n = 9; 3 Shots / Can, 3 Cans)

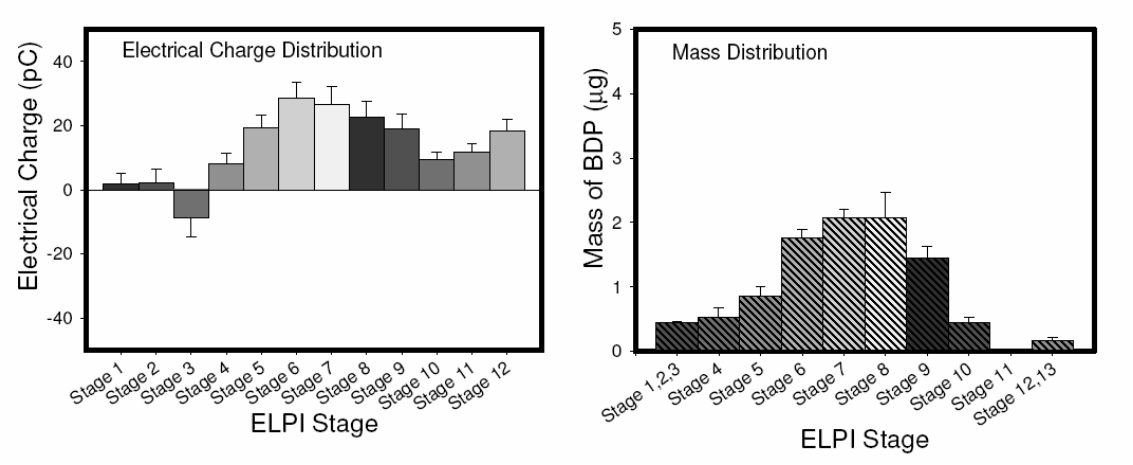


Figure VI.7 shows the electrostatic charge distribution and the corresponding mass distribution of the experimental BDP solution pMDIs; BDP predominantly deposited on stages 1 - 10. Except for stage 3 where net negatively charged particles deposited, the electrostatic charge measured on stages where BDP deposited was determined to be net positive.

QVAR 40 was used as the model solution pMDI and the influence of individual formulation components of BDP solution pMDIs on aerosol charge were investigated by a systematic study of a series of experimental solution formulations. Since the repackaged QVAR pMDIs produced aerosols with similar electrostatic charging characteristics compared to those of QVAR pMDIs (as obtained), the effect of formulation components of BDP solution pMDIs on the electrostatic charge of the aerosols could be systematically investigated using experimental HFA solution pMDIs packaged with Valois metering valves.

The addition of BDP to an ethanol / propellant HFA 134a blend did not affect the unipolar charge distribution profile observed for the ethanol - propellant blend alone. The water content for the control 100% HFA 134a ranged from 36 – 55 ppm, while the water content was higher for the ethanol containing control pMDIs (water content for ethanol-propellant blend and BDP solution in ethanol-propellant blend: 354 - 361 ppm and 357 - 362 ppm, respectively). The presence of water in the ethanol-containing pMDIs may contribute to their relatively polar nature and possibly influence the aerosol charging properties. It was hypothesized that since BDP solution pMDIs could be considered to be a homogeneous system, all the aerosol droplets exhibited uniform charging characteristics similar to the ethanol-propellant blend alone resulting in a unipolar charge distribution.

The predominant effect of ethanol as a polar cosolvent on the electrical properties of the control HFA based solutions was confirmed from the electrical resistivity measurements. Propellant HFA 134a has been reported to have a high electrical resistivity (180 MΩ.cm; Solvay Fluor Product Bulletin 2001). As observed in Chapter IV.B.2.2, the addition of ethanol decreased the resistivity of pure propellant HFA 134a; for example, the resistivity of 7% ethanol / 93% HFA 134a blend was 0.8 MΩ.cm suggesting that addition of ethanol increased the polar nature of the propellant as well as the conductivity of the solution. Addition of BDP to the ethanol-propellant blend only slightly increased the electrical resistivity (2.38 ± 1.31 MΩ.cm) in comparison to the ethanol / propellant blend alone. In summary, the presence of ethanol was shown to have a predominant effect on the electrical properties of BDP HFA solutions inside the canister as well as the electrostatic properties of the aerosols produced by these pMDIs.

## VI.C.2. Electrostatic Charge and Mass Distribution of HFA Propelled Albuterol Sulfate Suspension pMDIs

### VI.C.2.1. Electrostatic Charge and Mass Distribution of Ventolin HFA pMDI Aerosols

The mean electrostatic charge and mass distribution of aerosols produced by Ventolin HFA are shown in Figure VI.8. Ventolin HFA produced bipolar aerosol clouds with the particles depositing on stages 1 - 6 net electronegatively charged while particles depositing on stages 7 - 12 being net electropositively charged similar to that observed in the literature (Kwok *et al.* 2005).

Figure VI.8. Electrostatic Charge and Mass Distribution of Ventolin HFA pMDI aerosols. Error Bars Represent Standard Deviation (n = 5; 5 Shots / Can, 1 Can). Electrostatic Charge Data for the Individual Shots are Listed in Appendix A.IV.2.2.

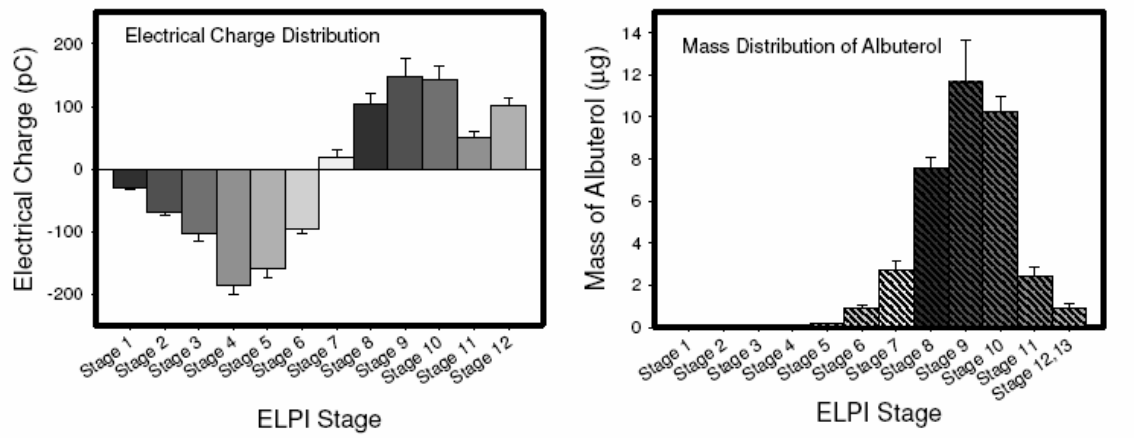

Background measurements were less than 0.06% of the net FPD charge. Appendix A.IV.2.1 shows the net charge obtained for background measurements. The mean net FPD charge was –232 ± 37 pC, which was comparable to the FPD charge (particles smaller than 5 μm) reported in the literature for Ventolin HFA (-231 ± 3 pC) measured using an aerosol electrometer (Kulphaisal 2003).

In contrast, the magnitude of the electrostatic charge produced by Ventolin HFA aerosols measured using a modified ELPI reported in literature was almost five fold higher (-1100 pC) (Glover and Chan 2004a, Kwok *et al.* 2005). A possible explanation for this difference in the total net aerosol charge of Ventolin HFA could be the manner in which the ELPI software analyzes the electrical current data. When the ELPI is used for sizing aerosol particles via electrical detection, the ELPI software uses a correction algorithm to account for diffusion losses of smaller particles such that some of the electrical current is transferred to the upper stages (Dekati Ltd. Technical Note 2002). Keil has illustrated for Ventolin CFC aerosols that the use of the corrected electrical current data for charge determination resulted in a higher mean total aerosol charge (–768 ± 136 pC) than that determined using the raw current data (–154 ± 26 pC) (Keil 2005). However, it is not possible to confirm from the data published by Kwok et al whether the correction algorithm was used in their experiments.

The total emitted dose for Ventolin HFA was 78.3 ± 6.0 μg while the impactor dose was 36.6 ± 2.8 μg. Figure VI.8 shows that albuterol was found to deposit on stages 6 - 13 of the ELPI, but predominantly on stages 7 - 11, which correspond to the stages where electropositive particles deposited. Negligible amount of drug was detected on stage 5;

albuterol was not detected on stages 1 - 4 of the ELPI using the HPLC method described in Chapter III.C.2.2.

### VI.C.2.2. Influence of Formulation Components on Electrostatic Properties of Experimental Albuterol Sulfate HFA Suspension pMDIs

Experimental albuterol sulfate HFA based suspension pMDIs were systematically tested to evaluate the contribution of individual components of the formulation to the electrostatic charge. Figure VI.9 shows the electrostatic charge distribution of 100% HFA 134a and 0.2% albuterol sulfate / 100% HFA 134a suspension pMDI aerosols.

Figure VI.9. Electrostatic Charge Distribution of Experimental HFA 134a pMDI Aerosols. Error Bars Represent Standard Deviations (n = 9; 3 Shots / Can, 3 Cans). Electrostatic Charge Data for the Individual Shots are Listed in Appendices A.IV.2.4 and A.IV.2.5.

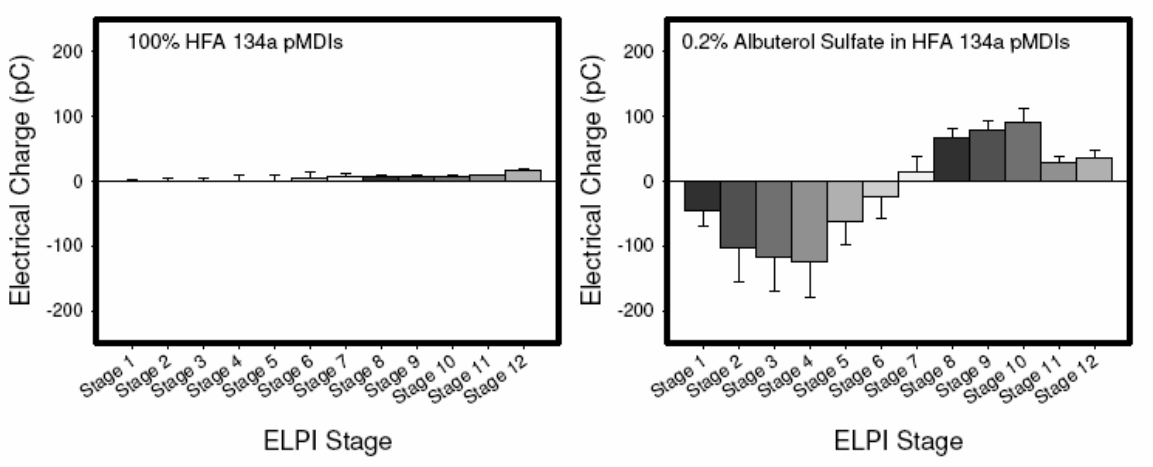


Propellant HFA 134a pMDIs produced primarily electropositive charge (mean total net charge: 59 ± 45 pC), although the total net charge varied from -12 pC to +137 pC.

Background measurements were less than 0.4% of the total net charge of propellant HFA 134a pMDIs (0.21 ± 0.25 pC; Appendix A.IV.2.3 provides a summary of the background measurements). The mean net charge of the propellant droplets on the individual stages, stages 1 - 12 of the ELPI, was found to be negligible in comparison to that of the experimental albuterol sulfate pMDI aerosols, as shown in Figure VI.9.

Albuterol sulfate pMDIs produced bipolar charged aerosol clouds with a mean net FPD charge of –227 ± 264 pC, similar to those produced by Ventolin HFA pMDI aerosols. Although the charge distribution profiles of the experimental albuterol sulfate pMDIs were similar for all the 3 canisters tested, there was can to can and shot to shot variability in the total net electrostatic charge of the aerosols. For example, aerosols from canister 1 produced a total net electronegative charge ranging from –370 to +546 pC. In contrast, canister 2 produced a total net aerosol charge ranging from –353 +175 pC; canister 3 produced aerosols with a total net charge ranging from –60 to +10 pC.

The systematic investigation of the electrostatic charging properties of propellant HFA 134a pMDIs and albuterol sulfate suspension pMDIs showed that the electronegative charge on the lower stages of the ELPI was not due to propellant droplets (Figure VI.9). This observation was in contradiction to Kwok *et al.* who speculated that the highly electronegative charges on stages 1 - 6 of the ELPI, detected for Ventolin HFA pMDI aerosols, were due to the propellant droplets since negligible amounts of albuterol sulfate was found to deposit on these stages (Kwok *et al.* 2005).

Table VI.6 compares the mass recovery data for the experimental albuterol sulfate pMDIs and Ventolin HFA aerosols.

Table VI.6. Actuator Dose, Emitted Dose, Throat Deposition, Impactor Dose, and FPD for Experimental Albuterol Sulfate HFA pMDIs (n = 9; 3 Shots / can, 3 Cans) and Ventolin HFA (n = 5; 5 Shots / Can, 1 Can). Results Represent Mean (S.D.).

| Formulation | Actuator Deposition* (μg) | Emitted Dose* (μg) | Throat Deposition* (μg) | Impactor Dose* (μg) | FPD* (μg) |
|---|---|---|---|---|---|
| Experimental Albuterol Sulfate pMDIs | 18.6 (2.8) | 62.5 (11.0) | 33.8 (6.0) | 28.7 (5.1) | 22.0 (3.0) |
| Ventolin HFA | 13.5 (5.9) | 78.3 (6.0) | 41.7 (4.6) | 36.6 (2.8) | 33.3 (2.8) |

*Difference between experimental albuterol pMDIs and Ventolin HFA pMDIs was significant

The mass of albuterol sulfate depositing within the actuator (18.6 ± 2.8 μg) from the experimental albuterol sulfate suspension pMDIs was significantly greater ($p < 0.05$) than that obtained for Ventolin HFA aerosols (13.5 ± 5.9 μg). The actuator orifice diameter (0.7 mm) for the experimental pMDIs is larger than that for the actuator used with Ventolin HFA (0.52 mm; Nithyanandan *et al.* 2007), which is reflected in the lower drug mass recovery from the actuator for the experimental pMDIs. It was therefore not unexpected that the emitted dose obtained for the experimental albuterol sulfate pMDIs (62.5 ± 11.0 μg) was significantly lower ($p < 0.05$) in comparison to the emitted dose obtained from Ventolin HFA aerosols (78.3 ± 6.0 μg). The emitted doses of the experimental albuterol sulfate suspension pMDIs, however, were found to be statistically comparable ($p = 0.4332$; one-way ANOVA) between the three canisters tested.

The difference in the total drug recovery between Ventolin HFA and the experimental albuterol sulfate suspension pMDIs may be related to the difference in the amount of drug metered per shot. The mass of Ventolin HFA formulation delivered per

shot ranged from 75 – 76 mg, which corresponds to a metering volume of 63 μL, while the shot weight for the experimental albuterol sulfate pMDIs ranged from 55 - 57 mg (metering volume: 50 μL). Both the formulations were intended to deliver a dose of 120 μg of albuterol sulfate per shot, thus the experimental albuterol sulfate suspension pMDI was formulated as a more concentrated suspension compared to Ventolin HFA. In addition, both the commercially available and the experimental albuterol sulfate HFA suspension pMDI tested in this study did not contain any surfactant, which would render the formulations inherently unstable. Owing to the increased drug mass in the experimental albuterol sulfate suspensions as well as the absence of a suspending agent, there may be an increased tendency for the suspended albuterol sulfate particles to aggregate and adhere to the canister inner walls as well as the metering chamber during storage and not be available for delivery.

Molecular modeling studies described in Chapter V have shown that the interactions between the molecules of albuterol sulfate and HFA 134a are predominantly unfavorable as suggested by the HINT scores. It would not be unexpected for albuterol sulfate particles to aggregate when suspended in HFA 134a in the absence of any suspending agent. The patent literature has documented the use of fluoropolymer coating on the canister inner walls as well as the metering chamber to minimize drug adhesion (Ashurst *et al.* 2000a, Riebe *et al.* 2003). The experimental albuterol sulfate pMDIs were packaged in uncoated aluminum canisters and untreated Valois metering valves, which may possibly be another factor responsible for the low drug recovery.

The ballistic fraction of the aerosols emitted from the experimental albuterol sulfate suspension pMDIs depositing in the USP induction port (54.1 ± 1.3 % of the emitted dose) was not significantly different from that obtained for Ventolin HFA pMDIs (53.2 ± 3.0 % of the emitted dose). As a consequence of the lower emitted dose recovery for the experimental albuterol sulfate pMDIs, the corresponding impactor dose (28.7 ± 5.1 μg) was significantly lower ($p < 0.05$) than the impactor dose for Ventolin HFA pMDI aerosols (36.6 ± 2.8 μg). However, the impactor doses for the experimental albuterol sulfate pMDIs were not significantly different ($p = 0.3644$, one-way ANOVA) between the canisters (3 cans) tested. Droplets depositing on stages 1 - 6 were net electronegatively charged while droplets depositing on stages 7 - 12 were net electropositively charged as shown in Figure VI.9.

FigureVI.10. Electrostatic Charge and Mass Distribution of Experimental Albuterol Sulfate pMDIs (n = 9; 3 Shots / Can, 3 Cans)

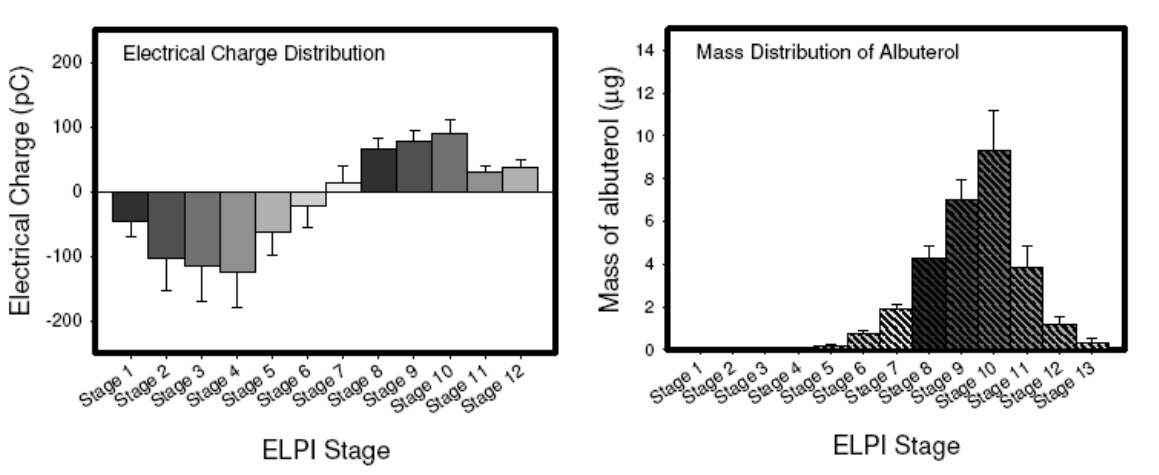


Chemical analysis using a validated HPLC method (Chapter III.C.2.2) showed that albuterol sulfate deposited on stages 6 - 13 of the ELPI, but predominantly on stages 7 - 12

where net electropositive charge was recorded. There was a negligible amount of albuterol sulfate on stage 5 while no drug was detected on stages 1 - 4 of the ELPI using the HPLC analysis with fluorescence detection (Figure VI.10). Interestingly, the net electrical charge recorded on these stages was highly electronegative.

The present study showed that the addition of albuterol sulfate to propellant HFA 134a appeared to modify the triboelectric properties of the non-drug droplets. However, the causative factors for the highly electronegative charges on stages 1 - 5 for albuterol sulfate pMDIs were not clearly understood. Trace amounts of albuterol sulfate on the lower stages 1 - 4 of the ELPI were detected using an LC-MS technique as described in Chapter III.C.2.3. From the analysis of albuterol sulfate recovered on the lower stages (Stages 1 - 4) of the ELPI, it was observed that the total mass of albuterol depositing on stages 1 - 4 was 0.05 ± 0.01 μg i.e. less than 0.1% of the emitted dose of albuterol sulfate penetrated beyond stage 5 (manufacturer-reported stage cut-off diameter: 0.27 μm). Further experiments were needed to address the origin of the electrostatic charge on stages 1 - 4 of the ELPI.

One possible explanation for the electronegative charge on the lower stages of the ELPI was considered to be the presence of trace quantities of soluble drug or related impurities. However the solubility of albuterol sulfate in 100% HFA 134a has been reported to be lower than 0.0005 μg/mg using a UV-Visible detection technique (Tzou *et al.* 1997). The effect of soluble impurities, if any, in the experimental albuterol sulfate suspension pMDIs was further investigated by filtering the suspensions and analyzing the electrostatic properties of the filtrates.

### VI.C.2.3. Influence of Soluble Impurities on Electrostatic Charge Distribution of Experimental HFA Suspension pMDIs

Figure VI.11 shows the electrostatic charge distribution of aerosols produced by filtrates of the experimental HFA pMDIs. Metered dose analysis using HPLC with fluorescence detection confirmed the absence of albuterol sulfate in filtrates of albuterol sulfate suspensions in HFA 134a. Filtrates of 100% HFA 134a produced aerosols with predominantly net positive charge (139 ± 110 pC). Background measurements were less than 0.1 % of the total net charge of the control HFA 134a filtrates (0.11 ± 0.18 pC; Appendix A.IV.2.6).

Figure VI.11. Electrostatic Charge Distribution of Aerosols Produced by Filtrates of Experimental HFA pMDIs (n = 9; 3 Shots / Can, 3 Cans). Electrostatic Charge Data for the Individual Shots are Listed in Appendices A.IV.2.7 and A.IV.2.8.

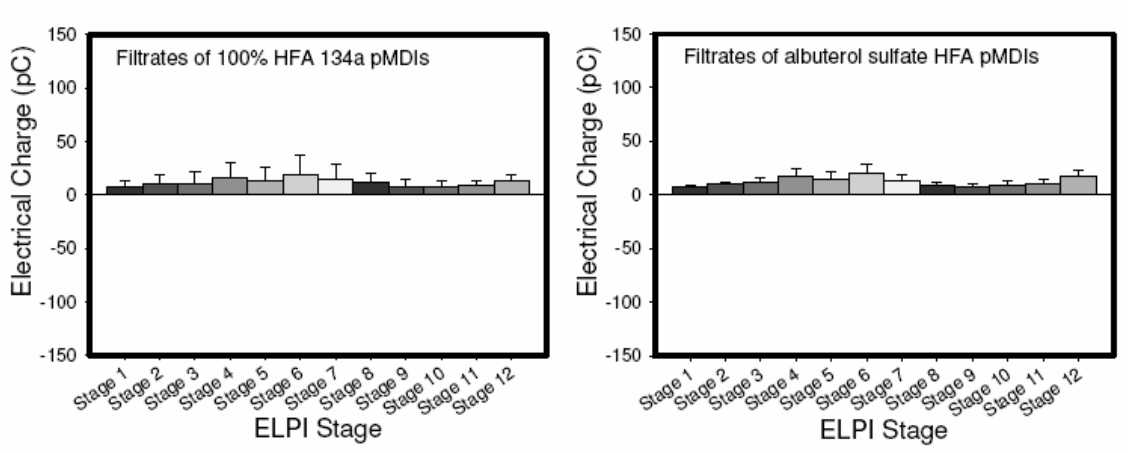


The aerosol clouds produced by filtrates from 0.2 % albuterol sulfate suspensions in 100 % HFA 134a were also net electropositively charged (151 ± 55 pC); the total net electrostatic charge was not statistically different (p = 0.7790) from that obtained for 100

% HFA 134a pMDIs post-filtration. In the absence of suspended albuterol sulfate particles in the formulation, the electrostatic charging characteristics of aerosols produced by the filtrates of experimental albuterol sulfate pMDIs were similar to those produced by the filtrates of 100% HFA 134a pMDIs. The mean net electrostatic charge on each stage of the ELPI for the filtrates of the control propellant pMDIs was higher than that obtained for the propellant pMDIs before filtration, although for some shots, net electronegative charge was observed on the ELPI stages.

The process of filtration and transfer of formulations via cold filling could possibly result in water ingress in the formulations. The water content of the experimental 100% HFA 134a pMDIs and 0.2% albuterol sulfate suspension pMDIs before filtration of the formulations measured by Karl Fischer titration was found to be 138 ± 4 ppm and 118 ± 38 ppm, respectively. After filtration, the water content of the filtrates of the experimental 100% HFA 134a and 0.02% albuterol sulfate / 100% HFA 134a pMDIs increased to 238 ± 41 ppm and 246 ± 55 ppm, respectively. The presence of water in the filtrates may have influenced the charging properties of the aerosols produced by them thus resulting in higher net electropositive aerosol charge for the HFA 134a filtrates and the formation of unipolar electropositive aerosol clouds for the filtrates of experimental albuterol sulfate pMDIs.

However, the absence of highly charged sub-micron particles suggests that the soluble albuterol impurities or the propellant HFA 134a itself may not be responsible for the highly electronegative charge on the lower stages of the ELPI in case of the albuterol sulfate pMDIs. An alternative explanation for the electrostatic charge on stages 1 - 4 may

be the presence of a very large number of small (particles smaller than 0.39 μm, manufacturer-reported cut-off diameter for stage 5) aerosol particles present on these stages. Crampton *et al.* have reported that HFA propelled pMDIs produce a higher sub-micron aerosol fraction compared to their CFC counterparts based on their measurements using electrical detection of charged aerosol particles in the ELPI and the Scanning Mobility Particle Sizer (SMPS) (Crampton *et al.* 2004). The authors determined that 0.269% of the labeled dose claim of Ventolin HFA had an aerodynamic size smaller than 0.1 μm. It was suggested that although sub-micron and ultrafine particles do not have appreciable mass; it might be relevant to measure the particle number or surface area to understand their physiological impact (Crampton *et al.* 2004). It was interesting to observe that the number of albuterol particles depositing on stages 1 - 4 of the ELPI contributed approximately 75% of the total number concentration calculated from the mass of albuterol deposited within the cascade impactor (Appendix A.V). It may be possible that this large number of sub-micron and ultrafine particles of albuterol detected on stages 1 - 4 could be responsible for the electronegative charge. It was hypothesized that the interactions between HFA 134a droplets and the valve stem on actuation of the pMDI would be influenced by albuterol sulfate particles such that the droplets emitted from the actuator orifice contained both positively and negatively charged species.

HFA 134a can be classified as a weakly polar solvent based on its dielectric constant ($\varepsilon = 9.5$) (Delgado *et al.* 2005). Although, the electrical resistivity of 100 % HFA 134a has been reported to be high (180 MΩ.cm; Solvay Fluor Product Bulletin 2001), albuterol sulfate particles were observed to acquire a positive zeta potential (75.9 ± 26.2

mV) when dispersed in 100% HFA 134a, which suggests that charge formation can occur within a weakly polar solvent. This observation compares favorably with the electrostatic properties of albuterol sulfate HFA pMDI aerosols; albuterol sulfate predominantly deposited on stages 7 - 12, on which a net electropositive aerosol charge was detected.

In summary, the systematic investigation of the electrical properties of droplets generated by HFA suspension and solution pMDIs demonstrated that surface electrification can be influenced by the formulation components. Characterization of these aerosol clouds from HFA propelled suspension and solution pMDIs using the modified ELPI has provided further insight into the droplet species that are likely generated, as well as their deposition behavior. Taken together with the studies investigating the electrical properties of HFA based solutions and suspensions, an improved understanding of charge formation within these formulations in relation with the electrostatic properties of the aerosols was provided.

# VII. CALIBRATION OF THE MODIFIED ELECTRICAL LOW PRESSURE IMPACTOR FOR USE WITH PRESSURIZED PHARMACEUTICAL AEROSOLS

## VII.A. Introduction

The modified Electrical Low Pressure Impactor (ELPI) has been employed to characterize the electrostatic properties of pressurized metered dose inhalers (Glover and Chan 2004a, Orban and Peart 2004, Kwok *et al.* 2005, Kwok *et al.* 2006), dry powder inhalers (Glover and Chan 2004b, Mikkanen *et al.* 2004, Kwok and Chan 2008, Telko *et al.* 2007, Young *et al.* 2007) and nebulizers (Kwok and Chan 2004) as a function of particle size. In most of these studies, it is not clear whether using the ELPI in this fashion yields an equivalent particle size distribution to other cascade impactor data (Glover and Chan 2004a, Kwok *et al.* 2005, Kwok *et al.* 2006). Telko *et al.* found that when aerosols produced by experimental DPIs containing micronized albuterol sulfate alone and those containing 1% albuterol sulfate in lactose were simultaneously sampled into a modified ELPI and an Andersen Cascade Impactor (ACI), the aerodynamic particle size distributions (aPSDs) obtained were comparable; however their study did not use the standard compendial experimental setup (Telko *et al.* 2007).

Recent evidence suggests that the ELPI appears to underestimate the particle size of aerosols produced by commercially available pMDIs (Orban and Peart 2004, Keil *et al.* 2006). While other studies have not directly compared the ELPI with other conventional cascade impactors, they have reported aPSDs determined using the modified ELPI. For example, the mass median aerodynamic diameter (MMAD) for Ventolin HFA pMDI (90 μg emitted dose of albuterol) was reported to be 1.82 ± 0.01 μm (Kwok *et al.* 2006) determined using the ELPI whereas the MMAD obtained with the ACI was reported to be 2.40 μm (Cripps *et al.* 2000).

Because of the current interest in apportioning charge to various size fractions of aerosols produced by pharmaceutical systems, the modified ELPI has been recalibrated using four independent, polydisperse pharmaceutical aerosols with different median diameters. After the recalibration procedure, the new ELPI cut-off diameters were validated using a previously untested commercially available pMDI.

**VII.B. Materials**

QVAR®, Ventolin CFC®, Flovent HFA® and Vanceril® (Table VII.1) were obtained commercially. These were tested before their expiry dates and used as "calibration standards". A fifth product, Ventolin HFA (Table VII.1) was tested after the ELPI recalibration procedure was complete, to validate the new calibration and compare the aPSDs obtained by performing side-by-side experiments in the ELPI and the ACI.

Table VII.1. Commercially Available pMDIs Used in this Study.

| Product | Active Drug (Labeled Dose)[a] | Supplier | Propellant System | Metering Valve Construction | | |
|---|---|---|---|---|---|---|
| | | | | Manufacturer | Valve Stem | Metering Chamber |
| Qvar | Beclomethasone Dipropionate 40 μg | Ivax Laboratories Inc., Miami, FL, USA, Lot # ED037A | HFA 134a | 3M | Stainless Steel | Stainless Steel |
| Ventolin | Albuterol Base 90 μg | GlaxoSmithKline, Raleigh, NC, USA, Lot # 1ZP0757 | CFC 11/12 | Bespak | Polymer | Polymer |
| Flovent HFA | Fluticasone Propionate 44 μg | GlaxoSmithKline, Raleigh, NC, USA, Lot # 0173 | HFA 134a | Valois | Polymer | Polymer |
| Vanceril | Beclomethasone Dipropionate 42 μg | Schering Corporation, Kenilworth, NJ, USA Lot # 1-AMA-226 | CFC 11/12 | Bespak | Polymer | Polymer |
| Ventolin HFA | Albuterol Sulfate 108 μg (Equivalent to 90 μg of Albuterol Base) | GlaxoSmithKline, Raleigh, NC, USA, Lot # 4ZP3714 | HFA 134a | Valois | Polymer | Polymer |

[a]Label claim doses represent the dose delivered from the mouthpiece actuator

## VII.C. Methods

### VII.C.1. Determination of Aerodynamic Particle Size Distributions (aPSDs) of Commercially Available pMDIs using the ACI and the Modified ELPI

An ACI was employed to generate the aPSD data for the four "calibration" pMDIs, which were used to calibrate the modified ELPI. The ACI used in this study was mensurated to ensure that the instrument was within its intended dimensional and engineering specifications by MSP Corporation (St Paul, MN, USA). Calibration of the ELPI used in the study was performed by Dekati Ltd., Tampere, Finland (ELPI); Appendix A.I provides the ELPI cut-off diameters. All pMDIs were tested under standard conditions at temperatures between 23-24 $^{\circ}$C and relative humidity ranging from 20-40%. Five replicate experiments were performed for a single canister of each product using a single ACI and modified ELPI.

#### VII.C.1.1. Andersen Cascade Impactor

Single actuation experiments were performed to assess the aPSDs of the emitted dose from each of the commercially available pMDIs listed in Table VII.1 using the ACI (8-stage Non-Viable Cascade Impactor Mark II; Thermo Electron Corporation, Franklin, MA) at a volumetric flow rate of 28.3 L/min according to standard compendial (USP 29/ NF 24 First Supplement 2006) methods. At a flow rate of 28.3 L/min the aerodynamic cut-off diameters of the stages are: 9.0, 5.8, 4.7, 3.3, 2.1, 1.1, 0.7 and 0.4 μm. A glass fiber

filter following the final impactor stage captures drug particles smaller than 0.4 μm. The impaction plates were coated to minimize any particle re-entrainment or "bounce" using 316 Silicone Release Spray (Dow Corning, Midland, MI, USA).

### VII.C.1.2. Modified Electrical Low Pressure Impactor

The pMDI products were also tested using the modified ELPI (Dekati Ltd., Tampere, Finland) as described in Chapter III.B. The ELPI was allowed to stabilize for an hour prior to operation while set-up requirements such as air leakage testing were performed in accord with the manufacturer's instructions and specifications. The ELPI was assembled as shown in Figure III.1 (the ELPI stages are numbered by the manufacturer starting from the base of the instrument). The manufacturer-reported cut-off diameters are shown in Table III.1. The modified ELPI was operated at a pressure of 100 mbar (below its lowest stage) to produce a flow rate of approximately 29 L/min, verified with an external flowmeter (Sierra Instruments Inc., Monterey, CA, USA). The aPSD of the drug clouds produced by each pMDI was characterized using single actuations into a previously cleaned ELPI with silicone-coated (DS-515 grease spray; Dekati Ltd., Tampere, Finland) aluminum substrates on each of the impaction plates.

### VII.C.1.3. Procedure for Determination of Aerodynamic Particle Size Distributions (aPSDs) of Commercially Available pMDIs using the ACI and the Modified ELPI

Prior to each experimental run, the canister was primed according to the patient information leaflet for each of the individual pMDIs. The primed canister, fitted with a clean actuator, was weighed, shaken for 5 sec, and actuated into the cascade impactor. The vacuum pump was turned off 10 or 20 sec after the actuation was completed for the ACI and the ELPI, respectively. The inhaler was reweighed as a procedural check to ensure accurate valve function, by checking to assess that the shot weight was within 5% of the target weight for that product. The mass of drug collected on the actuator, USP induction port, the ELPI inlet (in case of the ELPI) and the impactor stages for all the pMDIs was determined using validated HPLC analytical methods (Chapter III.C.2.1 & III.C.2.2).

The total emitted dose was determined for each actuation by summation of the masses collected in the induction port and the cascade impactor stages. The average emitted dose from each pMDI was determined from 5 single shot cascade impactor experiments in which drug recovery fell within the USP mass balance limits (label claim ± 25%; USP 29 / NF 24 First Supplement 2006). The amount of drug penetrating the impactor below the upper impaction stage of either ACI or ELPI was determined for each product and compared statistically using t-tests, to assure the comparability of the aerosol clouds being used as the ELPI calibration standards. Statistical significance was assessed at the $p < 0.05$ level throughout. The mass of drug penetrating both impactors and depositing on the individual stages below the top stage (Stage 0 of the ACI, Stage 13 of the ELPI) was

tabulated to produce cumulative percent drug undersize profiles of the output cloud from each pMDI.

**VII.C.2. Curve Fitting of the ACI aPSD Data for the Calibration Aerosols**

Four sets of n = 5 cumulative percent drug undersize data obtained from the ACI for the calibration pMDIs were fitted using least mean square nonlinear regression analysis to determine best estimates for the MMAD and the GSD of each cloud by fitting the data to the cumulative distribution function (CDF) (Dunbar and Hickey 2000) shown in Equation VII.1.

$$y = [100*(0.5+0.5\ ERF\ \{[1/(2^{0.5} * SIGMA)]*[\log_e(x) - MEAN]\})] \qquad \text{Equation VII.1}$$

ERF is the error function = $2/\pi^{0.5}$. $\int \exp -\{[1/(2^{0.5} *SIGMA)]*[\log_e(x) - MEAN]\}^2$. dx where $e^{MEAN}$ and $e^{SIGMA}$ are the MMAD and GSD of the log-normally distributed data (Tobias 1993).

The nonlinear regression software, SCIENTIST® for Windows (Micromath Research, St. Louis, MO), was used to fit the lognormal cumulative distribution function to the experimentally obtained ACI data. The program required three types of electronic files for curve fitting: a Model File (*.EQN), a Parameter File (*.PAR) and a Data File (*.MMD). The model file and parameter file are shown in Appendix A.VI.1. The model file defined the 50% aerodynamic cut-off diameter (x) as the independent variable in μm, cumulative % undersize (y) as a dependent variable and MEAN and SIGMA as the parameters. The parameters, MEAN and SIGMA, were assigned initial values obtained

from linear interpolation of the cumulative percent undersize vs. aerodynamic cut-off diameter profiles. The model file was compiled and a non-weighted non-linear least squares regression analysis was performed. This allowed for a more precise estimation of the parameters, MEAN and SIGMA, for the particle size distribution of the calibration pMDI aerosols. The analysis resulted in the SCIENTIST Plot for the cumulative % undersize vs. aerodynamic diameter and the Statistical Output, as shown in Appendix A.VI.2 and A.VI.3.

The parameters used to assess the goodness of fit of the lognormal distribution model for curve-fitting the ACI cumulative % undersize data were the coefficient of determination (COD) and the Model Selection Criteria (MSC).

Coefficient of Determination (COD) is calculated as follows by the SCIENTIST software:

$$COD = \frac{\sum_{i=1}^{n}(Y_{\exp,i} - \overline{Y_{\exp}})^2 - \sum_{i=1}^{n}(Y_{\exp,i} - Y_{calc,i})^2}{\sum_{i=1}^{n}(Y_{\exp,i} - \overline{Y_{\exp}})^2} \qquad \text{Equation VII.2}$$

where $Y_{exp,i}$ and $Y_{calc,i}$ are the experimental and calculated (model predicted) values of cumulative % undersize, respectively, n is the number of data points and $\overline{Y_{\exp}}$ is the mean of the experimental data. COD is a measure of the fraction of the total variance accounted for by the model. The closer the value of COD to 1, the better the model fits the data.

MSC is calculated by the SCIENTIST Software as follows:

$$MSC = \ln\left(\frac{\sum_{i=1}^{n}(Y_{\exp,i} - \overline{Y_{\exp}})^2}{\sum_{i=1}^{n}(Y_{\exp,i} - Y_{calc})^2}\right) - 2p/n \qquad \text{Equation VII.3}$$

where p is the number of parameters required to fit the data and n is the number of data points. The most appropriate model will have the highest MSC value. In this study, the lognormal cumulative distribution function was the only model used; for all the calibration pMDI aerosols, an MSC value greater than 5 was obtained which is considered to be an indication of a good model.

### VII.C.3. Calculation of Aerodynamic Cut-off Diameters of the Modified ELPI Using the ACI Curve Fitted Data

Individual values for the cumulative percentage of drug penetrating below a given ELPI stage were tabulated. The curves of best fit from the ACI and thus the best estimates for MMAD and GSD, were assumed also to describe the clouds entering the ELPI from each product. Equation VII.1 cannot be solved analytically for the aerodynamic cut-off diameter, hence MMAD and GSD were fixed at their product-specific best estimates and solutions for the cut-off diameters were determined for each stage of the ELPI by reiterating numerical solutions for Equation VII.1 using the LOGNORMDIST function in Microsoft® Office Excel 2003 (Microsoft Corp. Seattle, WA, USA).

For the cumulative percentage of drug penetrating below a particular stage of the ELPI (which represents the left hand side, LHS, of Equation VII.1), a series of assumed values for the cut-off diameter were used to calculate the value of the right hand side, RHS,

of Equation VII.1. The data was processed in an iterative manner until the quotient of LHS / RHS approached unity. Iteration ended when the following end point was obtained: 0.99999 < LHS / RHS < 1.00001; the cut-off diameter producing this condition was then noted as the new cut-off diameter value for the ELPI stage in question. Mean (±SD) values for the cut-off diameter, for each product and each stage, were determined from the 5 separate cascade impaction runs performed with each product. Confidence limits for these product-specific mean new ELPI cut-off diameter values were also calculated for each of the ELPI stages using the same procedure with estimates of the MMAD and GSD values set equal to their 95% confidence limits after curve fitting the ACI data for each calibration pMDI.

### VII.C.4. Validation of the Recalibration of the Modified ELPI

In order to validate the recalibration of the modified ELPI and the cut-off diameters calculated from the procedure, a single canister of a fifth product, Ventolin HFA, was studied after the ELPI recalibration procedure had been completed. Ventolin HFA was tested by collecting five single actuations in the ACI in accord with the USP and the procedures repeated in the modified ELPI to determine the aPSDs as described earlier in Section VII.C.1. Mass of drug penetrating both the impactors and depositing on the individual stages of the ACI and the ELPI (without excluding the mass deposited on the topmost stage of the impactor) was tabulated to produce cumulative percent drug undersize profiles of the output cloud from each pMDI.

## VII.D. Results and Discussion

### VII.D.1. Determination of Aerodynamic Particle Size Distributions (aPSDs) of Commercially Available pMDIs using the ACI and the Modified ELPI

In the present study, the corona charger as well as the charger frame of the ELPI was removed to create the modified ELPI; this arrangement shortens the aerosol flow path into the ELPI and makes the aerosol entry conditions comparable to those in the ACI. Most pharmaceutical investigators use the ELPI without the corona charger while keeping the hollow charger frame atop the impactor in place (Glover and Chan 2004a, Kwok *et al.* 2005, Kwok *et al.* 2006, Telko *et al.* 2007). As part of the ELPI validation studies, Keil determined the aPSD of Ventolin CFC using the ELPI by chemical analysis and has shown that the impactor dose recovered following pMDI actuation into the ELPI with the corona charger in place (29.7 ± 5.5 μg) or into the ELPI in the absence of both the corona charger and the frame (28.9 ± 3.0 μg) were statistically indistinguishable ($p = 0.7636$) (Keil 2005).

Table VII.2 shows that the mass of drug depositing in the actuator as well as the USP induction port for all the calibration pMDIs were comparable between the ACI and the ELPI experiments with the exception of Ventolin CFC for which the USP induction port dose was statistically different. The emitted doses from the calibration pMDIs for the ACI and the ELPI experiments were statistically comparable with the exception of the surfactant-free formulation, Flovent HFA, which showed a small but statistically significant difference ($p = 0.0189$) for the sprays used for calibration purposes in this study, as shown in Table VII.2.

Table VII.2. Emitted Dose, Actuator Dose, USP Induction Port Dose and Impactor Dose (Dose Collected on All the Stages of the Cascade Impactor) for Each of the Four pMDIs Used for Calibration Purposes.

| Product | Label Claim | Impactor | Mass collected (μg) ± SD | | | |
|---|---|---|---|---|---|---|
| | | | Total Emitted Dose | Actuator | USP Induction Port[a] | Impactor Dose[b] |
| Qvar | 40 μg | ACI | 36.87 (1.17) | 9.68 (1.29) | 17.45 (3.44) | 19.42 (4.53) |
| | | ELPI | 37.92 (2.74) | 12.76 (1.72) | 17.54 (1.09) | 20.71 (3.05) |
| Ventolin CFC | 90 μg | ACI | 88.54 (5.22) | 14.14 (1.43) | 47.77 (3.14)* | 40.76 (4.35)* |
| | | ELPI | 87.64 (9.68) | 12.07 (1.11) | 55.94 (5.00)* | 31.70 (5.48)* |
| Flovent HFA | 44 μg | ACI | 37.79 (1.92)* | 8.44 (0.84) | 16.92 (1.27) | 20.87 (1.39)* |
| | | ELPI | 34.43 (1.69)* | 6.62 (0.37) | 16.38 (0.91) | 18.04 (1.11)* |
| Vanceril | 42 μg | ACI | 37.34 (1.79) | 8.58 (2.31) | 20.98 (0.96) | 16.36 (1.42)* |
| | | ELPI | 34.45 (2.27) | 7.06 (1.70) | 22.65 (1.60) | 11.80 (1.52)* |

[a]Mass of drug recovered from the mouthpiece adaptor included. For the ELPI experiments, mass of drug recovered from the ELPI inlet also included.

[b]Mass of drug collected on all stages of the cascade impactor.

*Difference in the drug deposition between the ACI and the ELPI experiments statistically significant.

The mass of drug penetrating both impactors and depositing on all the individual stages for the ACI and the ELPI was tabulated to produce cumulative percent drug undersize profiles of the output cloud from each of the four calibration pMDIs as illustrated in Figure VII.1. Comparison of the aPSDs of the four calibration pMDIs determined in the present study using the ACI following standard compendial procedures and the modified ELPI provided evidence that the modified ELPI undersized pMDI aerosols (Figure VII.1). Table VII.3 summarizes the MMADs and GSDs for the four pMDIs determined by linear interpolation for both the ACI and the ELPI experiments along with the MMADs reported in the literature obtained using the ACI. For example, as shown in Table VII.3, the MMADs for both QVAR and Ventolin CFC determined in the present study using the modified ELPI with the manufacturer's calibration (0.60 ± 0.05 and 1.71 ± 0.05 μm, respectively) were smaller than those determined using the ACI (0.94±0.06 and 2.20±0.04 μm, respectively). In comparison, the literature reports MMADs for QVAR and Ventolin CFC, in the ACI, of 1.1 μm (Leach *et al.* 1998) and 2.2 μm (Mitchell *et al.* 1999), respectively. Kamiya *et al.* have reported that comparable aPSDs are obtained for Vanceril using the ACI (MMAD: 3.86 ± 0.12 μm) and the Next Generation Cascade Impactor (NGI) (MMAD: 3.69 ± 0.19 μm) (Kamiya *et al.* 2004); in contrast, it was observed that the MMAD of Vanceril (3.13 ± 0.07 μm) obtained using the ELPI in this study was smaller than those obtained using both the ACI and the NGI.

Figure VII.1. Comparison of Aerodynamic Particle Size Distributions of the Calibration pMDI Aerosols Determined from Single Actuations into the ACI and the Modified ELPI (n = 5). Error Bars Represent Standard Deviation.

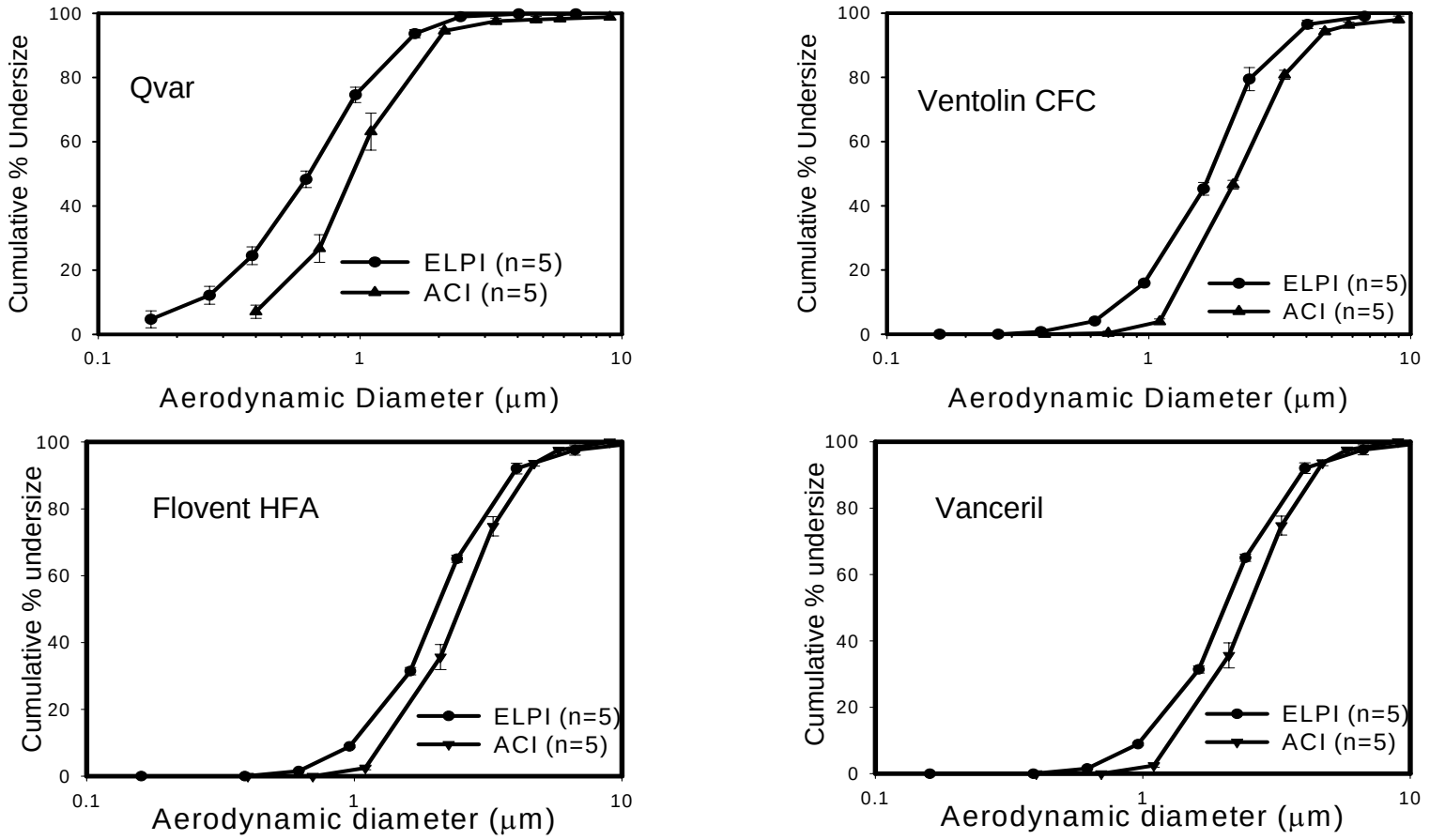

Table VII.3. Summary of MMADs and GSDs of the Calibration pMDI Aerosols Along with the Literature Reported Values for the MMADs

| Product | Impactor | MMAD (μm) | | GSD (Linear Inpterpolation) |
|---|---|---|---|---|
| | | Literature | Linear Interpolation | |
| Qvar | ACI | 1.1[a] | 0.94±0.06 | 1.80 |
| | ELPI | - | 0.60±0.05 | 2.21 |
| Ventolin CFC | ACI | 2.2[b] | 2.20±0.04 | 1.65 |
| | ELPI | - | 1.71±0.05 | 1.84 |
| Flovent HFA | ACI | - | 2.51±0.10 | 1.65 |
| | ELPI | - | 2.02±0.03 | 1.75 |
| Vanceril | ACI | 3.9[c] | 3.86±0.12 | 1.52 |
| | ELPI | - | 3.13±0.07 | 1.65 |

[a]Leach *et al.* 1998, [b]Mitchell *et al.* 1999, [c]Kamiya *et al.* 2004.

The ELPI was originally designed for real time particle sizing of aerosols using electrical detection (Keskinen *et al.* 1992). The performance of the ELPI as a particle size analyzer when used with the corona charger in comparison to a Scanning Mobility Particle Sizer (SMPS), for charged dioctyl sebacate (DOS) droplets in isopropyl alcohol, has been investigated and good agreement between the two techniques was reported (Maricq *et al.* 2000, Marjamaki *et al.* 2000). Telko *et al.* have also employed the ELPI in its standard mode of operation (with the corona charger switched on) to determine aPSDs of pharmaceutical aerosols via electrical detection (Telko *et al.* 2007). The authors found that the aPSDs of experimental DPIs containing albuterol sulfate-lactose blends determined using the ELPI via electrical detection compared well with those obtained subsequently via gravimetric analysis. There was a discrepancy in the particle size observed on the lower stages where the use of the gravimetric sizing technique was reported to be limited by the sensitivity of the analytical balance used (Telko *et al.* 2007). The aPSDs obtained by both

these techniques, however, were not specific to drug mass and the results obtained therefore may be of limited use for characterization of pharmaceutical aerosols.

In a separate experiment, Telko *et al.* also determined the aPSDs of these experimental albuterol sulfate - lactose blend DPIs sampled simultaneously into a ELPI and ACI and reported that the MMAD determined with the ELPI was 2.1 μm and with the ACI, 2.2 μm (Telko *et al.* 2007). However, these data were obtained with a non-compendial set up and the authors did not validate the data against the compendial apparatus. Furthermore, the flowrate used by the authors was slightly outside the acceptable range for the ACI (26.8 - 29.7 L/min; USP 29 / NF 24 First Supplement 2006). The cut-off diameters are not well established for the USP Apparatus III (ACI with a preseparator) in the airflow range 30 - 100 L/min (USP 29 / NF 24 First Supplement 2006). While it is not recommended that the cut-off diameters for the ACI at 30 L/min be calculated using Equation VII.4 (USP 29 / NF 24 First Supplement 2006), it is interesting to note that the calculated cut-off diameters ($D_{50}$) at Q = 30 L/min are smaller than the corresponding cut-off diameters at $Q_n$ = 28.3 L/min.

$$D_{50,Q} = D_{50,Qn}(Q_n / Q)^{0.5} \qquad \text{Equation VII.4}$$

For example, cut-off diameters for the ACI stages 1 and 6 at 28.3 L/min are 5.8 and 0.7 μm, respectively; in comparison, the calculated cut-off diameters at 30 L/min for stages 1 and 6 were 5.63 and 0.67 μm, respectively. Since, the aPSDs determined by Telko et al using the modified ELPI were in good agreement with those determined using the ACI at

30 L/min, it may also be speculated that the ELPI possibly undersized the experimental DPIs tested.

A possible explanation for undersizing of aerosols produced by pMDIs by the modified ELPI is likely found in the manner in which the ELPI was originally calibrated. Aerosols (e.g., polystyrene latex, oleic acid, ammonium fluorescein, sodium chloride particles) generated for calibration of instruments used for aerosol characterization can be monodisperse or polydisperse, wet or dry, charged or uncharged, spherical or nonspherical (Chen and John 2001). Since aerosol particles are usually charged by static electrification after formation, these aerosols are passed through a neutralizer containing a bipolar ion source (e.g. $^{63}$Ni, $^{85}$Kr, $^{241}$Am) in order to reduce the number of charges on particles to charge equilibrium. In addition, a concentrator or a diluter may be required to adjust the aerosol concentration (Chen and John 2001). Conventional cascade impactors are typically calibrated using charge neutralized aerosol particles of known size and these particles are collected in an electrically conductive impactor (Marple *et al.* 2003, Garmise and Hickey 2008).

For an instrument designed for real time particle size measurement, the calibration process would determine a relationship between the response of the instrument (e.g., electronic signal) and the property (e.g., particle size, mass concentration, number concentration) being measured (Chen and John 2001). The ELPI, which was originally designed to measure real time particle size distributions by electrical detection, has been calibrated using charged monodisperse aerosols of di-octyl sebacate (DOS) with the exception of the topmost stage, stage 13, which has been calibrated using a fluorimetric

method (Keskinen *et al.* 1999, Marjamaki *et al.* 2000). In order to produce aerosol droplets in the wide size range of 0.03 - 10 μm corresponding to the ELPI cut-off diameters, two different aerosol generation techniques were employed (Marjamaki *et al.* 2000). Droplets in the size range of 0.015 - 0.9 μm were generated using an evaporation-condensation generator that produced polydisperse aerosols, which were then size classified according to their electrical mobility using a differential mobility analyzer before introducing them into the ELPI. The vibrating orifice aerosol generator was used to produce monodisperse aerosol droplets ranging in size from 0.9 - 11 μm; these aerosols were first neutralized to charge equilibrium and then highly charged by passing through the corona discharge unit before they entered the impactor (Marjamaki *et al.* 2000). Finally, the impactor was calibrated using the electrical current, rather than mass data, since the current signal produced by the charged monodisperse calibration aerosol droplets was related to the number and mass concentration (Keskinen *et al.* 1999, Marjamaki *et al.* 2000).

Because the basis of the ELPI's calibration assumes the sizing of highly charged aerosol particles and droplets, the particle size data reported for pharmaceutical aerosols in earlier studies in which the modified ELPI has been employed should be viewed with caution. In those studies the calibration of the ELPI was assumed to remain unchanged even though triboelectrification, as commonly seen in many pharmaceutical systems, cannot impart charges of the same magnitude as the corona discharge employed by the unmodified ELPI. Therefore, in order to use the modified ELPI as a sizing instrument paired with chemical analysis of drug depositing on its stages, recalibration was required.

As an alternative to a comprehensive and expensive recalibration of the ELPI with monodisperse aerosols, the present study utilized four commercially available pMDIs, representing small (Qvar), medium (Ventolin CFC and Flovent HFA) and large (Vanceril) aerosols as polydisperse calibration standards. The ACI, USP Apparatus I, (USP 29 / NF 24 First Supplement 2006) was used as the reference cascade impactor for determination of each calibration aPSD. The use of a polydisperse calibration method precludes the determination of the cut-off properties of the topmost stage (Stage 13) of the ELPI. Hence, it was necessary to recalculate the cascade impactor doses of the pMDIs used as 'calibration' aerosols for the ACI and the ELPI experiments in order to exclude the drug collected on the top stages (Stage 0 of the ACI, Stage 13 of the ELPI).

Table VII.4 summarizes the emitted dose, actuator dose, USP induction port dose, top stage dose, and impactor dose (dose collected below top stage of the impactor) for each of the four pMDIs used for calibration purposes. It was observed that the mass of drug depositing on the ELPI inlet port and the upper stage (stage 13) were consistently < 3% of the total emitted dose for all tested pMDIs; the deposition on the upper stage (stage 0) of the ACI for each inhaler was also found to be less than 3% of the impactor dose. The ballistic portion of each pMDI's output was collected primarily within the USP induction port (Table VII.4) and it was therefore considered reasonable that selective sampling into the different aerosol inlets directly atop the ACI and the ELPI would not pose a problem when using the ACI data for each pMDI product to recalibrate the modified ELPI.

Table VII.4. Emitted dose, Actuator Dose, USP Induction Port Dose, Top Stage Dose, and Impactor Dose (Dose Collected Below Top Stage of the Impactor) for Each of the Four pMDIs Used for Calibration Purposes

| Product | Label Claim | Impactor | Mass collected (SD) in μg | | | | |
|---|---|---|---|---|---|---|---|
| | | | Total Emitted dose | Actuator | Inlet port | | Impactor Dose[c] |
| | | | | | USP Induction Port[a] | Top Stage[b] | |
| Qvar | 40 μg | ACI | 36.87 (1.17) | 9.68 (1.29) | 17.45 (3.44) | 0.21 (0.07) | 19.22 (4.59) |
| | | ELPI | 37.92 (2.74) | 12.76 (1.72) | 16.69 (1.10) | 0.73 (0.10) | 20.51 (3.06) |
| Ventolin CFC | 90 μg | ACI | 88.54 (5.22) | 14.14 (1.43) | 47.77 (3.14)* | 0.84 (0.51) | 39.93 (4.12)* |
| | | ELPI | 87.64 (9.68) | 12.07 (1.11) | 55.94 (5.00)* | 0.33 (0.21) | 31.37 (5.31)* |
| Flovent HFA | 44 μg | ACI | 37.79 (1.92)* | 8.44 (0.84) | 16.92 (1.27) | 0.46 (0.14) | 20.41 (1.38)* |
| | | ELPI | 34.43 (1.69)* | 6.62 (0.37) | 16.38 (0.91) | 0.15 (0.24) | 17.90 (1.17)* |
| Vanceril | 42 μg | ACI | 37.34 (1.79) | 8.58 (2.31) | 20.98 (0.96) | 0.96 (1.08) | 15.40 (0.70)* |
| | | ELPI | 34.45 (2.27) | 7.06 (1.70) | 22.65 (1.60) | 0.16 (0.06) | 11.64 (1.49)* |

[a]Includes mass of drug recovered from the mouthpiece adaptor for both the ACI and the ELPI experiments.
[b]Includes mass of drug recovered from the ELPI inlet (Figure III.3) for the ELPI experiments which was consistently < 3% of the emitted dose for all the pMDIs tested.
[c]Mass of drug collected below the topmost stage (Stage 0 of the ACI, Stage 13 of the ELPI) of each impactor.
*Difference in the drug deposition between the ACI and the ELPI experiments statistically significant.

The total dose collecting on all the stages below the top stage (Stage 0 of the ACI, stage 13 of the ELPI), i.e., the recalculated impactor dose was statistically comparable ($p > 0.05$) between the ACI and ELPI experiments for QVAR whereas there was a small but statistically significant difference ($p < 0.05$) in the recalculated impactor doses between the ACI and the ELPI for its higher variance suspension counterparts as shown in Table VII.4. Because these apparent statistical differences in impactor dose could not be attributed to differences in the masses of drug collected in the experimentally variable portion of each inlet configuration, i.e., the ELPI inlet and top stage deposition (Table VII.4), it was reasonable to assume that the aerosols depositing from each pMDI in the ACI and the modified ELPI had comparable aPSDs. This assumption would be reasonable provided the droplet evaporation for the pMDI aerosols sampled inside the two cascade impactors was comparable.

The ELPI is a low-pressure impactor and in comparison to the ACI (which operates at atmospheric pressure), the downstream pressure measured at the ELPI stage 5 is equivalent to the pressure at the base of the ACI (90 - 100 kPa); stages 1 - 4 of the ELPI are at pressures lower than 90 kPa (Appendix A.I, Greenspan 2008). Since the downstream pressures for stages 5 - 13 of the ELPI and all the ACI stages are equivalent, droplet evaporation of the pMDI aerosols may be considered to be comparable for those stages as well. From the mass distribution data obtained for the ELPI experiments, it was observed that drug deposited predominantly on stages 6 and above, with the exception of QVAR, suggesting therefore that the aerosol clouds being sampled into the ACI and the EPI would be comparable.

**VII.D.2. Curve Fitting of the ACI aPSD Data for the Calibration Aerosols**

The mass distribution data from stages 1 - 7 plus filter of the ACI in each single actuation experiment was expressed as a percentage of the total impactor dose, which is the total drug mass collected on the filter and stages 1 - 7, for each product (n = 5). Drug deposition on stage 0, the topmost stage of the ACI, was not included in the determination of total impactor dose since the upper limit of the size range of drug particles depositing on that stage is unknown. The aPSDs of each of these pMDI aerosols followed a lognormal distribution. The lognormal distribution of the aPSDs of pMDIs can be described in terms of two variables, a single MMAD (μm) and a dimensionless geometric standard deviation (GSD) (Thiel 2002). The cumulative percent drug undersize data determined using the ACI was therefore fitted to a lognormal distribution function using non-linear regression analysis.

Figure VII.2 shows the mean results for cumulative percent drug undersize versus the aerodynamic cut-off diameter for each stage of this ACI after mensuration in accord with the USP (USP 29 / NF 24 First Supplement 2006). Also shown, as continuous curves, are the results of curve fitting for each product. The numerical results of curve fitting the ACI data and its 95% confidence limits are shown in Table VII.5. Also shown in the table are the MMADs for the calibration pMDIs reported in the literature obtained using the ACI. The MMADs obtained from curve fitting were not statistically different from those obtained for all the calibration pMDIs when calculated by linear interpolation of data, which included drug deposition on stage 0 of the ACI.

Figure VII.2. Mean Cumulative Percent of Drug Mass Undersize versus Aerodynamic Diameter (n = 5), Following Collection of Single Actuations of Qvar, Ventolin CFC, Flovent HFA, and Vanceril in the ACI at 28.3 L/min. The Solid Profiles are the Result of Curve Fitting to Equation VII.1. Model Selection Criteria Results Exceeded 5 in all Cases and Values for all Coefficients of Determination (COD) > 0.99. Error Bars are Sample Standard Deviations.

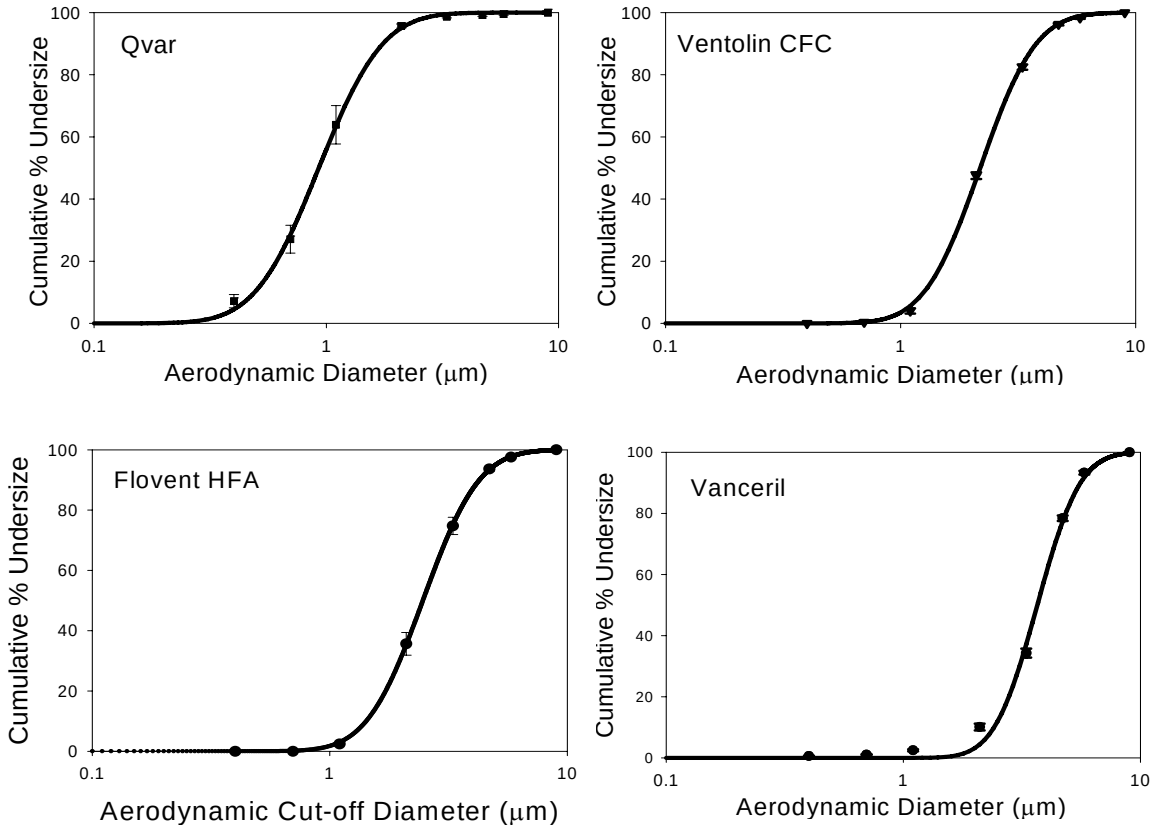

Table VII.5. Numerical Results of Curve-Fitting the Cumulative Percent Undersize Data from the ACI for Each Aerosol Product to Equation VII.1. The Best Estimates for MMAD and GSD are Shown with their 95% Confidence Intervals along with the MMADs Reported in Literature

| Product | MMAD (μm)[a] | | Confidence Interval (μm) | GSD | Confidence Interval | Model Selection Criteria (MSC) | Coefficient of Determination (COD) |
|---|---|---|---|---|---|---|---|
| | Curve Fit | Literature | | | | | |
| Qvar | 0.93 | 1.1[b] | 0.91 – 0.95 | 1.64 | 1.58 – 1.70 | 5.3828 | 0.9957 |
| Ventolin CFC | 2.18 | 2.2[c] | 2.16 – 2.20 | 1.54 | 1.52 – 1.55 | 7.7427 | 0.9996 |
| Flovent HFA | 2.46 | - | 2.44 – 2.50 | 1.55 | 1.51 – 1.56 | 6.6740 | 0.9962 |
| Vanceril | 3.67 | 3.9[d] | 3.62 – 3.73 | 1.4 | 1.36 – 1.42 | 5.4910 | 0.9985 |

[a]For numerical fitting of the ACI data in this study, drug deposition on stage 0 was not included in the determination of total impactor dose since the upper limit of the size range of drug particles depositing on stage 0 is not known.
[b]Leach *et al.* 1998, [c]Mitchell *et al.* 1999, [d]Kamiya *et al.* 2004.

The MMADs obtained from curve fitting were comparable with those reported in the literature even though the USP technique used in the literature for determination of MMADs includes drug deposition data on stage 0 of the ACI. The curve fitting procedure produced excellent fits of the ACI cumulative data which were well modeled as mono-modal and log-normally distributed as indicated by the goodness-of-fit parameters; MSC > 5 and COD > 0.99 for all the pMDIs. Although the fit for cumulative deposition of drug below stage 4 deviated slightly from the experimental results for Vanceril (Figure VII.2), the COD value suggested that 99.6% of the total variance was accounted for by the model used to fit the cumulative percent BDP undersize data for Vanceril. In addition, a MSC value of 5.4910 also gave an indication of the goodness-of-fit of the lognormal function used in curve fitting the Vanceril ACI data.

### VII.D.3. Calculation of the Aerodynamic Cut-off Diameters of the Modified ELPI Using the ACI Curve Fitted Data

The curves of best fit from the ACI (Figure VII.2), and thus the best estimates for MMAD and GSD (Table VII.5), were also assumed to describe the clouds penetrating beneath the topmost stage (stage 13) of the ELPI. Because Equation VII.1 cannot be solved analytically for aerodynamic diameter (and the cut-off diameter of the ELPI stages) (Thiel 2002), MMAD and GSD were fixed at their product-specific best estimates and solutions for the cut-off diameter were determined for each stage of the ELPI by the iterative technique described in Section VII.C.3. This procedure resulted in a series of product-

specific numerical solutions or "estimates" for the cut-off diameters for the major stages of the ELPI. For example, if 79% of the cloud from a single shot of Qvar was shown to have aerodynamic diameters that enabled penetration of the drug beneath stage 8 of the ELPI, this would enable the substitution of a value of 79 (%) for y (LHS of Equation VII.1) while MMAD and GSD are assigned their best estimates from Table VII.5 (0.93 μm and 1.64, respectively). Numerical solution of Equation VII.1 for aerodynamic diameter (x) would then produce a solution = 1.37 (μm). This value (1.37) was then assigned to the cut-off diameter of stage 8 for that individual experiment. Because each experiment was replicated, this resulted in 5 individual estimates along with a mean and sample standard deviation for the cut-off diameter of stage 8 from the Qvar experiments.

Table VII.6 shows the means and standard deviations of the cut-off diameters for the individual stages of the ELPI for each of the calibration products. The mean cut-off diameters calculated using each of the four calibration pMDIs have been tabulated in Appendix A.VI.4. The calibration aerosols used in this study were polydisperse in nature, hence on certain stages of the ELPI, no drug was detected and consequently cut-off diameters could not be calculated for those stages from some of the calibration pMDI aerosols. Cut-off diameter for stage 1 could not be obtained from any of the calibration pMDIs since no drug was detected on that stage. Cut-off diameters for stages 2 - 5 could be calculated using cumulative percent undersize data from QVAR pMDI aerosols alone since the drug clouds failed to penetrate beyond stage 6 for Ventolin CFC and beyond stage 7 for Flovent HFA and Vanceril.

Table VII.6. Calculated Aerodynamic Cut-off Diameters (μm) of the Different ELPI Stages Based on the Replicate Results (n = 5) for Each of the 4 pMDIs Studied as Calibration Standards. Results Expressed as Mean (SD).

| Stage # | Qvar | Ventolin CFC | Flovent HFA | Vanceril |
|---|---|---|---|---|
| 1 | [a] | [a] | [a] | [a] |
| 2 | 0.28 (0.01) | [a] | [a] | [a] |
| 3 | 0.35 (0.01) | [a] | [a] | [a] |
| 4 | 0.44 (0.02) | [a] | [a] | [a] |
| 5 | 0.56 (0.01) | [a] | [a] | [a] |
| 6 | 0.70 (0.02) | 0.77 (0.03) | [a] | [a] |
| 7 | 0.98 (0.06) | 1.03 (0.02) | 0.98 (0.01) | 1.79 (0.35) |
| 8 | 1.37 (0.14) | 1.42 (0.01) | 1.39 (0.02) | 1.65 (0.18) |
| 9 | 2.10 (0.12) | 2.08 (0.04) | 2.01 (0.04) | 2.31 (0.08) |
| 10 | 2.64 (0.24) | 3.15 (0.15) | 2.93 (0.06) | 3.01 (0.08) |
| 11 | 3.39 (0.22) | 5.08 (0.31) | 4.62 (0.08) | 4.54 (0.07) |
| 12 | [b] | [b] | [a] | 6.37 (0.21) |
| 13 | [c] | [c] | [c] | [c] |

[a] Drug mass < LOQ

[b]Stages 12 and 13 were combined since drug detected on individual stages in preliminary experiments was often < LOQ

[c]Polydisperse calibration provides no information on the cut-off of the uppermost stage

For stage 6, cut-off diameters could be calculated from two aerosols, QVAR and Ventolin CFC. Drug deposition data from all the calibration pMDI aerosols could be used to calculate cut-off diameters for stages 7 - 11; higher degree of confidence can be placed on the calculated cut-off diameters for stages 7 - 11 since most of the drug deposited predominantly within this size range for all the four calibration pMDIs. The cut-off diameter for stage 12 could be calculated from Vanceril data alone since no drug was detected on stage 12 for any of the other calibration pMDIs. The cut-off diameter for the topmost stage, stage 13, could not be calculated using this technique from any of the calibration aerosols since the upper cut-off diameter of the polydisperse calibration aerosols depositing on the topmost stage was not known.

An inclusion criterion was set for determining the final recalibrated cut-off diameters from the values obtained in Table VII.6. Those calculated cut-off diameters for which the mean cumulative percent of the impactor dose depositing below a given stage fell within the range of 3 - 97 % (Table VII.7) were chosen.

Table VII.7. Mean Cumulative Percent of the Impactor Doses of the Four Calibration pMDIs Used in the Study (n = 5).

| Stage No. | Qvar | Ventolin CFC | Flovent HFA | Vanceril |
|---|---|---|---|---|
| Stage 1 | 0 | 0 | 0 | 0 |
| Stage 2 | 0.75 | 0 | 0 | 0 |
| Stage 3 | 2.63 | 0 | 0 | 0 |
| Stage 4 | **6.41** | 0 | 0 | 0 |
| Stage 5 | **15.74** | 0 | 0 | 0.73 |
| Stage 6 | **28.48** | 0.77 | 0 | 0.73 |
| Stage 7 | **53.92** | **4.12** | 1.55 | 0.81 |
| Stage 8 | **77.91** | **16.07** | **8.98** | 2.01 |
| Stage 9 | **94.84** | **45.73** | **31.69** | **7.9** |
| Stage 10 | 98.09 | **80.22** | **65.59** | **27.18** |
| Stage 11 | 99.52 | **97.43** | **92.81** | **74.08** |
| Stage 12 | 99.52 | 97.43 | 98.38 | **95.27** |
| Stage 13 | 100 | 100 | 100 | 100 |

This inclusion criteria was chosen so that the data fell in the linear portion of the lognormal distribution for each of the products since the reliability of cut-off diameters obtained would decrease for stages when drug deposition is low, i.e., the tail ends of the lognormal curve. The values of cumulative percent undersize data for the pMDIs marked in bold in Table VII.7 fell within the linear portion of the cumulative percent undersize vs. aerodynamic size curve; the cut-off diameters calculated using those values were averaged. Table VII.8 summarizes the final cut-off diameters for the ELPI stages 4 - 12 calculated

using this technique. For comparative purposes, the manufacturer's claims of the cut-off diameter for each stage of the ELPI have also been tabulated (Table VII.8).

Table VII.8. Mean Recalibration Values for the Aerodynamic Cut-off Diameter of the ELPI Stages Compared to the Values Provided by Dekati.

| ELPI Stage # | Dekati Cut-off Diameter (μm) | Mean Calculated Cut-off Diameter (μm) | Dekati d50[a]/ Mean Calculated d50 |
|---|---|---|---|
| 1 | 0.03 | [b] | [b] |
| 2 | 0.06 | [b] | [b] |
| 3 | 0.10 | [b] | [b] |
| 4 | 0.16 | 0.44 | 0.37 |
| 5 | 0.27 | 0.56 | 0.48 |
| 6 | 0.39 | 0.70 | 0.56 |
| 7 | 0.62 | 1.01 | 0.62 |
| 8 | 0.96 | 1.40 | 0.69 |
| 9 | 1.62 | 2.12 | 0.76 |
| 10 | 2.42 | 3.03 | 0.80 |
| 11 | 4.05 | 4.75 | 0.85 |
| 12 | 6.67 | 6.37 | 1.05 |
| 13 | 10.08 | [c] | [c] |

[a]d50: Aerodynamic Cut-off Diameter
[b]Cumulative percent undersize data fell out of the inclusion criteria
[c]Polydisperse calibration does not provide information on the cut-off diameter of the topmost stage

Table VII.9 shows the cut-off diameters of the ELPI stages calculated using the 95% confidence intervals of the best estimates of the MMAD and GSD for all the four calibration pMDIs.

Table VII.9. Mean Values of 50% Cut-off Diameters for ELPI Stages 4 - 12 Calculated Using 95% Confidence Intervals of the Best Estimates of MMADs and GSDs Obtained from Curve-Fitting the ACI Cumulative Data for the Four Calibration pMDIs

| Stage No. | Mean Calculated Cut-Off Diameters (μm) of ELPI Stages 4 - 12 | | | | |
|---|---|---|---|---|---|
| | Using Mean Estimates of MMAD & GSD from ACI Curve Fit | Using Lower CIs[a] of MMAD & GSD from ACI Curve Fit | Using Upper CIs[a] of MMAD & GSD from ACI Curve Fit | Using Lower CI[a] of MMAD & Upper CI[a] of GSD from ACI Curve Fit | Using Upper CI[a] of MMAD & Lower CI[a] of GSD from ACI Curve Fit |
| Stage 4 | 0.44 | 0.45 | 0.42 | 0.40 | 0.47 |
| Stage 5 | 0.56 | 0.57 | 0.56 | 0.53 | 0.60 |
| Stage 6 | 0.70 | 0.70 | 0.70 | 0.67 | 0.73 |
| Stage 7 | 1.00 | 1.00 | 1.01 | 0.98 | 1.03 |
| Stage 8 | 1.40 | 1.38 | 1.41 | 1.37 | 1.42 |
| Stage 9 | 2.12 | 2.09 | 2.17 | 2.11 | 2.15 |
| Stage 10 | 3.03 | 2.99 | 3.07 | 3.00 | 3.06 |
| Stage 11 | 4.75 | 4.60 | 4.89 | 4.79 | 4.71 |
| Stage 12 | 6.37 | 6.06 | 6.70 | 6.50 | 6.25 |

[a]CIs: 95% Confidence Intervals on estimates of MMAD and GSD obtained from curve fitting the ACI cumulative data of the four calibration pMDIs (Qvar, Ventolin CFC, Flovent HFA and Vanceril) to a lognormal cumulative distribution function.

The cut-off diameters summarized in Table VII.9 were not statistically different ($p>0.05$) from those calculated using the best estimates of MMAD and GSD for the ELPI stages 4 - 11. However, the difference became statistically significant ($p < 0.05$) for stage 12 due to a larger variance in stage 12 deposition associated with testing Vanceril.

The manufacturer's reported cut-off diameters and the mean cut-off diameters calculated from the mean estimates of the MMAD and GSD have been compared in Table VII.8. Of greatest note is the increasing margin of error in the calculated cut-off diameters of the lower stages of the ELPI, i.e., the impactor stages with smaller cut-off diameters deviated more markedly than the upper stages from values claimed for corona-charged aerosols. For example, the calculated stage cut-off diameter for the ELPI Stages 4 and 12 were determined to be 0.44 and 6.37 μm, respectively as compared to the manufacturer's reported cut-off diameters (0.16 and 6.67 μm for Stages 4 and 12, respectively).

While particle charging theory is a complex function of size (Hinds 1999), the trend of increasing errors as aerosol size became smaller (Table VII.8) suggests that the ELPI may behave differently when separating corona-charged aerosol particles. Briefly, it is possible that deposition of charged particles in this impactor may be influenced by mechanisms in addition to impaction. Electrophoretic mobility of charged particles, for example, increases substantially as size decreases. Further investigation into the influence of electrostatics on in vitro aerosol separation during testing therefore appears warranted but is not included in the scope of this study.

**VII.D.4. Validation of the Recalibration of the Modified ELPI**

To validate the recalibration of the modified ELPI and the cut-off diameters calculated for the modified ELPI, a single canister of a fifth product, Ventolin HFA, was studied after the ELPI recalibration procedure had been completed. Ventolin HFA was tested by collecting five single actuations in the ACI in accord with the USP and the procedures repeated in the modified ELPI. Table VII.10 shows that both the actuator deposition as well as drug deposited in the USP induction port for Ventolin HFA aerosols were statistically comparable ($p > 0.05$) between the ACI and the ELPI experiments.

Table VII.10. Summary of Mass Recovery from Ventolin HFA using ACI and modified ELPI (n = 5, 5 shots / can, 1 can)

| Impactor | Mass Recovered (μg) | | | |
|---|---|---|---|---|
| | Emitted dose | Actuator | USP Induction Port[a] | Impactor Dose[b] |
| ACI | 97.46 (10.35)* | 13.57 (1.82) | 44.47 (4.66) | 52.99 (6.74)* |
| ELPI | 78.26 (6.03)* | 13.52 (1.59) | 41.70 (4.61) | 36.55 (2.79)* |

[a]Includes mass of drug recovered from the mouthpiece adaptor and the ELPI Inlet.
[b]Mass of drug collected on all stages of each impactor (Stages 0 - 7 & filter of the ACI, Stages 1-13 of the ELPI).
*Difference in the drug deposition between the ACI and ELPI experiments statistically significant.

The mean emitted dose of Ventolin HFA was statistically higher ($p < 0.05$) for the ACI when compared to that obtained from the ELPI experiments (Table VII.10). While the total mass recovery for these single shot experiments was more variable for Ventolin HFA (a surfactant-free formulation of albuterol sulfate in HFA 134a) than for any of the other

products, the mass depositing on the ELPI inlet was less than 0.5% of the emitted dose in all cases. Not surprisingly, the mean impactor dose of Ventolin HFA obtained in the ACI was significantly higher ($p < 0.05$) than that obtained from the ELPI.

Cumulative percent mass undersize for Ventolin HFA was calculated for each experiment and plotted using the ACI cut points taken from (USP 29 / NF 24 First Supplement 2006) while the single actuation data from the modified ELPI was treated in two ways; cut-off diameter values were taken either from Dekati (Table III.1) or from the results of the recalibration shown in Table VII.8. Figure VII.3 shows the results of this procedure.

Figure VII.3. Mean Cumulative Percent Undersize Versus Aerodynamic Diameter (n = 5), Following Collection of Single Actuations of Ventolin HFA in ACI (Circle), Ventolin HFA in the Modified ELPI with Cut-Off Diameters taken from Dekati (Triangle) or Calculated in this Study (Inverted Triangle). The Profiles are Simple Linear Interpolations Between Data Points. Error Bars are Sample Standard Deviations.

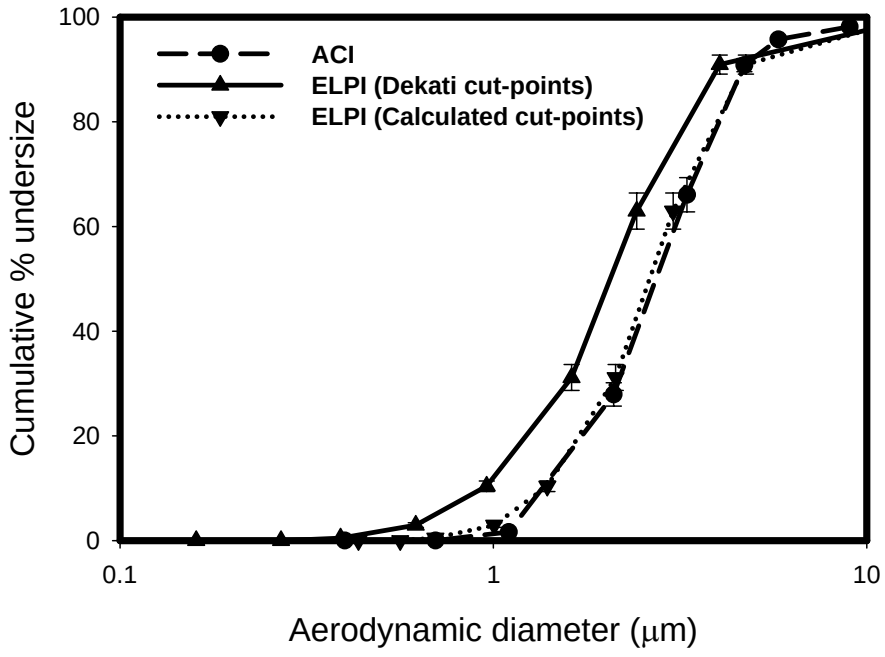

The MMAD for Ventolin HFA pMDI aerosols using the modified ELPI with the manufacturer-supplied cut-off diameters was 2.06 ± 0.08 μm. The MMAD of Ventolin HFA obtained using the calculated cut-points for the ELPI (Table VII.8) was 2.63 ± 0.09 μm, which was statistically comparable ($p = 0.0852$) to that determined using the ACI (2.73 ± 0.09 μm). This study showed that the aPSDs for Ventolin HFA were indistinguishable when determined in the modified ELPI or the ACI, provided the new cut points described in Table VII.8 were used for the aerodynamic particle size analysis.

The use of an instrument at operating conditions and parameters different from those utilized when the instrument was originally calibrated may render that calibration inappropriate and hence recalibrating the instrument under the modified conditions is essential to operate the instrument with confidence (Chen and John 2001). It is reasonable to assume that the modified ELPI subdivides particles primarily by impaction, in a similar fashion to the ACI and other cascade impactors, which was the basis of this recalibration exercise in which the stage cut points for known aerosols in the ELPI were determined by direct comparison to a mensurated ACI, used as a calibration instrument. Previous studies have shown that aPSDs of pharmaceutical aerosols determined using different ACIs can be variable due to inter-impactor stage cut-points variability (Stein and Olson 1997). However, the present study was an attempt to calibrate a single ELPI in comparison with an ACI, both of which have been utilized in the same research laboratory and was not intended to investigate inter-impactor variability of PSD data from multiple ELPI and ACI cascade impactors. To this end, it was ensured that both the ACI and the ELPI used for

these experiments were duly mensurated by MSP Corporation of St. Paul, MN, USA and Dekati, Inc. of Tampere, Finland, respectively.

In summary, the study showed that in the absence of a comprehensive recalibration of the ELPI using monodisperse aerosols, commercially available, polydisperse aerosols may be used as calibration standards in a reference cascade impactor and that this constitutes a practical way of calibrating alternative particle sizing instruments.

# VIII. OVERALL DISCUSSION AND SUMMARY

Aerosol electrostatics is considered to be an important property of pharmaceutical aerosols. Previous studies have shown that the electrostatic properties of pMDI aerosols characterized using the aerosol electrometer and the modified electrical low pressure impactor (ELPI) are a function of both formulation and packaging components (Peart *et al.* 1998, Glover and Chan 2004a, Kwok *et al.* 2005). The modified Electrical Low Pressure Impactor (ELPI) enables measurement of the charge distribution of aerosol clouds as a function of particle size, and the simultaneous determination of the mass distribution using chemical analysis. However, in order to fully assess the cause and effects of pMDI aerosol electrostatics in terms of its biological and regulatory implications, it is necessary to understand the basic charging mechanisms inside the pMDI formulation as well as the electrostatic properties of aerosols produced by these HFA based pMDI formulations.

Electrical properties of the formulation within the pMDI canister are not well characterized, primarily due to a lack of consensus on charge generation mechanisms and the experimental difficulties associated with the measurement of electrical properties in non-aqueous liquefied propellants (Sidhu *et al.* 1993, Sandstrom *et al.* 1994, Rogueda 2002, Traini *et al.* 2005). Electrical resistivity of experimental HFA 134a based beclomethasone dipropionate (BDP) solutions and albuterol sulfate suspensions were

determined in order to establish the presence of ionic species in these systems. Although HFA 134a has high resistivity, which could not be measured reliably, the presence of ethanol in the control HFA solutions tested increased the conductivity of the formulation, which resulted in a decrease in the resistivity. The mean electrical resistivity of a 7% ethanol / 93% HFA 134a blend (0.83 ± 0.02 MΩ.cm) was significantly lower in magnitude than that reported for HFA 134a in the literature (180 MΩ.cm; Solvay Fluor Product Bulletin 2001). The presence of water in ethanol may confound the results obtained for resistivity measurements of the ethanol - HFA based formulations. For albuterol sulfate suspensions in HFA 134a containing ethanol and oleic acid, the resistivity measurements decreased with increased ethanol concentrations. The mean resistivity of an albuterol sulfate suspension containing 0.02% oleic acid in 5% ethanol / 95% HFA 134a was 1.74 ± 0.02 MΩ.cm, which was higher than that obtained for a suspension in 10% ethanol / 90% HFA 134a (0.37 ± 0.01 MΩ.cm). The resistivity measurements suggested that ethanol-containing HFA formulations are relatively polar and may likely produce charged species in these systems.

Electrophoretic mobility studies were performed to investigate the surface charge of albuterol sulfate suspensions in HFA 134a. Albuterol sulfate demonstrated a positive zeta potential (75.9 ± 26.2 mV) in a simple suspension in 100% HFA 134a, although, there was variability in the measurements. It may be hypothesized that surface charge formation in such formulations may be due to the presence of trace water (59 ± 7 ppm) or impurities. In addition to these simple albuterol sulfate suspensions, albuterol sulfate suspensions in HFA 134a containing oleic acid and ethanol were also investigated. The electrophoretic

mobility and the corresponding zeta potential of albuterol sulfate decreased in the presence of oleic acid and ethanol. The zeta potential value decreased from 39.5 ± 7.8 mV for an albuterol sulfate suspension containing 0.02% oleic acid in a 5% ethanol / 95% HFA 134a blend to 15.4 ± 9.7 mV for a suspension in a 15% ethanol / 85% HFA 134a blend. However, the limitation of this technique is that dilute particle concentrations are required. Unfortunately, these dilute concentrations do not reflect the concentration of drug present in commercially available suspension pMDIs and hence the results obtained are difficult to extrapolate to commercial products.

In order to gain an improved understanding of the possible interactions within pMDI suspensions on the molecular level, a pilot study was performed, wherein molecular models of a simple pMDI formulation containing an albuterol sulfate crystal unit cell in HFA 134a were constructed and optimized using molecular modeling software, Sybyl. The interactions between the drug and propellant molecules were investigated using the Hydropathic INTeractions (HINT) program. The total HINT score was predominantly negative (-7597 ± 2063) signifying unfavorable interactions between the albuterol sulfate unit cell and the surrounding HFA 134a molecules. In practice, this observation is not unexpected. It is well recognized that HFA based suspension pMDIs have an increased propensity for drug adhesion to the canister inner surface and the use of fluorocarbon polymer coating, e.g., PTFE (polytetrafluoroethylene), on the canister inner surfaces to minimize drug adhesion has been documented in the patent literature (Ashurst *et al.* 2000a).

Although the majority of the interactions between the albuterol sulfate unit cell and individual HFA 134a molecules were unfavorable, approximately 23% of the total number of HFA 134a molecules surrounding the albuterol sulfate unit cell showed net favorable interactions with the unit cell. Unfavorable hydrophobic-polar interactions were likely between carbon atoms of HFA 134a and polar groups of albuterol sulfate, while base-base interactions may be accounted for by the unfavorable interactions between the fluorine atoms of HFA 134a and sulfate group of albuterol sulfate. Hydrophobic interactions between carbon atoms of HFA 134a and those present on the side chain of albuterol sulfate and polar acid-base interactions between the hydroxyl or amine group of albuterol sulfate with the fluorine atoms of HFA 134a contributed to the favorable or positive interaction scores.

Molecular modeling studies of interactions within a complex formulation, e.g., interactions within a molecular model containing albuterol sulfate unit cell, oleic acid and ethanol molecules solvated in a HFA 134a solvent box, were significantly more challenging compared to the two-component system. Since, the oleic acid and ethanol molecules were arbitrarily placed around the albuterol sulfate unit cell in the molecular model, it was not possible to take into consideration the interactions between the solvated components within the model for every likely conformation with respect to the interacting molecules. However, an indication of the likely types of interactions could be obtained from the analysis of these models. In order to gain confidence in the HINT score analysis of the likely types of interactions within these pMDIs, an increased number of replicates would be required. Molecular modeling in conjunction with the analysis of interactions

using the HINT program may serve as a useful tool to provide a better understanding of interactions between pMDI formulation components on a molecular level in a propellant medium. Studies could also usefully be extended to the investigation of canister coating materials used in pMDI canisters.

Electrostatic charge characterization of commercial HFA based solution and suspension pMDIs using a modified ELPI has previously been reported (Kwok *et al.* 2005), however, a systematic study investigating the differences in the electrostatic charging characteristics of solution and suspension HFA pMDIs is deficient. HFA propelled beclomethasone dipropionate (BDP) solution pMDIs and albuterol sulfate suspension pMDIs were chosen as the model pMDIs to investigate the influence of formulation components on the aerosol charge determined using the modified ELPI. It was hypothesized that since BDP solution pMDIs are a homogeneous system each aerosol droplet would have a uniform distribution of drug and excipients, and may exhibit similar charging characteristics resulting in a unipolar charge distribution. Not surprisingly, QVAR 40, a commercially available BDP HFA solution pMDI, produced predominantly unipolar electropositive aerosol clouds with a mean total net electrostatic charge of +449 ± 254 pC.

The experimental 100% HFA 134a pMDIs produced primarily net electropositively charged aerosol clouds (mean net inherent charge: 68 ± 100 pC). The mean net inherent charge for ethanol / propellant blend aerosol clouds was also predominantly net electropositive (108 ± 11 pC). The experimental BDP solution pMDIs produced predominantly electropositive clouds with a mean net electrostatic charge of 160 ± 30 pC,

which was significantly higher ($p = 0.0069$) than that obtained for the ethanol / propellant blend pMDIs. The addition of BDP to an ethanol / propellant HFA 134a blend did not affect the unipolar charge distribution profile observed for the ethanol - propellant blend. The predominant effect of ethanol as a polar cosolvent on the electrical properties of the control HFA based solutions was confirmed from the electrical resistivity measurements. The addition of ethanol decreased the resistivity of pure propellant HFA 134a suggesting that addition of ethanol increased the polar nature of the propellant as well as the conductivity of the solution.

Ventolin HFA, an albuterol sulfate HFA suspension pMDI, produced bipolar aerosol clouds with a mean net FPD charge (particles smaller than 4.05 μm, manufacturer reported cut-off diameter for ELPI stage 11) of –232 ± 37 pC, which was comparable to the FPD charge (particles smaller than 5 μm) reported in the literature for Ventolin HFA (-231 ± 3 pC), measured using an aerosol electrometer (Kulphaisal 2003). Propellant HFA 134a pMDIs produced primarily net electropositively charged clouds (mean net inherent charge: 59 ± 45 pC). The mean net charge of the propellant droplets on the individual stages, stages 1 - 12 of the ELPI, was found to be negligible in comparison to that of the experimental albuterol sulfate pMDI aerosols, which produced bipolar charged aerosol clouds. Particles depositing on stages 1 - 6 were net electronegatively charged. Interestingly, negligible albuterol sulfate was detected on stage 5, while 0.05 ± 0.01 μg (less than 0.1% of the emitted dose) penetrated beyond stage 5. Particles depositing on stages 7 - 12 were net electropositively charged; chemical analysis showed that albuterol deposited predominantly on stages 7 - 12. This observation compares favorably with the

zeta potential measurements for albuterol sulfate suspensions in HFA 134a since albuterol sulfate particles were observed to acquire a positive zeta potential (75.9 ± 26.2 mV) in HFA 134a. The electronegative charge on the ELPI stages 1 - 5 has previously been attributed to non-drug (propellant) containing droplets (Kwok *et al.* 2005). However, the systematic investigation of the electrostatic charging properties of propellant HFA 134a pMDIs and albuterol sulfate suspension pMDIs adopted in the study demonstrated that the electronegative charge on the lower stages of the ELPI was not due to propellant droplets.

The influence of soluble impurities in the experimental albuterol sulfate suspension pMDIs on the electrostatic charge was investigated by filtering the suspensions and analyzing the electrostatic properties of the filtrates. In the absence of suspended albuterol sulfate particles in the formulation, the electrostatic charging characteristics of aerosols produced by the filtrates of the experimental albuterol sulfate pMDIs were similar to those produced by the filtrates of control 100% HFA 134a pMDIs. The absence of highly charged particles on the Stages 1-4 of the ELPI suggests that soluble albuterol impurities or the propellant HFA 134a itself may not be responsible for the highly electronegative charge on the lower stages of the ELPI for the albuterol sulfate pMDIs.

Interestingly, the number concentration of albuterol particles deposited on stages 1-4 of the ELPI calculated on the basis of the mass of albuterol (0.05 ± 0.01 μg) deposited on those stages for the experimental albuterol sulfate pMDIs was approximately 75% of the total particle number concentration on stages 1-13 of the ELPI. It may be possible that this large number of submicron particles of albuterol detected on stages 1 - 4 could be responsible for the electronegative charge. Although sub-micron particles do not have

appreciable mass, it might be more relevant to measure the particle number or surface area to understand their impact. Furthermore, the addition of albuterol sulfate to propellant HFA 134a appeared to modify the triboelectric properties of the non-drug droplets. It was hypothesized that the interactions between HFA 134a droplets and the valve stem on actuation of the pMDI would be influenced by albuterol sulfate particles such that the droplets emitted from the actuator orifice contained both positively and negatively charged species.

Recent evidence suggests that the modified ELPI appears to underestimate the particle size of aerosols produced by commercially available pMDIs in comparison to that obtained using the ACI (Orban and Peart 2004, Keil *et al.* 2006). The ELPI, which was originally designed to measure real time particle size distributions by electrical detection, has been calibrated using charged monodisperse aerosols of di-octyl sebacate (DOS) with the exception of the topmost stage, stage 13, which has been calibrated using a fluorimetric method (Keskinen *et al.* 1999, Marjamaki *et al.* 2000). The modified ELPI (charger-free), however, has been used for sizing pharmaceutical aerosols by chemical analysis of drug deposited on each stage of the ELPI. Triboelectrification, as commonly seen in many pharmaceutical systems, cannot impart charges of the same magnitude as the corona discharge employed by the unmodified ELPI, hence the electrical calibration of the ELPI cannot be assumed to remain unchanged in the modified ELPI.

The present study utilized four commercially available pMDIs, representing small (Qvar), medium (Ventolin CFC and Flovent HFA) and large (Vanceril) aerosols as polydisperse calibration standards. The ACI was used as the reference cascade impactor

for determination of each calibration aPSD. The use of a polydisperse calibration method precluded the determination of the cut-off properties of the topmost stage (Stage 13) of the ELPI. The mean cut-off diameters for stages 4 - 12 obtained following recalibration of the modified ELPI were 0.44, 0.56, 0.70, 1.01, 1.40, 2.12, 3.03, 4.75, 6.37 μm, respectively, which were found to deviate increasingly from the manufacturer-supplied values (0.16, 0.26, 0.39, 0.62, 0.96, 1.62, 2.42, 4.05, 6.67 μm, respectively) as aerodynamic diameter decreased suggesting that the ELPI may behave differently when separating corona-charged aerosol particles. It is possible that deposition of charged particles in this impactor may be influenced by mechanisms in addition to impaction. Further investigation into the influence of electrostatic charge on *in vitro* aerosol separation during *in vitro* testing appears warranted but is not included in the scope of this study. Validation of the ELPI recalibration was performed by determining the aPSD of Ventolin HFA using the modified ELPI and the ACI. Ventolin HFA's MMAD determined using the modified ELPI with the manufacturer-supplied d50s was 2.06 ± 0.08 μm. The MMAD calculated using the recalibrated d50s was 2.63 ± 0.09 μm, which was statistically indistinguishable ($p = 0.0852$) from that determined for Ventolin HFA using the ACI (2.73 ± 0.09 μm). The aPSDs for Ventolin HFA were indistinguishable when determined in the modified ELPI or the ACI, provided the calculated cut-off diameters were used for the aerodynamic particle size analysis.

In summary, the electrical resistivity and electrophoretic mobility measurements confirmed the presence of charged species within HFA based solutions and suspensions although the nature of these species remains unknown. These measurements

were influenced by the concentration of cosolvent (ethanol) and to a lesser extent by the presence of soluble drug (BDP) and surfactant (oleic acid). The presence of moisture in the formulations was also considered to influence the formation of charged species. Pilot molecular modeling studies, in conjunction with the analysis of interactions using HINT, provided an improved understanding of the possible interactions within albuterol sulfate HFA suspension pMDIs. A systematic investigation of the electrical properties of droplets generated by HFA solution and suspension pMDIs demonstrated that the electrical properties were a function of the formulation type (solution or suspension) and the formulation components, as well as the particle size. Taken together with the studies investigating the electrical properties of HFA based solutions and suspensions, an improved understanding of charge formation within these formulations in relation with the electrostatic properties of the aerosols was provided. Finally, the present study also showed that in the absence of a comprehensive recalibration of the ELPI using monodisperse aerosols, commercially available, polydisperse aerosols may be used as calibration standards in a reference cascade impactor and that this constitutes a practical way of calibrating alternative particle sizing instruments.

# LIST OF REFERENCES

# LIST OF REFERENCES

Ali, M., Reddy, R.A. and Mazumder, M.K. (2007). Electrostatic charge effects on deposition of asthma drugs in the human oral-pharyngeal-laryngeal regions. In.: Crowley, J., Barringer, S., and Sundararajan, R. editors. *Proceedings of the ESA Annual Meeting on Electrostatics 2007*, Laplacian Press, Cambria, California, 199-209.

Ashurst, I.C., Herman, C.S., Li-Bovet, L. and Riebe, M.T. (2000a). Metered dose inhaler for albuterol. U.S. Patent No. 6,131,566, Glaxo Wellcome Inc.

Ashurst, I.C., Herman, C.S., Li-Bovet, L. and Riebe, M.T. (2000b). Metered dose inhaler for salmeterol. U.S. Patent No. 6,143,277, Glaxo Wellcome Inc.

ASTM Standard D1169-02 (2002). Standard test method for specific resistance (resistivity) of electrical insulating liquids. ASTM International, West Conshohocken, PA.

ASTM Standard D4308-95 (2005). Standard test method for electrical conductivity of liquid hydrocarbons by precision meter. ASTM International, West Conshohocken, PA.

Balachandran, W., Ahmad, C.N. and Barton, S.A. (1991). Deposition of electrically charged drug aerosols in lungs. *Institute of Physics Conference Series*, **118**, 57-62.

Balachandran, W., Machowski, W., Gaura, E. and Hudson, E. (1997). Control of drug aerosol in human airways using electrostatic forces. *Journal of Electrostatics*, **40 &41**, 579-584.

Balachandran, W., Kulon, J., Koolpiruck, D., Dawson, M. and Burnell, P. (2003). Bipolar charge measurement of pharmaceutical powders. *Powder Technol.*, **135-136**, 156-163.

Bisgaard, H., Anouj, J. and Wildhaber, J. (2002). Spacer Devices. In: Bisgaard, H. and O'Calloghan, C. editors. *Drug Delivery to the Lung*. Marcel Dekker, Inc., New York, NY, 389-420.

Blondino, F.E. (1995). Novel solution aerosols for inhalation, Ph.D. Dissertation, Virginia Commonwealth University, USA.

Britto, I.L. (2000). Metered dose inhaler for beclomethasone dipropionate. U.S. Patent No. 6,149,892, Glaxo Wellcome Inc.

Britto, I.L. (2001). Metered dose inhaler for fluticasone propionate. U.S. Patent No. 6,253,762, Glaxo Wellcome Inc.

Byron, P.R., Miller, N.C., Blondino, F.E., Visich, J.E. and Ward, G.H. (1994). Some aspects of alternative propellant solvency. In: Dalby, R.N., Byron, P.R., and Farr, S.J. editors. *Respiratory Drug Delivery IV*, Interpharm Press, Buffalo Grove, IL, 231-242.

Byron, P.R., Peart, J. and Staniforth, J.N. (1997). Aerosol electrostatics I: Properties of fine powders before and after aerosolization by dry powder inhalers. *Pharmaceutical Research*, **14**, 698-705.

Chan, T.L., Lippmann, M., Cohen, V.R. and Schlesinger, R.B. (1978). Effect of electrostatic charges on particle deposition in a hollow cast of the human-tracheobronchial tree. *J. Aerosol. Sci.*, **9**, 463-468.

Chen, B. T. and John, W. (2001). Instrument Calibration. In.: Baron, P.A. and Willeke, K. editors. *Aerosol Measurement: Principles, Techniques and Measurements*, Wiley-Interscience, Inc, New York, 627-666.

Clark, A.R. and Hollingworth, A.M. (1993). The relationship between powder inhaler resistance and peak inspiratory conditions in healthy volunteers – Implications for in vitro testing. *Journal of Aerosol Medicine*, **6**, 99-110.

Clarke, S.G., Wicks, S.R. and Farr S.J. (1993). Surfactant mediated effects in pressurized metered dose inhalers formulated as suspensions. I. Drug / surfactant interactions in a model propellant system. *International Journal of Pharmaceutics*, **93**, 221-231.

Crampton, M., Kinnersley, R. and Ayres, J. (2004). Sub-micrometer particle production by pressurized metered dose inhalers. *Journal of Aerosol Medicine*, **17**, 33-42.

Cripps, A., Riebe, M., Schulze, M. and Woodhouse, R. (2000). Pharmaceutical transition to non-CFC pressurized metered dose inhalers. *Respir. Med.*, **94** Suppl B, S3-S9.

Cummings, R.H. (1999). Pressurized metered dose inhalers: chlorofluorocarbon to hydrofluoroalkane transition-valve performance. *Journal of Allergy and Clinical Immunology*, **104**, S230-S236.

Dalby R.N. (1990). Special considerations in the formulation of suspension type Metered Dose Inhalers. In.: Dalby R.N. and Evans, R., editors. *Respiratory Drug Delivery II*, University of Kentucky, Lexington, KY, 390-415.

Dalby, R.N., Phillips, E.M. and Byron, P.R. (1991). Determination of drug solubility in aerosol propellants. *Pharm. Res.*, **8**, 1206-1209.

Dekati Ltd. Technical Note. (2002). Negative current values in ELPI data, Version 2.0, 3-19-2002.

Delgado, A.V., Gonzalez-Caballero, F., Hunter, R.J., Koopal, L.K. and Lyklema, J. (2005). Measurement and interpretation of electrokinetic phenomena. *Pure Appl. Chem.*, **77**, 1753-1805.

Derjaguin, B.V. and Landau, L.D. (1941). Theory of the stability of strongly charged lyophobic sols and of the adhesion of strongly charged particles in solutions of electrolytes. *Acta Physicochimica U.S.S.R.*, **14**, 663.

DeStefano, G.A. and McNamara, D.P. (1996). Viscosity measurements of metered dose inhalers. In: Dalby R.N., Byron P.R., and Farr S.J. editors. *Respiratory Drug Delivery V*, Interpharm Press, Buffalo Grove, IL, 209-219.

Dunbar, C.A. and Hickey, A.J. (2000). Evaluation of probability density functions to approximate particle size distributions of representative pharmaceutical aerosols. *Journal of Aerosol Science*, **31**, 813-831.

Eriksson, P.M., Sandstrom, K.B. and Rosenholm, J.B. (1995). The Distribution of Oleic Acid Between Salbutamol Base Drug and Different Propellant Blends. *Pharm. Res.*, **12**, 715-719.

Farr, S.J., McKenzie, L. and Clarke, J.G. (1994). Drug-surfactant interactions in apolar systems: relevance to the optimized formulation of suspension pMDIs. In: Dalby R.N., Byron P.R., and Farr S.J. editors. *Respiratory Drug Delivery IV*, Interpharm Press, Buffalo Grove, IL, 221-229.

Fowkes, F.M., Jinnai, H., Mostafa, M.A., Anderson, F.W. and Moore, R.J. (1982). Mechanism of electric charging of particles in non-aqueous liquids. *ACS Symposium Series*, **200**, 307-324.

Fraser, D.A. (1966). The deposition of unipolar charged particles in the lungs of animals. *Archives of Environmental Health*, **13**, 152-157.

Garmise, R.J. and Hickey, A.J. (2008). Calibration of the Andersen Cascade Impactor for the characterization of nasal products. *Journal of Pharmaceutical Sciences*, published online 14 December 2007, doi 10.1002/jps.21267.

Gelotte, K.M. and Shaheed, D.J. (1998). Water solubility in metered dose inhalers media containing different propellants. *Journal of Pharmaceutical Sciences*, **1**, 210.

Glover, W. and Chan, H-K. (2004a). Electrostatic charge characterization of pharmaceutical aerosols using electrical low-pressure impaction (ELPI). *Journal of Aerosol Science*, **35**, 755-764.

Glover, W. and Chan, H-K. (2004b). Electrostatic charge characterization of pharmaceutical aerosols. In: Dalby R.N., Byron P.R., Peart, J., Suman, J. D., and Farr S.J. editors. *Respiratory Drug Delivery IX,* Davis Healthcare International Publishing, River Grove, IL, **3**, 825-828.

Greenspan, B (2008). Personal Communication.

Hinds, W. C. (1999). *Aerosol technology: Properties, behavior and measurement of airborne particles.* 2nd edition, Wiley Interscience, New York, 327-330.

Hunter, R.J. (1998). Review: Recent developments in the electroacoustic characterization of colloidal suspensions and emulsions. *Colloids and Surfaces A: Physicochemical and Engineering Aspects*, **141**, 37-65.

Jannick, P. (2006). CFC phase-out scenarios of pressurized metered dose inhalers: Current status. In: Dalby R.N., Byron P.R., Peart, J., Suman, J. D., and Farr S.J. editors. *Respiratory Drug Delivery 2006,* Davis Healthcare International Publishing, River Grove, IL, LLC, 789-792.

Kamiya, A., Sakagami, M., Hindle, M. and Byron, P.R. (2004). Aerodynamic sizing of metered dose inhalers: An evaluation of the Andersen and Next Generation Pharmaceutical Impactors and their USP methods. *Journal of Pharmaceutical Sciences*, **93**, 1828-1837.

Keil, J. (2005). Relationship of particle size distribution with electrical properties of pharmaceutical aerosols, Masters Thesis, Virginia Commonwealth University, USA.

Keil, J., Kotian, R. and Peart, J. (2006). Using and interpreting aerosol electrostatic data from the Electrical Low Pressure Impactor. In.: Dalby R.N., Byron P.R., Peart, J., Suman, J. D., and Farr S.J. editors. *Respiratory Drug Delivery 2006*, Davis Healthcare International Publishing, LLC, River Grove, IL, **1**, 267-278.

Kellogg, G.E. and Abraham, D.J. (2000). Hydrophobicity: is $LogP_{o/w}$ more than the sum of its parts? *European Journal of Medicinal Chemistry*, **35**, 651-661.

Keskinen, J., Pietarinen, K. and Lehtimaki, M. (1992). Electrical low pressure impactor. *J. Aerosol Sci.*, **23**, 353-360.

Keskinen, J., Marjamaki, M., Virtanen, A., Makela, T. and Hillamo, R. (1999). Electrical calibration method for cascade impactors. *Journal of Aerosol Science*, **30**, 111-116.

Kitahara, A. and Watanabe, A. (1984). *Electrical phenomena at interfaces: Fundamentals, measurements and applications*, Marcel Dekker, New York.

Kulphaisal, P. (2003). Importance of metering valve-formulation interactions on electrical properties in hydrofluoroalkane based pressurized metered dose inhalers. Masters Thesis, Virginia Commonwealth University.

Kwok, P. and Chan, H-K. (2004). Measurement of electrostatic charge of nebulised aqueous droplets with the electrical low pressure impactor. In: Dalby R.N., Byron P.R., Peart, J., Suman, J. D., and Farr S.J. editors. *Respiratory Drug Delivery IX*, Davis Healthcare International Publishing, River Grove, IL, 833-836.

Kwok, P., Glover, W. and Chan, H-K. (2005). Electrostatic charge characteristics of aerosols produced from metered dose inhalers. *Journal of Pharmaceutical Sciences*, **94**, 2789-2799.

Kwok, P., Collins, R. and Chan, H-K. (2006). Effect of spacers on the electrostatic charge properties of metered dose inhaler aerosols. *Journal of Aerosol Science*, **37**, 1671-1682.

Kwok, P.C. and Chan, H-K. (2008). Effect of relative humidity on the electrostatic charge properties of dry powder inhaler aerosols. *Pharm. Res.*, **25**, 277-288.

Larson, J.R., Morrison, I.D. and Robinson, T.S. (1992). A thermodynamic approach to liquid toner particle charging. Proceedings of the 8th International Congress on Advances in Non-Impact Printing, Williamsburg, VA, 193-197.

Leach, C.L., Davidson, P.J. and Boudreau, R.J. (1998). Improved airway targeting with the CFC-free HFA-beclomethasone Metered Dose Inhaler compared with CFC-beclomethasone. *Eur. Respir. J.*, **12**, 1346-1353.

Leach, C.L. (2005). The CFC to HFA transition and its impact on pulmonary drug development. *Respiratory Care*, **50**, 1201-1206.

Leger, J.M., Goursolle, M., Gadret, M. and Carpy, A. (1978). Structure crystalline du sulfate de salbutamol [tert-butylamino-2-(hydroxy-4-hydroxmethyl-3-phenyl)-1-ethanol.0.5$H_2SO_4$]. *Acta Crystallographica Section B: Structural Science*, **B34**, 1203-1208.

Levitt, M. (1983). Molecular dynamics of native protein: I. Computer simulation of trajectories. *Journal of Molecular Biology*, **168**, 595-617.

Levitt, M. and Perutz, M.F. (1988). Aromatic rings act as hydrogen bond acceptors. *Journal of Molecular Biology*, **201**, 751-754.

Lewis, D., Johnson, S., Meakin, B., Ganderton, D., Brambilla, G., Garzia, R. and Ventura, P. (1998). Effects of actuator orifice diameter on beclomethasone dipropionate delivery from a pMDI HFA solution formulation. In.: Dalby R.N., Byron P.R., and Farr S.J. editors. *Respiratory Drug Delivery VI*, Interpharm Press, Buffalo Grove, IL, 363-364.

Looker, B.E., Lunniss, C.J. and Redgrave, A.J. (2003). Compounds for use as surfactants. WIPO Patent No. WO/2003/035237, Glaxo Group Ltd.

Louca, E., Leung, K., Coates, A.L., Mitchell, J. and Nagel, M. (2006). Comparison of three valved holding chambers for the delivery of fluticasone propionate-HFA to an infant face model. *Journal of Aerosol Medicine*, **19**, 160-167.

Lyklema, J. (1968). Principles of the stability of lyophobic colloidal dispersions in non-aqueous media. *Advances in Colloid and Interface Science*, **2**, 67-114.

Malvern Zetasizer Nano ZS Manual 2003. Chapter 16. Zeta Potential Theory.

Maricq, M.M., Podsiadlik, D.H. and Chase, R.E. (2000). Size distribution of motor vehicle exhaust PM: A comparison Between ELPI and SMPS measurements. *Aerosol Science and Technology*, **33**, 239-260.

Marjamaki, M., Keskinen, J., Chen, D.R. and Pui, D.Y.H. (2000). Performance evaluation of the Electrical Low Pressure Impactor (ELPI). *J. Aerosol Sci.*, **31**, 249-261.

Marple, V.A., Olson, B.A., Santhanakrishnan, K., Mitchell, J., Murray, S.S. and Hudson-Curtis, B.L. (2003). Next Generation Impactor (a new impactor for pharmaceutical inhaler testing), Part II: Archival Calibration. *Journal of Aerosol Medicine*, **16**, 301-324.

Matthews, M.B. and Hirschhorn, E. (1953). Solubilization and micelle formation in a hydrocarbon medium. *Journal of Colloid Science*, **8**, 86-96.

McGown, D.N.L. and Parfitt, G.D. (1966). Stability of non-aqueous dispersions. Part 4 - Rate of coagulation of rutile in aerosol OT + p-xylene solutions. *Discuss. Faraday Soc.*, **42**, 225-231.

Melandri C., Tarroni G., De Zaiacomo, T.Formignani M. and Lombardi C. (1983). Deposition of charged particles in the human airways. *J. Aerosol Sci.*, **14**, 657-669.

Meurer, C., Pietsch, G. and Haacke, M. (2001). Electrical properties of CFC- and HCFC-substitutes. *International Journal of Refrigeration*, **24**, 171-175.

Mikkanen, P., Moisio, M., Ristimaki, J., Ronkko, T., Keskinen, J. and Korpiharju, T. (2004). Measuring DPI charge properties using ELPI. In: Dalby R.N., Byron P.R., Peart,

J., Suman, J.D., and Farr S.J. editors. *Respiratory Drug Delivery IX*, Davis Healthcare International Publishing, LLC, River Grove, IL, **2**, 465-468.

Mitchell, J., Nagel, M. and Archer, A.D. (1999). Size analysis of a pressurized metered dose inhaler - Delivered suspension formulation by the API Aerosizer time-of-flight Aerodynamic Particle Size Analyzer. *Journal of Aerosol Medicine*, **12**, 255-264.

Mitchell, J., Morton, R. W., Schmidt, J., Snyder, S., Doyle, C. and Nagel, M. (2004). Overcoming electrostatic charge retention in a new valved holding chamber (VHC). In: Dalby R.N., Byron P.R., Peart, J., Suman, J. D., and Farr S.J. editors. *Respiratory Drug Delivery IX*, Davis Healthcare International Publishing, LLC, River Grove, IL, **3**, 705-708.

Mitchell, J., Coppolo, D.P. and Nagel, M. (2007). Electrostatics and inhaled medications: Influence on delivery via pressurized metered dose inhalers and add-on devices. *Respiratory Care*, **52**, 283-300.

Morrison, I.D., Thomas, A.G. and Tarnawskyj, C.J. (1991). A method to measure the average charge to mass ratio of particles in low-conductivity media. *Langmuir*, **7**, 2847-2852.

Morrison, I.D. (1993). Electrical charges in nonaqueous media. *Colloids and Surfaces A: Physicochemical and Engineering Aspects*, **71**, 1-37.

Nithyanandan, P., Hoag, S.W. and Dalby, R.N. (2007). The analysis and prediction of functional robustness of inhaler devices. *Journal of Aerosol Medicine*, **20**, 19-37.

Orban, J. and Peart, J. (2004). Simultaneous electrostatic charge characterization and particle size analysis of metered dose inhalers (pMDIs) Using the electrical low pressure impactor. In: Dalby R.N., Byron P.R., Peart, J., Suman, J.D., and Farr S.J. editors. editors. *Respiratory Drug Delivery IX*, Davis Healthcare International Publishing, LLC, River Grove, IL, **3**, 877-880.

Parsons, G.E., Buckton, G. and Chatham, S.M. (1992). The use of surface energy and polarity determinations to predict physical stability of non-polar, non aqueous suspensions. *International Journal of Pharmaceutics*, **83**, 163-170.

Peart, J., Magyar C. and Byron, P.R. (1998). Aerosol electrostatics – Metered dose inhalers (MDIs): Reformulation and device design issues. In: Dalby R.N., Byron P.R., and Farr S.J. editors. *Respiratory Drug Delivery VI*, Interpharm Press, Buffalo Grove, IL, 227-233.

Pischtiak, A. (2000a). Qualification of HFA 227ea versus HFA 134a for use as a propellant in MDIs. In: Dalby R.N., Byron P.R., Farr S.J., and Peart, J. editors. *Respiratory Drug Delivery VII*, Davis Horwood International Publishing, Raleigh, NC, 519-522.

Pischtiak, A. (2000b). Material compatibility of plastics and elastomers with 5 % w/w of ethanol in HFA 134a and HFA 227ea. In: Dalby R.N., Byron P.R., Farr S.J., and Peart, J., editors. *Respiratory Drug Delivery VII*. Davis Horwood International Publishing, Raleigh, NC, 515-518.

Pugh, R.J., Matsunaga, T. and Fowkes, F.M. (1983). The dispersibility and stability of carbon black in media of low dielectric constant: I. Electrostatic and steric contribution to colloid stability. *Colloids Surf.*, **7**, 183-207.

Purewal, T.S. (1998). Formulation of metered dose inhalers. In: Purewal, T.S. and Grant, D.J.W. editors, *Metered dose inhaler technology*, Interpharm Press, Buffalo Grove, IL, 9-68.

Rau, J.L., Coppolo, D.P., Nagel, M., Avvakoumova, V.I., Doyle, C., Wiersema, K.J. and Mitchell, J. (2006). The importance of non-electrostatic materials in holding chambers for delivery of hydrofluoroalkane albuterol. *Respiratory Care*, **51**, 503-510.

Riebe, M. T., Dwivedi, S. K. and Li-Bovet, L. (2003). Aerosols containing annealed particulate salbutamol and tetrafluoroethane. U.S. Patent No. 6,558,651, Smithkline Beecham Corporation.

Rogueda, P. (2002). Particle interactions in HFA formulations: Experiment, theory and practice. In: Dalby R.N., Byron P.R., Farr S.J., and Peart, J. editors. *Respiratory Drug Delivery VIII*, Davis Horwood International Publishing, Raleigh, NC, **1**, 215-222.

Rogueda, P. (2005a). Novel hydrofluoroalkane suspension formulations for respiratory drug delivery. *Expert Opinion on Drug Delivery*, **2**, 625-638.

Rogueda, P. (2005b). Personal Communication.

Romo, L.A. (1966). Effects of C3, C4 and C5 alcohols and water on the stability of dispersions with alumina and aluminum hydroxide. *Discuss. Faraday Soc.,* **42**, 232-237.

Sandstrom, K.B., Eriksson, P.M. and Rosenholm, J.B. (1994). Electrophoretic mobility of salbutamol drug powder in mixed propellant solvents. *Journal of Pharmaceutical Sciences*, **83**, 1380-1385.

Schlick, T. (2002). *Molecular modeling and simulation: an interdisciplinary guide*. Springer, New York.

Shell Chemicals (2005). Methyl ethyl ketone Datasheet. 9-19-2005.

Sidhu, B.K., Washington, C., Davis, S.S. and Purewal, T.S. (1993). Electrophoretic properties of lactose and salbutamol sulfate suspensions in halogenated solvents. *Langmuir*, **9**, 839-843.

Solvay Chemicals Solkane 134a Material Safety Data Sheet (MSDS) 2003.

Solvay Fluor Und Derivate GmbH (2001). Electrical properties of solkane refrigerants. Product Bulletin no. I/10.01/11/E.

Solvay Fluor Und Derivate GmbH (2003). HFA 227 and HFA 134a Datasheet.

Stefely, J.S. (2002). Novel excipients for inhalation drug delivery: Expanding the capability of the MDI. *Drug Delivery Technology*, **2**, 6-69.

Stein, S. and Olson, B.A. (1997). Variability in size distribution measurements obtained using multiple Andersen Mark II Cascade Impactors. *Pharmaceutical Research*, **14**, 1718-1725.

Stein, S. and Myrdal, P. (2004). A theoretical and experimental analysis of formulation and device parameters affecting solution MDI size distributions. *Journal of Pharmaceutical Sciences* **93**, 2158-2175.

Telko, M.J., Kujanpaa, J. and Hickey, A.J. (2007). Investigation of triboelectric charging in dry powder inhalers using electrical low pressure impactor (ELPI). *Int. J. Pharm.*, **336**, 352-360.

Thiel, C.G. (1996). From Susie's question to CFC free: An inventor's perspective on forty years of MDI development and regulation. In: Dalby R.N., Byron P.R., and Farr S.J. editors. *Respiratory Drug Delivery V*, Interpharm Press, Buffalo Grove, IL, 115-123.

Thiel, C.G. (2002). Cascade impactor data and the lognormal distribution: Nonlinear regression for a better fit. *Journal of Aerosol Medicine*, **15**, 369-378.

Tobias, M. L. (1993). Using the log-normal distribution in analyzing aerosols: The mathematical reasoning underlying the various diameters used and the plotting procedure. Technical Document No. 12669 (Office of Scientific and Technical Information (OSTI) ID No. DE94006459), Oak Ridge, TN, Oak Ridge National Laboratory (ORNL), 1-24.

Traini, D., Rogueda, P., Young, P.M. and Price, R. (2005). Surface energy and interparticle forces correlations in model pMDI formulations. *Pharmaceutical Research* **22**, 816-825.

Traini, D., Young, P.M., Rogueda, P. and Price, R. (2006). The use of AFM and surface energy measurements to investigate drug-canister material interactions in a model

pressurized metered dose inhaler formulation. *Aerosol Science and Technology*, **40**, 227-236.

Tripos Bookshelf, Force Field Manual Sybyl version 7.3 (2006). Tripos Inc., St. Louis, MO.

Tripos Bookshelf, HINT® Manual Sybyl version 7.3 (2006). Tripos Inc., St. Louis, MO.

Tzou, T.Z., Pachuta, R.R., Coy, R.B. and Schultz, R.K. (1997). Drug form selection in albuterol-containing metered-dose inhaler formulations and its impact on chemical and physical stability. *Journal of Pharmaceutical Sciences*, **86**, 1352-1357.

United States Pharmacopeia (Vol. 29) and National Formulary (Vol. 24) First Supplement. (2006). General Chapter 601 Aerosols. Physical tests and determinations: aerosols, metered-dose inhalers, and dry powder inhalers. United States Pharmacopeial Convention, Inc., Rockville, MD, 2617-2636.

van Oss, C. J. (1994). *Interfacial forces in aqueous media*. Marcel Dekker, New York.

Vervaet, C. and Byron, P. (1999). Drug–surfactant–propellant interactions in HFA-formulations. *International Journal of Pharmaceutics*, **186**, 13-30.

Verwey, E.J.W. and Overbeek, J.T.G. (1948). *Theory of the stability of lyophobic colloids*, Elsevier, Amsterdam.

Williams, G. and Tcherevatchenkoff, A. (1998). Moisture transport into CFC-free MDIs. In. Dalby, R.N., Byron, P.R. and Farr, S.J. *Respiratory Drug Delivery VI*, Interpharm Press, Buffalo Grove, IL, 471-474.

Williams, G. (1999). Moisture transport into chlorofluorocarbon-free metered dose inhalers. *Journal of Allergy and Clinical Immunology*, **104**, S227-S229.

Wohlfarth, C. (2007). Section 6: Fluid properties: Permittivity (dielectric constant) of liquids. In: Lide, D.R. editor-in-chief. *CRC Handbook of Chemistry and Physics*, 18th edition, CRC Press, Cleveland, Ohio, 6-151.

Wyatt, D.A. and Vincent, B. (1989). Electrical effects in non-aqueous systems. *J. Biopharm. Sci.*, **3**, 27-31.

Young, P.M., Sung, A., Traini, D., Kwok, P., Chiou, H. and Chan, H.K. (2007). Influence of humidity on the electrostatic charge and aerosol performance of dry powder inhaler carrier based systems. *Pharmaceutical Research*, **24**, 963-970.

# APPENDIX

## A.I Dekati Ltd. Charger Efficiency Curve and Impactor Data Sheet for the ELPI used for Electrostatic Charge and Mass Distribution of pMDIs

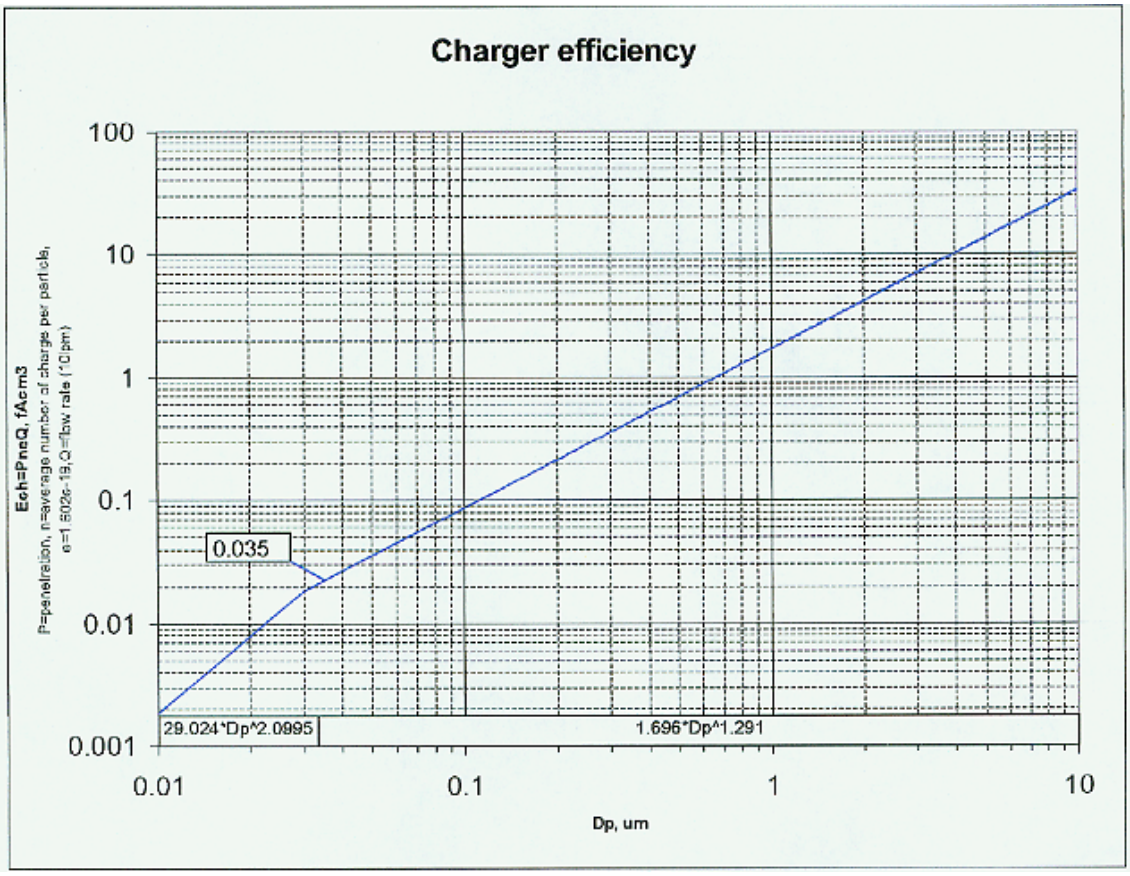

DEKATI

# 30 LPM IMPACTOR DATA SHEET

Below is given the correct settings for DEKATI Impactor # 6235

Cut points, downstream stagnation pressures and residence times:

| Stage | Number of jets | D50% (µm) | Pressure (kPa) | Res Time |
|---|---|---|---|---|
| 1 | 207 | 0.0283 | 10.00 | 0.0057 |
| 2 | 174 | 0.0555 | 21.91 | 0.0100 |
| 3 | 63 | 0.0952 | 38.21 | 0.0177 |
| 4 | 57 | 0.159 | 69.34 | 0.0231 |
| 5 | 81 | 0.266 | 89.09 | 0.0252 |
| 6 | 150 | 0.388 | 97.20 | 0.0259 |
| 7 | 144 | 0.622 | 99.70 | 0.0261 |
| 8 | 60 | 0.961 | 100.55 | 0.0333 |
| 9 | 51 | 1.62 | 101.00 | 0.0333 |
| 10 | 42 | 2.42 | 101.16 | 0.0367 |
| 11 | 9 | 4.05 | 101.24 | 0.0400 |
| 12 | 1 | 6.67 | 101.28 | 0.0467 |
| 13 | 1 | 10.08 | 101.32 | 0.0000 |
| inlet | | | 101.33 | |

Inlet pressure: 1013.3 mbar
Outlet pressure: 100 mbar
Flow Rate: 29.02 lpm

Calibration information
Date: 9.3.2007
Temperature: 21.5 °C

Timo Alanen

**A.II. Dielectric Constant of Ethanol / HFA 134a Blend**

The dielectric constant of a binary mixture can be approximately calculated based on the simple equation (Jouyban *et al.* 2004)*:

$$\varepsilon_m = \varepsilon_1\varphi_1 + \varepsilon_2\varphi_2$$

where $\varepsilon_m$, $\varepsilon_1$ and $\varepsilon_2$ are the dielectric constants of the ethanol/HFA134a blend, HFA 134a and ethanol, respectively, $\varphi_1$ and $\varphi_2$ are the weight fractions of HFA 134a and ethanol in the mixture. For example, the dielectric constant for a 5% ethanol/95% HFA 134a blend would be given by:

$$\varepsilon_m = 9.5*0.95 + 25.3*0.05 = 10.29$$

Similarly, the dielectric constant for other compositions of the ethanol/HFA 134a blends was calculated using the above equation as shown below:

| Composition of Binary Mixture | Weight Fraction of HFA 134a | Weight Fraction of Ethanol | Dielectric Constant of the Mixture |
|---|---|---|---|
| 7% ethanol / 93% HFA 134a blend | 0.93 | 0.07 | 10.61 |
| 10% ethanol / 90% HFA 134a blend | 0.90 | 0.10 | 11.08 |
| 15% ethanol / 85% HFA 134a blend | 0.85 | 0.15 | 11.87 |

*Jouyban, A., Soltanpur, S. and Chan, H-K. (2004). A Simple Relationship between Dielectric Constant of Mixed Solvents with Solvent Composition and Temperature. *International Journal of Pharmaceutics*, **269**, 353-360.

## A.III Summary of Net Positive and Negative HINT scores for interactions in albuterol sulfate HFA suspension pMDI molecular models

### A.III.1 Summary of Net Positive HINT scores for interactions between albuterol sulfate unit cell and HFA 134a molecules in a model containing albuterol sulfate unit cell solvated in HFA 134a alone

| Albuterol sulfate unit cell in HFA 134a | No. of HFA 134a molecules | Hydrophobic | H-bond | Acid/Base | Hydrophobic/ Polar | Base/Base | Total | Total Score/ HFA 134a molecule | Range of Total Score/ HFA 134a molecule |
|---|---|---|---|---|---|---|---|---|---|
| 1 | 21 | 1173 | 181 | 426 | -610 | -377 | 793 | 38 | 1.3 to 152 |
| 2 | 20 | 1359 | 373 | 542 | -754 | -480 | 1040 | 52 | 0.8 to 239 |
| 3 | 26 | 789 | 321 | 432 | -632 | -499 | 411 | 16 | 0.4 to 82 |
| Mean | 22 | 1107 | 292 | 467 | -666 | -452 | 748 | 35 | - |
| SD | 3 | 291 | 99 | 66 | 78 | 66 | 317 | 18 | - |

### A.III.2 Summary of Net Negative HINT scores for interactions between albuterol sulfate unit cell and HFA 134a molecules in a model containing albuterol sulfate unit cell solvated in HFA 134a alone

| Albuterol sulfate unit cell in HFA 134a | No. of HFA 134a molecules | Hydrophobic | H-bond | Acid/Base | Hydrophobic/ Polar | Base/Base | Total | Total Score/ HFA 134a molecule | Range of Total Score/ HFA 134a molecule |
|---|---|---|---|---|---|---|---|---|---|
| 1 | 74 | 2985 | 1230 | 1493 | -9497 | -6127 | -9915 | -134 | -1to -1080 |
| 2 | 56 | 2925 | 2210 | 1525 | -9204 | -6915 | -9460 | -169 | -1 to -897 |
| 3 | 54 | 2584 | 1210 | 1274 | -6288 | -4441 | -5660 | -105 | -1 to -962 |
| Mean | 61 | 2832 | 1550 | 1431 | -8330 | -5828 | -8345 | -136 | - |
| SD | 11 | 216 | 571 | 136 | 1774 | 1264 | 2336 | 32 | - |

A.III.3 Summary of Net Positive HINT scores for interactions between albuterol sulfate unit cell and HFA 134a molecules in a model containing albuterol sulfate unit cell solvated in HFA 134a in the presence of oleic acid and ethanol

| Albuterol sulfate unit cell in HFA 134a | No. of HFA 134a molecules | Hydrophobic | H-bond | Acid/Base | Hydrophobic/ Polar | Base/Base | Total | Total Score/ HFA 134a molecule | Range of Total Score/ HFA 134a molecule |
|---|---|---|---|---|---|---|---|---|---|
| 1 | 41 | 1447 | 658 | 635 | -1007 | -648 | 1085 | 26 | 0 to 249 |
| 2 | 31 | 357 | 156 | 200 | -207 | -220 | 286 | 9 | 0 to 62 |
| 3 | 30 | 350 | 87 | 195 | -239 | -169 | 225 | 7 | 0 to 52 |
| Mean | 34 | 718 | 301 | 343 | -484 | -346 | 532 | 14 | - |
| SD | 6 | 631 | 312 | 253 | 453 | 263 | 480 | 11 | - |

A.III.4 Summary of Net Negative HINT scores for interactions between albuterol sulfate unit cell and HFA 134a molecules in a model containing albuterol sulfate unit cell solvated in HFA 134a in the presence of oleic acid and ethanol

| Albuterol sulfate unit cell in HFA 134a | No. of HFA 134a molecules | Hydrophobic | H-bond | Acid/Base | Hydrophobic/ Polar | Base/Base | Total | Total Score/ HFA 134a molecule | Range of Total Score/ HFA 134a molecule |
|---|---|---|---|---|---|---|---|---|---|
| 1 | 63 | 1752 | 728 | 986 | -5629 | -3881 | -6043 | -829 | 0 to -829 |
| 2 | 76 | 2091 | 1379 | 1218 | -6844 | -5337 | -7492 | -1026 | 0 to -1026 |
| 3 | 79 | 1926 | 1296 | 1097 | -6626 | -5345 | -7653 | -1119 | 0 to -1119 |
| Mean | 73 | 1923 | 1135 | 1100 | -6366 | -4854 | -7063 | -97 | - |
| SD | 9 | 170 | 354 | 116 | 648 | 843 | 887 | 1 | - |

A.III.5 Summary of Net Positive HINT scores for interactions between oleic acid and HFA 134a molecules in a model containing albuterol sulfate unit cell solvated in HFA 134a in the presence of oleic acid and ethanol

| Oleic Acid in HFA 134a | No. of HFA 134a molecules | Hydrophobic | H-bond | Acid/Base | Hydrophobic/ Polar | Base/Base | Total | Total Score/ HFA 134a molecule | Range of Total Score/ HFA 134a molecule |
|---|---|---|---|---|---|---|---|---|---|
| 1 | 27 | 1446 | 0 | 25 | -318 | -30 | 1123 | 42 | 0 to 170 |
| 2 | 35 | 1250 | 0 | 51 | -265 | -72 | 965 | 28 | 0 to 105 |
| 3 | 59 | 3415 | 0 | 97 | -532 | -131 | 2845 | 48 | 0 to 156 |
| Mean | 40 | 2037 | 0 | 58 | -372 | -78 | 1314 | 39 | - |
| SD | 17 | 1197 | 0 | 37 | 142 | 51 | 475 | 11 | - |

A.III.6 Summary of Net Negative HINT scores for interactions between oleic acid and HFA 134a molecules in a model containing albuterol sulfate unit cell solvated in HFA 134a in the presence of oleic acid and ethanol

| Oleic Acid in HFA 134a | No. of HFA 134a molecules | Hydrophobic | H-bond | Acid/Base | Hydrophobic/ Polar | Base/Base | Total | Total Score/ HFA 134a molecule | Range of Total Score/ HFA 134a molecule |
|---|---|---|---|---|---|---|---|---|---|
| 1 | 26 | 726 | 444 | 618 | -2130 | -1413 | -1755 | -68 | 0 to -249 |
| 2 | 15 | 390 | 240 | 303 | -1079 | -619 | -765 | -51 | 0 to -215 |
| 3 | 14 | 630 | 348 | 516 | -1310 | -1178 | -994 | -71 | 0 to -296 |
| Mean | 18 | 582 | 344 | 479 | -1506 | -1070 | -1171 | -63 | - |
| SD | 7 | 173 | 102 | 161 | 552 | 408 | 518 | 11 | - |

A.III.7 Summary of Net Positive HINT scores for interactions between ethanol and HFA 134a molecules in a model containing albuterol sulfate unit cell solvated in HFA 134a in the presence of oleic acid and ethanol

| Ethanol in HFA 134a | No. of HFA 134a molecules | Hydrophobic | H-bond | Acid/Base | Hydrophobic/ Polar | Base/Base | Total | Total Score/ HFA 134a molecule | Range of Total Score/ HFA 134a molecule |
|---|---|---|---|---|---|---|---|---|---|
| 1 | 68 | 3087 | 301 | 315 | -1442 | -856 | 1405 | 21 | 0 to 94 |
| 2 | 73 | 4163 | 538 | 456 | -1680 | -1354 | 2123 | 29 | 0 to 128 |
| 3 | 81 | 4395 | 605 | 507 | -1797 | -1441 | 2269 | 28 | 0 to 109 |
| Mean | 74 | 3882 | 481 | 426 | -1640 | -1217 | 1932 | 26 | - |
| SD | 7 | 698 | 160 | 100 | 181 | 316 | 462 | 5 | - |

A.III.8 Summary of Net Negative HINT scores for interactions between ethanol and HFA 134a molecules in a model containing albuterol sulfate unit cell solvated in HFA 134a in the presence of oleic acid and ethanol

| Ethanol in HFA 134a | No. of HFA 134a molecules | Hydrophobic | H-bond | Acid/Base | Hydrophobic/ Polar | Base/Base | Total | Total Score/ HFA 134a molecule | Range of Total Score/ HFA 134a molecule |
|---|---|---|---|---|---|---|---|---|---|
| 1 | 81 | 3036 | 2409 | 1081 | -6802 | -3529 | -3804 | -47 | 0 to -213 |
| 2 | 63 | 2949 | 2147 | 1017 | -7014 | -3456 | -4357 | -69 | 0 to -326 |
| 3 | 62 | 2692 | 2057 | 901 | -6228 | -3179 | -3757 | -61 | 0 to -292 |
| Mean | 69 | 2892 | 2204 | 1000 | -6681 | -3388 | -3973 | -59 | - |
| SD | 11 | 179 | 183 | 91 | 407 | 185 | 334 | 11 | - |

## A.IV. Summary of Background Measurements and Electrical Properties of Commercial and Control HFA Solution and Suspension pMDIs

### A.IV.1. Commercial and Control HFA Solution pMDIs

A.IV.1.1. Background Measurements for QVAR 40 pMDIs – Total Net Inherent Charge

| Measurement # | Total Net Charge (pC) | |
|---|---|---|
| | Before pMDI Actuation | After pMDI Actuation |
| 1 | 0.04 | 0.29 |
| 2 | 0.06 | 0.29 |
| 3 | -0.08 | 0.44 |
| 4 | 0.01 | 0.04 |
| 5 | -0.03 | 0.25 |
| Mean | 0.00 | 0.26 |
| SD | 0.06 | 0.14 |
| % CV | 4.04E+18 | 54.87 |

A.IV.1.2.Background Measurements for QVAR 80 pMDIs – Total Net Inherent Charge

| Measurement # | Total Net Charge (pC) | |
|---|---|---|
| | Before pMDI Actuation | After pMDI Actuation |
| 1 | 0.13 | -0.40 |
| 2 | 0.00 | 0.20 |
| 3 | -0.06 | -0.10 |
| 4 | -0.04 | -0.14 |
| 5 | -0.10 | -0.03 |
| Mean | -0.01 | -0.09 |
| SD | 0.09 | 0.22 |
| % CV | -630.03 | -229.60 |

| Shot No. | A.IV.1.3. QVAR 40 - Net Inherent Charge (pC) 5 shots/ can, 1 can | | | | | | | | | | | | Total net charge (pC) | FPD charge (pC) |
|---|---|---|---|---|---|---|---|---|---|---|---|---|---|---|
| | Stage 1 | Stage 2 | Stage 3 | Stage 4 | Stage 5 | Stage 6 | Stage 7 | Stage 8 | Stage 9 | Stage 10 | Stage 11 | Stage 12 | | |
| 1 | -0.44 | 3.96 | 2.85 | 15.36 | 28.34 | 47.77 | 51.38 | 47.51 | 22.37 | 12.54 | 8.36 | 24.93 | 264.93 | 231.64 |
| 2 | 5.73 | 12.62 | 14.35 | 47.25 | 74.99 | 135.11 | 144.48 | 117.32 | 65.44 | 33.84 | 33.85 | 53.34 | 738.32 | 651.13 |
| 3 | 1.28 | 0.65 | -9.11 | 15.16 | 36.43 | 61.12 | 59.60 | 45.30 | 31.23 | 18.49 | 33.03 | 49.36 | 342.55 | 260.15 |
| 4 | 1.67 | 7.25 | 4.86 | 27.30 | 39.56 | 76.02 | 70.60 | 62.84 | 29.76 | 20.38 | 20.21 | 30.28 | 390.73 | 340.24 |
| 5 | 5.04 | 7.81 | 1.50 | 30.43 | 43.10 | 80.97 | 85.29 | 74.89 | 43.78 | 32.76 | 36.46 | 58.66 | 500.70 | 405.57 |
| Mean | 2.66 | 6.46 | 2.89 | 27.10 | 44.48 | 80.20 | 82.27 | 69.57 | 38.52 | 23.60 | 26.38 | 43.31 | 447.44 | 377.75 |
| SD | 2.63 | 4.48 | 8.38 | 13.20 | 17.90 | 33.35 | 37.03 | 29.28 | 16.90 | 9.32 | 11.88 | 14.84 | 183.70 | 167.40 |
| % CV | 98.90 | 69.40 | 290.05 | 48.73 | 40.25 | 41.58 | 45.01 | 42.09 | 43.89 | 39.51 | 45.04 | 34.25 | 41.06 | 44.32 |

| Shot No. | A.IV.1.4. QVAR 80 - Net Inherent Charge (pC) 5 shots/ can, 1 can | | | | | | | | | | | | Total net charge (pC) | FPD charge (pC) |
|---|---|---|---|---|---|---|---|---|---|---|---|---|---|---|
| | Stage 1 | Stage 2 | Stage 3 | Stage 4 | Stage 5 | Stage 6 | Stage 7 | Stage 8 | Stage 9 | Stage 10 | Stage 11 | Stage 12 | | |
| 1 | 15.78 | 20.45 | 9.46 | 68.43 | 107.34 | 182.96 | 196.88 | 188.91 | 125.86 | 78.53 | 59.38 | 79.16 | 1133.14 | 994.60 |
| 2 | 14.88 | 37.62 | 78.92 | 174.34 | 228.44 | 275.56 | 253.46 | 225.41 | 146.37 | 93.25 | 85.38 | 98.21 | 1711.84 | 1528.25 |
| 3 | 12.49 | 21.53 | 11.92 | 43.30 | 78.27 | 146.03 | 148.08 | 125.49 | 68.71 | 38.48 | 35.75 | 69.01 | 799.05 | 694.30 |
| 4 | 13.99 | 7.63 | 36.34 | 155.25 | 201.93 | 246.48 | 225.54 | 198.94 | 130.95 | 105.76 | 117.26 | 142.60 | 1582.66 | 1322.81 |
| 5 | 5.66 | 16.28 | 56.76 | 136.40 | 154.48 | 190.24 | 199.86 | 176.95 | 119.27 | 89.15 | 86.99 | 108.83 | 1340.87 | 1145.05 |
| Mean | 12.56 | 20.70 | 38.68 | 115.54 | 154.09 | 208.25 | 204.76 | 183.14 | 118.23 | 81.03 | 76.95 | 99.56 | 1313.51 | 1137.00 |
| SD | 4.04 | 10.92 | 29.67 | 56.81 | 62.75 | 52.03 | 39.06 | 36.85 | 29.43 | 25.71 | 30.84 | 28.68 | 363.68 | 317.78 |
| % CV | 32.20 | 52.78 | 76.71 | 49.16 | 40.72 | 24.98 | 19.08 | 20.12 | 24.89 | 31.73 | 40.07 | 28.80 | 27.69 | 27.95 |

| Shot No. | A.IV.1.5. QVAR 40 - Charge to mass ratio (pC/µg), 5 shots/can, 1 can | | | | | | |
|---|---|---|---|---|---|---|---|
| | Stage 4 | Stage 5 | Stage 6 | Stage 7 | Stage 8 | Stage 9 | Stage 10 |
| 1 | 10.62 | 10.91 | 9.91 | 9.48 | 9.56 | 10.33 | 29.36 |
| 2 | 38.63 | 30.10 | 28.34 | 24.96 | 23.83 | 30.02 | 88.50 |
| 3 | 9.24 | 11.69 | 10.60 | 9.49 | 8.70 | 15.00 | 55.33 |
| 4 | 19.18 | 18.31 | 14.49 | 12.02 | 11.81 | 11.42 | 21.62 |
| 5 | 21.58 | 19.13 | 15.73 | 14.07 | 13.83 | 19.60 | 61.82 |
| Mean | 19.85 | 18.03 | 15.81 | 14.00 | 13.55 | 17.27 | 51.32 |
| SD | 11.77 | 7.71 | 7.43 | 6.42 | 6.09 | 7.99 | 26.80 |
| % CV | 59.28 | 42.77 | 46.96 | 45.82 | 44.95 | 46.28 | 52.22 |

| Shot No. | A.IV.1.6. QVAR 80 - Charge to mass ratio (pC/µg), 5 shots/can, 1 can | | | | | | |
|---|---|---|---|---|---|---|---|
| | Stage 4 | Stage 5 | Stage 6 | Stage 7 | Stage 8 | Stage 9 | Stage 10 |
| 1 | 25.67 | 23.29 | 21.17 | 17.89 | 19.75 | 25.45 | 63.68 |
| 2 | 74.00 | 53.84 | 32.18 | 29.78 | 35.43 | 63.09 | 366.34 |
| 3 | 15.71 | 15.23 | 14.89 | 12.80 | 11.95 | 12.38 | 25.38 |
| 4 | 72.59 | 51.81 | 30.00 | 27.14 | 29.78 | 55.73 | 313.79 |
| 5 | 51.18 | 35.93 | 23.31 | 22.48 | 26.77 | 54.47 | - |
| Mean | 47.83 | 36.02 | 24.31 | 22.02 | 24.74 | 42.22 | 192.30 |
| SD | 26.61 | 17.04 | 6.96 | 6.87 | 9.11 | 22.02 | 172.68 |
| % CV | 55.63 | 47.30 | 28.64 | 31.19 | 36.84 | 52.16 | 89.80 |

A.IV.1.7 Background Measurements for repackaged QVAR 40 pMDIs – Total Net Inherent Charge

| Can # | Shot # | Total Net Charge (pC) | |
|---|---|---|---|
| | | Before pMDI Actuation | After pMDI Actuation |
| 1 | 1 | 0.47 | 0.30 |
| | 2 | 0.01 | 0.32 |
| | 3 | -0.17 | 0.26 |
| 2 | 1 | 0.08 | 0.28 |
| | 2 | 0.05 | 0.12 |
| | 3 | 0.26 | 0.66 |
| 3 | 1 | -0.03 | -0.60 |
| | 2 | -0.02 | 0.09 |
| | 3 | 0.02 | 0.06 |
| Mean | | 0.07 | 0.17 |
| SD | | 0.19 | 0.34 |
| % CV | | 250.51 | 204.10 |

| Can # | Shot # | A.IV.1.8. Repackaged QVAR 40 (Transferred to Al canister fitted with Valois DF10/50 metered valve) - Net Inherent Charge (pC) 3 shots/ can, 3 cans | | | | | | | | | | | | Total net charge (pC) | FPD charge (pC) |
|---|---|---|---|---|---|---|---|---|---|---|---|---|---|---|---|
| | | Stage 1 | Stage 2 | Stage 3 | Stage 4 | Stage 5 | Stage 6 | Stage 7 | Stage 8 | Stage 9 | Stage 10 | Stage 11 | Stage 12 | | |
| 1 | 1 | -0.53 | 0.09 | 2.47 | 9.15 | 20.63 | 26.73 | 26.77 | 21.41 | 11.72 | 6.39 | 3.08 | 16.63 | 144.54 | 124.83 |
| | 2 | -3.24 | -4.79 | -1.26 | 8.44 | 19.08 | 22.92 | 21.09 | 16.72 | 12.42 | 4.38 | 8.17 | 12.58 | 116.51 | 95.76 |
| | 3 | -5.66 | -5.50 | -0.64 | 9.61 | 23.66 | 31.09 | 29.38 | 23.30 | 17.87 | 9.27 | 17.85 | 29.68 | 179.92 | 132.38 |
| 2 | 1 | -3.04 | -3.12 | -1.44 | 13.29 | 29.04 | 40.06 | 36.38 | 29.14 | 17.26 | 7.47 | 12.91 | 22.79 | 200.73 | 165.04 |
| | 2 | -2.12 | -2.64 | -2.95 | 8.48 | 18.92 | 31.02 | 36.09 | 28.35 | 22.19 | 9.81 | 12.05 | 23.26 | 182.47 | 147.15 |
| | 3 | -4.34 | -3.34 | 1.65 | 16.41 | 30.19 | 42.31 | 38.20 | 28.83 | 26.09 | 13.25 | 18.52 | 28.11 | 235.88 | 189.25 |
| 3 | 1 | -3.21 | -4.73 | -17.36 | 2.80 | 10.86 | 14.67 | 17.92 | 11.72 | 15.09 | 3.22 | 10.25 | 6.83 | 68.06 | 50.98 |
| | 2 | 1.44 | 4.88 | 9.18 | 20.84 | 23.78 | 34.59 | 28.14 | 20.51 | 20.03 | 14.03 | 14.70 | 18.81 | 210.92 | 177.42 |
| | 3 | -3.22 | -2.53 | 1.82 | 17.19 | 32.21 | 43.69 | 37.14 | 28.50 | 24.15 | 13.77 | 15.49 | 28.00 | 236.22 | 192.72 |
| Mean | | -2.66 | -2.41 | -0.95 | 11.80 | 23.15 | 31.90 | 30.12 | 23.17 | 18.54 | 9.07 | 12.56 | 20.74 | 175.03 | 141.73 |
| SD | | 2.08 | 3.19 | 7.09 | 5.58 | 6.70 | 9.53 | 7.38 | 6.18 | 5.03 | 4.04 | 4.89 | 7.73 | 56.20 | 46.67 |
| % CV | | -78.19 | -132.29 | -747.61 | 47.31 | 28.93 | 29.88 | 24.49 | 26.69 | 27.12 | 44.58 | 38.96 | 37.27 | 32.11 | 32.93 |

| Can # | Shot # | A.IV.1.9. Repackaged QVAR (Transferred to Al canister fitted with Valois DF10/50 metered valve) - Charge to mass ratio (pC/µg), 3 shots/can, 3 cans | | | | | | |
|---|---|---|---|---|---|---|---|---|
| | | Stage 4 | Stage 5 | Stage 6 | Stage 7 | Stage 8 | Stage 9 | Stage 10 |
| 1 | 1 | 9.15 | 20.62 | 17.77 | 12.76 | 9.91 | 8.31 | 13.55 |
| | 2 | 15.47 | 17.88 | 13.69 | 10.20 | 8.34 | 10.93 | 11.36 |
| | 3 | 16.44 | 23.99 | 18.91 | 14.84 | 11.34 | 15.73 | 21.70 |
| 2 | 1 | 26.96 | 32.95 | 26.66 | 18.68 | 14.81 | 14.86 | 18.83 |
| | 2 | 16.84 | 18.74 | 20.23 | 18.87 | 13.47 | 16.89 | 21.75 |
| | 3 | 21.89 | 23.41 | 23.13 | 18.93 | 16.64 | 27.73 | 36.36 |
| 3 | 1 | 2.92 | 7.80 | 5.32 | 4.91 | 3.24 | 5.89 | 2.89 |
| | 2 | 38.05 | 25.83 | 20.36 | 14.49 | 9.77 | 11.80 | 16.52 |
| | 3 | - | 28.94 | 25.93 | 19.47 | 14.81 | 19.25 | 25.46 |
| Mean | | 18.47 | 22.24 | 19.11 | 14.79 | 11.37 | 14.60 | 18.71 |
| SD | | 10.77 | 7.24 | 6.56 | 4.92 | 4.12 | 6.49 | 9.43 |
| % CV | | 58.32 | 32.56 | 34.31 | 33.26 | 36.25 | 44.47 | 50.37 |

A.IV.1.10 Background measurements for HFA 134a Solution pMDIs – Total net inherent charge

| Can # | Shot # | Total Net Charge (pC) | |
|---|---|---|---|
| | | Before pMDI Actuation | After pMDI Actuation |
| 1 | 1 | 0.30 | 0.82 |
| | 2 | 0.02 | -0.06 |
| | 3 | -0.03 | 0.01 |
| 2 | 1 | 0.66 | 0.68 |
| | 2 | 0.43 | 0.39 |
| | 3 | -0.53 | -0.10 |
| 3 | 1 | 0.23 | 0.64 |
| | 2 | -0.36 | -0.81 |
| | 3 | 0.09 | 0.39 |
| Mean | | 0.06 | 0.21 |
| SD | | 0.36 | 0.49 |
| % CV | | 594.02 | 237.89 |

| Can # | Shot # | A.IV.1.11. 100% HFA 134a with Valois DF 10/50 EPDM valves - Net Inherent Charge (pC) 3 shots/ can, 3 cans | | | | | | | | | | | | Total net charge (pC) | FPD charge (pC) |
|---|---|---|---|---|---|---|---|---|---|---|---|---|---|---|---|
| | | Stage 1 | Stage 2 | Stage 3 | Stage 4 | Stage 5 | Stage 6 | Stage 7 | Stage 8 | Stage 9 | Stage 10 | Stage 11 | Stage 12 | | |
| 1 | 1 | 14.25 | 18.10 | 23.15 | 22.26 | 22.85 | 20.77 | 10.92 | 7.03 | 8.46 | 3.24 | 10.49 | 7.61 | 169.12 | 151.03 |
| | 2 | 12.32 | 16.60 | 20.20 | 14.06 | 11.66 | 2.36 | -5.63 | -5.68 | -0.69 | -10.93 | -0.72 | -13.24 | 40.31 | 54.27 |
| | 3 | 15.38 | 20.17 | 25.15 | 20.46 | 17.06 | 10.48 | 3.88 | 4.23 | 7.02 | -0.50 | 7.58 | 0.70 | 131.61 | 123.33 |
| 2 | 1 | 2.73 | 1.63 | 2.40 | 0.32 | 0.71 | -0.13 | -1.77 | -0.86 | -0.60 | -1.61 | -0.15 | -2.58 | 0.09 | 2.82 |
| | 2 | 6.55 | 3.43 | -0.13 | -9.98 | -11.60 | -20.83 | -15.64 | -9.08 | -6.57 | -11.21 | -7.12 | -15.30 | -97.47 | -75.06 |
| | 3 | 7.17 | 7.56 | 6.77 | 1.31 | 0.82 | -5.13 | -6.15 | -3.88 | -0.47 | -4.38 | 0.07 | -4.67 | -0.96 | 3.62 |
| 3 | 1 | 9.89 | 9.63 | 7.64 | -1.93 | -5.79 | -12.14 | -4.64 | -1.27 | 4.77 | 0.94 | 3.89 | 6.57 | 17.56 | 7.10 |
| | 2 | 13.48 | 18.08 | 23.27 | 20.93 | 18.68 | 12.77 | 5.33 | 5.85 | 8.59 | 2.06 | 9.00 | 1.94 | 139.98 | 129.04 |
| | 3 | 14.64 | 20.31 | 28.52 | 28.60 | 26.16 | 20.56 | 9.97 | 10.27 | 14.10 | 9.20 | 16.02 | 14.93 | 213.27 | 182.33 |
| Mean | | 10.71 | 12.83 | 15.22 | 10.67 | 8.95 | 3.19 | -0.41 | 0.73 | 3.85 | -1.46 | 4.34 | -0.45 | 68.17 | 64.28 |
| SD | | 4.39 | 7.34 | 10.94 | 13.45 | 13.37 | 14.36 | 8.66 | 6.46 | 6.40 | 6.59 | 7.09 | 9.78 | 100.38 | 86.16 |
| % CV | | 40.98 | 57.19 | 71.86 | 126.09 | 149.41 | 449.72 | -2086.68 | 880.72 | 166.32 | -450.24 | 163.28 | -2181.93 | 147.26 | 134.04 |

| Can # | Shot # | A.IV.1.12. 7% Ethanol/93% HFA 134a pMDIs with Valois DF 10/50 EPDM valves - Net Inherent Charge (pC) 3 shots/ can, 3 cans | | | | | | | | | | | | Total net charge (pC) | FPD charge (pC) |
|---|---|---|---|---|---|---|---|---|---|---|---|---|---|---|---|
| | | Stage 1 | Stage 2 | Stage 3 | Stage 4 | Stage 5 | Stage 6 | Stage 7 | Stage 8 | Stage 9 | Stage 10 | Stage 11 | Stage 12 | | |
| 1 | 1 | -7.11 | -2.91 | 7.51 | 15.19 | 16.79 | 18.52 | 15.97 | 11.54 | 14.31 | 5.95 | 10.01 | 17.36 | 123.15 | 95.76 |
| | 2 | -5.62 | -0.51 | 9.25 | 16.35 | 15.23 | 18.12 | 14.34 | 9.89 | 8.54 | 4.25 | 5.78 | 13.60 | 109.22 | 89.84 |
| | 3 | -5.96 | -2.02 | 5.81 | 12.10 | 13.84 | 15.44 | 14.06 | 9.60 | 9.43 | 3.51 | 6.90 | 8.61 | 91.32 | 75.81 |
| 2 | 1 | -6.63 | -1.37 | 8.86 | 16.25 | 16.90 | 17.14 | 13.64 | 10.18 | 10.43 | 5.63 | 10.74 | 11.95 | 113.70 | 91.03 |
| | 2 | -8.15 | -3.17 | 10.62 | 17.30 | 17.11 | 19.91 | 15.91 | 11.21 | 14.59 | 4.02 | 8.53 | 8.61 | 116.48 | 99.35 |
| | 3 | -6.67 | -1.07 | 9.97 | 17.70 | 15.93 | 18.26 | 13.95 | 9.49 | 8.83 | 4.20 | 4.35 | 9.72 | 104.66 | 90.59 |
| 3 | 1 | -5.56 | -1.34 | 7.06 | 15.76 | 15.91 | 17.37 | 14.20 | 10.75 | 9.26 | 5.16 | 9.71 | 12.11 | 110.41 | 88.57 |
| | 2 | -6.20 | -1.33 | 9.51 | 16.19 | 16.92 | 17.45 | 13.01 | 8.32 | 8.48 | 4.35 | 7.90 | 16.85 | 111.46 | 86.70 |
| | 3 | -6.35 | -2.58 | 6.34 | 11.55 | 13.05 | 14.21 | 11.07 | 7.55 | 9.24 | 4.14 | 6.42 | 13.70 | 88.35 | 68.22 |
| Mean | | -6.47 | -1.81 | 8.33 | 15.38 | 15.74 | 17.38 | 14.02 | 9.84 | 10.35 | 4.58 | 7.82 | 12.50 | 107.64 | 87.32 |
| SD | | 0.81 | 0.91 | 1.70 | 2.15 | 1.45 | 1.69 | 1.48 | 1.30 | 2.40 | 0.81 | 2.13 | 3.24 | 11.33 | 9.66 |
| % CV | | -12.46 | -50.18 | 20.38 | 14.00 | 9.22 | 9.72 | 10.53 | 13.17 | 23.19 | 17.75 | 27.29 | 25.89 | 10.53 | 11.06 |

| Can # | Shot # | A.IV.1.13. 0.08% BDP/7% Ethanol/93% HFA 134a pMDIs with Valois DF 10/50 EPDM valves - Net Inherent Charge (pC) 3 shots/ can, 3 cans | | | | | | | | | | | | Total net charge (pC) | FPD charge (pC) |
|---|---|---|---|---|---|---|---|---|---|---|---|---|---|---|---|
| | | Stage 1 | Stage 2 | Stage 3 | Stage 4 | Stage 5 | Stage 6 | Stage 7 | Stage 8 | Stage 9 | Stage 10 | Stage 11 | Stage 12 | | |
| 1 | 1 | 1.41 | 7.38 | -6.25 | 11.30 | 23.42 | 31.73 | 28.45 | 24.97 | 19.27 | 9.85 | 10.90 | 22.70 | 185.14 | 151.53 |
| | 2 | 0.16 | 3.30 | -7.33 | 4.77 | 15.39 | 23.84 | 20.88 | 17.70 | 14.69 | 6.95 | 8.62 | 18.55 | 127.53 | 100.35 |
| | 3 | 2.03 | 3.20 | -7.62 | 9.15 | 15.61 | 26.58 | 24.89 | 22.66 | 16.37 | 8.61 | 9.45 | 20.07 | 150.99 | 121.48 |
| 2 | 1 | -2.67 | -2.41 | -0.84 | 12.53 | 25.16 | 32.98 | 30.36 | 24.94 | 17.12 | 8.72 | 11.79 | 20.56 | 178.24 | 145.89 |
| | 2 | -0.28 | 6.39 | -2.58 | 8.74 | 19.88 | 24.97 | 24.23 | 21.27 | 17.74 | 10.78 | 16.28 | 20.84 | 168.27 | 131.14 |
| | 3 | 4.35 | -5.43 | -15.61 | 3.59 | 14.90 | 25.79 | 26.08 | 22.27 | 17.78 | 8.02 | 8.90 | 12.39 | 123.02 | 101.74 |
| 3 | 1 | 8.70 | 4.40 | -19.24 | 5.33 | 18.00 | 27.53 | 26.09 | 24.08 | 22.74 | 12.09 | 14.10 | 20.20 | 164.02 | 129.72 |
| | 2 | 2.17 | 3.52 | -8.28 | 11.00 | 24.23 | 38.46 | 38.76 | 32.04 | 29.85 | 13.23 | 12.37 | 14.60 | 211.95 | 184.98 |
| | 3 | 0.39 | -0.24 | -11.16 | 7.53 | 16.78 | 24.64 | 20.34 | 14.58 | 16.42 | 7.87 | 13.80 | 14.90 | 125.85 | 97.15 |
| Mean | | 1.81 | 2.23 | -8.77 | 8.22 | 19.26 | 28.50 | 26.68 | 22.72 | 19.11 | 9.57 | 11.80 | 18.31 | 159.45 | 129.33 |
| SD | | 3.23 | 4.16 | 5.84 | 3.14 | 4.07 | 4.88 | 5.55 | 4.91 | 4.62 | 2.09 | 2.61 | 3.50 | 30.44 | 28.65 |
| % CV | | 178.72 | 186.51 | -66.65 | 38.28 | 21.10 | 17.13 | 20.81 | 21.58 | 24.15 | 21.88 | 22.12 | 19.10 | 19.09 | 22.15 |

## A.IV.2 Commercial and Control HFA Suspension pMDIs

A.V.2.1 Background Measurements for Ventolin HFA – Total Net Inherent Charge

| Measurement # | Total Net Charge (pC) | |
|---|---|---|
| | Before pMDI Actuation | After pMDI Actuation |
| 1 | 0.17 | -0.25 |
| 2 | -0.07 | -0.05 |
| 3 | 0.00 | -0.30 |
| 4 | 0.09 | -0.12 |
| 5 | -0.03 | -0.88 |
| Mean | 0.03 | -0.32 |
| SD | 0.10 | 0.33 |
| % CV | 303.30 | -102.67 |

| Shot No. | A.IV.2.2. Ventolin HFA - Net Inherent Charge (pC) 5 shots/ can, 1 can | | | | | | | | | | | | Total net charge (pC) | FPD charge (pC) |
|---|---|---|---|---|---|---|---|---|---|---|---|---|---|---|
| | Stage 1 | Stage 2 | Stage 3 | Stage 4 | Stage 5 | Stage 6 | Stage 7 | Stage 8 | Stage 9 | Stage 10 | Stage 11 | Stage 12 | | |
| 1 | -25.29 | -62.29 | -90.05 | -167.02 | -140.42 | -96.29 | 0.24 | 82.19 | 98.47 | 117.23 | 39.02 | 106.55 | -137.66 | -283.23 |
| 2 | -26.02 | -65.54 | -96.02 | -180.13 | -154.15 | -99.99 | 20.51 | 99.71 | 143.87 | 126.45 | 47.90 | 94.09 | -89.33 | -231.31 |
| 3 | -31.23 | -70.95 | -108.87 | -200.63 | -168.01 | -97.10 | 21.14 | 95.12 | 164.08 | 146.13 | 53.29 | 92.66 | -104.36 | -250.32 |
| 4 | -34.68 | -75.61 | -117.75 | -194.95 | -160.58 | -85.67 | 31.91 | 127.74 | 153.67 | 165.24 | 55.65 | 97.80 | -37.24 | -190.68 |
| 5 | -28.58 | -66.83 | -108.14 | -189.98 | -176.03 | -104.17 | 22.08 | 113.83 | 174.36 | 157.95 | 58.52 | 117.97 | -29.00 | -205.51 |
| Mean | -29.16 | -68.24 | -104.17 | -186.54 | -159.84 | -96.64 | 19.18 | 103.72 | 146.89 | 142.60 | 50.88 | 101.81 | -79.52 | -232.21 |
| SD | 3.87 | 5.16 | 11.04 | 13.26 | 13.59 | 6.87 | 11.56 | 17.55 | 29.37 | 20.40 | 7.69 | 10.52 | 45.92 | 36.64 |
| % CV | -13.28 | -7.56 | -10.60 | -7.11 | -8.50 | -7.10 | 60.30 | 16.93 | 19.99 | 14.31 | 15.12 | 10.34 | -57.74 | -15.78 |

A.IV.2.3 Background measurements for Control Suspension pMDIs (Prefiltration) – Total net inherent charge

| Can # | Shot # | Total Net Charge (pC) | |
|---|---|---|---|
| | | Before pMDI Actuation | After pMDI Actuation |
| 1 | 1 | 0.16 | 0.20 |
| | 2 | -0.43 | 0.03 |
| | 3 | 0.15 | 0.14 |
| 2 | 1 | 0.26 | 0.08 |
| | 2 | 0.48 | 0.24 |
| | 3 | 0.68 | 0.47 |
| 3 | 1 | 0.50 | 0.32 |
| | 2 | 0.15 | 0.27 |
| | 3 | 0.12 | -0.09 |
| Mean | | 0.23 | 0.18 |
| SD | | 0.32 | 0.17 |
| % CV | | 137.85 | 90.44 |

| Can # | Shot # | A.IV.2.4. 100% HFA 134a (Prefiltration) net inherent charge (pC) on each stage of the ELPI (3 shots/ can, 3 cans) | | | | | | | | | | | | Total net charge (pC) | FPD charge (pC) |
|---|---|---|---|---|---|---|---|---|---|---|---|---|---|---|---|
| | | Stage 1 | Stage 2 | Stage 3 | Stage 4 | Stage 5 | Stage 6 | Stage 7 | Stage 8 | Stage 9 | Stage 10 | Stage 11 | Stage 12 | | |
| 1 | 1 | 1.30 | 2.42 | 4.78 | 8.39 | 9.23 | 15.84 | 12.35 | 11.16 | 8.33 | 7.46 | 9.18 | 13.59 | 104.04 | 81.26 |
| | 2 | 1.07 | 1.66 | 3.34 | 5.83 | 5.74 | 8.71 | 6.47 | 8.04 | 6.51 | 4.92 | 7.40 | 10.43 | 70.10 | 52.29 |
| | 3 | 1.06 | 1.47 | 3.61 | 6.95 | 7.09 | 10.49 | 8.13 | 9.05 | 7.13 | 5.94 | 8.23 | 11.77 | 80.93 | 60.92 |
| 2 | 1 | 3.72 | 6.69 | 8.62 | 14.03 | 13.57 | 22.40 | 16.81 | 10.07 | 6.64 | 7.71 | 7.83 | 19.20 | 137.29 | 110.26 |
| | 2 | -0.53 | -2.79 | -4.11 | -6.62 | -4.54 | -2.16 | 3.26 | 5.61 | 5.49 | 7.78 | 9.11 | 18.73 | 29.23 | 1.39 |
| | 3 | -2.08 | -7.09 | -10.39 | -18.31 | -15.74 | -14.94 | -1.29 | 6.99 | 7.75 | 10.73 | 10.84 | 21.77 | -11.76 | -44.37 |
| 3 | 1 | 1.00 | 0.53 | 0.22 | -0.46 | -0.39 | 0.05 | 4.99 | 6.85 | 9.53 | 8.70 | 9.61 | 15.73 | 56.35 | 31.02 |
| | 2 | 0.51 | -0.57 | -1.47 | -2.58 | -1.89 | -1.70 | 3.58 | 5.53 | 7.26 | 6.84 | 8.73 | 16.19 | 40.43 | 15.51 |
| | 3 | -0.22 | -1.90 | -3.15 | -5.01 | -4.23 | -3.20 | 4.42 | 6.48 | 8.50 | 6.64 | 7.00 | 11.89 | 27.22 | 8.33 |
| Mean | | 0.65 | 0.05 | 0.16 | 0.25 | 0.98 | 3.94 | 6.53 | 7.75 | 7.46 | 7.41 | 8.66 | 15.48 | 59.31 | 35.18 |
| SD | | 1.58 | 3.84 | 5.68 | 9.75 | 8.90 | 11.40 | 5.35 | 1.98 | 1.21 | 1.67 | 1.19 | 3.88 | 44.74 | 46.52 |
| % CV | | 244.01 | 8408.43 | 3531.04 | 3961.07 | 905.25 | 289.23 | 82.03 | 25.50 | 16.27 | 22.46 | 13.77 | 25.06 | 75.44 | 132.23 |

| Can # | Shot # | A.IV.2.5. 0.2% Albuterol sulfate/100% HFA 134a (Prefiltration) - Net inherent charge (pC) (3 shots/ can, 3 cans) | | | | | | | | | | | | Total net charge (pC) | FPD charge (pC) |
|---|---|---|---|---|---|---|---|---|---|---|---|---|---|---|---|
| | | Stage 1 | Stage 2 | Stage 3 | Stage 4 | Stage 5 | Stage 6 | Stage 7 | Stage 8 | Stage 9 | Stage 10 | Stage 11 | Stage 12 | | |
| 1 | 1 | -85.39 | -182.68 | -188.85 | -177.42 | -87.88 | -43.33 | 16.12 | 85.87 | 112.15 | 125.25 | 30.44 | 26.18 | -369.56 | -426.16 |
| | 2 | -67.98 | -160.06 | -184.20 | -205.63 | -132.12 | -86.90 | -31.25 | 48.59 | 84.31 | 121.99 | 26.30 | 41.52 | -545.45 | -613.25 |
| | 3 | -70.16 | -154.26 | -169.30 | -175.65 | -84.82 | -36.35 | -9.84 | 58.41 | 68.75 | 71.25 | 12.11 | 19.36 | -470.51 | -501.97 |
| 2 | 1 | -22.70 | -56.72 | -69.00 | -68.87 | -27.46 | 11.88 | 31.36 | 82.28 | 89.86 | 103.11 | 45.81 | 56.32 | 175.82 | 73.74 |
| | 2 | -45.03 | -104.95 | -128.80 | -154.24 | -78.88 | -46.30 | -16.48 | 42.77 | 59.29 | 73.39 | 20.45 | 25.33 | -353.42 | -399.23 |
| | 3 | -16.23 | -39.36 | -45.80 | -48.63 | -15.00 | 18.79 | 36.54 | 79.36 | 76.02 | 72.42 | 29.19 | 39.04 | 186.33 | 118.11 |
| 3 | 1 | -23.25 | -54.95 | -70.10 | -87.20 | -45.40 | -6.80 | 32.60 | 76.20 | 69.20 | 65.20 | 26.10 | 28.90 | 10.41 | -44.50 |
| | 2 | -37.77 | -86.42 | -98.50 | -107.00 | -47.30 | -9.20 | 33.90 | 62.50 | 71.00 | 85.00 | 31.40 | 42.10 | -60.35 | -133.79 |
| | 3 | -37.31 | -83.18 | -92.10 | -98.30 | -44.80 | -11.00 | 28.20 | 57.10 | 73.00 | 90.60 | 38.10 | 47.70 | -32.11 | -117.79 |
| Mean | | -45.09 | -102.51 | -116.30 | -124.77 | -62.64 | -23.25 | 13.45 | 65.90 | 78.17 | 89.81 | 28.87 | 36.28 | -162.09 | -227.20 |
| SD | | 24.24 | 51.72 | 53.71 | 54.90 | 36.36 | 33.12 | 25.73 | 15.55 | 15.56 | 22.40 | 9.66 | 12.06 | 277.11 | 264.01 |
| % CV | | -53.77 | -50.46 | -46.18 | -44.00 | -58.04 | -142.44 | 191.32 | 23.60 | 19.91 | 24.94 | 33.45 | 33.24 | -171.00 | -116.20 |

A.IV.2.6 Background measurements for Control Suspension pMDIs (Postfiltration) – Total net inherent charge

| Can # | Shot # | Total Net Charge (pC) | |
|---|---|---|---|
| | | Before pMDI Actuation | After pMDI Actuation |
| 1 | 1 | 0.13 | 0.07 |
| | 2 | 0.39 | -0.04 |
| | 3 | 0.2 | 0.09 |
| 2 | 1 | 0.31 | 0.01 |
| | 2 | 0 | -0.11 |
| | 3 | 0.15 | -0.18 |
| 3 | 1 | 0.03 | 0.08 |
| | 2 | 0.55 | 0.09 |
| | 3 | 0.21 | 0.06 |
| Mean | | 0.22 | 0.01 |
| SD | | 0.17 | 0.10 |
| % CV | | 79.77 | 1259.37 |

| Can # | Shot # | A.IV.2.7. 100% HFA 134a (Postfiltration) net inherent charge (pC) on each stage of the ELPI (3 shots/ can, 3 cans) | | | | | | | | | | | | Total net charge (pC) | FPD charge (pC) |
|---|---|---|---|---|---|---|---|---|---|---|---|---|---|---|---|
| | | Stage 1 | Stage 2 | Stage 3 | Stage 4 | Stage 5 | Stage 6 | Stage 7 | Stage 8 | Stage 9 | Stage 10 | Stage 11 | Stage 12 | | |
| 1 | 1 | 14.95 | 21.02 | 18.79 | 25.37 | 22.38 | 37.45 | 35.37 | 28.49 | 18.40 | 17.24 | 16.48 | 25.20 | 281.14 | 239.46 |
| | 2 | 9.92 | 13.03 | 12.39 | 19.64 | 19.70 | 30.75 | 23.31 | 13.80 | 8.21 | 8.65 | 8.04 | 12.76 | 180.21 | 159.4 |
| | 3 | 8.78 | 11.41 | 10.84 | 17.17 | 16.73 | 27.22 | 21.77 | 14.46 | 9.04 | 9.65 | 8.92 | 14.99 | 170.98 | 147.07 |
| 2 | 1 | -1.01 | -6.10 | -7.52 | -10.94 | -9.18 | -15.68 | -10.26 | -2.25 | -1.02 | -0.53 | 1.88 | 8.57 | -54.05 | -64.49 |
| | 2 | 0.82 | -1.70 | -1.74 | -2.73 | -2.54 | -5.14 | -2.93 | 2.49 | 2.56 | 2.19 | 3.50 | 7.42 | 2.21 | -8.72 |
| | 3 | 4.29 | 4.42 | 6.15 | 11.35 | 10.66 | 14.59 | 10.66 | 10.11 | 8.06 | 8.33 | 9.46 | 15.69 | 113.77 | 88.62 |
| 3 | 1 | 9.90 | 16.81 | 23.73 | 34.89 | 31.53 | 40.61 | 24.55 | 15.23 | 15.61 | 15.48 | 16.19 | 18.26 | 262.79 | 228.34 |
| | 2 | 6.31 | 9.46 | 12.03 | 16.55 | 13.57 | 15.04 | 13.16 | 8.87 | 4.97 | 3.53 | 3.99 | 5.77 | 113.26 | 103.49 |
| | 3 | 14.65 | 20.96 | 22.63 | 26.99 | 22.09 | 22.60 | 12.59 | 9.44 | 7.20 | 6.33 | 6.78 | 10.28 | 182.56 | 165.48 |
| Mean | | 7.63 | 9.93 | 10.81 | 15.37 | 13.88 | 18.61 | 14.25 | 11.18 | 8.11 | 7.88 | 8.36 | 13.21 | 139.21 | 117.63 |
| SD | | 14.95 | 21.02 | 18.79 | 25.37 | 22.38 | 37.45 | 35.37 | 28.49 | 18.40 | 17.24 | 16.48 | 25.20 | 281.14 | 101.35 |
| % CV | | 9.92 | 13.03 | 12.39 | 19.64 | 19.70 | 30.75 | 23.31 | 13.80 | 8.21 | 8.65 | 8.04 | 12.76 | 180.21 | 86.16 |

| Can # | Shot # | A.IV.2.8. 0.2% Albuterol sulfate/ 100% HFA 134a (Postfiltration) Net inherent charge (pC) (3 shots/ can, 3 cans) | | | | | | | | | | | | Total net charge (pC) | FPD charge (pC) |
|---|---|---|---|---|---|---|---|---|---|---|---|---|---|---|---|
| | | Stage 1 | Stage 2 | Stage 3 | Stage 4 | Stage 5 | Stage 6 | Stage 7 | Stage 8 | Stage 9 | Stage 10 | Stage 11 | Stage 12 | | |
| 1 | 1 | 8.66 | 8.06 | 7.34 | 9.99 | 8.39 | 10.61 | 8.00 | 8.04 | 5.90 | 8.14 | 10.86 | 17.92 | 111.91 | 83.13 |
| | 2 | 9.75 | 11.85 | 12.97 | 20.88 | 18.33 | 25.94 | 16.64 | 12.31 | 11.89 | 15.01 | 15.55 | 20.80 | 191.93 | 155.57 |
| | 3 | 8.71 | 10.67 | 12.42 | 19.63 | 16.81 | 23.87 | 14.28 | 12.58 | 12.50 | 12.93 | 11.75 | 14.80 | 170.93 | 144.4 |
| 2 | 1 | 5.84 | 11.97 | 16.13 | 25.78 | 21.40 | 25.22 | 16.53 | 10.03 | 9.10 | 12.31 | 17.50 | 25.42 | 197.24 | 154.31 |
| | 2 | 4.75 | 10.50 | 14.22 | 24.69 | 23.36 | 32.46 | 22.03 | 13.69 | 9.70 | 10.09 | 11.46 | 17.18 | 194.14 | 165.49 |
| | 3 | 4.80 | 11.56 | 16.90 | 27.84 | 22.99 | 27.84 | 17.03 | 10.14 | 7.77 | 8.29 | 13.43 | 27.90 | 196.49 | 155.16 |
| 3 | 1 | 10.77 | 13.32 | 12.74 | 17.62 | 13.66 | 18.71 | 13.81 | 9.99 | 8.62 | 10.73 | 11.08 | 14.75 | 155.79 | 129.97 |
| | 2 | 6.25 | 7.13 | 6.33 | 7.97 | 6.27 | 7.76 | 5.80 | 4.96 | 3.46 | 4.27 | 3.98 | 6.81 | 70.98 | 60.2 |
| | 3 | 5.65 | 6.48 | 5.93 | 7.13 | 4.87 | 7.08 | 5.61 | 5.50 | 4.17 | 4.79 | 4.50 | 7.38 | 69.08 | 57.21 |
| Mean | | 7.24 | 10.17 | 11.66 | 17.95 | 15.12 | 19.94 | 13.30 | 9.69 | 8.12 | 9.62 | 11.12 | 17.00 | 150.94 | 122.83 |
| SD | | 2.32 | 2.08 | 3.79 | 7.22 | 6.49 | 8.57 | 5.21 | 2.79 | 2.97 | 3.35 | 3.99 | 6.63 | 53.39 | 43.66 |
| % CV | | 32.03 | 20.44 | 32.46 | 40.21 | 42.93 | 43.00 | 39.15 | 28.80 | 36.61 | 34.81 | 35.91 | 38.98 | 35.37 | 35.55 |

## A.V. Calculation of Number Concentration of Albuterol Particles using the Mass of Albuterol Depositing Within the ELPI

The calculation of the particle volume of albuterol is simplified by assuming that albuterol particles are spherical. The volume of a spherical particle is:

$$V = \pi.d^3/6$$

where V is the volume of the particle and d is the cut-off diameter of the ELPI stages calculated in Chapter VII.

The mass of one particle is calculated by utilizing the known density of albuterol,

D = 1.31 g/cm$^3$ (D = 1.31 x $10^{-12}$ g/μm$^3$).

M = D * V

Where M is the mass of one particle and D is the density of albuterol.

The number of particles depositing on each ELPI stage is calculated as:

Number of particles = FPD / mass per particle

The volume of air that has been pulled through the ELPI during the sampling time of 20 seconds at a flow rate of 29.04 L/min i.e. the sample volume is calculated to be 9680 cm$^3$.

The number concentration of albuterol particles per cm$^3$ for each ELPI stage is calculated as:

Number concentration (per cm$^3$) = Number of particles / 9680 cm$^3$

| Can # | Shot # | A.V.1. Number Concentration (per $cm^3$) for 0.2% Albuterol sulfate / 100% HFA 134a pMDI Aerosols (3 shots / can, 3 cans) based on mass of albuterol deposited in the ELPI | | | | | | | | | | | | Total (Stages 1-12)* | Total (Stages 1-4) |
|---|---|---|---|---|---|---|---|---|---|---|---|---|---|---|---|
| | | Stage 1 | Stage 2 | Stage 3 | Stage 4 | Stage 5 | Stage 6 | Stage 7 | Stage 8 | Stage 9 | Stage 10 | Stage 11 | Stage 12 | | |
| 1 | 1 | 2009 | 1702 | 1175 | 71 | 163 | 321 | 246 | 212 | 98 | 46 | 4 | 1 | 6048 | 4958 |
| | 2 | 893 | 1123 | 1046 | 58 | 94 | 255 | 252 | 211 | 105 | 50 | 5 | 1 | 4093 | 3120 |
| | 3 | - | 356 | 634 | 52 | 94 | 312 | 244 | 203 | 97 | 35 | 4 | 1 | 2033 | 1043 |
| 2 | 1 | - | 2330 | 1994 | 65 | 163 | 325 | 254 | 213 | 99 | 46 | 4 | 1 | 5495 | 4389 |
| | 2 | 2121 | 4207 | 1867 | 98 | 275 | 439 | 367 | 295 | 146 | 70 | 9 | 1 | 9895 | 8293 |
| | 3 | - | 5009 | 735 | 50 | 120 | 308 | 260 | 235 | 110 | 49 | 5 | 1 | 6883 | 5794 |
| 3 | 1 | - | 1744 | 1094 | 75 | 150 | 328 | 261 | 275 | 103 | 41 | 5 | 1 | 4077 | 2913 |
| | 2 | - | 1570 | 1350 | 58 | 158 | 311 | 297 | 240 | 118 | 60 | 6 | 1 | 4168 | 2978 |
| | 3 | - | 2518 | 1337 | 76 | 162 | 330 | 289 | 237 | 115 | 55 | 6 | 1 | 5126 | 3931 |
| Mean | | 1674 | 2284 | 1248 | 67 | 153 | 325 | 274 | 236 | 110 | 50 | 5 | 1 | 5313 | 4158 |
| SD | | 679 | 1474 | 456 | 15 | 54 | 48 | 39 | 31 | 15 | 10 | 1 | 0 | 2212 | 2069 |
| % CV | | 41 | 65 | 37 | 22 | 35 | 15 | 14 | 13 | 14 | 21 | 27 | 33 | 42 | 50 |

*Number Concentration of albuterol particles depositing on Stage 13 was not detected.

## A.VI. SCIENTIST Model and Output and the Modified ELPI recalibration cut-off diameters calculated from individual calibration aerosols

### A.VI.1 SCIENTIST Model file and an example of the Parameter File

**Model File name: c:\scientis\lognmcdf.eqn**

```
//Lognormal Cumulative distribution function - fitting Model (Mean and Sigma not conventional)
//MEAN is the mean of the (ln x) values; SIGMA is the std dev of the (ln x) values
//Take EXP(MEAN,SIGMA) for best fits for (MMAD,SIGMAG) respectively
//The ERF function below performs the integration of the usual pdf expression but the function removes
//2/SQRT(PI) from the pdf equation by using it as a coefficient in front of the integration symbol
IndVars: X
DepVars: Y
Params: MEAN,SIGMA
Y=100*(0.5+0.5*ERF((1/(SIGMA*SQRT(2)))*(LN(X)-MEAN)))
***
```

**Parameters File Name: c:\scientis\lognmdif.par**

| Parameter Name | Lower Limit | Value | Upper Limit |
|---|---|---|---|
| MEAN | 0.000000000 | 0.903279562 | 5.00000000 |
| SIGMA | 0.000000000 | 0.428846956 | 10.0000000 |

## A.VI.2 Example of a SCIENTIST Plot of the Overlay of Experimental and Calculated Data

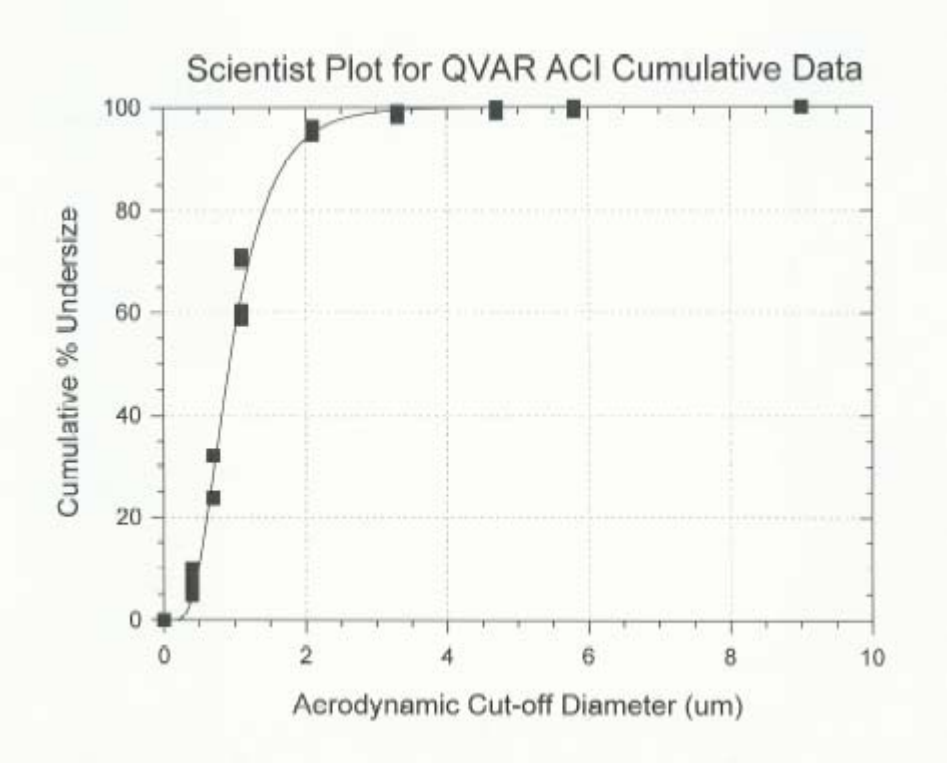

## A.VI.3 Example of the SCIENTIST Statistical Report for the non-linear regression analysis

*** MicroMath Scientist Statistics Report ***

Model File Name: c:\scientis\lognmcdf.eqn
Data File Name: c:\scientis\qvarargb.mmd
Param File Name: c:\scientis\lognmdif.par

Goodness-of-fit statistics for data set: c:\scientis\qvarargb.mmd

Data Column Name: Y

| | Weighted | Unweighted |
|---|---|---|
| Sum of squared observations: | 267773.3192 | 267773.3192 |
| Sum of squared deviations: | 309.439812 | 309.439812 |
| Standard deviation of data: | 2.68258731 | 2.68258731 |
| R-squared: | 0.998844396 | 0.998844396 |
| Coefficient of determination: | 0.995795932 | 0.995795932 |
| Correlation: | 0.997951600 | 0.997951600 |

Data Set Name: c:\scientis\qvarargb.mmd

| | Weighted | Unweighted |
|---|---|---|
| Sum of squared observations: | 267773.3192 | 267773.3192 |
| Sum of squared deviations: | 309.439812 | 309.439812 |
| Standard deviation of data: | 2.68258731 | 2.68258731 |
| R-squared: | 0.998844396 | 0.998844396 |
| Coefficient of determination: | 0.995795932 | 0.995795932 |
| Correlation: | 0.997951600 | 0.997951600 |
| Model Selection Criterion: | 5.38281365 | 5.38281365 |

Confidence Intervals:

| | | |
|---|---|---|
| Parameter Name: | MEAN | |
| Estimate Value = | -0.0748528851 | |
| Standard Deviation = | 0.0113635050 | |
| 95% Range (Univar) = | -0.0977695770 | -0.0519361932 |
| 95% Range (S-Plane) = | -0.103665501 | -0.0460402690 |
| Parameter Name: | SIGMA | |
| Estimate Value = | 0.496699907 | |
| Standard Deviation = | 0.0180281352 | |
| 95% Range (Univar) = | 0.460342707 | 0.533057107 |
| 95% Range (S-Plane) = | 0.450988858 | 0.542410956 |

Variance-Covariance Matrix:

| | |
|---|---|
| 0.000129129246 | |
| 1.65836853E-5 | 0.000325013659 |

Correlation Matrix:

| | |
|---|---|
| 1.00000000 | |
| 0.0809502015 | 1.00000000 |

Residual Analysis:
The following are normalized parameters with an expected value of 0.0. Values are in units of standard deviations from the expected value.
The serial correlation is -2.14 which is probably not significant.
Skewness is -1.79 indicating the likelihood of a few large negative residuals having an unduly large effect on the fit.
Kurtosis is 0.00 which is probably not significant.
The weighting factor was 0.00 leading to a heteroscedacticity of -0.79 which suggests an optimal weight factor for this fit of about -0.79

## A.VI.4 Mean values for the 50% Cut-off Aerodynamic Diameters (μm) of the Different ELPI Stages Based on the Replicate Results (n=5) for Each of the 4 pMDI Products studied as Calibration Standards Along with 95% Confidence Intervals

A.VI.4.1 Mean Calculated Cut-off Diameters of the ELPI Stages using Qvar

| Stage No. | Manufacturer-Reported Cut-Off Diameter (μm) | Calculated Cut-Off Diameter (μm) for ELPI Stages from QVAR | | | |
|---|---|---|---|---|---|
| | | Mean | SD | Lower 95% CI | Upper 95% CI |
| 1 | 0.03 | | | | |
| 2 | 0.06 | 0.28 | 0.01 | 0.26 | 0.29 |
| 3 | 0.1 | 0.35 | 0.01 | 0.34 | 0.37 |
| 4 | 0.16 | 0.44 | 0.02 | 0.41 | 0.46 |
| 5 | 0.27 | 0.56 | 0.01 | 0.55 | 0.57 |
| 6 | 0.39 | 0.70 | 0.02 | 0.68 | 0.72 |
| 7 | 0.62 | 0.98 | 0.06 | 0.91 | 1.05 |
| 8 | 0.96 | 1.37 | 0.14 | 1.21 | 1.54 |
| 9 | 1.62 | 2.10 | 0.12 | 1.94 | 2.25 |
| 10 | 2.42 | 2.64 | 0.24 | 2.34 | 2.94 |
| 11 | 4.05 | 3.39 | 0.22 | 3.12 | 3.66 |
| 12 | 6.67 | | | | |
| 13 | 10.08 | | | | |

A.VI.4.2 Mean calculated cut-off diameters of the ELPI Stages using Ventolin CFC

| Stage No. | Manufacturer-Reported Cut-Off Diameter (μm) | Calculated Cut-Off Diameter (μm) for ELPI Stages from Ventolin CFC | | | |
|---|---|---|---|---|---|
| | | Mean | SD | Lower 95% CI | Upper 95% CI |
| 1 | 0.03 | | | | |
| 2 | 0.06 | | | | |
| 3 | 0.1 | | | | |
| 4 | 0.16 | | | | |
| 5 | 0.27 | | | | |
| 6 | 0.39 | 0.77 | 0.03 | 0.73 | 0.80 |
| 7 | 0.62 | 1.03 | 0.02 | 1.01 | 1.06 |
| 8 | 0.96 | 1.42 | 0.01 | 1.41 | 1.44 |
| 9 | 1.62 | 2.08 | 0.04 | 2.03 | 2.13 |
| 10 | 2.42 | 3.15 | 0.15 | 2.96 | 3.34 |
| 11 | 4.05 | 5.08 | 0.31 | 4.69 | 5.47 |
| 12 | 6.67 | | | | |
| 13 | 10.08 | | | | |

A.VI.4.3 Mean calculated cut-off diameters of the ELPI Stages using Flovent HFA

| Stage No. | Manufacturer-Reported Cut-Off Diameter (µm) | Calculated Cut-Off Diameter (µm) for ELPI Stages from Flovent HFA | | | |
|---|---|---|---|---|---|
| | | Mean | SD | Lower 95% CI | Upper 95% CI |
| 1 | 0.03 | | | | |
| 2 | 0.06 | | | | |
| 3 | 0.1 | | | | |
| 4 | 0.16 | | | | |
| 5 | 0.27 | | | | |
| 6 | 0.39 | | | | |
| 7 | 0.62 | | | | |
| 8 | 0.96 | 1.39 | 0.02 | 1.36 | 1.41 |
| 9 | 1.62 | 2.01 | 0.04 | 1.97 | 2.06 |
| 10 | 2.42 | 2.93 | 0.06 | 2.86 | 3.00 |
| 11 | 4.05 | 4.62 | 0.08 | 4.53 | 4.71 |
| 12 | 6.67 | | | | |
| 13 | 10.08 | | | | |

A.VI.4.4 Mean calculated cut-off diameters of the ELPI Stages using Vanceril

| Stage No. | Manufacturer-Reported Cut-Off Diameter (µm) | Calculated Cut-Off Diameter (µm) for ELPI Stages from Vanceril | | | |
|---|---|---|---|---|---|
| | | Mean | SD | Lower 95% CI | Upper 95% CI |
| 1 | 0.03 | | | | |
| 2 | 0.06 | | | | |
| 3 | 0.1 | | | | |
| 4 | 0.16 | | | | |
| 5 | 0.27 | | | | |
| 6 | 0.39 | | | | |
| 7 | 0.62 | ***1.79*** | ***0.35*** | | |
| 8 | 0.96 | 1.65 | 0.18 | 1.43 | 1.88 |
| 9 | 1.62 | 2.31 | 0.08 | 2.20 | 2.41 |
| 10 | 2.42 | 3.01 | 0.08 | 2.91 | 3.11 |
| 11 | 4.05 | 4.54 | 0.07 | 4.46 | 4.63 |
| 12 | 6.67 | 6.37 | 0.21 | 6.11 | 6.64 |
| 13 | 10.08 | | | | |

# VITA

Reshma Kotian was born on April 28, 1978 in Mumbai, India and is an Indian citizen. She graduated from Mumbai University Institute of Chemical Technology, Mumbai, India with a Bachelor of Pharmaceutical Sciences in 2000 and a Master of Pharmaceutical Sciences in 2002. She worked as a Research & Development Officer (Formulations) at Ipca Laboratories Ltd., Mumbai, India before joining the Department of Pharmaceutics, Virginia Commonwealth University (VCU) in 2003.

During the course of her Ph.D. studies, Reshma has submitted one research article and published three abstracts. She has presented her research at the Graduate Research Association of Students in Pharmacy (GRASP) Annual Meeting (2005), the Annual Meetings of the American Association of Pharmaceutical Scientists (AAPS, 2006) and the Electrostatic Society of America (ESA, 2007) in addition to poster presentations within VCU. She received the VCU Graduate School Student Travel Grant in 2006. Reshma was awarded the 2005 Jyotsna and Mavji Thacker Award for academic excellence in the Department of Pharmaceutics, VCU. In 2000, she received a Junior Research Fellowship for Master of Pharmaceutical Sciences program from the University Grants Commission, Government of India.

Reshma served as the School of Pharmacy representative at the VCU GSA during which she chaired the VCU GSA Research Symposium (2006). She served as the Secretary-Treasurer and Vice-Chair of the GSA in the Department of Pharmaceutics and the AAPS-VCU Student Chapter in 2005 and 2004, respectively. She is a member of the AAPS, ESA and the Phi Kappa Phi Honor Society.

Publication and Abstracts:

1. **Kotian R.**, Peart J., Bryner J. and Byron P. R. Calibration of the modified electrical low pressure impactor for use with pressurized pharmaceutical aerosols. *J Aerosol Med 2008. (Manuscript submitted)*
2. **Kotian R.** and Peart J. Using the modified electrical low pressure impactor (ELPI) to characterize the electrostatic properties of hydrofluoroalkane (HFA) pressurized metered dose inhalers (pMDIs). Annual Meeting of the AAPS, San Antonio, Texas *(Poster & The AAPS Journal 8 (S2): W4224; Nov. 2006)*
3. **Kotian R.** and Peart J. Influence of formulation components on inherent electrostatic properties of HFA propelled solution pMDIs. Respiratory Drug Delivery Conference, Boca Raton, Florida *(Poster & Respiratory Drug Delivery 2006*, In: Dalby, R.N., Byron, P.R., Peart, J., Suman, J.D., and Farr, S.J., editors, Davis Healthcare International Publishing, LLC, River Grove, IL, 3, 947-950).